Reactive MgO and Self-healing Microcapsules for Enhanced Well Cement System Performance

Wenting Mao

Department of Engineering

University of Cambridge

This dissertation is submitted for the degree of

Doctor of Philosophy

Downing College

September 2018

Dedicated to My Loving Parents …

ii

Declaration

I hereby declare that except where specific reference is made to the work of others, the contents of this dissertation are original and have not been submitted in whole or in part for consideration for any other degree or qualification in this, or any other University. This dissertation is the result of my own work and includes nothing which is the outcome of work done in collaboration, except where specifically indicated in the text. This dissertation contains less than 65,000 words including appendices, bibliography, footnotes, tables and equations and has less than 150 figures.

Wenting Mao

September 2018

iv

Acknowledgements

Publications

W.Mao, F.Jin and A.Al-Tabbaa., 2017. Expansion performance of Class G oil well cement with reactive MgO as an expansive additive under different temperatures. In 9th International Symposium on Cement & Concrete, November, Wuhan, China.

W.Mao and A.Al-Tabbaa., 2017. Survivability and Self-healing Efficiency of Microencapsulated Sodium Silicate in Class G Oil Well Cement. In 6th International Conference on Self-Healing Materials, June, Friedrichshafen, Germany.

W.Mao and A.Al-Tabbaa., 2015. Self-healing expansive oil well cement. In 5th International Conference on Self-Healing Materials, June, Durham, North Carolina, USA.

Abstract

The annular cement sheath plays a crucial role in ensuring well integrity by providing adequate zonal isolation, stabilizing the formation, and protecting the casing from corrosion. A majority of well integrity problems originate from oil well cement shrinkage and shrinkage-induced cracking, as well as cracking induced by other external stresses. The addition of expansive additives is a commonly used way to compensate for shrinkage. Compared to conventional ettringite-based and CaO-based expansive additives, MgO has many advantages including a thermally stable hydration product, relatively low water requirements for hydration, and designable expansion properties. These make MgO a promising candidate for delivering the desired expansion under the complex and variable underground wellbore environment. Self-healing materials which have the capability for autonomous crack repair are an attractive solution for addressing cracking problems in oil well cement. Engineered additions of healing agents for autonomic self-healing via a delivery system have been reported as effective ways to promote self-healing in cementitious materials. Microcapsules that can be easily added to cement pastes and dispersed through the cement matrix are considered particularly suitable for use in oil well cement. This research project investigates the efficacy of reactive MgO expansive additives to reduce shrinkage, and of sodium silicate microcapsules to improve the self-healing properties of oil well cement, and explores the feasibility of their combined use in a high temperature oil well environment.

Three types of reactive MgOs from different reactivity grades, high reactivity N50, medium reactivity MAG-R, and low reactivity 92/200, were characterised in terms of their expansion characteristics in cement paste prisms cured in water, and further tested on their autogenous shrinkage reduction at 80°C. The highly reactive N50 could only partially compensate for autogenous shrinkage, while the less reactive MAG-R and 92/200 completely compensated for autogenous shrinkage. MAG-R and 92/200 also showed effective drying shrinkage reduction at 90% RH. The restrained expansion of MAG-R and 92/200 during an early age was found to significantly improve the cracking resistance of oil well cement. The free expansion of 92/200, with low reactivity, caused significant strength reduction, but under restrained conditions the effect was mitigated as its compressive strength was enhanced by confined expansion. The addition of MAG-R increased compressive strength under both free and restrained conditions.

Two groups of sodium silicate microcapsules, T1 with rigid polyurea shells and T2 with rubbery polyurea shells, were characterised in terms of their thermal stability, alkalinity resistance and survivability during cement mixing, and the results verified their suitability for use in oil well cement at the high temperature of 80 °C. The effects of the two types of microcapsules on the self-healing performance of oil well cement at 80 °C were monitored using a variety of techniques. Oil well cement itself showed very little healing capability when cured at 80 °C, but the addition of microcapsules significantly promoted its self-healing performance, showing reduced crack width and crack depth, enhanced tightness recovery against gas permeability and water sorptivity, as well as strength recovery. Microstructure analyses of the cracking surface further verified the successful release of the sodium silicate core and its reaction with the cement matrix to form C-S-H healing products. Both groups of microcapsules showed comparable self-healing efficiency. Their different shell properties mainly influenced the strength of oil well cement, with rigid shell microcapsules causing less strength reduction than rubbery shell microcapsules.

The overall performance of oil well cement containing both reactive MgO and microcapsules were evaluated. The combined addition of MgO MAG-R and T1 microcapsules showed similar expansion performance and self-healing efficiency compared to their individual use. The use of MgO MAG-R compensated for the strength reduction caused by the addition of microcapsules, achieving an overall improvement in the cement strength.

Table of Contents

List of Figures

List of Tables

Nomenclature

τ	Shear stress
$\dot{\gamma}$	Shear rate
τ_Y	Yield stress
μ_{pl}	Plastic viscosity
$\varnothing$	Diameter
3PB	Three-point bending
AEA	Ettringite-based expansive additive
C_2S	Dicalcium silicate
C_3A	Tri-calcium aluminate
C_3AH_6	Hydrogarnet
$Ca_2(Fe,Al)_2O_5$, C_4AF	Tetracalcium aluminoferrite
$CaSO_4$	Calcium sulphate, gypsum
CaO	Calcium oxide
$Ca(OH)_2$, CH	Calcium hydroxide, portlandite
C-S-H	Calcium silicate hydrate
$CaCO_3$	Calcite, calcium carbonate
$CaSO_4$	Calcium sulphate
$C_6A\bar{S}_3H_{32}$	Ettringite
$C_6S_2H_3$	Jaffeite
α-C_2SH	α–dicalcium silicate hydrate
CS	Colloidal silica
Ca^{2+}	Calcium ions
CO_2	Carbon dioxide

CMOD	Crack mouth opening displacement
DCPD	Dicyclopentadiene
EDS, EDX	Environmental scanning electron microscopy
HSR	High Sulphate Resistant
MgO	Magnesium oxide
$Mg(OH)_2$	Magnesium hydroxide, brucite
$MgCO_3$	Magnesium carbonate magnesite
MEA	MgO expansive additives
MMA	Methylmethacrylate
MICP	Microbiologically induced calcite precipitation
MSR	Moderate Sulphate Resistant
MF	Melamine-formaldehyde
OPC	Ordinary Portland cement
OWC	Oil well cement
PF	Phenol formaldehyde
PU	Polyurethane
PUrea	Polyurea
PS	polystyrene
RH	Relative humidity
SAPs	Super absorbent polymers
SCMs	Supplementary cementitious materials
SEM	Scanning electron microscope/microscopy
SIS	Styrene–isoprene–styrene
SBS	Styrene–butadiene–styrene
SSA	Specific surface area

SS	Sodium silicate
TGA	Thermogravimetric analysis
UCS	Unconfined compressive strength
UF	Urea-formaldehyd
w/c	Water-to-cement ratio
XCT	X-ray computed tomography
XRD	X-ray diffraction

Chapter 1 Introduction

1.1 Research problem and rationale

Cementing is one of the most important and crucial operations performed on oil and gas wells (Nelson, 2006). It delivers zonal isolation, completely sealing off oil and gas from the wellbore, preventing fluid communication between producing zones in the borehole, and blocking the escape of fluids to the surface. The cement barrier plays a key role in well's operational safety. It also provides stability to the formation and protects the casing from corrosion. The importance of effective well sealing in the protection of groundwater has also been highlighted (Jackson et al. 2013).

Despite the rapid and extensive development of well construction technology, well integrity and safety issues are still significant concerns in the oil and gas industry. One of the major causes of catastrophic accidents in oil and gas operations is the failure of well cementing jobs, which leads to severe hazards including fire, explosions, and oil spills on the sea surface or subsea. It also poses great risks to the workers and the environment. The Macondo well blowout in the Gulf of Mexico was one of the worst oil spills, which claimed 11 lives and caused severe injuries, marine and atmospheric pollution, and enormous economic and energy resource losses. It was reported that improper cementing operations may have been one of the major causes of this catastrophic accident (Bea 2011; National Academy of Engineering and National Research Council 2011). Therefore, improvements to well integrity that target existing deficiencies are highly desirable.

The properties of cement-based materials are key factors to cementing performance. Conventional oil well cement systems exhibit unfavourable characteristics that adversely affect their sealing capacity such as their brittle nature, shrinkage, and weak bonding to the casing and formation. A majority of well integrity problems originate from cement shrinkage, deformation, and cracking induced by shrinkage strains and stress concentrations imposed by external restraints (Carey 2010; Shadravan et al. 2014; Jafariesfad et al. 2016). Cement shrinkage can result in increased permeability of the cement sheath and microannulus at the cement/formation and cement/casing interfaces, further leading to gas/oil leakage. The cracks

and flaws in the cement sheath also create pathways for the migration of gas/oil fluids. Downhole pressure and temperature fluctuations will also aggravate the formation and propagation of micro-cracks through the cement sheath. Therefore, to improve well integrity, great importance should be attached to addressing the shrinkage and cracking issues of oil well cement.

Expansive additives have been commonly used for shrinkage reduction in oil well cement. Proper expansion within the limited spaces between the casing and the formation can seal the cement against its boundaries and even deliver some initial pre-stressing which resists a higher level of tensile stress before it cracks. Magnesium oxide (MgO) is one of the expansive additives used in cementitious systems to produce expansion based on the internal pressure exerted upon crystallization of the hydration product brucite ($Mg(OH)_2$). MgO is commonly produced either from magnesite or from seawater/brines. Generally, MgOs produced from magnesite are divided into four categories depending on the calcination temperature: light-burned or reactive (700-1000 ºC), hard-burned (1000-1400 ºC), dead-burned (1400-2000 ºC), and fused (above 2800 ºC) (Jin & Al-Tabbaa 2014). Compared to the magnesite production route, MgOs produced from seawater and brine usually possess higher reactivity. MgO expansive additive has several advantages for application in oil well cement including: (1) good thermal stability of hydration products (up to 332 ºC) (Marbun 2012), suitable for use in high-temperature downhole conditions; (2) lower water demand for hydration (Mo et al. 2014), allowing for use in low moisture downhole conditions; and (3) designable expansion properties by controlling its microstructure and hydration activity through changing the calcining temperature and residence time (Mo et al. 2010; Mo et al. 2012; Lau & Mo 2014). The latter provides the possibility of delivering the desired expansion under different downhole conditions.

The expansion performance of MgO is strongly dependent on its hydration reactivity. Most MgO additives currently used in oil well cement are hard-burned or dead-burned grade with low reactivity, which are suitable for high-temperature borehole conditions (>90 ºC) and the wellbore temperature can be up to 260 ºC in many cases. But under lower temperatures, these low reactivity MgOs cannot generate effective expansion and even cause unsoundness due to

their slow hydration process (Saidin et al. 2008a). By contrast, reactive MgOs with high reactivity hydrate much more rapidly than hard-burned or dead-burned MgOs, producing more effective expansion at a lower temperature. In ordinary Portland cement systems, reactive MgO additives have been explored for their expansion properties as well as shrinkage reduction performance under normal temperature, and they showed effectiveness in compensating for both autogenous shrinkage and drying shrinkage (Li 2010; Mo et al. 2012; Lau 2017). Reactive MgO is therefore deemed to possess great potential for application in oil well cement under low-temperature wellbore conditions. However, the reactivity and hydration properties of reactive grade MgO samples vary significantly depending on their origin and calcination temperatures. There is also very little research into the effect of different reactive MgOs on the expansion performance of oil well cement. Studies into their influence on other essential properties of oil well cement are also lacking.

The conventional solution to the cracking issue is remedial cementing by injecting cement slurry into cracking locations, which is usually untimely and ineffective. Self-healing cementitious materials with a built-in capability to repair micron-sized cracks autonomously show promise for use in oil well cement sheaths. The self-healing properties of the cement can provide a durable cement sheath, long-term zonal isolation, and reliable repair of the cement sheath to preserve well integrity (Schlumberger 2014). Cement itself has some inherent self-healing capability to heal limited-width cracks without the need for an external healing agent. This is referred as autogenous healing. However, the autogenous healing capability is very limited and external interventions are needed to help promote the autogenous healing. Various techniques have been explored to enhance autogenous healing. For example, the use of mineral additives such as crystalline or silica-based additives and expansive agents have been widely investigated for promoting crystallization and sedimentation of healing products in the cracking area (Jaroenratanapirom 2010; Sisomphon et al. 2012; Huang et al. 2014; Qureshi 2016). Superabsorbent polymers (SAP) and nanoclays are reported to be effective internal water reservoirs for supplying adequate water to assist healing (Qian et al. 2010; Van Tittelboom & De Belie 2013). The swelling of SAP, nanoclays or other hydrocarbon swellable polymers can also be used to achieve crack sealing (Lu et al. 2016). However, direct addition of self-healing

agents like mineral additives may render the agents ineffective because they usually start reacting immediately upon addition and may be consumed prior to the occurrence of cement cracking.

The engineered additions of healing agents via specialized delivery systems (vascular networks or discrete capsules) to provide controlled release of healing agents, endow the cementitious system with autonomic self-healing capability. Compared to continuous delivery networks, discrete microcapsules are more suitable for practical use in oil well cement systems. Capsule-based self-healing systems sequester the healing agent in discrete capsules until cracking triggers the rupture and release of the agent at the region of the crack (White et al. 2010). A variety of adhesive or mineral-based healing agents have been encapsulated for use in self-healing cementitious materials. The mineral-based sodium silicate has received increasing attention due to its good compatibility with the cementitious matrix. The self-healing effectiveness of encapsulated sodium silicate agents in terms of strength recovery and durability recovery has been reported in cementitious materials (Pelletier et al. 2010; Huang & Ye 2011a; Gilford III et al. 2014; Mostavi et al. 2015; Giannaros et al. 2016). However, current research into microcapsule-based self-healing cement systems has mainly focused on their application under ambient conditions. Their use under extreme environments such as underground wellbores is rarely reported. The stability of microcapsules (both the shell and core materials) when exposed to challenging high temperature downhole conditions is a major concern for their application in oil well cement systems. Their self-healing performance as well as influence on oil well cement properties also needs comprehensive investigation.

Both reactive MgO expansive additives and self-healing microcapsules can be considered respectively as prospective solutions to the current problems of shrinkage and micro-cracks in oil and gas well cement. In this work, three oil well cement systems were investigated: an expansive system with reactive MgO, a self-healing system with sodium silicate microcapsules, and a combined system with both types of additive. In the expansive system, three types of reactive MgO with different reactivity values, produced from seawater or calcination of magnesia, were investigated in terms of their expansion characteristics and shrinkage reduction performance in oil well cement as well as their influences on other properties of oil well cement.

Meanwhile, for the self-healing system, two groups of microcapsules consisting of polyurea shell and sodium silicate healing agent manufactured by industrial partners were used. The suitability of the microcapsules for use in oil well cement under elevated temperature was examined by testing their thermal stability, resistance to alkalinity and survivability during mixing. The effects of microcapsule addition on self-healing efficiency as well as other properties of oil well cement were investigated. Based on investigations of the two individual systems above, a hybrid system that combines the reactive MgO and sodium silicate microcapsules was proposed. The combined use of expansive and self-healing additives was expected to further enhance the structural integrity and resilience of oil well cement sheath.

1.2 Research objectives

This research project focuses on investigating the use of reactive MgOs and sodium silicate microcapsules in oil well cement to deliver expansion properties and self-healing properties respectively under elevated temperatures up to 80 ℃. The temperature and pressure in oil/gas wells increases with well depth. Typically, the well temperature increases by about 3 ℃ per 100 m depth and the pressure increases by about 10 bar per 100 m depth. High temperature is the main wellbore condition factor investigated in this research. The temperature from 50 ℃ to 120 ℃ covers 90% of the oil/gas wells and 80 ℃ is chosen as the target temperature in this research. Although wellbore pressure also increases, the high-pressure condition was not investigated in this research. The overall performance of a hybrid oil well cement combining both expansive and self-healing additives is also the interest of this study. The objectives for each oil well cement system are as follows:

1. The expansive oil well cement system

   1) Characterise the reactivity of three types of reactive MgO and investigate their expansion characteristics in oil well cement. Different variables including MgO reactivity and addition contents, temperature, and restrained conditions were investigated.

   2) Investigate the performance of reactive MgOs in the shrinkage reduction of oil well cement under sealed or drying conditions at 80 ℃.

3) Evaluate the effects of three reactive MgOs on oil well cement properties including rheology, cement hydration rate, and mechanical strength.

2. The self-healing oil well cement system

1) Characterise the two groups of polyurea/sodium silicate microcapsules, including their morphology, particle size distribution, shell thickness, thermal stability, resistance to alkalinity, and survivability during mixing, and verify their suitability for use in oil well cement at the elevated temperature of 80 ºC.

2) Investigate the self-healing efficiency of oil well cement containing different groups of microcapsules under the curing temperature of 80 ºC.

3) Evaluate the effects of microcapsule addition on oil well cement properties including rheology, cement hydration rate, and mechanical strength.

3. The combined oil well cement system

Suitable reactive MgO and microcapsules will be selected from the above two individual systems. The effects of the mixed addition of reactive MgO and microcapsules on the expansion, self-healing, and other properties of oil well cement will be all examined to assess the compatibility of the two types of additives in the combined system.

1.3 Structure of the thesis

This thesis is formatted into six chapters. **Chapter 1** illustrates the background of the research problem, the prospective solution, and the aims and objectives of the current PhD research work. **Chapter 2** presents an in-depth overview of well cementing and the typical problem of gas migration induced by shrinkage and cracking in the cement sheath. MgO as an expansive additive is discussed in terms of its expansion properties and potential application for shrinkage reduction in oil well cement. Meanwhile, autonomic self-healing techniques for cementitious material are reviewed. The self-healing mechanisms and self-healing performances of different delivery systems (mainly microcapsule-based) and healing agents are evaluated based on their suitability for addressing cracking problems in oil well cement system. **Chapter 3** gives a detailed description of the materials, sample preparation and experimental methods and

procedures. **Chapter 4** is dedicated to the expansive system and presents the results on the expansion properties of three different types of reactive MgOs and their shrinkage reduction performance in oil well cement pastes. Analysis on the effects of reactive MgOs on cement properties such as rheology, cement hydration rate and mechanical strength is also carried out. **Chapter 5** reports the results from the self-healing system including the characterisation of two different groups of sodium silicate microcapsules and their effects on self-healing efficiency and various properties of oil well cement. In the final part of this Chapter, suitable reactive MgO and sodium silicate microcapsules are selected for combined addition in oil well cement following the results from the two individual systems. The compatibility of the two additives and the overall performance of their joint use in the combined system are assessed. Finally, in **Chapter 6**, conclusions are drawn from the whole research work on utilising reactive MgO and self-healing microcapsules to improve well integrity, based on which recommendations for future research were provided.

Chapter 2 Literature review

This chapter presents a critical literature review of topics relevant to the research work presented in this thesis. It starts with introducing well cementing operations and outlining the shrinkage and cracking problems of oil well cement sheaths that severely undermine the well integrity. The details of oil well cements and their properties are also presented. Expansive additives and self-healing materials are presented as potential approaches to improving the well integrity, and the following sections present extensive reviews of these two fields. The former targets the shrinkage problem, while the latter focuses on repairing the cracks. The review of expansive additives focuses on magnesium oxide (MgO) and its application for shrinkage reduction in cementitious materials. Autogenous and autonomic self-healing research in the literature are both reviewed in the context of self-healing techniques in cementitious materials. In particular, autonomic self-healing cementitious materials using microcapsule-based delivery systems are thoroughly discussed. The different shell materials and healing agents used in microcapsules are reported in terms of their self-healing performance and effects on other cement properties. To conclude, this chapter summarises the research problems and current research gaps in the literature which motivate this research project.

2.1   Well Cementing

2.1.1   Well cementing process

Well cementing is one of the most critical steps in the construction of oil/gas wells. In essence, oil/gas well construction involves drilling a borehole, inserting a series of casings or liners, and fixing them in place using cement (Nelson, 2006). Well cementing is the phase responsible for introducing cement to the annular space between the wellbore and casing, or between two successive casing strings. In a typical wellbore as shown in Figure 2.1a, the oil well cement (OWC) slurries need to be pumped to a depth of several thousand metres underground. The cement slurries are subjected to a high-temperature and high-pressure downhole environment. As mentioned in Section 1.2, the temperature and pressure in oil/gas wells increases with well depth. A typical oil/gas well can be thousands of metres (from 1000 to 5000 m). Therefore, the cement slurry can be subjected to high temperatures up to 150 ℃ and high pressures up to

500 bar. These extreme conditions make well cementing operations more challenging than common cementing work above ground. Cementing jobs have always been given great importance by the oil industry, since good cementing is an important guarantee for the subsequent phases from operation and production to abandonment.

Well cementing mainly consists of two principal operations: primary cementing and remedial cementing, as illustrated in Figure 2.1b. Primary cementing is the process of pumping down the cement slurry to form the cement sheath and then hydraulically sealing the annulus between the casing and the formation, while remedial cementing occurs after primary cementing, and it refers to the operation phase of injecting cements into well locations for the purposes of well repair or well abandonment. The main purpose of the well cement sheath is to provide zonal isolation, preventing fluids (oil, gas) flowing between different subsurface zones as well as pressurized formation fluids outside the casing from entering the well. It also mechanically stabilises the formation and keeps the casing in place, protects the casing from corrosion, which are key to safe production of hydrocarbons and preventing contamination (Jackson et al. 2013; Lavrov & Torsaeter 2016).

A typical primary cementing process is shown in Figure 2.2. Primary cementing operations first involve conditioning the borehole after proper placement of the casing string. Chemical washes and spacer fluids are pumped down to displace drilling fluids. In the next step, a bottom plug is inserted, followed by a volume of cement slurry that is sufficient to fill the annulus. Continued pumping of cement slurry forces the drilling fluid out of the casing interior, up the annulus, and eventually out of the wellbore. When the bottom plug lands at the bottom of the casing string, a membrane in the plug ruptures, opening a pathway for the cement slurry to enter the annulus. A top plug is placed after the addition of the cement slurry is complete, and a displacement fluid is pumped in to force the top plug downward until it lands on the bottom plug, thereby isolating the casing interior and annulus and filling the annulus with cement slurry (Nelson 2012). The cement sheath formed within the annulus is responsible for mechanically stabilising the wellbore, providing zonal isolation and preventing the communication of pressurised formation fluids between different subsurface zones. This cement barrier also protects the steel casing against corrosion by formation fluids.

The remedial cementing process requires as much technical, engineering, and operational experience as primary cementing. Squeeze cementing and plug cementing are the two main remedial cementing techniques used to repair flaws in primary cement or damage incurred by corrosive fluids (Nelson, 2006).

(a)   (b)
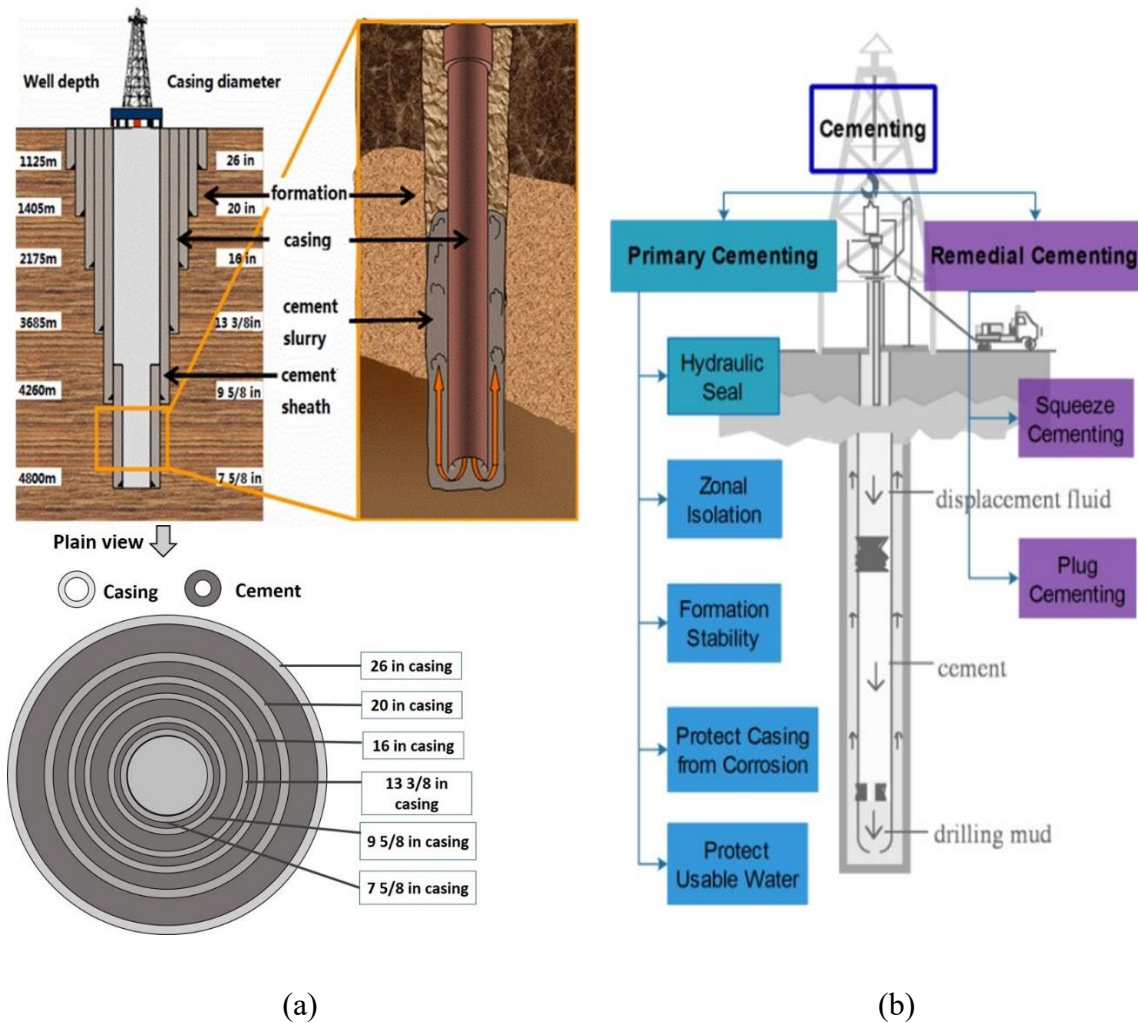
Figure 2.1 Typical wellbore cementing processes: (a) a schematic of a typical cemented well, adapted from (Plank 2018); and (b) principal operations of well cementing and their main objectives, adapted from (Mangadlao et al. 2015).
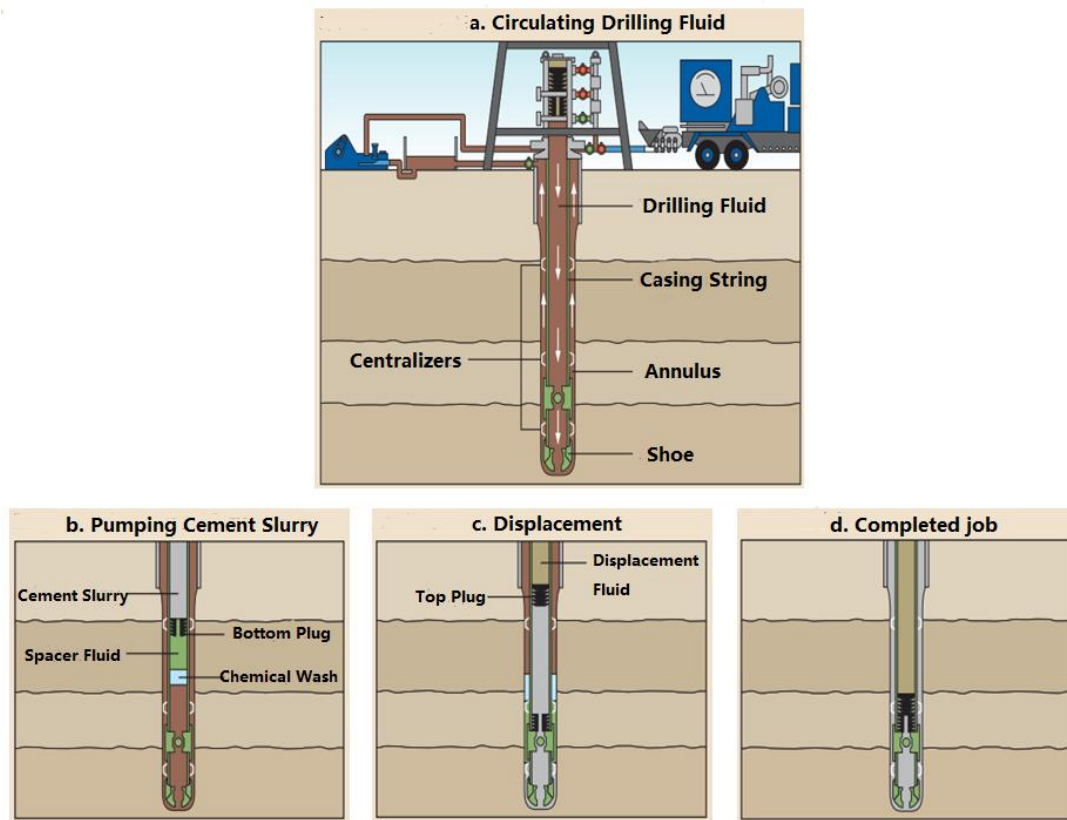
Figure 2.2 Illustration of primary cementing procedure (Nelson 2012).

2.1.2   Well integrity

Maintaining well integrity during all well operations has long been a major concern in the oil and gas industry. The life cycle of a well stretches from the initial drilling and construction phase, through its operational phase, and ends with the final abandonment phase. For a well to be operated and produced safely and effectively, it is extremely important to maintain well integrity throughout its life cycle. Technically, "well integrity" refers to the zonal isolation of liquids and gases from the target formation or from intermediate layers through which the well passes. In a practical sense, it means that a well doesn't leak (Jackson 2014). The severe consequences of well integrity loss, such as leakages and blowouts, can cause loss of production, costly repairs, environmental damage, and, in the rarest of cases, can cost lives, as in the Deepwater Horizon disaster in the Gulf of Mexico in 2010. Carey (2010) classified typical causes of wellbore integrity issues which occur during pre-production (mainly drilling)

and production stages, as shown in Table 2.1. Well integrity problems are mostly associated with improper well cementing and/or cement sheath stability problems.

Table 2.1 Main causes for well integrity issues (Carey 2010).

Pre-Production Stage	Production Stage
• Formation damage during drilling (caving) • Casing decentralization (incomplete cementing) • Inadequate drilling mud removal • Inadequate cement placement (pockets) • Inadequate formation–cement/cement-casing bond • Cement shrinkage • Excessive fluid loss (Filtration into permeable formation) • Contamination of cement slurry by mud or formation fluids	• Microannulus at casing-cement interface • Disruption of formation cement bond • Cracking formation within cement sheath • Degradation of cement • Corrosion of casing

From a cementing perspective, the factors contributing to the loss of zonal isolation can be categorized into: immediate migration (during cement placement), short-term migration (before setting of cement) and long-term migration (after setting of cement) according to when a path for fluid (gas/oil) migration is created (Nelson 2006; Jafariesfad et al. 2016), as illustrated in Figure 2.3.
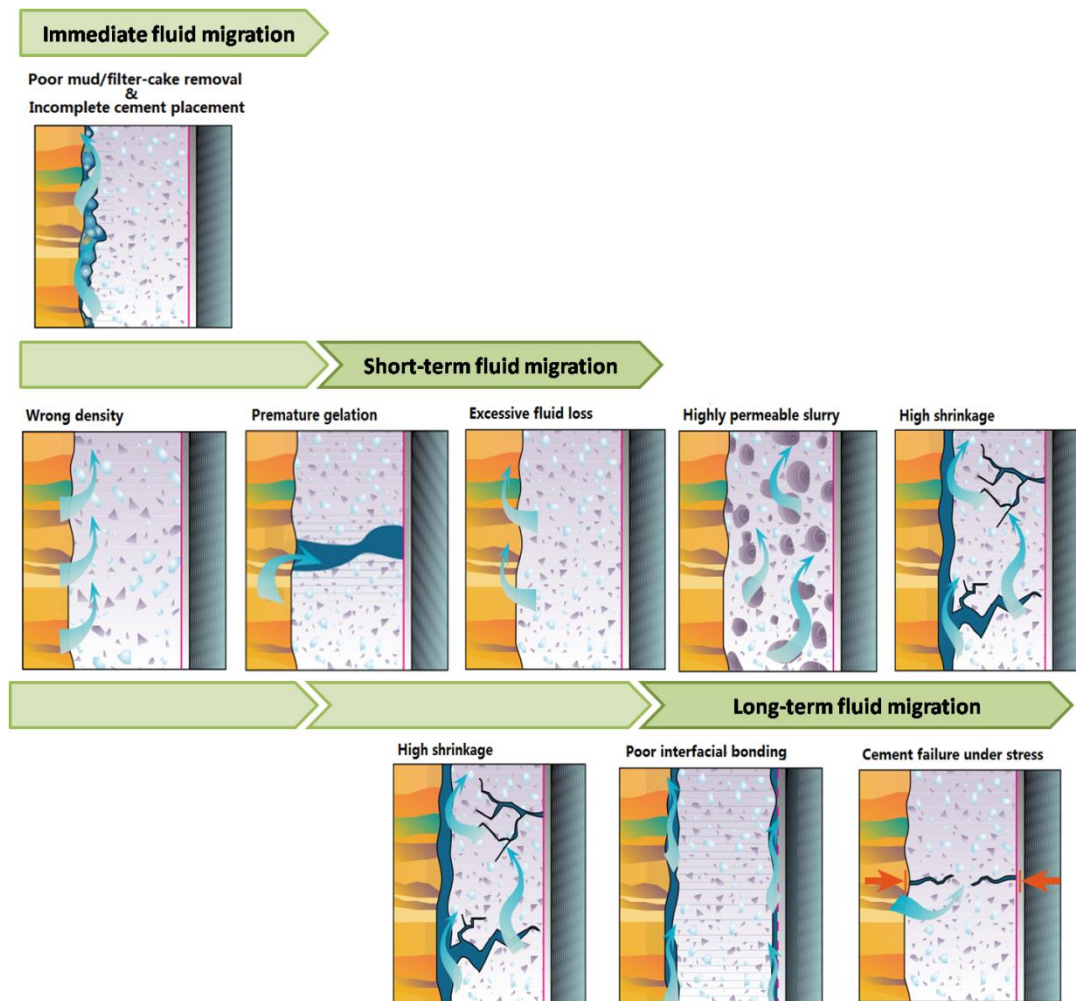
Figure 2.3 Influencing factors for fluid migration occurring at different stages during the cementing process, adapted from (Bonett & Pafitis 1996).

Immediate fluid migration occurs from the start of the cementing job to the end of cement placement. Poor mud and filter-cake removal can leave a route for fluid to flow up the annulus. Incomplete cement placement will also cause pockets in the annulus between the casing and the formation. To eliminate fluid migration during this phase, it is essential to ensure adequate drilling mud removal as well as to preserve the flowability of the slurry by controlling the thickening time and viscosity during placement.

Short-term fluid migration occurs during the cement setting process after cement placement. As cement gels, it loses the ability to transmit hydrostatic pressure. During this period, fluids (water and/or gas) can invade the cement and form channels. Cement properties influencing

zonal isolation in this period include wrong cement density, fluid loss (filtration), free fluid development (bleeding), gel strength development, chemical shrinkage, and permeability, as shown in Figure 2.3. Incorrect cement densities can cause hydrostatic imbalance which is the driving force behind fluid flow. Premature gelation can also lead to loss of hydrostatic pressure control. Excessive fluid loss (bleeding and filtration) contributes to the development of available space in the cement slurry column for fluid flow. Highly permeable slurries result in poor zonal isolation and offer little resistance to fluid flow.

The short-term properties of cement slurry are usually the main focus for oil industries, and many technological efforts have been made by engineers to optimise the short-term properties of cement slurries. However, even when the cement slurry is placed properly and its short-term properties provide adequate zonal isolation, the long-term zonal isolation can be compromised.

Long-term fluid migration can occur at any time during the long lifetime of the well after the cement slurry sets. After the slurry sets, changes in pressure and temperature, which occur during expansion and contraction of the casing and cement sheath, can cause the cement to debond from the casing or the formation. Portland cement is a brittle material and susceptible to cracking when exposed to thermal and stress induced tensile loads (Bourgoyne et al. 1999). The potential failure modes of long-term migration can be classified into three groups: formation-cement debonding (outer microannulus). cement-casing (inner microannulus) and failure of the cement sheath itself, as characterised in Figure 2.4 (J. Liu 2012; Shadravan et al. 2014).

- Formation-cement debonding. The cement sheath could debond at the formation-cement interface due to bulk shrinkage of cement, differences in stiffness between the formation and cement sheath, or temperature and pressure changes inside the casing. Incomplete mud removal at the rock-cement interface could also lead to the formation of microannulus.
- Cement-casing debonding. The cement sheath could debond at the cement-casing interface due to differences in stiffness, where drilling mud could also exist due to incomplete mud displacement. With changes of temperature and pressure in the casing,

the casing diameter reduces or expands, thus a microannulus is formed, which could lead to vertical migration of fluids.

- Failure of the cement sheath. The cement sheath could crack due to bulk shrinkage and temperature and pressure fluctuations in the casing causing tensile failure, which is the most dominant failure mode. Cyclic loads, formation pressure and formation subsidence and movement can also lead to shear failure of the cement sheath. Additionally, cement degradation over time also contributes to cement sheath failure.
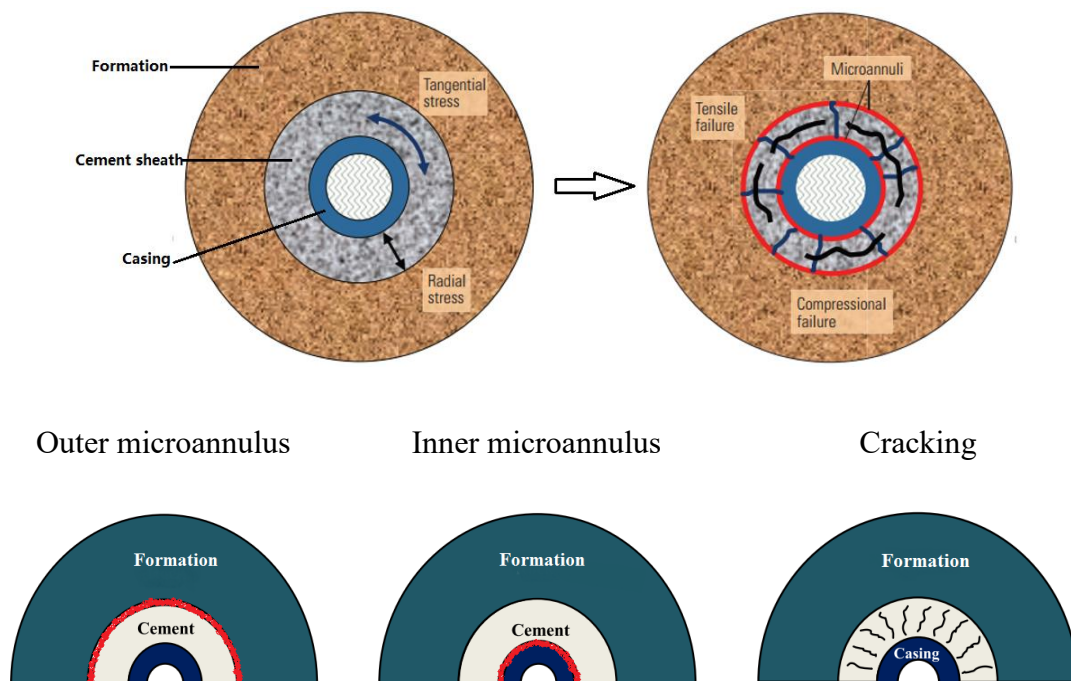
Figure 2.4 The basic failure modes of long-term migration, adapted from (J. Liu 2012; Shadravan et al. 2014).

Improper cementing operation and defective cement sheath properties are apparently principal factors that compromise well integrity. The average life time of an oil and gas well is normally about 20 to 30 years. To ensure long-term zonal isolation throughout the long life of the well, the primary concern is that the cement system meets both required short-term and long-term properties. In addition to optimal cement system performance, long-term zonal isolation also requires that the drilling and cement placement procedures are done ideally, with proper casing

centralization, adequate mud removal, complete cement placement, adequate cement-formation/cement-casing bonds, and no cement slurry contamination.

2.1.3 Oil well cement properties

As previously mentioned, the well integrity of an oil/gas well is significantly affected by the quality of the cement system between the casing and the rock formation. The performance of the cement system depends on its short-term and long-term properties. Short-term concerns regarding the properties of oil well cement in the slurry/paste state include density, rheology, and thickening time, while the long-term concerns refer primarily to the mechanical properties of the hardened cement sheath such as strength, bulk shrinkage, bonding, and its resistance to downhole chemical attack. Thorough evaluation of the properties that affect the short-term and long-term performance of the cement sheath is crucial for designing a cement system that is able to provide sustained zonal isolation and withstand high downhole temperature and pressure differentials (Wilcox et al. 2016).

2.1.3.1   Oil well cements and additives

Most cements used in the oil and gas industry are one type of Portland cement (PC), produced from grinding clinker or blended hydraulic cements. Oil well cements (OWCs) are usually exposed to conditions underground which significantly differ from the ambient surface conditions associated with buildings, roads and bridges. For example, OWCs must perform over a wide temperature range from below freezing in permafrost zones to temperatures as high as $400^{\circ}C$ in geothermal wells (Nelson 2012). Compared to regular Portland cement, OWCs usually have lower C_3A content, are coarsely ground, and may contain friction-reducing additives and special retarders such as starch, sugars, etc., in addition to or in place of gypsum (Shahriar 2011). According to the API specifications for Materials and Testing for Well Cements (API Specification 10A 2010), there are eight classes of OWCs, designated A through H. For each class, OWCs are available on several grades based on their C_3A (Tricalcium Aluminate) content: Ordinary (O), Moderate Sulphate Resistant (MSR), and High Sulphate Resistant (HSR). Each class is applicable for a certain range of well depth, temperature, pressure and sulphate environments.

Table 2.2 Classes of oil well cement (OWC) and their main characteristics and requirements on strength (API Specification 10A 2010; Shahriar 2011).

Class	Available Grade	Range of Depth (m)	Key Characteristics	Requirement on compressive strength[##], @8-hour curing time
A	O[*]	0 – 1830	For use when special properties are not required	1.7 MPa curing at 38 ºC
B	MSR[**], HSR[***]	0 – 1830	Lower C_3A content than Class A, for use when conditions require moderate or high sulphate-resistance	1.4 MPa curing at 38 ºC
C	O[*], MSR[**], HSR[***]	0 – 1830	Relatively high C_3S content and surface area, for use when conditions require high early strength	2.1 MPa curing at 38 ºC
D	MSR[**], HSR[***]	1830 – 3050	Retarded cement[#] for use under conditions of moderately high temperature and pressure	–
E	MSR[**], HSR[***]	3050 – 4270	Retarded cement[#] for use under conditions of high temperature and pressure	–
F	MSR[**], HSR[***]	3050 – 4880	Retarded cement[#] for use under conditions of extremely high temperature and pressure	–
G	MSR[**], HSR[***]	0 – 2440	Basic well cement, can be used with accelerators and retarders to cover a wider range of well depths and temperatures	2.1 MPa curing at 38 ºC 10.3 MPa curing at 60 ºC
H	MSR[**], HSR[***]	0 – 2440	Basic well cement, can be used with accelerators and retarders to cover a wider range of well depths and temperatures; coarser surface area than that of Class G	2.1 MPa curing at 38 ºC 10.3 MPa curing at 60 ºC

O[*]: Ordinary; MSR[**]: Moderate Sulphate Resistant; HSR[***]: High Sulphate Resistant; Retarded cement[#]: retardation is achieved by reducing C_3S and C_3A and increasing the particle size of the cement grains; Compressive strength[##] is tested under atmospheric pressure.

The main class characteristics of OWCs and their suitable conditions of use are summarised in

Table 2.2. The requirements for OWCs are also shown in Table 2.2. API Classes G and H are

currently the most commonly used oil well cements. These two classes of OWC have similar chemical compositions but differ in their surface area. Class H is coarser than Class G cement and thus has a lower water requirement.

Various types of additives are used to adjust the performance of OWCs to accommodate a particular well environment. The principal objective is to formulate a cement that is pumpable for a time sufficient for placement in the annulus, develops strength within a few hours after placement, and remains durable throughout the lifetime of the well (Nelson 2012). Typically, additives for OWCs can be classified into eight groups according to the functions they perform including accelerators, retarders, extenders, weighting agents, fluid loss control agents, lost circulation control agents, and dispersants, as well as other special additives such as expansive additives, antifoam agents, and fibrous additives (Nelson 2012; Broni-bediako et al. 2016).

2.1.3.2   Properties of fresh cement slurries

The properties of fresh cement slurry are crucial for a primary cementing job, since they control the pumpability of the cement slurry and determine how cement displaces other fluids as it is placed in the annulus between the casing and formation. Rheology is concerned with the flow and deformation of materials in response to applied stresses. It not only determines the flow of cement slurry but also directly affects the quality of the hardened cementitious matrix. The rheology of cement slurry is usually characterized by rheological parameters such as yield stress, plastic viscosity, and apparent viscosity. Cement slurries are non-Newtonian fluids, which means that their rheological properties are dependent on the applied shear rate and the time over which the shear rate is applied. The Bingham plastic model is the simplest model used to characterise the behaviour of non-Newtonian fluids. The Bingham model, as shown in Equation 2.1, stipulates that the shear stress is a linear function of the shear rate when the shear stress is above the yield stress (Figure 2.5) (Lavrov & Torsaeter 2016).

$$\tau = \tau_Y + \mu_{pl}|\dot{\gamma}| \qquad\qquad \text{Equation 2.1}$$

where τ is the shear stress (Pa), and $\dot{\gamma}$ is the shear rate (s^{-1}), τ_Y is the yield stress (Pa), μ_{pl}.is the plastic viscosity (Pa s).
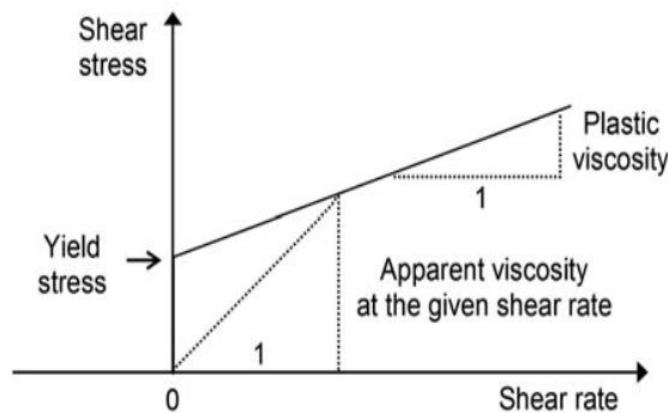
Figure 2.5 Shear stress-shear rate relationship in the Bingham plastic model (Lavrov & Torsaeter 2016).

The yield stress indicates the minimum effort needed for the cement slurries to start flowing, which means that cement slurries behave like a solid below the yield stress. In the Bingham model as shown in Figure 2.5, the yield stress τ_Y is the value of shear stress τ when the shear rate $\dot{\gamma} = 0$. For a non-Newtonian cement slurry, the yield stress usually increases over time if the slurry is at rest. The gel strength is then defined as the minimum shear stress required to shear the cement slurry after a given period of rest. Viscosity is defined as the ratio of the shear stress to the shear rate. The apparent viscosity is the slope of the straight line connecting the origin and any point on the shear stress-shear strain rate flow curve. In other words, it is the viscosity at a particular shear rate. In the Bingham model where the flow curve is fitted to a straight line, the slope represents the plastic viscosity μ_{pl}. Oil well cement slurries typically have yield stress of the order of 1–100 Pa, while their plastic viscosity is of the order of 0.01– 0.1 Pa s. Rheological properties should be taken into consideration during cement design and be adjusted according to the conditions of specific wells. In addition to the rheological properties mentioned above, thickening time, density, and free fluid are also important properties of cement slurry. Typical requirements for the properties of the commonly used class G and H cement slurries can be referred to API Specification 10A (2010).

2.1.3.3   Hydration of oil well cement

The hydration of OWCs is a function of various conditions such as the chemical composition of the cement, curing temperatures and pressures, addition of additives, and stirring conditions, etc.

At ambient conditions, the hydration of OWCs (typically Class G or Class H) is similar to ordinary Portland cement (OPC). The main constituents of OWCs (Class G or Class H) are tricalcium silicate (Ca_3SiO_5, or C_3S), dicalcium silicate (Ca_2SO_4, or C_2S), calcium aluminoferrite ($Ca_2(Fe,Al)_2O_5$, or C_4AF), and a small quantity of gypsum ($CaSO_4 \cdot 2H_2O$). The main hydration process is the conversion of the silicate phases to an amorphous calcium silicate referred to as C-S-H, and portlandite $Ca(OH)_2$. However, OWCs are subjected to a wide range of temperatures and pressures in situ, which strongly influences their hydration processes. Pang et al. (2013) used isothermal calorimetry to study the effect of temperatures and pressures on the hydration of Class H cement. As the temperature is raised, the rate of heat flow increases significantly during the acceleration period while the duration of the acceleration period decreases (Figure 2.6), which demonstrates the acceleration of cement hydration at high temperatures. They also found that increased pressure has a similar effect on cement hydration, but its effect is much less significant than that of temperature.

At sufficiently high temperatures (usually above $40\,^{\circ}C$), certain changes occur in the microstructure and morphology of the hydration products. C-S-H gel will become more fibrous and individualized, and a higher degree of silicate polymerisation is observed. Previous studies have reported that when the temperature exceeds $110\,^{\circ}C$, the C-S-H gel is transformed into highly crystalline and much denser calcium silicate hydrates, α–dicalcium silicate hydrate (α-C_2SH), and then into jaffeite ($C_6S_2H_3$) at even higher temperatures. Meanwhile, the formation of ettringite is also affected at elevated temperatures. Ettringite is reported to be unstable above $70\,^{\circ}C$ (Bentz 2009; Nelson 2006). As the temperature increases, the initially formed ettringite decomposes to calcium monosulfate and ultimately converts to a more stable crystalline hydrogarnet (C_3AH_6) (Jupe et al. 2005).
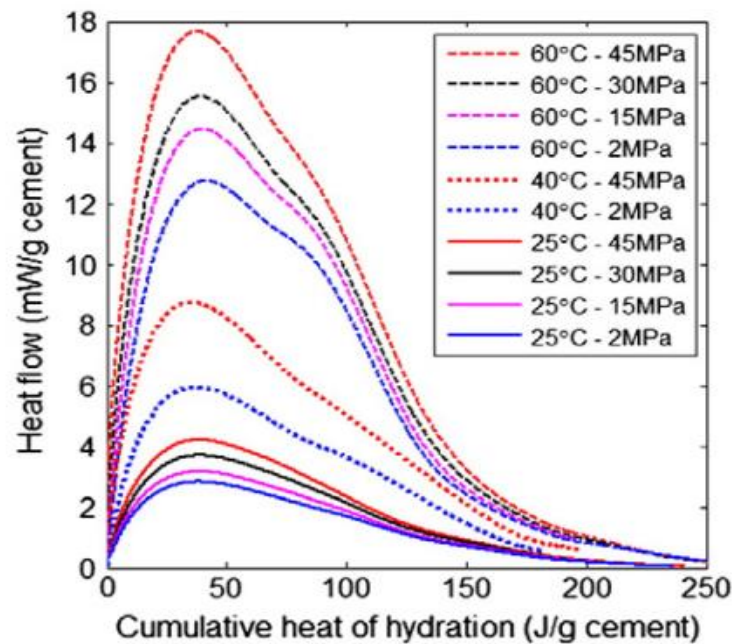
Figure 2.6 Effect of temperature and pressure on the hydration of Class H cement (Pang et al. 2013).

2.1.3.4 Properties of hardened cement pastes

The properties of hardened cement significantly affect its sealing capacity, and a thorough understanding of those properties is crucial for maintaining well integrity.

The mechanical properties of hardened oil well cement are important for casing bonding support and zonal isolation. Compressive strength and other mechanical properties such as tensile strength, flexural strength, and elastic properties, are very important in the design to ensure an effective and durable well integrity. The mechanical properties depend on the chemical composition, admixtures, and curing regime. The downhole temperature is a key factor for strength development of OWCs as it dramatically affects the kinetics and mechanism of the hydration process, and the nature of the hydrated products, as mentioned above. Under high temperatures, the cement may undergo strength retrogression, depletion of microstructure, and degradation of the pore structure. Reduction in durability, increase in drying shrinkage and structural cracking are further consequences. To mitigate the strength loss and other influences caused by thermal conditions on mechanical properties, the addition of various types of admixtures has been investigated. Studies showed that the addition of silica flour (30–40% by

weight of cement) can effectively prevent the cement strength retrogression and improve stability of the cement under hydrothermal conditions., leading to improved compressive strength, refined pore structure and reduced permeability (Souza et al. 2012; Fathaddin & Condition 2005). Fibrous materials such as glass fibres and nylon fibres are added to OWCs (0.15–0.5% by weight of cement) to increase the tensile strength, flexural strength, and toughness of the cement matrix (Nelson 2006).

Apart from the compressive strength, the bonding properties at the cement-formation and cement-casing interfaces have also been highlighted since flow paths (microannulus, radius cracks) situated at the interfaces could lead to failures of zonal isolation. The bonding of cement to the casing and to the formation is normally reported as the shear bond or hydraulic bond strength (Radonjic & Oyibo 2014). The force required to initiate movement of the casing in the cement sheath or the movement of the cement from the formation is defined as the shear bond strength. The hydraulic bond strength is the bond between the casing and the cement, or the cement and the formation, that prevents fluids flow. Proper cementing operations including drilling mud removal and cement placement are essential to ensure good interfacial bonding. Moreover, a cement system with high elasticity and low shrinkage is desired. The bonding strength of the cement sheath can be improved by the addition of expansive agents such as Calcium oxide (CaO) and Magnesium oxide (MgO), which will be discussed in detail in Section 2.2.

As mentioned in Section 2.1.2, cement shrinkage is considered to be one of the major causes of well integrity problems. Given the detrimental effects of shrinkage, solutions to shrinkage reduction have become of great interest to the oil industry. This has led to the development of a series of products such as expanding cements in which various additives counteract shrinkage. This is achieved either by chemical interaction with cement constituents so as to produce expansion during hydration, or by adding gaseous or mechanical energizing materials that expand themselves and thereby compensate for shrinkage (Goboncan et al. 2003). In the following section, the main types of shrinkage and their mechanisms, the shrinkage of OWCs, and shrinkage control strategies will be systematically discussed.

2.1.4 Shrinkage of oil well cements

2.1.4.1   Overview of cement shrinkage types

Typically, shrinkage of Portland cement can be classified into autogenous, drying, and carbonation shrinkage as well as thermal deformation. Cement shrinkage can take place in two distinct stages: early age and later age, as shown in Figure 2.7 (Holt 2001). Early age is broadly defined as the first 24 hours during which the cement slurry is setting and developing strength. Autogenous and drying shrinkages and thermal deformation may occur during the early age, while long-term shrinkage comprises the same shrinkage components and thermal deformation as well as carbonation shrinkage.
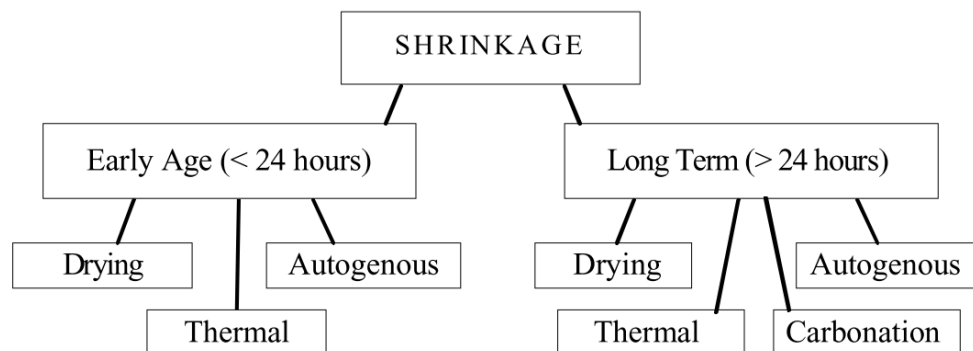
Figure 2.7 Typical shrinkage types in cement (Holt 2001).

Autogenous shrinkage of cement paste is defined as the macroscopic volume change occurring in the absence of moisture exchange conditions, as a result of chemical shrinkage. Hydraulic cements undergo hydration reactions in the presence of water, and the volume of the products formed is less than the volume occupied by the reactants (water and cement) (Mehta & Monteiro 2006). This volume reduction is referred to as chemical shrinkage, or total shrinkage. Chemical shrinkage occurs as soon as the cement reacts with water, and reaches a maximum when the cement is completely hydrated. Chemical shrinkage is one of the main driving forces behind autogenous shrinkage. Autogenous shrinkage occurs over three different phases after cement mixing:

(1) Liquid phase. Autogenous shrinkage of the liquid phase is equivalent to chemical shrinkage. As long as the cement paste is fluid, the chemical shrinkage may be totally converted into an external volume change.

(2) Skeleton formation stage. This is a transition stage during which the cement starts setting and a self-supportive skeleton is gradually formed. Chemical shrinkage beyond the setting time results in the creation of empty pores and menisci in cement paste. Since the skeleton is formed to resist chemical shrinkage, capillary forces will develop due to the localized drying of the internal pores, referred to as self-desiccation, and thus causes autogenous shrinkage. The contribution of chemical shrinkage to autogenous shrinkage decreases while self-desiccation becomes more dominant.

(3) Hardened stage. After the cement has hardened at later stages, any further autogenous shrinkage is mostly due to self-desiccation.

Drying shrinkage refers to the volume reduction resulting from the loss of excess water from the internal pores through evaporation at the surface of the cement (Holt 2001). The differential relative humidity between the cement and the environment is the driving force behind drying shrinkage, and thus water evaporation from the interior cement mass results in shrinkage (Mehta & Monteiro 2006).

Thermal deformation occurs when the cement undergoes temperature fluctuations caused by cement hydration and/or the surrounding environment. In the early age, the cement temperature is changing due to cement hydration. In the later age, thermal deformation is typically a result of temperature fluctuations in the surrounding environment (Holt 2001). For example, the temperature differences between the cement and the casing or between the cement and the formation can induce thermal deformation and corresponding stresses in the cement sheath, and can further result in radial cracks or debonding at the cement-casing and cement-formation interfaces (Lavrov& Torsaeter, 2016).

Carbonation shrinkage occurs when the hardened cement reacts with moisture and carbon dioxide (CO_2) in the air, resulting in a slight volume reduction. Carbonation is generally

considered to be a durability issue which can cause chemical degradation of the cement due to the relatively acidic environments created by CO_2 (Mehta & Monteiro 2006).

2.1.4.2   Shrinkage in oil well cements

There are two ways that shrinkage of oil well cements can be divided into two parts: internal shrinkage and external shrinkage (K.R.Backe 1997). Internal shrinkage is caused by the formation of contraction pores in the cement paste, which is mainly attributed to chemical shrinkage after cement setting. Contraction pores may contribute to the connectivity between pores in a set cement and hence to increased permeability for gas/liquid flow. External shrinkage is the bulk or external dimensional volume change of the cement slurry, which may lead to microannulus between the cement and formation/casing, and/or tensile cracks. Autogenous shrinkage, caused by chemical shrinkage during the liquid stage and self-desiccation after hardening at later stages, is an important component of external shrinkage. Other types of shrinkage, including drying shrinkage, carbonation, and thermal deformation may also contribute to the external volume reduction depending on the wellbore environment.

The shrinkage of oil well cements has been investigated by several researchers, which have mainly focused on the total chemical shrinkage and autogenous shrinkage at the early age. Justnes et.al. (1995) used the traditional dilatometry method to measure the total chemical shrinkage of Class G cement slurries for the first 48h of curing at 20 $^{\circ}$C and atmospheric pressure. The dilatometry test follows Le Chatelier's principle where an Erlenmeyer flask containing a diluted cement paste sample is connected to a pipette from which the dropping water level that is equal to chemical shrinkage was monitored (Figure 2.8) (Holt 2001). As shown in Figure 2.8b, the chemical shrinkage of the cement pastes with w/c of 0.3 was measured as 2.2ml/100g cement (2.6 vol.%), and the chemical shrinkage measured at w/c=0.4 and w/c=0.5 were almost identical to the value measured at w/c=0.3.The authors also measured autogenous shrinkage using the membrane method based on the Archimedes principle that a water-submerged sample will register a volume reduction by a weight increase. This method seals a cement sample in a thin latex membrane and then takes the mass over time when the sample is continuously submerged in water (Figure 2.9a). The results showed 1.05, 1.47 and 2.2 ml/100 g cement (1.2, 1.68, 2.5 vol.%) for w/c = 0.3, 0.4 and 0.5, respectively, at 48h under

the same curing conditions (Figure 2.9b). By comparing the developing trends of these two types of shrinkages, the authors observed that autogenous shrinkage is roughly equivalent to the total chemical shrinkage in the first few hours before setting, but deviates from the total chemical shrinkage after setting and gradually reaches a plateau.

The external volumetric reduction caused by autogenous shrinkage occuring after intitial set, which could be responsible for microannlus or debonding defect as discussed above, is generally less than 1% (usually a few tenth of 1%) (Gotsis et al.1984; Nelson, 2006). For example, for cement placed across 26 in. to 20 in. casing in a wellbore as shown in Figure 2.1, a homogeneous volumertic bulk shrinkage of 1% would result in a retraction of around 1.35 mm. For smaller annualr space across 9 $^5/_8$ in to 7 $^5/_8$ in, a retraction of 0.46 mm can be induced by 1% volumertic bulk shrinkage. The resulting volumetric shrinkage can induce microannulus at the cement/casing interfaces for gas/oil migragation.

Since OWC is subjected to hostile downhole conditions, the elevated temperature and pressure will have a prominent impact on its shrinkage performance. Pang et al. (2015) developed a specialized steel pressure cell to monitor the in situ chemical shrinkage of oil well cement under simulated high temperature and pressure wellbore conditions. The test results (Figure 2.10a,b) suggested that the evolution of chemical shrinkage was significantly accelerated at elevated temperatures. Increasing the temperature can speed up the cement hydration process and hence the chemical shrinkage. By contrast, the effect of increasing pressure on chemical shrinkage is much less significant. At a constant temperature, the chemical shrinkage rate appears to increase only slightly with increasing curing pressure during the early age (Figure 2.10a,c).
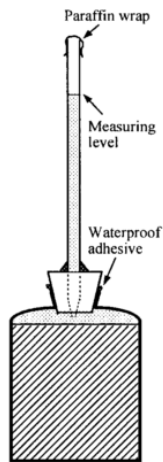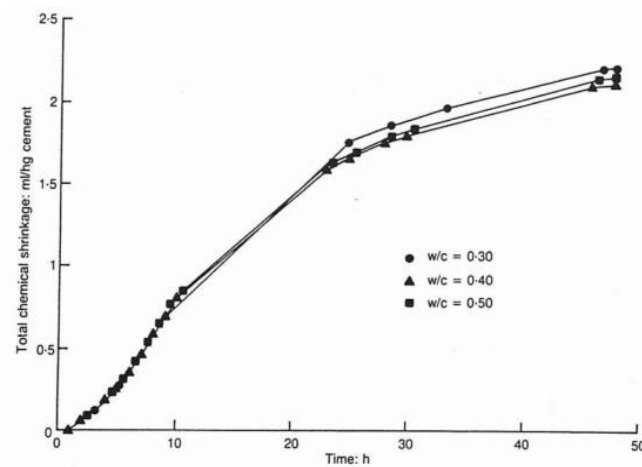
<p style="text-align: center;">(a)   (b)</p>

Figure 2.8 (a) Set-up of the dilatometry method for chemical shrinkage measurement (Holt 2001); (b) Chemical shrinkage of class G cement slurries at the early age of 0–48 h, w/c=0.3, 0.4, 0.5 (Justnes et al. 1995).
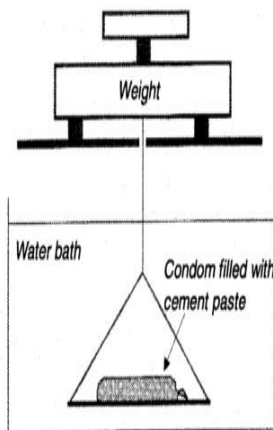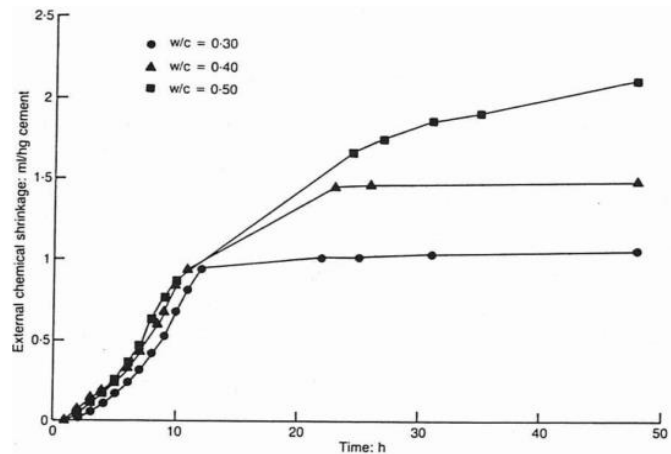
<p style="text-align: center;">(a)   (b)</p>

Figure 2.9 (a) Membrane method for autogenous shrinkage measurement (Holt 2001); (b) Autogenous shrinkage of class G cement slurries at the early age of 0-48 h, w/c=0.3, 0.4, 0.5 (Justnes et al. 1995).

(a)

(b)   (c)
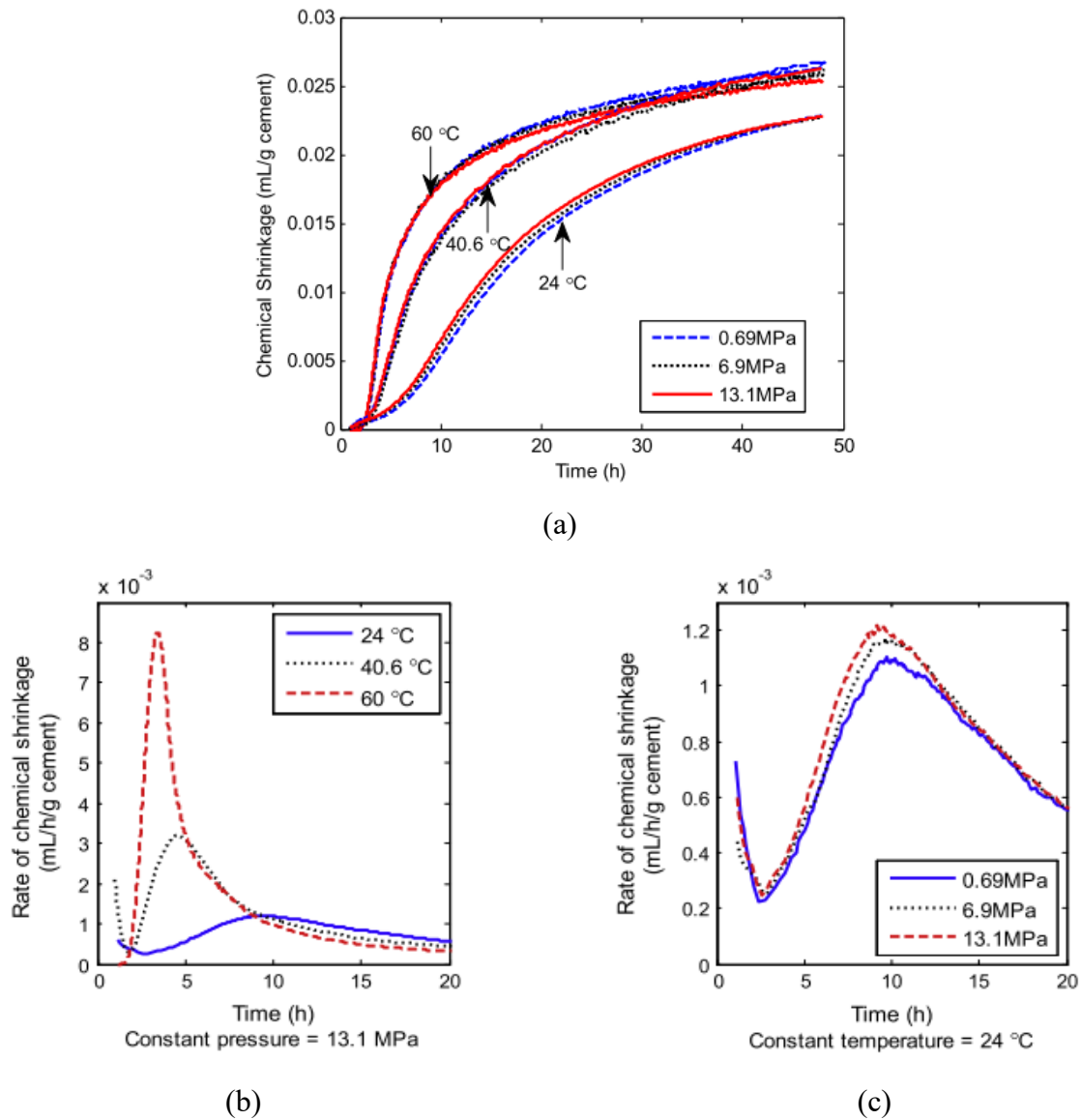
Figure 2.10 Total chemical shrinkage of Class H cement with w/c=0.4 at different temperatures of 24, 40.6 and 60 ºC , and different pressures of 0.69, 6.9, 13.1 MPa (Pang et al. 2015).

The strong dependence of autogenous shrinkage on curing temperature has also been reported in the literature, although most of the studies were carried out with ordinary Portland cement. The records on OWCs are very limited. The effect of temperature increase on the development of autogenous shrinkage is unsystematic, and varies for different types of cement. Nonetheless, the high curing temperature at early ages was generally found to increase the rate of the development of autogenous shrinkage as well as the shrinkage amplitude (Jensen & Hansen 1999; Mounanga et al. 2006; Chu et al. 2012). This is attributed to autogenous shrinkage, or

rather, chemical shrinkage as one of its components, being strongly interrelated with the degree of hydration. A high curing temperature normally causes the hydration reaction to be accelerated, leading to early completion of the hydration reaction and hence autogenous shrinkage.

Additionally, the shrinkage of OWCs can also be affected by water availability from the surrounding formations. The access to external water depends on the nature of the facing rock formations, whether they are porous or not, and their content of water, oil, gas or a mix of each. Water availability reduces the bulk shrinkage caused by drying and self-desiccation, and may even cause bulk expansion due to increased pore pressure when water enters into the cement pore spaces. In some cases, the cement is placed between an impermeable rock formation and casing, or between two concentric casings of different diameters and has no access to any external fluid (Blanc et al. 2013). In a sealed condition without moisture exchange, autogenous shrinkage becomes more dominant.

2.2   Expansive additives in cementitious materials

2.2.1 Expansive additives for shrinkage reduction in oil well cement

Given the detrimental effects of shrinkage, different strategies have been developed to control shrinkage and shrinkage-induced cracking of concrete structures, and to some extent the cement sheath of oil wells. These shrinkage control strategies can be broadly divided into two categories: (1) chemical interventions through reducing the tensile stresses, including shrinkage reducing admixtures, expansive additives, supplementary cementitious materials, and internal curing; (2) physical interventions through resisting the tensile stresses in the cement/concrete matrix, such as reinforcement with fibres.

Among various shrinkage control methods, the addition of expansive additives has been commonly used in OWC systems. Within the limited spaces between the casing and the formation, proper expansion of the cement sheath can eliminate microannulus and reduce the cement porosity, leading to improved bonding properties. As mentioned above, there are two groups of expansive additives for oil well cements based on their distinctive expansion mechanisms: (1) gas-generation systems that produce expansion due to the pressure of gas

bubbles produced by gas generation agents (Nelson 2006); (2) crystal-growth systems that produce expansion due to the internal pressure exerted upon crystallization of the reaction products.

In a gas-generating system, the cement expands through artificially entrapping swelling gas holes upon the generation of hydrogen by the reaction of metallic powders like Al, Zn, or Fe with the alkaline constituents of the cement (Narayanan & Ramamurthy 2000; Liu et al. 2013). Apart from for compensating volume shrinkage, the swelling gas holes are also beneficial to improving cement flexibility by reducing the Young's modulus and brittleness of the cement. However, a gas-generating system needs careful controlling and monitoring during the cementing process, otherwise gas bubbles may merge and create paths for formation fluid to flow in, leading to undesired fluid migration and even loss of well integrity (Ghofrani& Plack 1993). The effectiveness of this phenomenon is limited to the shallow depth of the borehole.

A crystal-growth system mainly comprises three types of expansive additives: ettringite-based, CaO-based, and MgO-based.

The ettringite-based additives are mainly used for drying shrinkage compensation based on the formation of ettringite to produce the expansion force. The ettringite ($C_6A\bar{S}_3H_{32}$) formation in the expansive cement is attributed to the reaction of CaO, Al_2O_3, SO_3 and H_2O, as shown in equation 2.2. The crystallisation pressure due to the formation and growth of ettringite crystals (Mehta 1973) and the swelling pressure due to the absorption of water molecules on colloidal ettringite grains (Cohen & Richards 1982), are considered to be the main driving forces behind the expansion.

$$6CaO + Al_2O_3 + 3SO_3 + 32H_2O \rightarrow C_6A\bar{S}_3H_{32}$$
<div align="right">Equation 2.2</div>
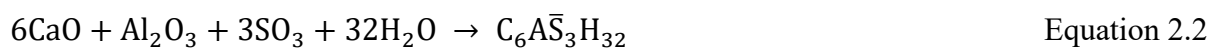
The CaO-based and MgO-based additives, also referred to as lime and magnesia, respectively, can provide expansions that are dependent on the formation of calcium hydroxides ($Ca(OH)_2$) and magnesium hydroxides ($Mg(OH)_2$). The hydration of CaO and MgO, as noted in Table 2.3, will result in increases of the volume of solids (theoretically 98% for CaO and 117% for MgO) and thus expansion of the cement.

Good thermal stability is required for expansive additives to be used under high-temperature wellbore conditions. The ettringite-based additives have a major limitation of use at high temperatures due to the instability of ettringite above ~70 °C (Bentz 2009; Nelson 2006). Such a limitation has made researchers turn to CaO-based and MgO-based expansive additives. Compared to ettringite-based additives, CaO and MgO additives, as well as their hydration products, have better thermal stability.

Table 2.3 Hydration and Expansion properties and products of CaO and MgO.

Expansive additive	CaO	MgO
Equation of hydration	$CaO + H_2O \rightarrow Ca(OH)_2$ 56.08 18.02 74.10 (Mass) 3.35 1.0 2.23 (Density) 16.74 18.02 33.23 (Volume)	$MgO + H_2O \rightarrow Mg(OH)_2$ 40.30 18.02 58.03 (Mass) 3.59 1.0 2.39 (Density) 11.20 18.02 24.30 (Volume)
Increase in volume of solids (%)	98%	117%

More importantly, the reactivity of the expansive additives must be controllable to produce the required expansion at the right time. If crystallization occurs when the cement slurry is in the fluid phase, the cement system will be unable to sustain the expansive forces, and therefore the expansive additive will not effectively compensate for bulk shrinkage. For additives with very low reactivity, the crystallization pressure of the expansive additive developing at the late age might result in cracking and loss of mechanical properties, or so-called unsoundness. Consequently, the reactivity of the additive must be such that its expansion occurs mainly in the late plastic phase and at the beginning of the cement-hardening phase (Ghofrani& Plack 1993). Oil well cement systems can be subjected to a wide range of temperatures from below freezing in permafrost zones to 350 °C in thermal recovery and geothermal wells, which strongly affects the hardening behaviour. Therefore, the expansion of expansive additives is preferably designable to accommodate such variations in conditions.

Industrially, CaO and MgO are usually manufactured by the calcining of calcium and magnesium carbonates. Their expansion behaviour can be controlled by changing their hydration reactivity through modifying the manufacturing process, either through decreasing the reactivity by increasing the calcining temperature, or increasing the reactivity by augmenting the specific surface area or fineness during the grinding process (Rubiandini et al., 2005). However, compared to MgO, CaO exhibits a considerably higher free enthalpy and thus a higher reactivity, even in the dead-burnt state (manufactured above 1600 °C) (Ghofrani and Plack 1993). Light-burnt CaO can begin hydrating very rapidly at a very early stage of cement hydration. The calcium hydroxide formed during this period will be consumed by reacting with the ferrite phase to form AFt phase instead of acting on expansion. The hard-burnt CaO can generate expansion mainly within the early age. Especially under elevated borehole temperatures, the hydration of CaO will be accelerated, leading to less effective expansion. In the literature, CaO-type expansive additives were reported to be efficient at lower temperatures (below 50 °C).(Ghofrani & Plack 1993; Marbun 2006; Jafariesfad et al. 2017). As a result, CaO has very limited capability of designable expansion.

By contrast, MgO additives with a wider range of reactivities are better at fulfilling the designable expansion properties. Several studies have reported controlling MgO expansion in given cement systems and curing conditions through pretreatment (Mo et al. 2010; F. X. Li et al. 2010; Mo et al. 2012; Lau & Mo 2014). MgO produced using a lower calcination temperature and finer particle size has higher reactivity and thus generates faster expansion at the early age, while low-reactivity MgO produced with a high calcination temperature and coarse particle size exhibits "delayed" expansion occurring mainly at the later age. Such expansion characteristics permit the use of MgO at wellbore conditions ranging from ambient temperature to even higher temperatures (Marbun 2006). High reactivity MgO can be used under lower temperature conditions while low reactivity MgO fits higher temperature to produce effective expansion.

A general comparison between the properties and performance of ettringite-based, CaO-based and MgO-based expansive additives was summarized by Lau (2017), as shown in Table 2.4. Of the three types of additive, MgO appears to be the most suitable expansive additive for use

in oil well cement systems. Its advantages include: (1) good thermal stability of hydration products, which is suitable for use in high-temperature downhole conditions; (2) designable expansion properties (Mo et al. 2010) which provide the possibility of delivering the desired expansion under different downhole conditions; (3) lower water demand for hydration, which allows use in low moisture downhole conditions; (4) the hydration product, brucite, has chemically and physically stable properties which provide the ability for autogenous, thermal and drying shrinkage reduction.

Table 2.4 Comparison between ettringite-based, CaO and MgO-based expansive additives (Lau 2017).

	Ettringite	CaO	MgO
Hydration			
Hydration rate	Fast	Fast	Designable
Heat of hydration	High	High	Depends on reactivity
Hydration Product			
Decomposed at high temp.	Yes	No	No
Reaction with Portlandite	No	Yes	No
Solubility in water	Low	High	Low
Hydration in cement			
Expansion	Early expansion	Early expansion	Early or delay
Water demand	High	High	Low
Shrinkage reduction			
Autogenous	No	Nil	Yes
Drying	Yes	Yes	Yes
Thermal	No	Nil	Yes
Application			
Hydraulic structures	Yes	No	Yes
Mass concrete	No	Yes	Yes

2.2.2 Magnesium oxide-based expansive additives

The use of MgO-based expansive additives was first proposed for OWC systems by Danjusevsky in 1983 (Danjusevsky 1983; Rubiandini et al. 2005). MgO was found to provide a good expansion effect in special wellbore conditions. This finding raised the interest of oil industries and research has been carried out accordingly in the following decades, to investigate the expansion performance of MgO and its efficiency in improving wellbore integrity under various wellbore conditions. In addition to special oil well environments, MgO has more extensive applications outside of oil well fields. Its effectiveness in thermal shrinkage reduction

was first discovered as early as the 1970s, in the case of the Baishan concrete dam construction in China. MgO expansive additives have been widely used in the construction of large concrete structures such as dams, foundations, tunnels and spillways in China for reducing thermal shrinkage. Their use has also extended to airport runways for drying shrinkage reduction. These applications have generated a significant amount of research, mainly in China, that was recently reviewed by Mo et al. (2014) and Lau (2017). This section systematically reviews the production, classification, and characteristics of MgO and its expansion behaviour in cement pastes, especially oil well cement.

2.2.2.1   Production of MgO

MgO is commonly obtained either from the calcination of natural magnesite or from the synthesis of seawater or brine (Shand 2006). The former production route accounts for ~85% of global MgO production, and is commonly used to produce MgO in the construction industry in China. The remaining ~15% of MgO is produced from seawater and brine, mainly in the Western world and a few shares in China (Lau 2017). The properties of MgO are highly dependent on the production process. The MgO content and reactivity produced from natural magnesite are of lower quality than the seawater or brine type due to the higher impurity level.

The production process of MgO from natural magnesite ($MgCO_3$) mainly comprises mining, crushing, sizing, and calcination (Shand 2006). The essential reaction that occurs during calcination is the loss of carbon dioxide from magnesite, with the corresponding formation of magnesium oxide, as shown in Equation 2.3 (Shand 2006). The decomposition temperature of magnesite varies from 402 ^{o}C to 750 ^{o}C depending on the source of magnesite (Cui 2008).

$$MgCO_3 \xrightarrow{\text{Heat}} MgO + CO_2 \qquad \text{Equation 2.3}$$

The calcination temperature and residence time have a strong influence on the chemical and physical properties of the MgO product. Research shows that MgO reactivity decreases with increased calcination temperature and prolonged residence time. Mo et al. (2010) studied the effect of calcination conditions on the chemical composition of MgO produced from magnesite, as shown in Table 2.5. It was found that the MgO content increases and the LOI (loss on

ignition) decreases with increasing calcination temperature and residence time, indicating that magnesite approaches complete decomposition.

The production of MgO from seawater and brine sources comes through heating the precipitated magnesium oxide ($Mg(OH)_2$) synthesized from seawater or brine, as shown in Equation 2.4 (Shand 2006). Compared to the magnesite production route, MgO produced from seawater and brine has a higher MgO content and reactivity because of the lower impurity level. However, it is an energy extensive production, requiring over four times as much energy to produce a tonne of MgO, and is also far more expensive than the magnesite production route.

$$Mg(OH)_2 \xrightarrow{\text{Heat}} MgO + H_2O \qquad \qquad \text{Equation 2.4}$$

Table 2.5 Effect of calcination conditions on the chemical composition of MgO (Mo et al. 2010).

Sample	Calcination condition		Chemical compositions / wt.%					
	Temperature /°C	Time /h	MgO	SiO_2	Fe_2O_3	Al_2O_3	CaO	Loss
S900-0.5	900	0.5	78.56	3.68	0.64	0.59	2.33	14.20
S900-1.0	900	1.0	80.95	4.35	0.97	0.58	2.41	8.83
S900-1.5	900	1.5	87.65	4.90	1.01	0.57	2.21	2.03
S1000-0.5	1000	0.5	88.05	4.45	1.86	0.55	1.96	3.83
S1000-1.0	1000	1.0	89.29	4.86	1.02	0.58	2.13	2.11
S1000-1.5	1000	1.5	90.35	4.88	1.00	0.56	2.23	1.03
S1100-0.5	1100	0.5	89.79	4.67	1.06	0.54	2.31	1.63
S1100-1.0	1100	1.0	89.24	4.30	0.98	0.55	2.34	0.64
S1100-1.5	1100	1.5	90.36	4.26	0.99	0.54	2.30	0.56
S1200-0.5	1200	0.5	90.23	4.22	1.04	0.57	2.28	0.31
S1200-1.0	1200	1.0	91.08	4.21	0.92	0.56	2.08	0.02
S1200-1.5	1200	1.5	91.63	4.31	1.03	0.46	2.16	0.04
S1300-0.5	1300	0.5	91.56	4.28	1.06	0.49	2.22	0.05
S1300-1.0	1300	1.0	91.94	4.03	0.90	0.55	2.35	0.03
S1300-1.5	1300	1.5	92.01	4.14	0.89	0.56	2.34	0.03

2.2.2.2   Characteristics of MgO

Reactivity is one of the most important properties directly related to the hydration and expansion behaviour of MgO. Reactivity is a measure of MgO quality, defined in terms of the neutralisation time of an acid. Thus a smaller neutralisation time indicates a higher reactivity (Shand 2006). The higher the reactivity, the faster and higher the hydration rate, and thus the faster the expansion. The production sources and the calcination conditions are the key factors that affect the reactivity of MgOs. As mentioned above, synthetic MgO from seawater and brine has a higher reactivity than MgO calcined from magnesite. Figure 2.11 displays the

reactivity of MgOs from both resources tested by the acetic acid reactivity test (Jin& Al-Tabbaa 2014). MgOs from the synthetic group exhibited higher reactivity than those from the calcined group.
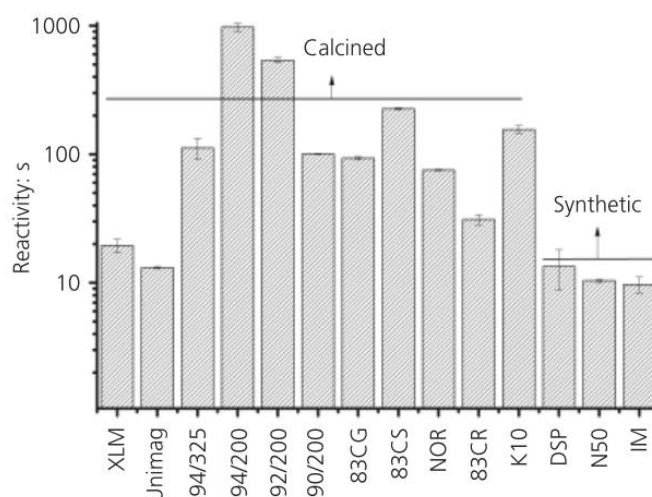
Figure 2.11 Reactivity of MgO from different sources based on the acetic acid test (Jin& Al-Tabbaa 2014).

Similarly, the physical properties, including specific surface area (SSA), pore structure, and grain size, are also affected by the production sources and calcination conditions. The synthetic MgOs generally have a higher SSA than MgOs from calcination of magnesite (Jin& Al-Tabbaa 2014). Among calcined-type MgOs, the SSA, pore structure and grain size vary significantly with different calcination temperatures and residence times. According to the results from Mo et al. (2010) as shown in Table 2.6, the SSA of MgO and the pore volume decrease with increasing calcination temperature and residence time, while the grain size increases with an increase in temperature and residence time. During the decomposing process of magnesite, porous MgO microcrystals are first formed as CO_2 escapes, and then the MgO grains grow due to the continued sintering. MgO grains under high temperature and/or long residence times result in large grain sizes and highly crystalline structures with small lattice distortion, reduced total pore volume, and enlarged pore size, and thus a low SSA. The evolution of MgO grain growth as calcination temperature and residence time increase has been confirmed under SEM. The morphology of MgO particles in Figure 2.12 revealed that MgO calcined at 900ºC had a smaller grain size and less regular surface, with defects as well as many interior pores, thus a

higher surface area. As the calcination temperature increased to 1100 ºC and 1300 ºC, MgO particles were seen to have larger grain size, regular surfaces with fewer crystal defects, and a denser structure with fewer interior pores, thus a lower surface area.

The reactivity of MgO is closely interrelated with those physical properties mentioned above. Mo et al. (2014) summarised the results from several studies on the relationship between the specific surface area (SSA) and the reactivity of MgO as shown in Figure 2.13. They revealed that the reactivity value of MgO decreases with increasing specific surface area, indicating an increase in the reactivity of MgO. Li et al. (2010) analysed the reactivity of three different MgO expansive additives (MEA) on their pore size distribution, average pore diameter, and SSA (Figure 2.14). It was found that MgO with a higher reactivity (smaller reactivity value) had a higher porosity and smaller pore size, accordingly with a higher specific surface area (SSA).

Table 2.6 Physical properties of MgO calcined under different calcination conditions (Mo et al. 2010).

Sample	Crystal grain size (nm)	Lattice distortion (%)	Specific surface area (m²/g)	Pore volume (cm³/g)	Average pore width (nm)	Density (g/cm³)
S900-0.5	21.2	0.1648	52.7	0.193	14.62	2.97
S900-1.0	29.3	0.0560	55.2	0.223	16.10	3.02
S900-1.5	36.8	0.0350	45.9	0.179	15.57	3.12
S1000-0.5	30.4	0.0208	49.8	0.235	18.84	3.13
S1000-1.0	43.2	0.0149	39.8	0.235	23.61	3.26
S1000-1.5	66.3	0.0092	18.9	0.103	25.12	3.32
S1100-1.0	>100	–	4.2	0.024	22.46	3.43
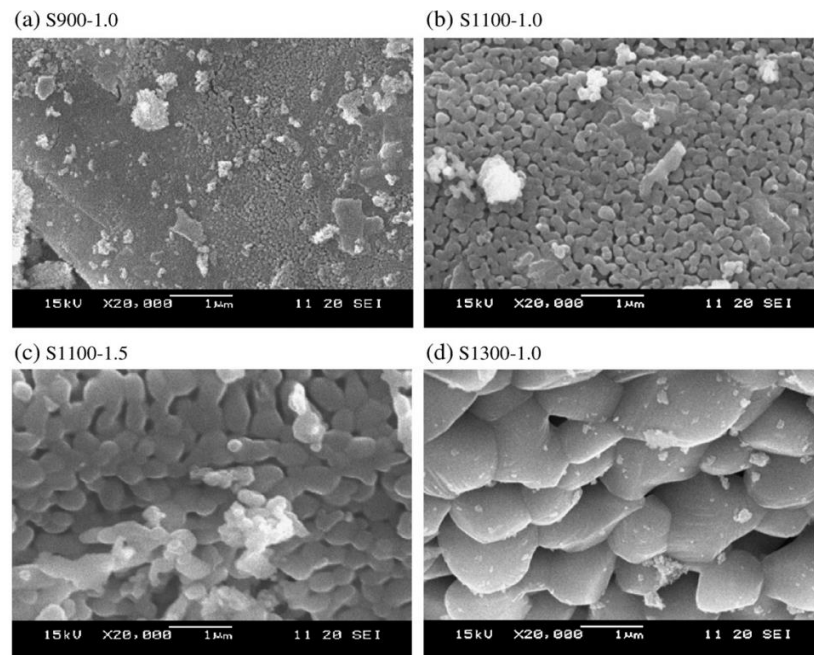
Figure 2.12 Morphology of MgO expansive additives produced at different calcination temperatures and residence times under SEM (Mo et al. 2010).
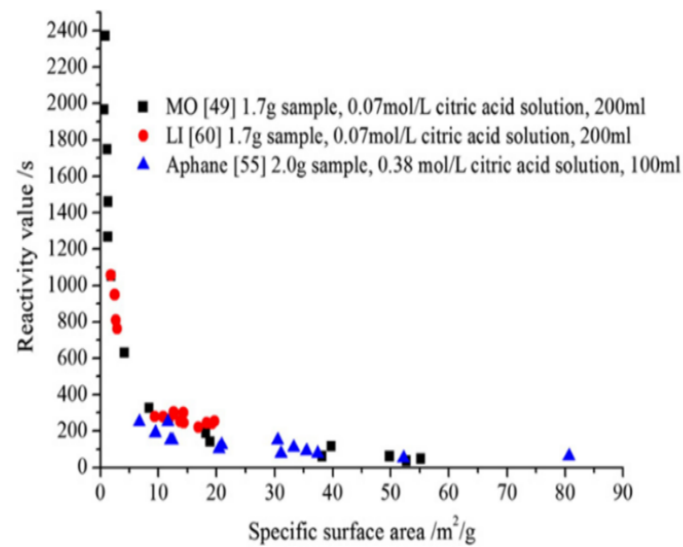
Figure 2.13 Relationship between the specific surface area and reactivity value of MgO (Mo et al. 2014).
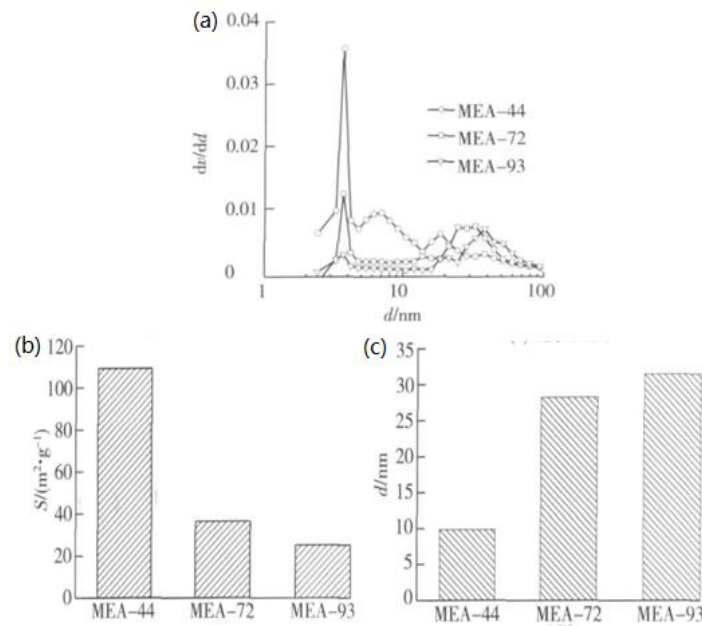
Figure 2.14 The properties of three MgO expansive additives (MEA) with different reactivities: 44s (MEA-44), 72s (MEA-72), 93s (MEA-93). (a) pore size distribution; (b) specific surface area; (c) average pore diameter (H. Li et al. 2010).

2.2.2.3   Classification of MgO

Generally, MgOs are divided into four categories depending on the calcination temperature: light-burned (reactive or caustic-calcined), hard-burned, dead-burned, and fused. The classification and corresponding calcination temperature grades vary between different researchers, and are summarized in Table 2.7. The MgO type can also be defined by the reactivity corresponding to the calcination temperature range (Strydom et al. 2005) as shown in Table 2.7. A further classification according to reactivity was proposed by Jin et al. (2014) based on the characteristics of different reactive MgOs produced from calcined or synthetic sources. The reactive MgOs are classified into three categories based on the reactivity value and SSA: highly reactive, medium reactive, and low reactive (Table 2.8).

Table 2.7 Classification of MgO depending on calcination temperature.

	Classification by calcination temperature (ºC)			
	Light-burned (reactive or caustic calcined)	Hard-burned	Dead-burned	Fused
(Canterford 1985)	<900	-	>1200	>2800
(Shand 2006)	800 - 930	1300 -1550	>1550	>2800
(Jin & Al-Tabbaa 2014)	700 -1000	1000 - 1400	1400 - 2000	>2800
	Classification by reactivity (s)[*]			
	Soft-burnt	Medium reactive	Hard-burnt	Dead-burnt
(Strydom et al. 2005)	<60	180 - 300	>600	>900

[*]: the reactivity is determined by the citric acid reactivity test.

Table 2.8 Classification of reactive MgOs depending on reactivity values and specific surface area (Jin & Al-Tabbaa 2014).

Category	Reactivity	Reactivity Value (s)	Specific surface area (m^2/g)
I	Highly reactive	≤ 30	≥ 60
II	Medium reactive	30 - 300	10 - 60
III	Low reactive	≥ 300	≤ 10

2.2.2.4   Hydration of MgO

As aforementioned, the expansion property of MgO is based on its hydration process. MgO reacts with water to form brucite ($Mg(OH)_2$) which is chemically stable with a low solubility in water. The hydration mechanism is based on the dissolution and precipitation processes of MgO particles and involves three main steps: (1) water absorbs at the surface and diffuses through interior pores into the MgO grains; (2) MgO dissolution occurs within particles, accompanied by a change of porosity; (3) the supersaturation of the solution with Mg^{2+} and OH^- ions leading to nucleation and growth of $Mg(OH)_2$ crystals at the surface and/or inside of the MgO grains (Rocha et al. 2004). The hydration of MgO is highly dependent on the area of

reaction region and the activity of MgO grains (Mo et al. 2010). The former is closely related to the specific surface area, and the latter strongly depends on the crystal structure of the MgO grains. The larger specific surface area and more porous crystal structures accelerate the dissolution process of MgO and provide more spaces for $Mg(OH)_2$ crystal growth. As previously mentioned, MgO with higher reactivity has higher porosity and a higher specific surface area. Therefore, MgO with higher reactivity has a faster hydration rate and reaches a higher degree of hydration.

According to the results of Mo et al. (2010), the hydration of an MgO expansive additive (MEA) with a reactivity of 46s was completed within 7 days while only 1.0 % hydration was reached for an MEA with a reactivity of 1966s, as shown in Table 2.9. The SEM images of MEA hydration products in Figure 2.15 show the MEA-46 with the highest reactivity hydrated most rapidly and formed a large number of hexagonal platelets of $Mg(OH)_2$ crystals at the early age of 2d (Figure 2.15a), reaching a hydration degree of 97% (Table 2.9). The platelet thickness of $Mg(OH)_2$ increased as the hydration proceeded (Figure 2.15b) and the hydration was completed at 7d. In contrast, the MEA-325 with less reactivity only formed a few fine sheets of $Mg(OH)_2$ grown at the surface of MgO grains or filling in the pores at 2 d and the hydration crystals increased at 7d, but only achieved a hydration degree of 9.9%. The MEA-1966 with the lowest reactivity hydrated most slowly and showed almost no sign of hydrate formation until 7d when only a thin layer of lamellar $Mg(OH)_2$ (Figure 2.15f) formed, at a hydration degree of only 1%.

In addition to the intrinsic reactivity of MgO itself, the exterior temperature is also an important influencing factor of the hydration process. At higher temperatures, MgO has a faster hydration rate and reaches a higher degree of hydration. Amaral et al. (2010) used ionic conductivity measurement to analyse the influence of temperature on MgO hydration. As shown in Figure 2.16, an increasingly rapid release of the Mg^{2+} and OH^- ions into solution by MgO dissolution occurred with increasing the temperature from 10 to 80 °C, followed by rapid hydroxide precipitation. Rocha et al. (2004) and Mo et al. (2014) also reported the promotion of the degree of hydration of MgO at elevated temperature.
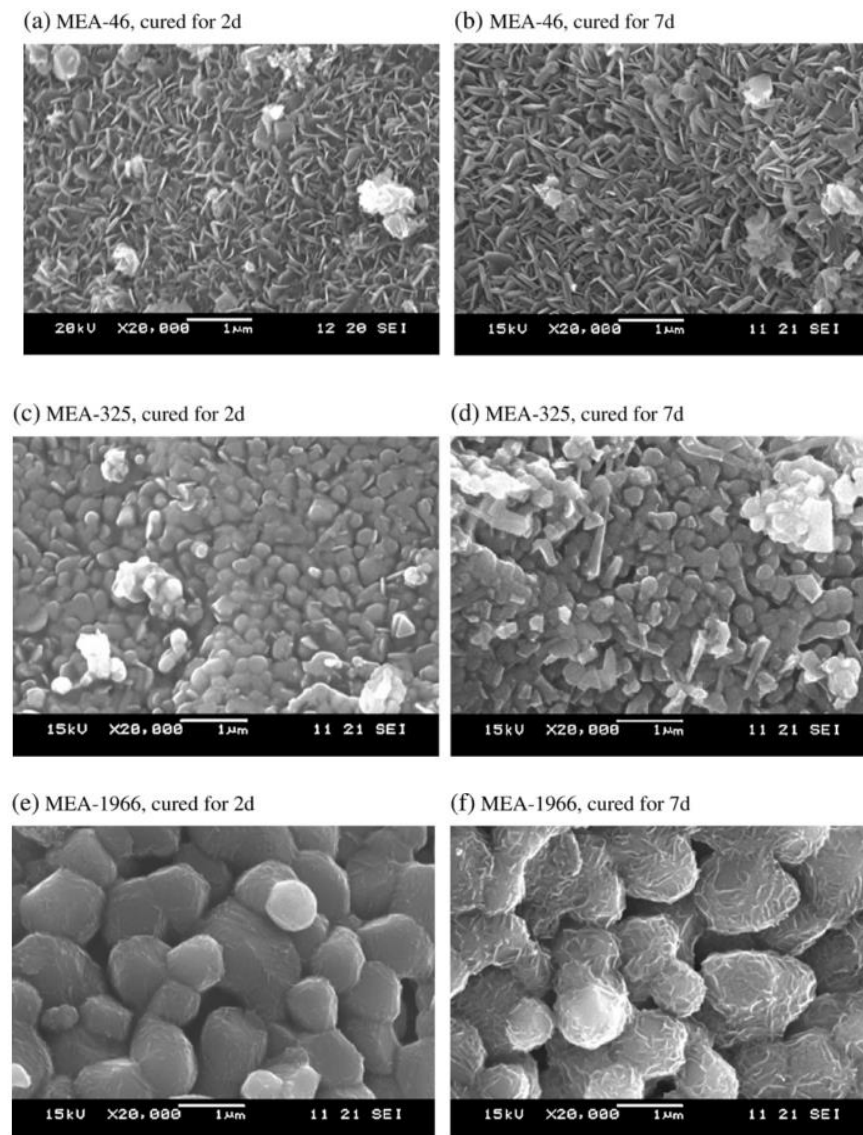
Figure 2.15 SEM images of the hydration products of MgO expansive additive (MEA) with different reactivities of 46 s, 325 s and 1966 s cured in water at 20 ^{o}C, at 2 days and 7 days (Mo et al. 2010).

Table 2.9 Hydration degree of MgO of different reactivity hydrated in water at 20 °C (Mo et al. 2010).

Reactivity (s)	Hydration degree of MgO (%)			
	2 days	7 days	15 days	30 days
46	97	100	100	100
325	4.5	9.9	20.9	82.6
1966	-	1.0	1.9	7.9
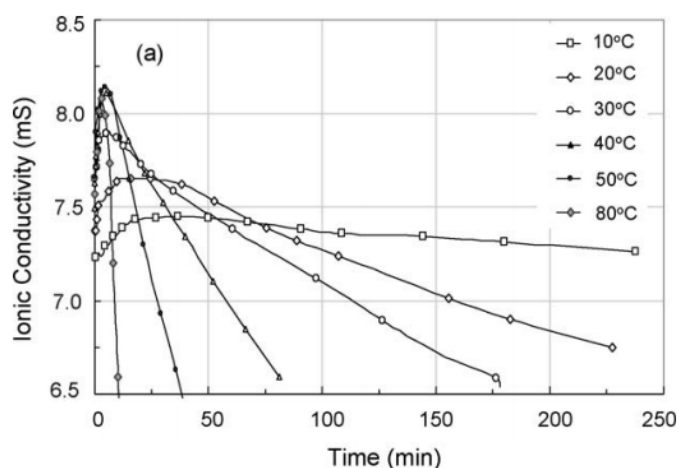
Figure 2.16 Ionic conductivity for magnesia suspensions at different temperatures from 10 to 80 °C (Amaral et al. 2010).

2.2.2.5   Expansion mechanisms of MgO

The hydration process of MgO is accompanied by volume expansion. From the view of the equation of hydration as shown in Table 2.3 in Scetion 2.2.2, the expansion of MgO can be explained based on the molecular mass and density calculations. The total volume of reactants is 29.22 compared to 24.3 of the volume of hydration product $Mg(OH)_2$, this means a chemical shrinkage of ~17% reduction in volume. On the other hand, the volume of solid increases by 117% from MgO into $Mg(OH)_2$, which contributes to the overall expansion. From the microstructure viewpoint, there are two main theories of the expansion mechanism of MgO:

(1) swelling pressure due to water absorption by fine crystals of MgO and (2) crystal growth pressure due to the growth of $Mg(OH)_2$ (Deng et al. 1990; Chatterji 1995). During the hydration of MgO, a supersaturated solution of Mg^{2+} and OH^- will first form and then $Mg(OH)_2$ crystals will precipitate and grow in a confined region, resulting in crystal growth pressure causing the expansion of the cement pastes. The pH environment in the cement paste was also reported to strongly affect the expansion of MgO (Deng et al. 1990). In a high pH environment, the high concentration of OH^- leads more Mg^{2+} ions to diffuse locally near the surface of MgO grains, contributing to a higher degree of supersaturation and thereby resulting in a larger expansion.

To better explain the expansion of MgO, Mo et al. (2010) proposed new hydration and expansion models of MgO expansive additive (MEA) and demonstrated the effects of reactivity on the expansion of MEA. As shown in Figure 2.17, MEA with high reactivity has a porous structures, a high volume of interior pores, and high SSA, which allows hydration to take place both at the surface of MEA grains and the interior pores inside MEA at an earlier age. The formed hydration products $Mg(OH)_2$ are first filled into the interior pores. As hydration proceeds, further formation of $Mg(OH)_2$ may cause the volume expansion of MEA grains.

Unlike MEA with high reactivity, the hydration of MEA with low reactivity mainly takes place at the MEA grain boundary (Figure 2.18). Because fewer interior pores accommodate the hydration products, the formed products accumulate at the MEA grain boundary. After an induction period, the hydration products at the boundary induce enough expansive force to break apart the sintered MEA grains, enlarging the reaction surface area, thus accelerating the hydration and resulting in faster and larger expansion at a later age. MEA with high activity hydrates rapidly and thus produce fast expansion at an early age, and a short time is needed to reach the "ultimate" expansion. The lower the reactivity of MEA, the longer the induction period and the larger "ultimate" expansion at a late age will be produced.
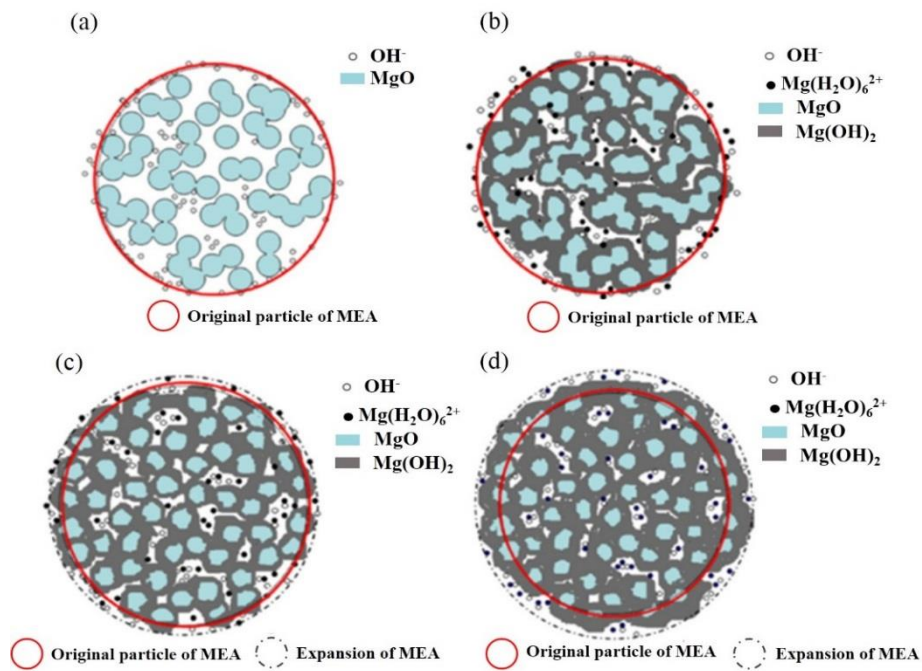
Figure 2.17 Hydration and expansion model of MEA with high reactivity in the cement paste (Mo et al. 2010).
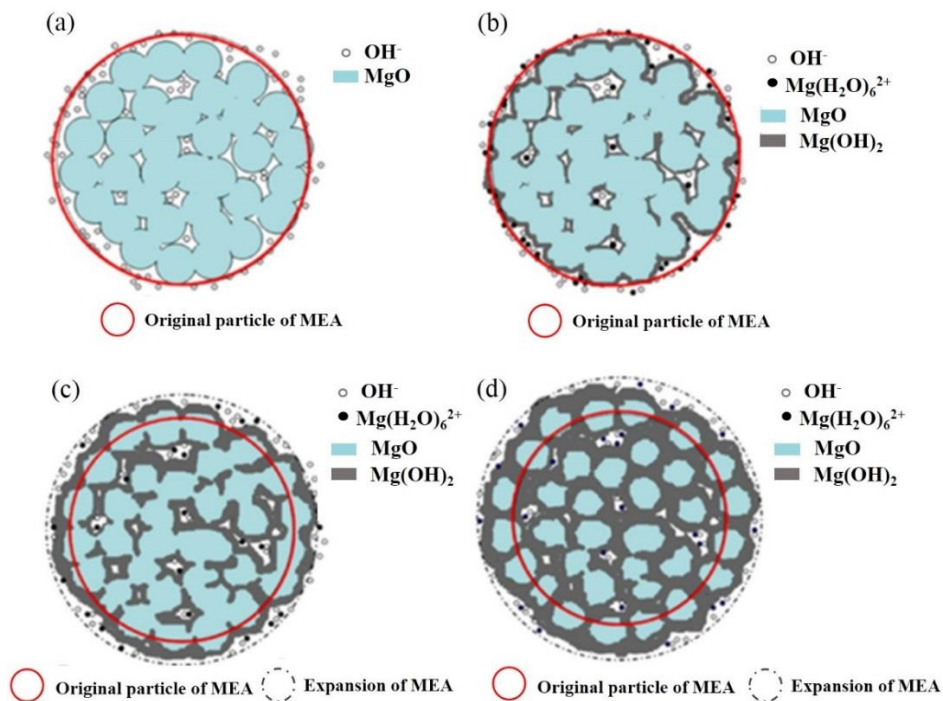
Figure 2.18 Hydration and expansion model of MEA with low reactivity in the cement paste (Mo et al. 2010).

2.2.3 Expansion performance of MgO in cement system

2.2.3.1   Expansion characteristics of MgO

Many studies have been carried out to evaluate the expansion characteristics of MgO in OPC systems, and have showed that MgO expansion is dependent on the MgO reactivity and MgO concentration as well as the curing temperature.

The reactivity is an inherent decisive factor influencing the expansion of MgO. Previous studies find that MgOs with high reactivity exhibit different expansion trends from MgOs with low reactivity. Mo et al. (2010) investigated the expansion performance of five kinds of MgO expansive additive (MEA) with a wider range of reactivity (46 s, 115 s, 325 s, 1266 s, 1966 s) at 20 ºC. The results in Figure 2.19a show that the MEA with higher reactivity has a higher expansion rate and greater magnitude of expansion at an earlier age, and reaches the ultimate expansion within a shorter period. A less reactive MEA with low reactivity has slower and smaller expansion at an early age, but faster and larger expansion at a later age. For instance, MEA-46 with the highest reactivity expanded the fastest and achieved the highest expansion values within the earlier age of 60 days. But at the later age, the expansion of MEA-115 and MEA-325 accelerated and reached a larger overall expansion than MEA-46. A recent study by Lau (2017) on the expansion of reactive MgOs with high reactivity: HR1-10s, HR2-14s, and medium reactivity: MR1-102 s, MR2-140 s (classified according to (Jin & Al-Tabbaa 2014)) in cement pastes also reported similar expansion trends as shown in Figure 2.19b. The higher the reactivity, the faster the expansion rate and the higher the expansion magnitude at an early age.

The expansion of MgO is affected by the curing temperature due to the strong influence of temperature on its hydration process. Mo et al. (2010) also studied the expansion performance of different reactivities of MEA in cement pastes at the elevated temperature of 40 ºC (Figure 2.20a). Compared to the results at 20 ºC in Figure 2.19a, it was found that MEAs showed faster expansion in cement pastes at 40 ºC, which was attributed to the faster hydration of MgO at higher temperature, resulting in faster $Mg(OH)_2$ crystal growth to expand the cement. It was also observed that the curing temperature had a more significant influence on the expansion of

MgO with lower reactivity. The expansion of MEA-1266 and MEA-1966 was significantly accelerated and a reached larger expansion within a shorter period. The author explained that low reactivity MEA with delayed expansion behaviour hydrates slowly to form hydration products at MgO grain boundaries during the induction period at 20 °C, and this process intensifies as the temperature increases. As a result, MgO grains are broken and the reaction surface area becomes enlarged, thus leading to noticeable increase in the expansion rate.

(a)   (b)
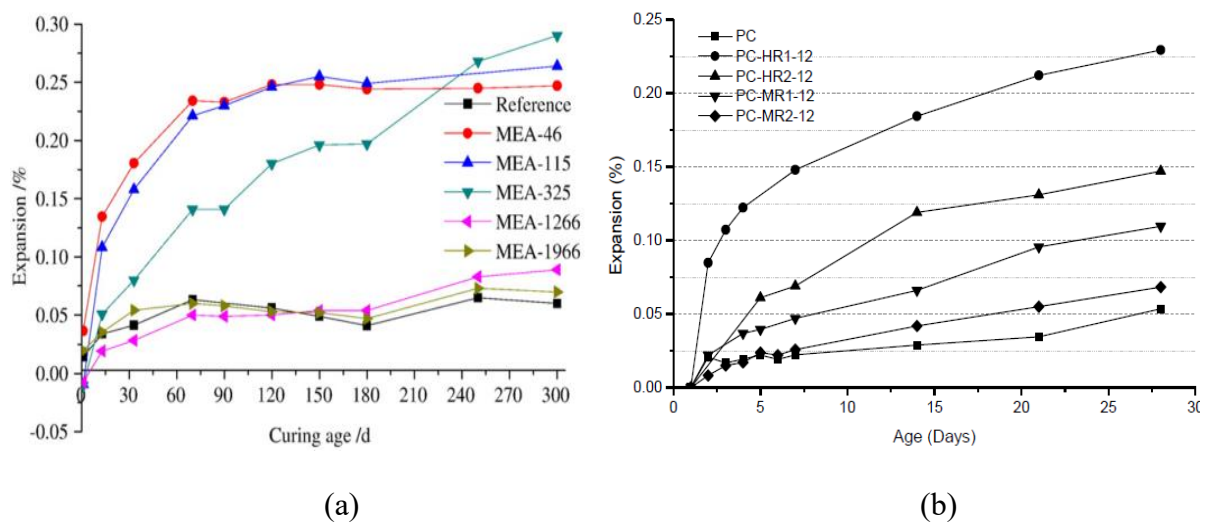
Figure 2.19 Effect of reactivity on the expansion of cement paste containing MgO at 20 °C (a). MgO expansive additive (MEA) with different reactivities at a content of 8% by weight of cement (Mo et al. 2010); (b) Reactive MgO with high reactivity and medium reactivity at a content of 12% by weight of cement (Lau 2017).
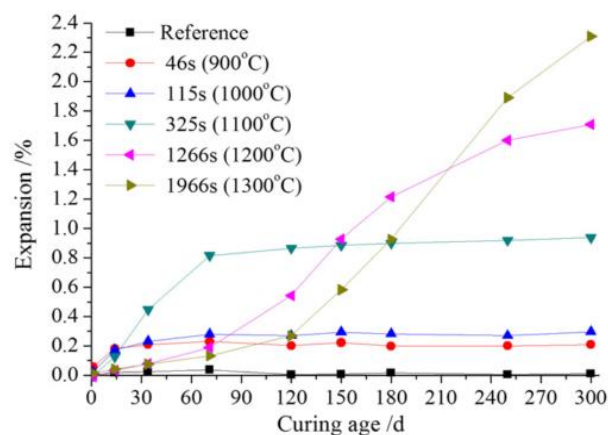
Figure 2.20 Expansion performance of cement paste containing different reactivities of MgO expansive additive (MEA) at a content of 8% by weight of cement cured at 40 °C (Mo et al. 2010).

In addition, the expansion has been reported to increase with increasing MgO content (H. Li et al. 2010; Li 2010; Lau 2017). More MgO in the cement paste produces more $Mg(OH)_2$, and thus produces a larger expansive stress in the cement pastes, leading to larger expansion. Lau (2017) observed that MgO expansion increased proportionally with increasing MgO content from 4% to 12% in both highly reactive MgO and medium reactive MgO (Figure 2.21).

(a)   (b)
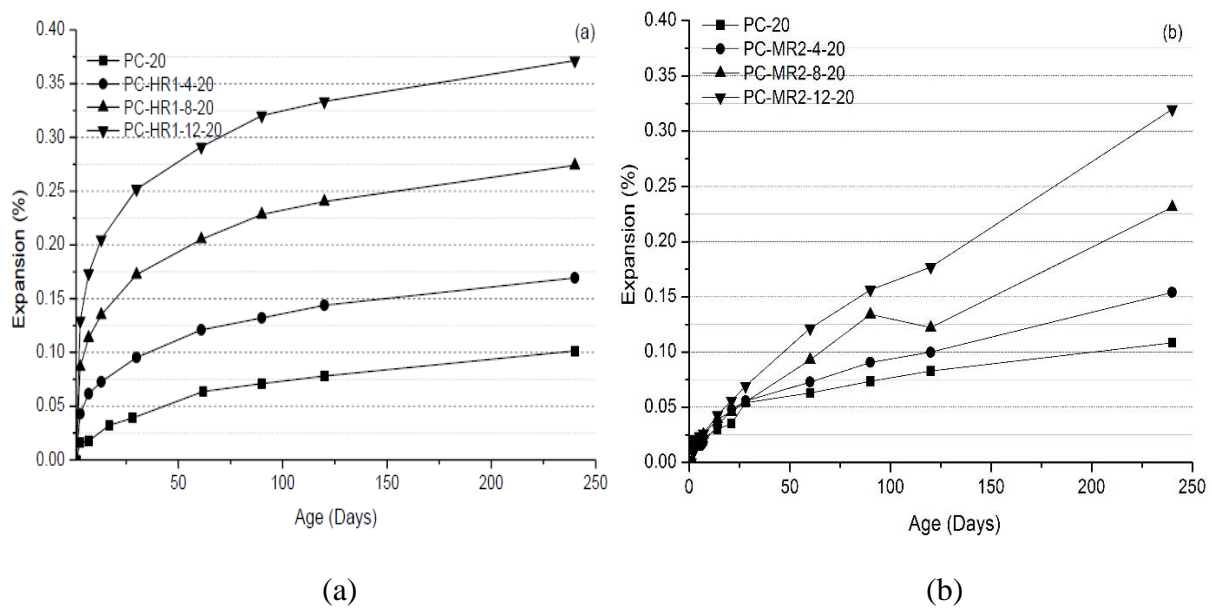
Figure 2.21 Effect of MgO content (4%, 8%, 12%) on the expansion of cement paste (a) Highly reactive MgO-HR1-10 s (b) Medium reactive MgO-HR2-140 s (Lau 2017).

MgO expansive additives used in OWCs are usually from the hard-burnt or dead-burnt categories with low reactivity. OWC systems containing hard-burnt or dead-burnt MgOs have been shown to provide excellent expansive performance at curing temperature up to 260 ℃ (Ghofrani & Plack 1993; Rubiandini et al. 2005; Saidin et al. 2008b; Thomas et al. 2014). However, at lower temperatures, the hydration reaction of MgO proceeds too slowly to be of practical benefit. Ghofrani & Plack (1993) examined the expansion performance of 20% hard-burnt MgO calcined at 1400 ℃ in Class G well cement pastes within the first 22 hours using an atmospheric expansion cell cured at 20 ℃, 50 ℃ and 90 ℃ in a water bath. The results in Figure 2.22a show that the cement pastes with hard-burnt MgO produced >1% volume expansion at a curing temperature of 90 ℃, but a much smaller expansion of less than 0.1% at lower temperatures of 20 and 50 ℃. A similar trend was also reported by Saidin et al. (2008) on the expansion of a Class G cement system contaning 1.0% dead-burnt MgO (>1400 ℃)

tested at higher temperatures up to 260 °C. The results in Figure 2.22b illustrate that the expansion sped up as the temperatrue increased from 79 °C to 260 °C, and a larger expansion was achieved at a higher temperature.

(a)   (b)
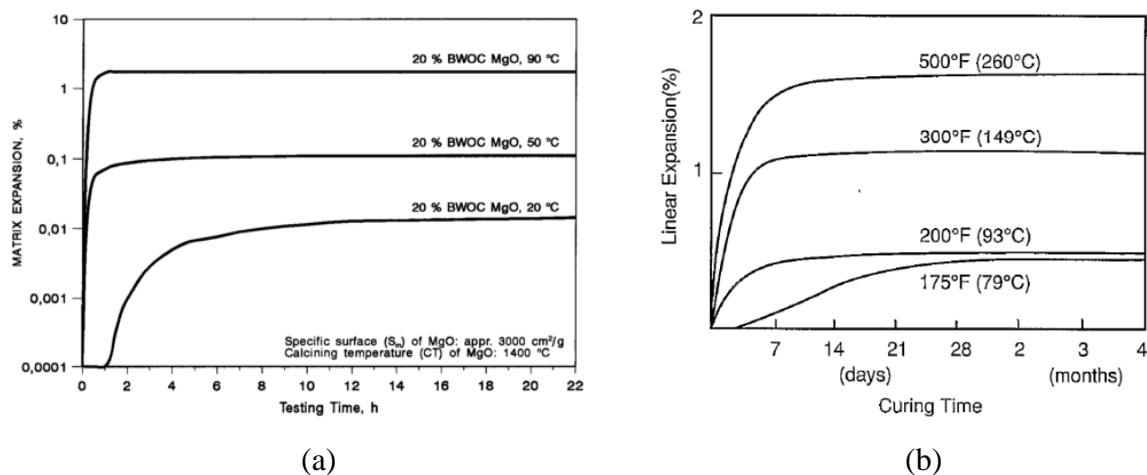
Figure 2.22 Expansion performance of hard-burnt or dead burnt MgO in Class G oil well cement systems under different curing temperatures: (a) Hard-burnt MgO calcined at 1400 °C at a content of 20%, cured at 20 °C, 50 °C and 90 °C (Ghofrani & Plack 1993); (b) Dead-burnt MgO calcined above 1400°C, at a content of 1%, and cured at 79 °C, 93 °C, 140 °C and 260 °C (Saidin et al. 2008b).
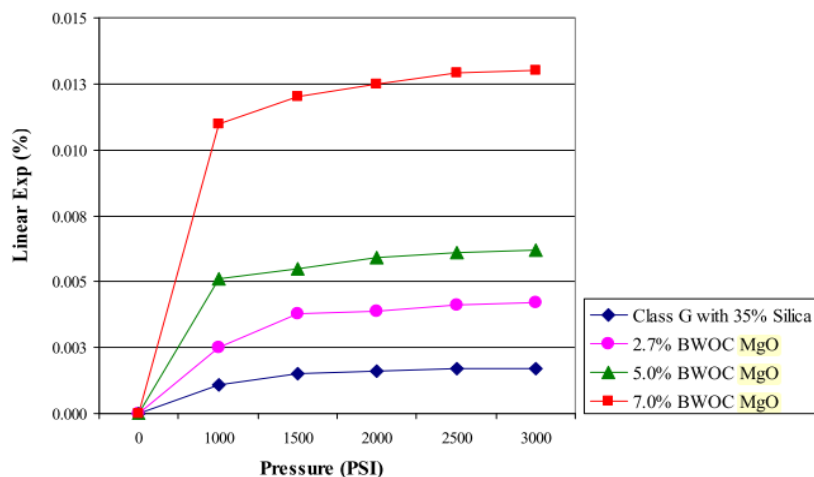
Figure 2.23 Expansion performance of class G cement with dead-burnt MgO (burnt above 1400°C) cured in an autoclave pressure curing vessel under different pressure gradients at a constant temperature of 49 °C for 2 d (Saidin et al. 2008b).

Apart from elevated temperature, oil well cement systems also sustain high borehole pressure. Saidin et al. (2008) studied the effect of pressure on the expansion of class G cement containing

dead-burnt MgO and found that the expansion did not change much with the pressure difference at a static borehole temperature (Figure 2.23).

2.2.3.2   Performance of MgO on shrinkage reduction in cement system

As introduced in Section 2.2.2, MgO has the ability to reduce autogenous, thermal and drying shrinkage in cement and concrete materials. In addition to the extensive use of MgO in compensating for thermal shrinkage in mass concrete structures, there are also reports of its performance in reducing autogenous shrinkage and drying shrinkage in cement materials.

Mo et al. (2012) evaluated the autogenous deformations of ordinary Portland cement pastes containing MgO expansive additive (MEA) (calcined at 1100 ºC) with low w/c ratio of 0.28 under non-wet curing conditions without moisture exchange with the environment (Figure 2.24). The results showed that the addition of MEA at 5% and 8% content led to significant reduction in autogenous shrinkage at an early age. With the continuous hydration and expansion of MgO, the shrinkage of cement paste was completely compensated for, followed by a continuous expansion of the cement paste at later ages. It was also found that cement paste containing a higher MEA content generated larger expansion, thus completely compensating for the shrinkage of the cement paste within a shorter period. The shrinkage reduction performance of the ettringite-based expansive additive (AEA) was also compared with MgO. AEA failed to produce effective expansion to compensate for shrinkage under autogenous conditions but resulted in even greater shrinkage of the cement paste due to its much higher water demand for hydration. Based on these findings, the authors concluded that MgO is suitable for the compensation of autogenous shrinkage under sealed curing conditions due to the relatively small water content required for its hydration.

Lau (2017) investigated the effects of different reactivities of MgO on the autogenous shrinkage reduction of ordinary Portland cement pastes at varied w/c ratios. The results in Figure 2.25 showed that at the same w/c, the addition of high reactivity MgO which had faster and larger expansion at an early age resulted in more autogenous shrinkage reduction than medium reactivity MgO. It was also found that higher shrinkage reduction was achieved as w/c ratio increased from 0.35 to 0.5. The author explained that increasing the w/c ratio provided

additional water for promoting MgO hydration, thus leading to larger expansion. In the meantime, increasing the w/c ratio also resulted in smaller autogenous shrinkage. Thus higher autogenous shrinkage reduction was observed.
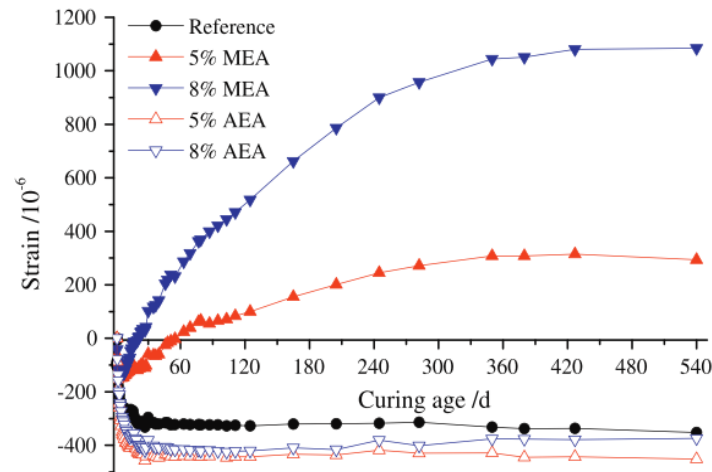
Figure 2.24 Autogenous deformations of cement pastes containing MgO expansive additive MEA or ettringite-based expansive additive AEA at content of 5% and 8% by weight of cement, under non-wet curing conditions at 20 °C (Mo et.al 2012).

| (a) | (b) |
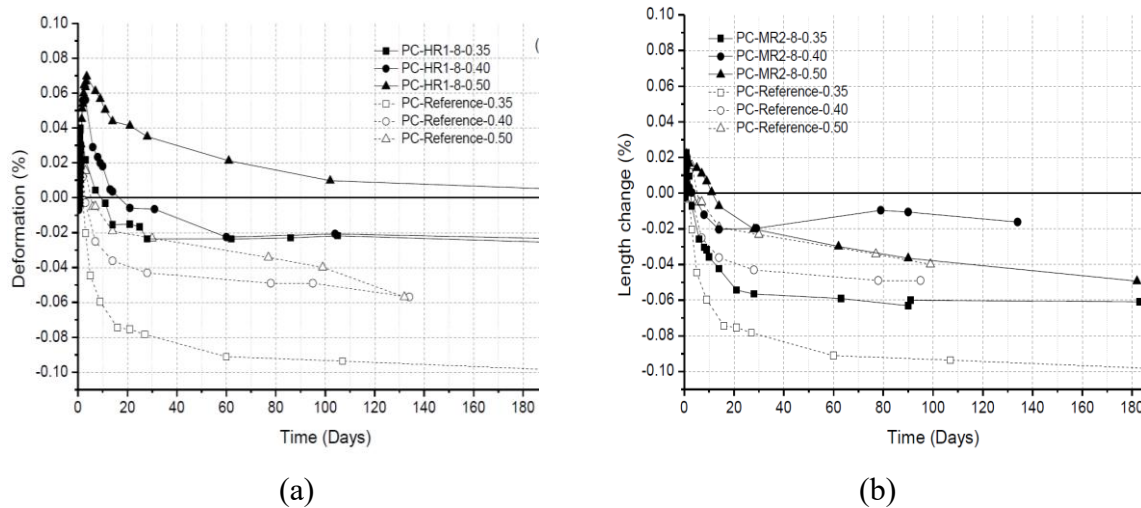
Figure 2.25 Effects of MgO with different reactivities: (a) HR1-10 s and (b) MR2-140 s at a content of 8% on autogenous shrinkage reduction in Portland cement pastes at varied w/c ratios of 0.35, 0.4, 0.5, under sealed conditions at 20 °C (Lau 2017).

Regarding shrinkage reduction under drying condition, Li (2010) tested four different reactivity MgOs ranging from 44 s to 93 s at content of 10% in OPC paste cured in air of RH 60% (Figure 2.26). The addition of all four MgOs partially reduced the drying shrinkage of the cement paste.

At 20 °C, the less reactive MgO (72 s and 74 s) showed more drying shrinkage reduction than did the MgO with a higher reactivity of 44 s. The drying shrinkage was further reduced when the temperature was increased to 30 °C. In particular, shrinkage of the cement contaning less reactive MgOs showed continous reducing trends at a later age. The increased temperature accelerated the hydration of MgO, thus producing a larger expansion to compensate for the shrinkage. However, Lau (2017) found that both highly reactive MgO (10 s) and less reactive MgO (140 s) showed no drying shrinkage reduction in cement paste cured in 40% RH at 20 °C. The addition of high reactivity MgO even led to increased drying shrinkage. The author speculated that the expansion of high reactivity MgO at the early age influenced the cement paste microstructure, resulting in a higher volume of micropores and increased loss of physical water from these micropores, thus producing higher drying shrinkage. But further analysis on the pore structure of cement paste was not provided in Lau (2017)'s study. Moreover, the author also pointed out that expansion of MgO under restrained condition was beneficial in reducing drying shrinkage. The restrained MgO expansion can induce prestress in cement to offset the tensile force induce by shrinkage.
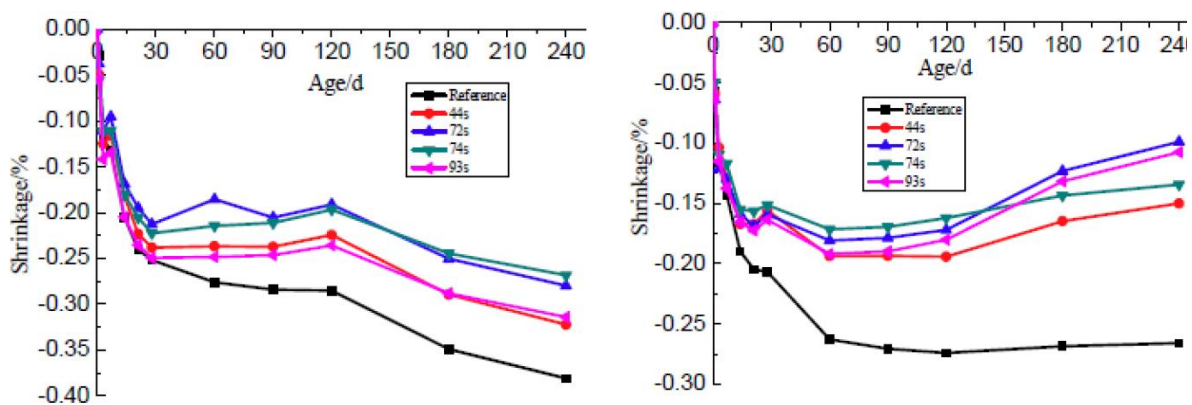
Figure 2.26 Effects of MgO with different reactivity MgOs ranging from 44 s to 93 s at a content of 10% on autogenous shrinkage reduction in Portland cement pastes cured in air of RH 60% at (a) 20 °C and (b) 30 °C (Li 2010).

For the use of MgO in OWC systems, Jafariesfad & Geiker (2017) recently investigated the effects of nano-sized MgO produced at lower temperatures (500–1000 °C) for compensating autogenous shrinkage at 40 °C. Compared to conventional hard-burnt or dead-burnt MgO additives, nano-sized MgO has higher reactivity due to its finer particle size and larger SSA.

53

Four types of nano-sized MgO with different reactivities, NM-500 >NM-700 >NM-900 >NM-1,000, were studied in their research. The results showed that the addition of all nano-sized MgOs generally reduced the shrinkage strains relative to the reference system and macro-sized MgO at 40 °C (Figure 2.27). Among four nano-sized MgOs, NM-700 with medium reactivity provided the highest early expansion and eliminated the bulk shrinkage of the cement system, while the most reactive NM-500 was less efficient at 40 °C because it hydrated too fast to provide adequate expansion in the cement system at the right time after cement setting. It was highlighted that the expansion provided in the cement system before the setting time was insufficient to compensate for the bulk shrinkage. Therefore, they concluded that highly reactive nano-MgO could be useful for low-temperature applications (less than 40 °C) but nano-MgO with lower reactivity might be required at higher curing temperatures. They also pointed out that the hybrid use of nano-MgOs with different reactivities might be a promising method to compensate for shrinkage at different ages.
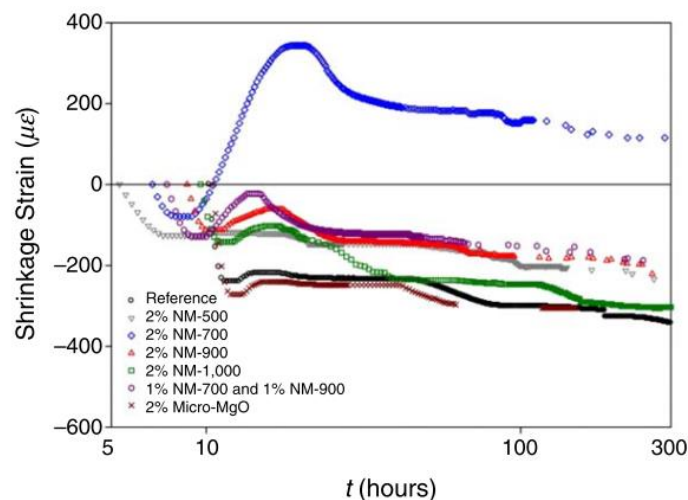
Figure 2.27 Bulk shrinkage reduction of four types of Nano-MgOs with different reactivity in class G cement systems cured at 40 °C (Jafariesfad & Geiker 2017).

2.2.3.3   Effect of MgO on the properties of oil well cement system

Compressive strength is one of the target values used to determine the wellbore integrity in current official guidelines and field practices. The effect of MgO on compressive strength in oil well cement has been investigated. Rubiandini (Rudi Rubiandini 2000) studied the effect of

MgO with different burnt temperatures on the compressive strength of class G cement. The results (Figure 2.28a,b) showed that the addition of MgO resulted in reduction of the cement compressive strength, which further decreased as the MgO content increased, although generally it was still higher than the recommended minimum value (1000 psi). For a lower curing temperature of 100 ^{o}C, cement pastes with MgO burnt at 1200 ^{o}C showed the least reduction in compressive strength. At a higher temperature of 150 ^{o}C, MgO burnt at 1300 ^{o}C was more efficient. Buntoro et al. (Buntoro et al. 2001) reported similar reduction trends in the influence of MgO (burnt at 1200 ^{o}C and 1300 ^{o}C) on the development of compressive strength of oil well cement pastes. The influence of MgO on the mechanical performance of cement depends on the influence of expansion produced on the microstructure of the cement matrix. Expansion may increase the pore size and total pore volume and induce microcracks in the matrix, which is detrimental to the mechanical strength as well to the durability of the cement matrix. Li (2010) investigated the pore structure development of mortar with MgO additives and reported an increase in porosity and volume of macropores (>50 nm) with increasing MgO content. This could be the main cause of strength reduction.

(a)   (b)
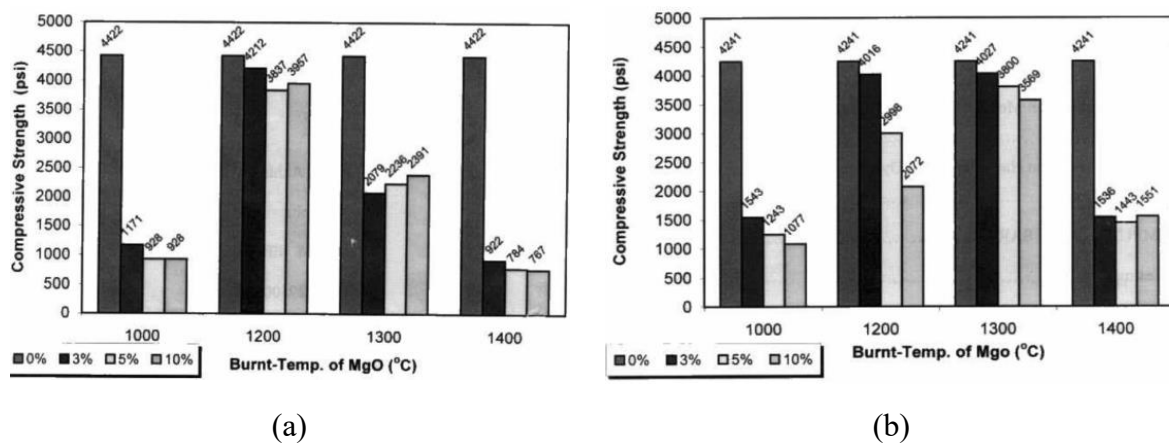
Figure 2.28 Effect of MgO with different burnt temperaturs (1000–1400 ^{o}C) at proportions of 3%, 5%, and 10% on the compressive strength of oil well cement cured at (a) 100 ^{o}C and (b) 150 ^{o}C (Rudi Rubiandini 2000).

However, restraints on the expansion were found to be able to make up for its negative effect on the strength. Under restrained conditions, the expansion of MgO causes densification in the cement matrix which in turn contributes to the increase in mechanical strength (Li et al. 2012; Zhu et al. 2013). Zhu et al. (2013) reported that under three-dimensional constraints the

expansive force generated by MgO hydration could improve the compressive strength and reduce the porosity of oil well cement.The compressive strengths of constrianed cement pastes with MgO curing at 80 ºC for 3 days and 7 days were 27. 5 MPa and 31. 6 MPa, which increased by 41. 8% and 49.1% compared to that of the free-expansion ones, respectively. The porosity of cement with MgO under three-dimensional constraints, was 22.7%, which decreased by 16.8% compared to that of the free-expansion oil well cement pastes, and the pore size tended to be smaller as well (harmless pores).

The addition of MgO has also been reported to be beneficial in improving the shear bond strength of oil well cement. According to Rubiandini (2000) and Buntoro et al. (2001), cement pastes with MgO had higher shear bond strengths compared to the control samples, and the shear bond strength generally increased with increasing MgO content. The cement expanded to eliminate void spaces between the interfaces, therefore improving the mechanical tightening of the cement against the casing and formation.

Apart from the mechanical properties of hardened cement, the addition of MgO can also affect the fresh properties of cement pastes. Liu et al. (1992) reported the retardation of cement hydration and the increase of the setting time by addition of MgO, which might be ascribed to both the decrease in the $Ca(OH)_2$ saturation ratio due to the formation of $Mg(OH)_2$ and the precipitation of $Mg(OH)_2$ on the surface of the cement grains forming a protective layer. The retardation influence of the MgO addition on oil well cement pastes was also reported by (Thomas et al. 2014). However, there are still very limited reports on the effects of MgO addition on other fresh properties of oil well cement such as the rheology.

2.3   Self-healing technology in cementitious materials

2.3.1 Overview

In recent years, self-healing technologies have been widely investigated for damage management in cement and concrete structures. Self-healing cement-based materials have the built-in capability to repair structural damage autonomously or with the minimal help of an external stimulus (De Rooij et al. 2013). Compared to conventional remedial cementing, this new damage management paradigm seems to be a very promising approach to addressing

cement damage issues in the wellbore. The self-healing properties of the cement can provide a durable cement sheath, long-term zonal isolation, and reliable cement sheath repair to preserve well integrity (Schlumberger 2014). Such potential for self-healing cements has raised great interest from the oil and gas industries, driving the extension of research into self-healing cement-based materials from the concrete structures on the ground to the underground wellbore cement sheath.

In general, self-healing in cementitious materials can be grouped into two major categories: autogenous healing and autonomic healing (Van Tittelboom & De Belie 2013). As shown in Figure 2.29, autogenous healing is the self-healing process where the recovery process uses its own generic materials components of the cementitious matrix. Autonomic healing depends on the intervention of external healing agents introduced by engineered approaches including microencapsulation, vascular networks, and other healing methods.
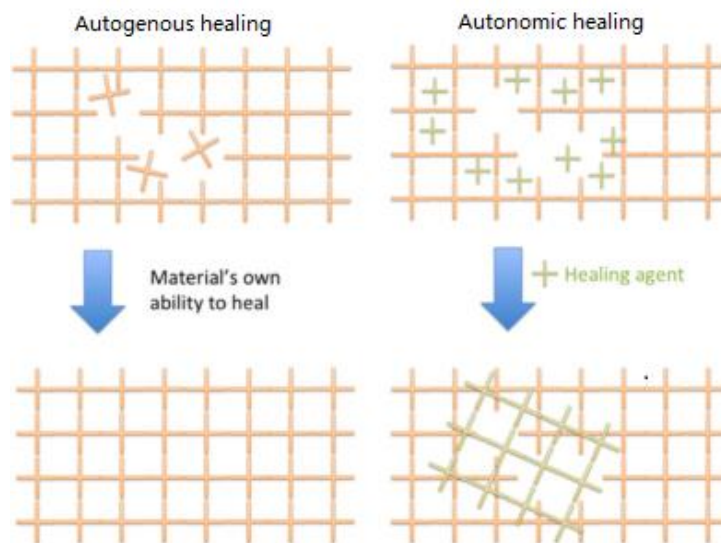
Figure 2.29 Two main categories of self-healing: Autogenous healing and Autonomic healing (Mangadlao et al. 2015).

2.3.2 Autogenous self-healing

All cementitious materials possess some innate self-healing capability and are able to repair limited-width cracks without the need for external healing agents under favourable conditions. The self-healing of cracks in fractured concrete was first observed by the French Academy of

Science in 1836 in water retaining structures, culverts, and pipes, as concrete possesses some natural autogenous healing properties (Hearn & Morley 1997). This self-healing phenomenon raised the attention of researchers and has been intensively studied.

The autogenous healing of cementitious materials is a combination of complicated physical, chemical and mechanical processes, as illustrated in Figure 2.30. Three main mechanisms are involved in the autogenous healing process: (1) further hydration of unhydrated cement particles; (2) recrystallization of portlandite ($Ca(OH)_2$) leached from the bulk paste; (3) formation of calcite ($CaCO_3$) (Huang et al. 2016). Continuing hydration is the main driving force for autogenous healing at an early age due to the relatively high content of unhydrated cement, while the recrystallization of portlandite and formation of calcium carbonates becomes dominant at a later age (Van Tittelboom & De Belie 2013). In addition, the swelling of the hydrated cementitious matrix in the crack flanks, blocks cracks by debris in the water and loose cement particles from the fracture surface can also contribute to autogenous healing (De Rooij et al. 2013).

Among all of the possible healing mechanisms, the formation of calcium carbonates is believed to contribute the most to self-healing (Edvardsen 1996). The crack closure can be attributed to the formation and growth of calcium carbonate crystals at both surfaces of the crack which then bridge the gap. This process starts with the leaching of calcium ions (Ca^{2+}) from the cement matrix and into cracks. In the presence of water and dissolved CO_2, Ca^{2+} will crystallise to form $CaCO_3$. The chemical reaction process is illustrated by the following equations (Wu et al. 2012):

$$H_2O + CO_2 \leftrightarrow H_2CO_3 \leftrightarrow H^+ + HCO_3^- \leftrightarrow 2H^+ + CO_3^{2-} \qquad \text{Equation 2.5}$$

$$Ca^{2+} + CO_3^{2-} \leftrightarrow CaCO_3 \ (pH_{water} > 8) \qquad \text{Equation 2.6}$$

$$Ca^{2+} + HCO_3^- \leftrightarrow CaCO_3 + H^+ \ (7.5 < pH_{water} < 8) \qquad \text{Equation 2.7}$$
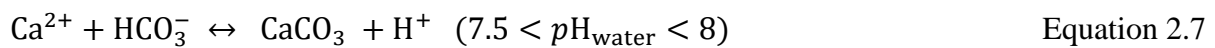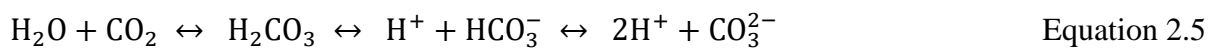
The $CaCO_3$ precipitation process is mainly affected by the concentration of calcium ions, dissolved inorganic carbon, the pH, and the availability of nucleation sites. In the cracking area, precipitation of $CaCO_3$ is reported to mainly occur at the crack mouth where the concentration of CO_3^{2-} is greatest (Sisomphon et al. 2012). As illustrated in Figure 2.31, a high concentration of calcium ions released from the matrix reacts with carbonates (CO_3^{2-}) and bicarbonates (HCO_3^-) from the surrounding water. Significant precipitation of calcium carbonates can be

then observed at the crack surface. Less precipitation can be seen at deeper locations due to the relatively lower concentrations of CO_3^{2-} and HCO_3^-.

However, this natural autogenous healing capability of cement is very limited and is hard to control. The autogenous healing is usually limited to tight crack widths up to 0.15 mm and preferably less than 0.05 mm (Reinhardt & Jooss 2003). Autogenous healing can be more difficult for oil well cement, especially in the extreme downhole environment. Elevated temperatures will significantly accelerate and enhance the hydration of the cement matrix. This means that most cement may be completely hydrated before cracking occurs, and thus very little unhydrated cement will be available for autogenous healing.

Therefore, external interventions are needed to help promote autogenous healing, such as an adequate water supply, enhancement of hydration and crystallisation, and addition of encapsulated healing agents (Van Tittelboom & De Belie 2013). These engineered methods for enhanced autogenous self-healing can also be categorised as autonomic self-healing, and will be discussed in detail in the following section.
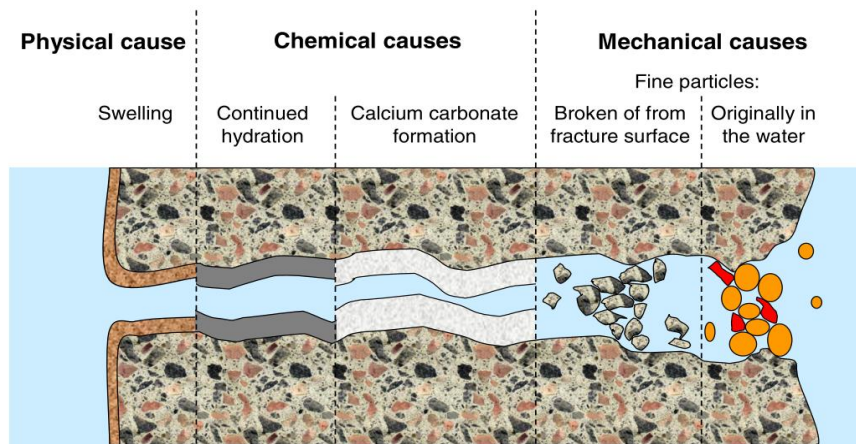
Figure 2.30 Physical, chemical and mechanical causes for autogenous healing process in cementitious materials (De Rooij et al. 2013).
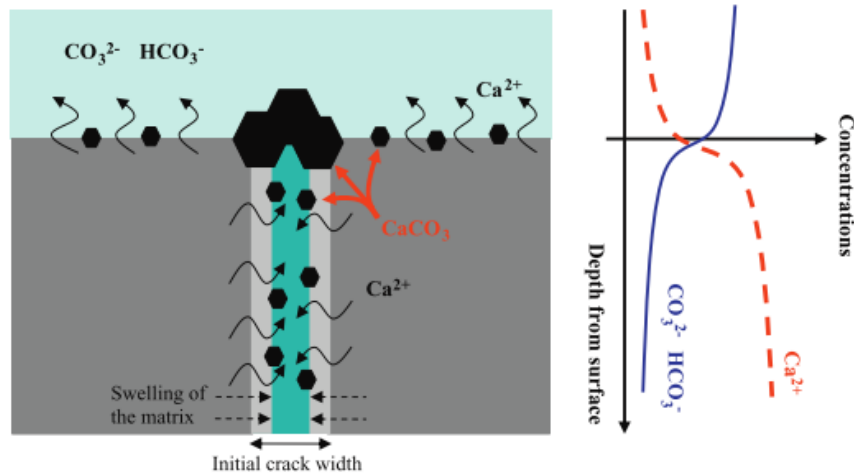
Figure 2.31 Illustration of calcium carbonate formation in the autogenous healing of a cementitious system (Sisomphon et al. 2012).

2.3.3 Autonomic self-healing

2.3.3.1   Overview

Autonomic self-healing is defined as a self-healing process where the recovery process uses materials components that would otherwise not be found in the material (engineered additions) (De Rooij et al. 2013). In autonomic self-healing systems, the healing can be achieved through three main routes: (1) the addition of super absorbent polymers (SAPs) or mineral admixtures to stimulate autogenous healing; (2) the use of bacterial spores and nutrients for microbiologically induced calcite precipitation (MICP); or (3) embedding encapsulated healing agents.

SAPs have been used in cementitious materials as a feasible way to provide additional water supply for promoting further hydration (Van Tittelboom & De Belie 2013). SAPs have the ability to absorb a large amount of water and swell substantially. As shown in Figure 2.32, they can release the water content slowly during cement hydration. After releasing water, the hydrogel particles shrink and leave behind small macro-pores. Concurrently, upon cracking, the crack is likely to propagate through the macro-pores created by the SAPs particles. The entry of moisture through the crack will cause the shrunk hydrogels at the cracking surface to swell again, eventually sealing the cracks (Lee et al. 2010; Mangadlao et al. 2015). Meanwhile, a variety of mineral admixtures have been proposed to improve autogenous healing by

promoting crystallization and sedimentation in the cementitious matrix. These include supplementary cementitious materials (SCMs) such as silica fume, blast furnace slag (Jaroenratanapirom 2010; Huang et al. 2014), which are able to react with $Ca(OH)_2$ to form crystalline products, mainly C-S-H. The use of expansive additives such as calcium sulfoaluminate (CSA), CaO and MgO has also been reported. The formation of products (such as ettringite, $Ca(OH)_2$ and $Mg(OH)_2$) with expanded volume can help bridge and seal the cracks (Sisomphon et al. 2012; Qureshi 2016).
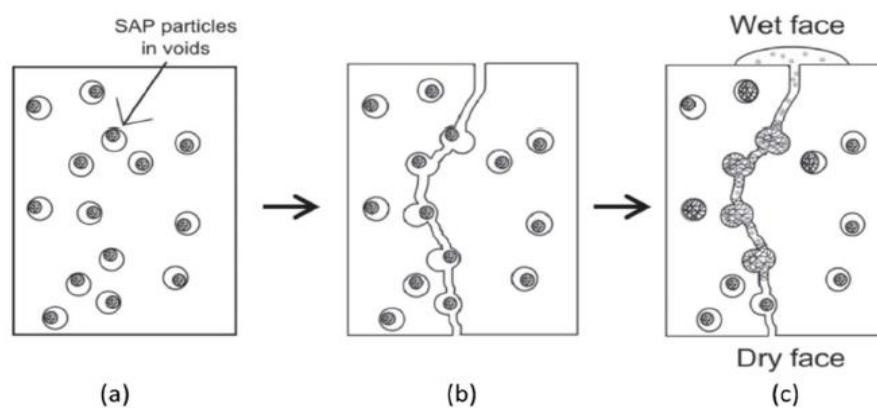
Figure 2.32 Mechanism of enhanced autogenous healing using hydrogels/super absorbent polymers (SAP) (Mangadlao et al. 2015).

Specially for OWC systems, a technology of Schlumberger used the swelling properties of the polymer styrene–isoprene–styrene (SIS) and styrene–butadiene–styrene (SBS) particles in the presence of gaseous hydrocarbons at various temperatures to give the oil well cement self-healing capabilities when exposed to hydrocarbons (Schlumberger 2010; Mangadlao et al. 2015). When hydrocarbons from the formation come in contact with the particles, the particles swell and then block the crack. Similarly, Lu et al. (2016) used an oil swellable polymer to modify the cement paste to improve the crack self-healing property triggered by oil leakage.

Other than the hydrocarbon or oil swellable polymers, research into most of the above mentioned additives for self-healing has focused on their use in ordinary cement systems, but very limited use has been found in OWC. The borehole environment with high temperature and high pressure can be very hostile to the survivability of bacterial species (Lu et al. 2016). This self-heling technique is therefore unsuitable for use in oil well cement systems. In contrast,

many mineral-based additives like MgO, CaO, and silica fume usually possess good stability under high temperature and high pressure conditions, which allows for their application in oil well cement systems. Furthermore, compared to hydrogels and oil/hydrocarbon swellable polymers, mineral additives have the advantage in that their healing products are compatible with the cement matrix. However, these mineral additives have the obvious disadvantage that they may react immediately on contact with water if they are added directly into the cement without protection. In fact some may even be completely consumed prior to cracking, resulting in reduced self-healing effectiveness. Accordingly, encapsulation of the healing agents has been proposed as a feasible way to ensure their release at suitable times.

2.3.3.2 Delivery methods of healing agents

The direct application of healing agents without protection and controlled release may render the agents ineffective and even cause negative effects on the cement and concrete properties. Accordingly, two main delivery systems have been proposed to provide controlled, sustained, or timed release of healing agents, namely vascular systems and capsule-based systems.

As shown in Figure 2.33a, a typical vascular system functions by delivering the healing agent via a network of hollow tubes embedded in the concrete matrix. Mechanical rupture of the tubes is a common triggering mechanism to release the healing agent (Ghosh 2009). When cracks occur, the pre-embedded tubes are broken by the cracks and then release the healing agents which are absorbed into the cracks due to capillary forces. The main advantage of a vascular system is its sufficient supply of healing agent to cracks by connecting with an external source, which ensures highly efficient self-healing (Dry 1994). However, practical application usually encounters difficulty in installing a vascular system inside the concrete matrix during construction (Huang et al. 2016). Particularly for oil wells, the installation of tubes within the deep annular space of a wellbore can be very impractical.

As shown in Figure 2.33b, capsule-based self-healing systems sequester the healing agent in discrete capsules until damage triggers rupture and release of the capsule to the region of damage. White et al. (White et al. 2001) first proposed a capsule based system for self-healing by encapsulating healing agent and catalyst particles into an epoxy matrix, achieving a

promising healing result. Since then, microcapsules have been extensively studied by many researchers due to their convenience of use, although the volume of healing agent carried by capsules is limited in comparison with that of a vascular system. The capsules can be mixed into concrete admixtures in a similar way to normal additives during the construction process. These capsules can be randomly and evenly dispersed throughout the cementitious matrix (Restuccia et al. 2017). From this point of view, a capsule-based system seems to be more practical for use in an oil well cement system.

(a)   (b)
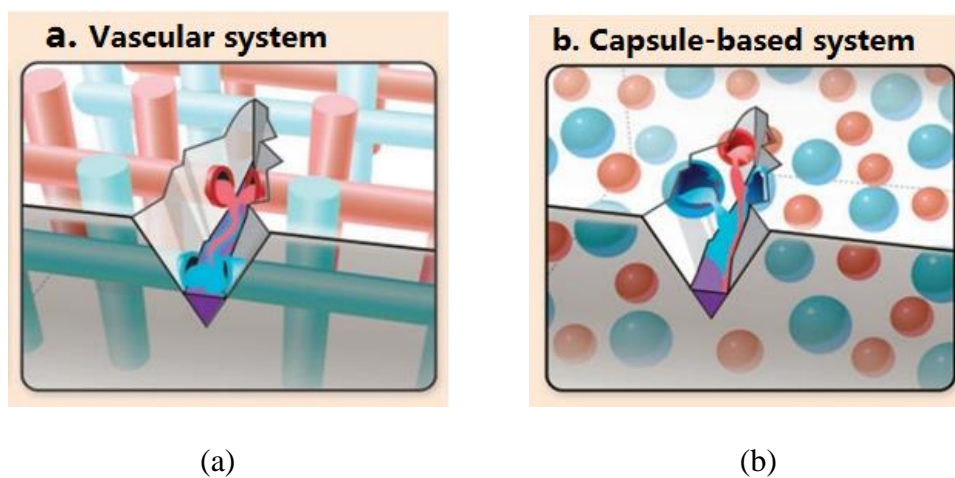
Figure 2.33 Delivery systems for healing agents (a) Vascular system; (b) Capsule-based system (White et al. 2010).

2.3.4 Capsule-based autonomic self-healing

2.3.4.1   Encapsulation methods

In a capsule based self-healing system, the capsules can be broadly divided into two groups according to their size: macrocapsule (>1 mm) and microcapsule ($\leqslant 1$ mm). Different encapsulation methods have been developed to produce macro- or microcapsules accordingly, as shown in Figure 2.34 (Souza 2017). The pan-coating and co-extrusion are commonly used for producing macron-sized capsules with solid or liquid healing agents (Ghosh 2006; Formia et al. 2015). However, macrocapsules usually have a large size that is analogous to the aggregates, but they are significantly weaker than the aggregates since they are designed to be easily ruptured upon damage. Their addition to cement and concretes can have a detrimental effect on the mechanical properties, particularly in well cementing, since there are usually no

aggregates added when preparing oil well cement slurries. The addition of such large size particles can have more negative effects on the cement sheath properties and even the well integrity. The production of smaller microcapsules thus became the interest of research.
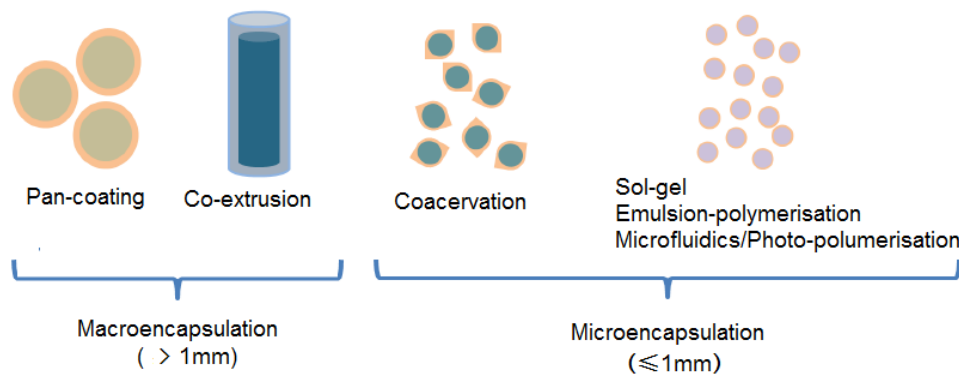
Figure 2.34 Encapsulation methods for macrocapsules ($>$1 mm) and microcapsules ($\leqslant$1 mm), adapted from (Souza 2017).

Typical production techniques for microcapsules include in situ polymerisation, interfacial polymerisation, coacervation, sol-gel and microfluidics (Ghosh 2006). In situ polymerisation is the most widely investigated chemical method used to produce microcapsules. The in situ polymerisation process generally involves the initial dispersion or emulsion of the core material (dispersed phase) within the continuous phase containing monomers and initiators that eventually form the shell material, followed by controlled capsule-shell deposition by precipitants, or a change in pH, temperature, or solvent quality, and ultimately formation of the microcapsules (Nguon et al. 2017). Interfacial polymerisation is another chemical encapsulation technique. It differs from in-situ polymerisation in that the reactants involved in the formation of the shell are present in both the dispersed and continuous phases. As a result, shell formation occurs at the emulsion interface(Nguon et al. 2017). Compared with in situ polymerisation, interfacial polymerisation is more simple and straightforward and can be accomplished as a one-step process (Perignon et al. 2015; Tan et al. 2016). This technique is therefore more conducive to industrial scale-up, which is very meaningful for the field use of self-healing microcapsules (Perignon et al. 2015). The microcapsules used in this study are produced via interfacial polymerisation.

2.3.4.2   Shell properties of microcapsules

The shells of microcapsules play a fundamental role in isolating and protecting the encapsulated core material from the environment, preventing its activation until triggered. The shell should protect the core material from the aggressive mixing process and high alkalinity of the cementitious environment during cement hydration and hardening. The shell mechanical properties are also very crucial in the triggering of healing. The shell must be sufficiently stiff to remain intact during processing, but must be brittle enough when subjected to mechanical triggering stimuli so that it can be successfully ruptured to release the core material. The shell should also have good bonding with the cement matrix at their interfaces. If the bonding is too weak, the microcapsules will debond from the matrix without rupture upon triggering. Cost is also an important concern when selecting shell materials. Table 2.10 summarises microcapsules reported in literature produced with different shell and core materials together with the encapsulation methods for self-healing cementitious materials.

Urea-formaldehyde (UF) and melamine-formaldehyde (MF) are the most commonly used shell materials in self-healing polymeric materials (White et al. 2001; Wang et al. 2009), and have also been used successfully for microencapsulation for pharmaceuticals and agricultural applications. Drawing from their advantages in other fields, they have found similar popularity for use as shell materials in self-healing cementitious materials. UF especially has become the dominant shell material as listed in Table 2.10. Apart from UF and MF, phenol-formaldehyde (PF), double walled-PU/PF, and polystyrene (PS) have also been used for the production of microcapsules via in situ polymerisation techniques. Meanwhile, polyurethane (PU) and polyurea (PUrea) are typical shell materials used to produce microcapsules by the interficial polymerisation technique. PU and PUrea have excellent mechanical properties and chemcial stability that are suited for microencapsulation. More importantly, PU and PUrea microcapsules have the advantage in terms of the simple polymerisation process as mentioned above in Section 2.3.4.1.

Table 2.10 Summary of microcapsules produced via different encapsulation methods for self-healing cementitious materials (adapted from (De Belie et al. 2018)).

Encapsulation method	Shell	Core	Diameter (µm)	Shell thickness (µm)	References
Emulsion polymerisation (in situ polymerisation or interfacial polymerisation)	UF	Epoxy	~166	4–8	(Wang et al. 2013) *
			100–250	5.46	(Dong et al. 2016)*;(Dong et al. 2017)*
			~122	5.46	(Wang et al. 2017)*
		DCPD	81-987	0.2–0.3	(Gilford III et al. 2014)*
		SS	134–701	0.4-0.7	
		MMA	~1.9	N/A	(Litina et al. 2014)** (Litina 2016)**
		Calcium nitrate	41–106	0.61–1.31	(Hassan et al. 2016)*; (Milla et al. 2016)*
	PU	MMA	~0.3	N/A	(Litina et al. 2014)*
		CS	60–120	N/A	(Tan et al. 2016)**
			30–60	N/A	(Litina 2016)*
		SS	40–800	N/A	(Pelletier et al. 2010)**
		SS	22–47	N/A	(Beglarigale et al. 2018)**
	PU/UF	SS	~322	N/A	(Mostavi et al. 2015)*
	PUrea	SS	~130	N/A	(Giannaros et al. 2016)**; Thies Technology Inc
	PS	Epoxy	100–150	N/A	(Li et al. 2013)**
	PF	DCPD	50–600	~10–40	(L. Lv et al. 2016)**
	MF	Epoxy	10–1000	1.1–2.4	(Li et al. 2016)**
Complex Coacervation	Gelatine/ Gum Acacia	SS solution in oil (1:1)	290–700	5–20	(A. Kanellopoulos et al. 2016); (Kanellopoulos et al. 2017) Lambson Ltd
Sol-gel	Silica	Epoxy	5–180	2	(Perez, Erkizia, et al. 2015)
		MMA	~1.9	N/A	(Litina et al. 2014)
		MMA	~4	N/A	(Yang et al. 2011)
Microfluidics/ Photo-polymerisation	Acrylate	CS, SS, Oil, CS,SS in oil	80–120	7, 12	(Souza 2017)

* in situ polymerisation, ** interfacial polymerisation
CS: Colloidal silica, DCPD: dicyclopentadiene, MMA: methylmethacrylate, PF: phenol formaldehyde, PU: polyurethane, PUrea: polyurea, PS: polystyrene; MF: melamine-formaldehyde, UF: urea formaldehyde, SS: Sodium silicate

The mechanical properties of microcapsules are very crucial since the fracture behaviour upon triggering stimuli as well as survival during mixing largely depend on their mechanical properties. First of all, the nature of shell material essentially determines the mechanical properties of microcapsules. Therefore, those polymeric shell materials with adequate stiffness as well as brittleness as introduced above are favourable for production of microcapsules. In the meantime, parameters such as the diameter and shell thickness also have significant influence on the mechanical properties of microcapsules, and further affect their fracture behaviour. Lv et al. (2016) investigated the rupture force of PF microcapsules with different sizes and shell thicknesses using nanoindentation as well as their fracture behaviour when embedded in cement paste using X-ray computed tomography (XCT). It was found that both an increase in diameter and in shell thickness led to a higher rupture force, as shown in Figure 2.35. By looking at 3D reconstructed images of the crack surface obtained by XCT (Figure 2.36), it was observed that smaller sized microcapsules tend to be more mechanically triggered by the crack while larger sized microcapsules were more prone to be pulled out from the matrix without rupture. It is therefore important to control and optimize the capsule size and shell thickness to obtain microcapsules with optimal mechanical strength.

(a)   (b)
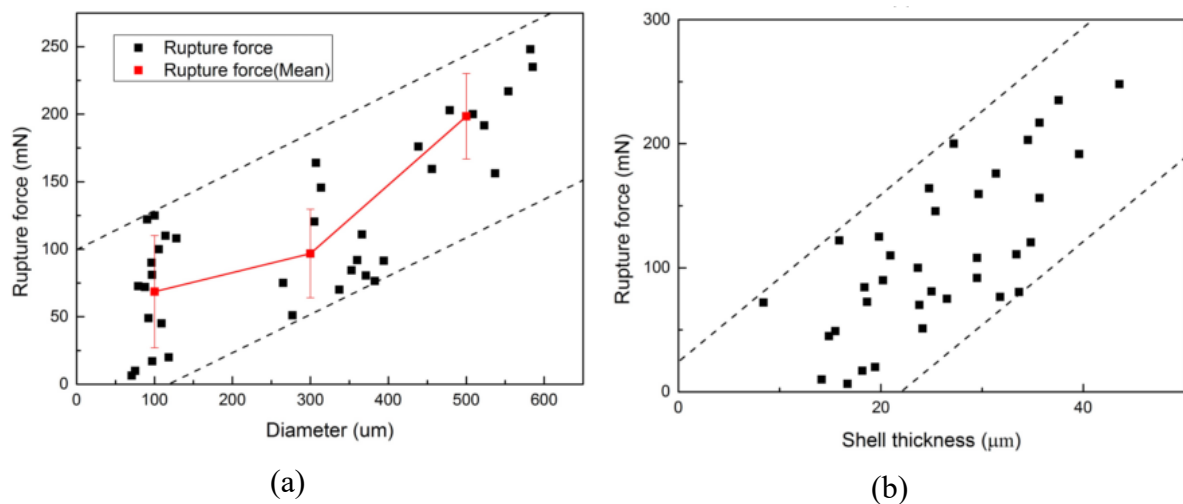
Figure 2.35 The relationship between the rupture force of PF microcapsules and their (a) diameter; (b) shell thickness (Leyang Lv et al. 2016).
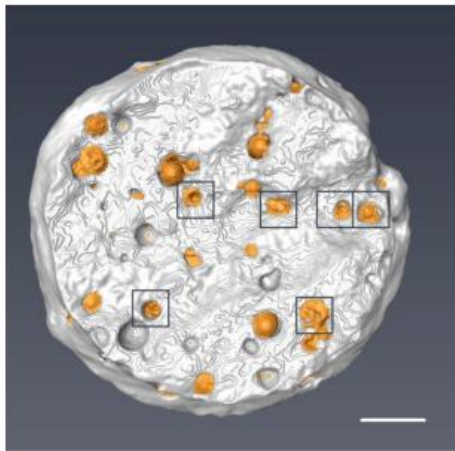
Trigger ratio of microcapsules		
Diameter(μm)	Rupture MC (%)	Unruptured MC +voids (%)
400-600	8.6	91.4
200-400	20.7	79.3
50-200	34.7	65.3

Figure 2.36 3D reconstructed images of the fractured cement surface with the ruptured microcapsules marked with black box, and the trigger ratio of microcapsules with different diameters (Lv et al. 2016).

To achieve good survivability and long shelf life, the chemical resistance and thermal stability of microcapsules are just as important as their mechanical properties. Good chemical resistance ensures the survival of the microcapsules in the aggressively high alkaline cementitious environment. The polymeric materials such as PF, PU and PUrea, are well known for their excellent chemical resistance. Therefore, the resultant microcapsules are very likely to be able to survive well in the highly alkaline environment. For example, Lv et al. (2016) investigated the chemical resistance of PF microcapsules by exposing them to a saturated $Ca(OH)_2$ solution ($pH_{max}>13$) that simulated the alkaline cementitious matrix pore solution for 48 h. The authors found that the highly alkaline environment of the concrete pore solution has minor influence on the synthesized microcapsules.

On the other hand, in a special high-temperature environment such as an underground wellbore, thermal stability is a particularly important concern for the survival of microcapsules under exposure to sustained high temperature. Research into microcapsules for self-healing cementitious materials has so far mainly focused on their use under ambient conditions, and less attention has been paid to the thermal stability issue. Nonetheless, the thermal stability of microcapsules has been widely investigated in their application with self-healing polymer composites that are subjected to a wide range of processing temperatures. The commonly used shell wall materials UF, MF, PU, PF, and PUrea generally possess good thermal stability up to

~150–250 ºC (Wang et al. 2009; Qiao et al. 2018; Chowdhury et al. 2015; Jinglei et al. 2008; Scarfato et al. 2007), which makes it possible to use the resultant microcapsules under high temperature conditions. For each category of shell material, the thermal properties of the shell wall are mainly dependent on the shell composition, that can vary with the monomer types and ratios used for wall formation. For example, Hong & Park (2000) reported that the reactivity of diamine monomer and the length of flexible methylene chain in diamine have decisive influence on the thermal properties of resultant polyurea shell membrane. The polyurea shell membrane composed of hard diamine monomer has higher thermal stability than the shell composed of soft monomer or a mix of hard and soft ones. Therefore, for each type of newly developed microcapsule, it is necessary to examine its thermal properties before applying to high temperature condition.

2.3.4.3   Healing agents

2.3.4.3.1   Adhesive healing agents and mineral-based healing agents

There are several main considerations for suitable healing agents in a capsule-based self-healing system (Joseph et al. 2010; Van Tittelboom & De Belie 2013). Firstly, a suitable agent should be sufficiently mobile to allow migration to the areas of damage following release. Secondly, in addition to the air and water tightness of the crack after healing, regaining mechanical properties is also desirable so that crack re-opening can be resisted post-healing. Thirdly, in order to improve long-term durability, the agent should also have sufficient longevity and compatibility with the cementitious matrix over the lifetime of the structure. Healing agents may need to be resistant to extreme environments such as high temperatures, dependent on the application. Additionally, for practical field application, it is important that the chosen healing agent be cost-effective and readily available for encapsulation.

Generally, healing agents usually work in four different ways after successful release: (1) they can either react with moisture, air or heat (one-component system); (2) reaction with a second component which is present in the matrix; (3) reaction with components provided by additional capsules (two or multi-components system); or (4) reaction with the cementitious matrix itself (Mangadlao et al. 2015). The healing agents microencapsulated for self-healing cementitious

materials listed in Table 2.11 can be broadly categorized into two groups: (1) adhesive healing agents, including epoxy, methylmethacrylate (MMA) and dicyclopentadiene (DCPD); and (2) mineral-based healing agents, including sodium silicate, colloidal silica, and calcium nitrate.

Table 2.11 Summary of the two main groups of healing agents encapsulated for self-healing cementitious materials in the literature: (1) adhesive agents and (2) mineral based agents.

Category	Healing agent	Healing mechanism	References
Adhesive agents	Epoxy resin	Two components react and become hardened	(Wang et al. 2013); (Wang et al. 2017); (Dong et al. 2016); (Dong et al. 2017); (Li et al. 2013); (Perez, Erkizia, et al. 2015); (Perez, Gaitero, et al. 2015); (Li et al. 2016)
	MMA	Two or multiple components react and become hardened	(Yang et al. 2011)
	DCPD	Two components react and become hardened	(Gilford III et al. 2014); (Leyang Lv et al. 2016); (L. Lv et al. 2016)
Mineral-based agents	Sodium silicate	Reacts with the cementitious matrix itself to produce further hydration products	(Gilford III et al. 2014); (Mostavi et al. 2015); (A. Kanellopoulos et al. 2016); (Kanellopoulos et al. 2017); (Giannaros et al. 2016); (Beglarigale et al. 2018)
	Colloidal silica		(Kanellopoulos et al. 2015); (Tan et al. 2016); (Litina 2016)
	Calcium nitrate		(Hassan et al. 2016); (Milla et al. 2016)

Adhesive agents are advantageous in helping seal cracks rapidly and restoring the mechanical properties of cementitious materials. Nonetheless, long-term durability after healing is a great concern for self-healing cementitious materials. Adhesive agents possess a certain inferiority due to their aging problems and low compatibility with the cementitious matrix. Meanwhile, adhesive agents also show some disadvantages in terms of their use under extreme temperatures. For example, microencapsulated DCPD has been reported to have low thermal stability because of the higher expansibility of DCPD during the heating process that can easily fracture the microcapsules (Yuan et al. 2006). MMA adhesive agents are not suitable for use at extreme temperatures due to their flammability. In addition, their relative high cost as well as safety and

environmental concerns have brought more challenges when it comes to practical field application. Therefore, researchers have turned to mineral-based materials as alternative healing agents.

Mineral-based agents have been widely reported to have good compatibility and cost-effective performance. They generally rely on chemical reaction with the cement matrix or with water or CO_2, producing hydration and carbonation products similar to the cementitious matrix. The use of mineral healing agents in cementitious material is likely to cause fewer material compatibility problems than their polymeric counterparts (Schlangen & Joseph 2009). Alkali-silica based mineral agents such as sodium silicate and colloidal silica can react with calcium hydroxide in the cement matrix to form further hydration products (C-S-H gel) which can seal the cracks and provide increased strength recovery (Mihashi et al. 2000). Sodium silicate is the most frequently investigated alkali-silica based agent for autonomic self-healing cementitious materials. As shown in Table 2.11, sodium silicate agents either in the liquid or solid state have been microencapsulated with different shell walls (UF, PUrea, UF/PF, gelatine/gum acacia). More details on sodium silicate healing agents will be reviewed in the following section.

2.3.4.3.2   Sodium silicate healing agent

Sodium silicate, also known as waterglass, is the common name for compounds with the formula $(Na_2SiO_2)_nO$. This series of materials is available in aqueous solution and in solid form. In well cementing, sodium silicate is the most commonly used chemical extender for cement slurries, reducing slurry density and increasing the yield of cement slurry (Broni-bediako et al. 2016). It is also used as a sealer to enhance waterproofing and improve the durability of concrete. In recent years, sodium silicate has found a promising new application as a self-healing agent in cementitious materials.

Sodium silicate can react with calcium hydroxide, a main product of cement hydration, and produce calcium-silica-hydrate (C-S-H) gel which is a binding material natural to the cementitious matrix. The newly formed C-S-H gel acts as a binder and healer in cracks and pores, bridging the gaps between cracking surfaces and allowing some recovery of strength (Pelletier et al. 2010; Huang & Ye 2011b). The relevant chemical reaction is shown in Equation

2.8. It is generally agreed among researchers that the main mechanism of self-healing promoted by sodium silicate is the reaction between dissolved sodium silicate and calcium cations available within the cracking area to yield C-S-H gel (Mihashi et al. 2000; Huang & Ye 2011a; Pelletier et al. 2010; Ouarabi et al. 2017). If there are insufficient calcium cations to react with, the still available sodium silicate crystallizes when the water of the solution evaporates or is transported into the cementitious matrixes, which also contributes to healing the cracks (Huang & Ye 2011a).

$$Na_2O \cdot SiO_2 + Ca(OH)_2 \rightarrow x\,(CaO \cdot SiO_2) \cdot H_2O + Na_2O \qquad \text{Equation 2.8}$$
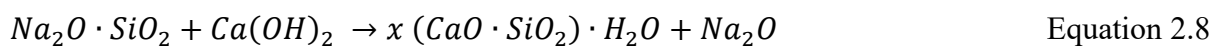
To better understand the reaction mechanism of sodium silicate as a healing agent, Irico et al. (2017) recently investigated the chemical reactivity of sodium silicate with hydrated Portland cement. In situ X-ray powder diffraction was used to assess the degree of reaction of the crystalline hydrated cement phases with sodium silicate over a timescale of hours and days (up to 7 days). According to the XRD patterns of cement samples mixed with sodium silicate in Figure 2.37a, a very quick consumption of ettringite (at 9.1, 15.8, 22.9 and 34.9º2θ) was observed within the first few hours, along with a gradual decrease of portlandite peak intensities accompanied by a significant increase in the main peaks of crystalline C-S-H (tobermorite) within the region around 30º2θ. These results indicate the reaction of sodium silicate with the aluminate hydrated phases (AFt/AFm) and portlandite to produce both C-S-H and C-A-S-H phases. In contrast, the presence of crystalline C-S-H was not detected in the samples mixed with water alone (Figure 2.37b). Similarly, Giannaros et al. (2016) tested the reactions between sodium silicate agents released from microcapsules with hydrated cement pastes using XRD analysis and observed a clear reduction in portlandite peak intensities when C-S-H peaks increased.

Based on the healing products formed by these reactions, sodium silicate as a healing agent is able to provide effective healing in terms of mechanical strength recovery and durability recovery, which will be discussed in detail in the following Section 2.3.5.

(a)

(b)
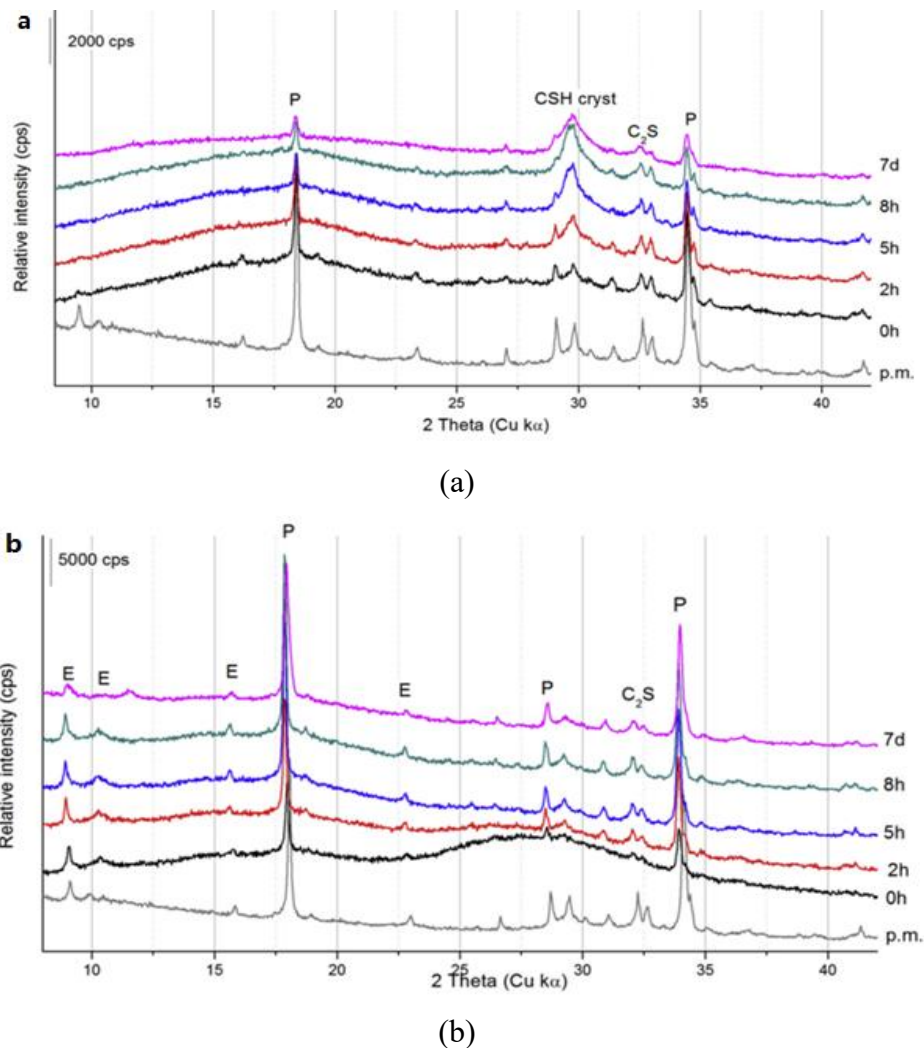
Figure 2.37 XRD diffraction of ground cement pastes; (a) Treated with sodium silicate solution (sample S); (b) Treated with water (sample W), P= Portlandite, E=Ettringite (Irico et al. 2017).

2.3.5 Self-healing efficiency of microcapsule-based cementitious materials

Self-healing efficiency in cementitious systems is usually assessed according to three aspects: (1) regained tightness, such as gas tightness, water tightness, corrosion resistance, etc.; (2) regained mechanical properties, such as compressive strength, flexural strength, stiffness, etc.; (3) visualisation of the healing process and determination of crack healing and healing products, such as visualisation of the release of agent, measurement of crack width and crack depth, characterisation of healing products, etc. Commonly used techniques for evaluating self-healing efficiency are listed in listed in Table 2.12. This section reviews the healing

performance of microcapsule-based self-healing cementitious materials reported in the literature. A summary is given in Table 2.13.

Table 2.12 Commonly used techniques for self-healing efficiency in cementitious materials (adapted from (Van Tittelboom & De Belie 2013)).

Recovery properties	Evaluation techniques	Description of techniques
Recovery in tightness	Water permeability/low or high pressure	Water flow through cracks
	Gas permeability	Gas flow through cracks
	Capillary water uptake	Capillary water uptake by crack
	Neutron radiography	Visualize capillary water uptake by crack
	Corrosion test	Resistance against corrosion
	Frost salt scaling Chloride	Resistance against frost salt scaling
	Chloride diffusion	Resistance against chloride ingress
	Osmotic pressure	Resistance against ion ingress
	Ultrasonic transmission measurements	Continuity of material and crack depth measurement
Recovery in mechanical properties	Compression test	Regained strength, stiffness and/or energy when reloading the healed specimen
	Tensile test	
	Three/four point bending test	
	Acoustic emission analysis	Regained energy/Notice capsule breakage
	Resonance frequency analysis	Regained stiffness
Visualization and determination	Optical microscopy and image analysis	Visualization of healing products and determination of healing rate
	Scanning electron microscopy	Visualization and determination of healing products
	X-ray radiography/ tomography	Visualization release of healing agent (in 3D with X-ray tomography)
	Digital image correlation	Visualization of crack closure
	Thin section analysis	Visualization of healing products inside crack
	X-ray diffraction analysis	Determination of crystalline materials
	Thermogravimetric analysis	Quantitative material characterisation
	Raman spectroscopy	Determination of chemical composition
	Infrared analysis	Determination of precipitated products

Table 2.13 Summary of the healing performance of microcapsule-based self-healing cementitious materials.

Shell	Core	D (μm)	Content (%)	Self-healing performance	References
UF	Epoxy	~166	3, 6, 9 *	Compressive strength (↑) Flexural strength (↑) Chloride ion permeability (↓)	(Wang et al. 2013)
		100–250	2, 4, 6, 8*	Compressive strength (13%↑) Healing ratio against chloride ion penetration (21–46%)	(Dong et al. 2016);(Dong et al. 2017)
		~122	3, 6, 9*	Compressive strength (↑) Dynamic modulus (↑) Porosity (↓)	(Wang et al. 2017)
	DCPD	81–987	0.25*	Modulus of elasticity (30%↑)	(Gilford III et al. 2014)
	SS	134–701	0.5, 1, 2.5, 5*	Modulus of elasticity (11%↑)	
	Calcium nitrate	41–106	0.25, 0.5, 1, 2 *	Modulus of elasticity (↑) Surface resistivity (↑)	(Hassan et al. 2016)
	CS	30–60	1, 5 *	Crack area healing (43–100%) Flexural strength (18%↑) Gas permeability (30↓)	(Litina 2016)
	SS	40–800	2 ***	Flexural strength (12%↑) Corrosion inhibition (↑)	(Pelletier et al. 2010)
PU/UF	SS	~322	2.5, 5 *	Crack depth (↓) Ultrasonic wave transmission time (↓)	(Mostavi et al. 2015)
PUrea	SS	~130	4 ****	Capillary absorption (45%↓)	(Giannaros et al. 2016)
Gelatine / Gum Acacia	SS	290–700	4, 8, 12, 16, 24, 32 ****	Crack mouth healing (20–77%↑) Crack depth (↓) Capillary water absorption (54%↓)	(A. Kanellopoulos et al. 2016)
PS	Epoxy	100–150	1, 2 *	Compressive strength (↑) Stiffness (-) Water absorption (↓)	(Li et al. 2013)
MF	Epoxy	10–1000	1, 2, 4 *	Flexural strength (↑)	(Li et al. 2016)
Silica	Epoxy	5–180	5, 10 *	Capillary water absorption (↓)	(Perez, Gaitero, et al. 2015)
	MMA	~4	1.5 *	Gas permeability (67%↓)	(Yang et al. 2011)

* Addition by weight of cement, ** Addition by volume of total concrete, *** Addition by volume of water, **** Addition by volume of cement.

2.3.5.1   Self-healing performance on regaining mechanical properties

The experimental investigations on self-healing efficiency by many researchers have been focused on regaining mechanical properties. Regain will depend on many factors including the type of capsules and healing agents, the volume of released healing agents, damage levels, as well as curing conditions, etc.

Wang et al. (2013) tested the self-healing performance in terms of the strength of mortar specimens embedded with microencapsulated epoxy along with a catalyst. The effects of proportions of microcapsules, w/c ratio and preloading rate on the recovery of compressive and flexural strength were investigated. Their results showed that the mechanical recovery rate was almost proportional to the amount of microcapsules added, whereas the influence of the preloading rate and w/c were relatively weak (Figure 2.38a). In their later work, mortar specimens with similar epoxy microcapsules were tested for the recovery of compressive strength and dynamic modulus, and showed an improved strength recovery rate with increased proportions of microcapsules.

The influence of the particle size of microcapsules on the strength recovery behaviour was also reported. Dong et al. (2016) tested microcapsules (shell: UF, core: epoxy) with three different average sizes of 132, 180 and 230 μm. The mortar specimens were loaded to 70% of their peak compressive strength and healed at 50 °C for 28 days. The authors found that the specimens with larger microcapsules revealed a relatively higher healing rate of compressive strength compared to those with smaller microcapsules at all healing stages (Figure 2.38b). Larger size microcapsules seemed to be able to provide more healing agent, thus improving the healing. However, a large particle size of microcapsules does not always have a positive effect on healing. The core/shell ratio and shell thickness should also be taken into account.

In the later research of Gilford III et al. (2014), microcapsule-containing concrete cylinders were loaded to 70% of their peak compressive strength and tested for strength recovery after 48 h steam curing. The microcapsules containing DCPD and SS prepared at different pH were added into the concrete mixtures at 0.25% and 5% by weight of cement, respectively. The preparation pH of microcapsules was found to have pronounced influence on the healing

performance due to its direct effect on the shell thickness: the shell thickness of the DCPD microcapsules increased as the pH was reduced, while the shell thickness of SS microcapsules decreased with decreasing pH (Figure 2.39). At pH=3.1, both DCPD microcapsules and SS microcapsules obtained the best healing, achieving 30% and 11% increase in the modulus of elasticity of the concrete respectively. The authors therefore concluded that too-low or too-high pH values (resulting in too-thin or too-thick shell thicknesses) were detrimental to the healing performance.

(a)   (b)
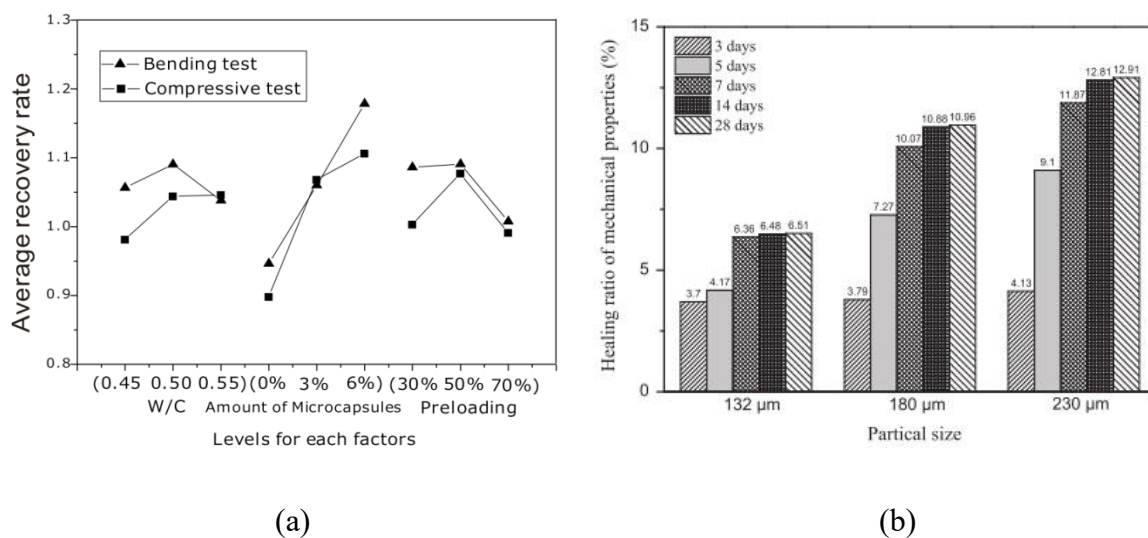
Figure 2.38 Self-healing recovery of the strength of mortar specimens containing microcapsule with UF shell and epoxy core: (a) Effect of w/c, number of microcapsules and pre-loading rate (Wang et al. 2013); (b) Effect of particle size (Dong et al. 2016).
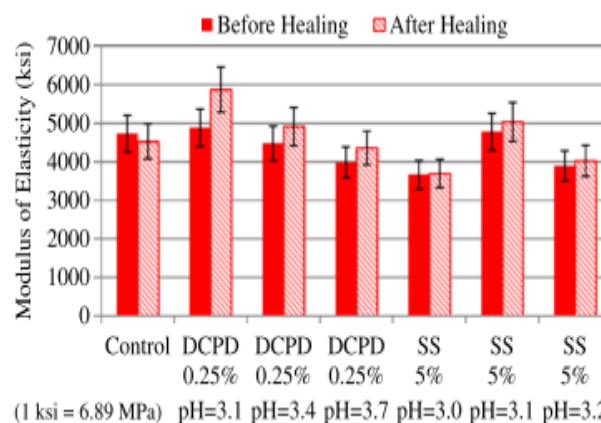
Figure 2.39 Self-healing recovery of the modulus of elasticity of concrete containing UF microcapsules with DCPD or SS with different preparation pH and addition contents (% of cement weight)(Gilford et al. 2014).

77

Pelletier et al. (2010) also assessed the mechanical strength recovery of concrete specimens containing 2% by volume PU microcapsules (40–800 μm) with SS mineral agent. The concrete specimens were loaded at 0.25 mm/min to induce internal microcracking within the sample, and were cured for 7 days in water. The microcapsule-containing specimens showed 20–26% flexural strength recovery, which was higher than the control specimens with only 10–14% recovery. However, information about influencing factors like microcapsule size and shell thickness were not reported in this study. Other types of microcapsules with mineral based agents such CS and calcium nitrate were also reported as effective in mechanical strength recovery, as shown in Table 2.13.

2.3.5.2   Self-healing performance on regaining water and gas tightness

Regaining tightness properties is another crucial criterion for evaluating the self-healing performance of cementitious materials. The durability can be increased when the self-healing of cracks results in the recovery of gas and water tightness as well as corrosion resistance. As previously mentioned, mineral healing agents have good compatibility with the cementitious matrix which can be beneficial for the durability of cement and concrete structures after healing. Therefore, researchers have paid great attention to recovery of tightness properties when investigating the self-healing performance of cementitious materials with mineral agent-based microcapsules like SS microcapsules, and various non-destructive methods have been used.

Mostavi et al. (2015) monitored and quantified the healing performance of cracked concrete specimens using portable ultrasonic non-destructive digital indicating testers to measure the crack depth and the transmission time. Double-walled polyurethane/urea-formaldehyde (PU/UF) microcapsules with SS agent were incorporated into self-healing concrete beams. The ultrasonic transmission time (Figure 2.40a) and crack depth (Figure 2.40b) measurements showed a steady decrease in the specimens with microcapsules, but largely remained unchanged in the control specimens during the healing period of 14 days. In terms of crack depth reduction, the specimens with higher microcapsule content (5% by weight of cement) had a higher healing efficiency (35%) than specimens with 2.5% microcapsules (25%). Faster healing during the first 7 days was also seen in the specimens with 5% microcapsules.
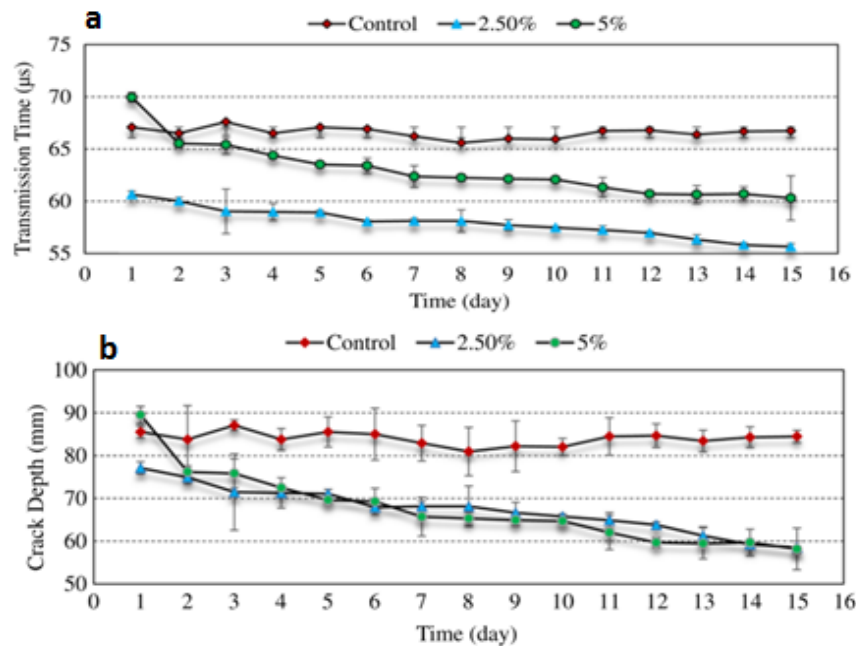
Figure 2.40 Self-healing performance of double-walled SS microcapsules in concrete specimens, measured by portable ultrasonic non-destructive digital indicating tester: (a) Ultrasonic wave transmission time; (b) Crack depth (Mostavi et al. 2015).

Kanellopoulos et al. (2016) investigated the self-healing performance of microcapsules with SS (in liquid solution) in cement pastes by combining multiple evaluation methods including capillary absorption, crack depth, and crack mouth closure measurments. The cement specimens with microcapsules added at a wide range of proportions (0–32% by volume of cement) were loaded by three point bending to induce crack mouth opening displacement (CMOD) of 0.4 mm and 0.5 mm, and were then cured in a water bath for 28 days. By increasing the concentration of microcapsules, the crack mouth healing was improved and the crack depth was also substantially reduced (Figure 2.41). These improvements were more noticeable in the case of specimens loaded at a CMOD of 0.4 mm with a smaller residual crack width range, where the crack mouth healing reached 100% and the crack depth was also reduced from ~28 mm to ~8.6 mm at 32% volume fractions of microcapsules. For the samples with a CMOD of 0.4 mm, the sorptivity coefficient showed a similar decreasing trend as that of crack depth with increasing microcapsule contents. The authors also pointed out that even 100% visual crack mouth healing did not indicate complete healing of the inner crack depth. Therefore, multiple methods should be employed to obtain a comprehensive evaluation of the self-healing

79

efficiency. Additionaly, in another macro-sized glass capsule system, the authors investigated the efficiency of SS healing agent on crack mouth healing under different curing conditions: in the air, high humdity, and immersed in water (Kanellopoulos et al. 2015). It was found that better crack mouth healing was achieved in high humidity or in water while very little healing took place in the air. This indicated that the presence of water is very crucial for the healing reaction of SS agent.

Giannaros (2017) compared the self-healing performance of two types of sodium silicate-containing microcapsules in cement pastes by the capillary absorption test: L1 with sodium silicate in liquid solution encapsulated in a gelatine/gum acacia shell (~500 μm), and T1 with solid sodium silicate encapulated in a polyurea shell (~130 μm). Compared to the control samples, the addition of 4% T1 microcapsules reduced the sorptivity drastically by 45% after a 7 day healing period which continued to 34% after 28 days of healing, while the addition of 4% microcapsules only reduced the sorptivity by 15% at 7 days but had almost the same sorptivity coefficient as the control samples at 28 days (Figure 2.42). The authors deduced that the preferable healing performance of T1 was due to several reasons. Smaller microcapsules produced smaller residual crack widths upon loading. Although loading at the same CMOD of 0.3 mm, samples with T1 had smaller residual crack widths (0.12 mm) than samples with L1 (0.22 mm). The water absorption capability of shell materials might also affect the sorptivity results. Apart from the cementitious matrix itself, the dried residual microcapsule shell material within the matrix also absorbed water. L1 with a hydrophilic gelatine/gum acacia shell had a higher water absorption capability than T1 with a hydrophobic polyurea shell, resulting in more water absorption, which could have skewed the results.

(a)   (b)
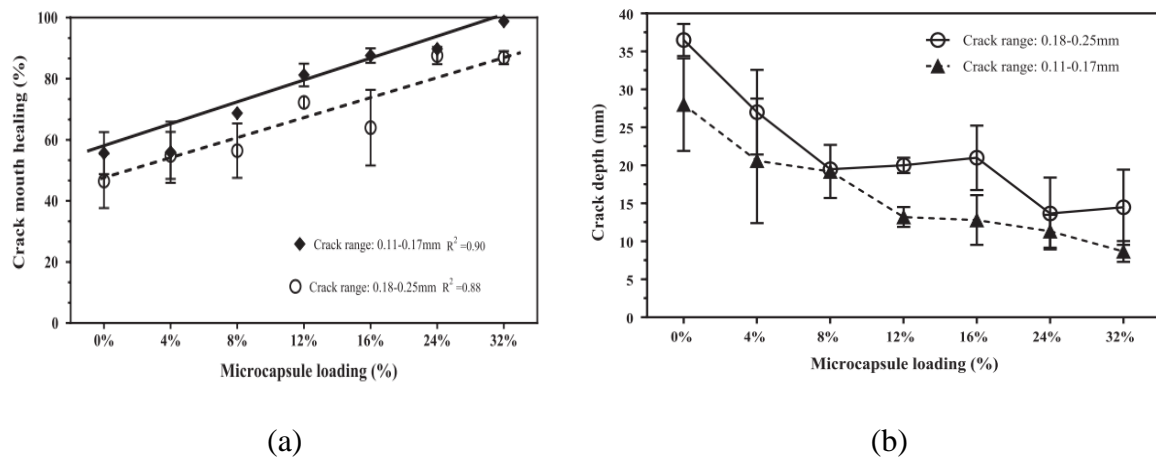
Figure 2.41 Self-healing recovery of cement specimens containing 0–32% by volume of cement sodium silicate microcapsules, cracked at two different crack ranges: 0.11–0.17 mm (CMOD=0.4 mm) and 0.18–0.25 mm (CMOD=0.5 mm) after 28 days healing in water. (a) crack mouth healing (%); (b) crack depth reduction (A. Kanellopoulos et al. 2016).
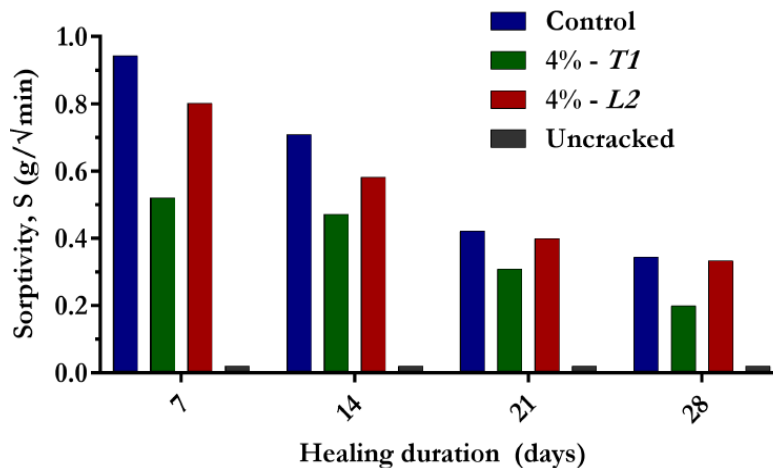
Figure 2.42 Self-healing effciency of water sorptivity of cracked specimens (at CMOD=0.3 mm) containing two types of sodium silicate microcapsules with polyurea shell (T1) and gelatine/gum acacia shell (L2) at 4% by volume of cement (Giannaros et al. 2016; Giannaros 2017).

The recovery of gas tightness has also been used to assess healing. Litina et al. (2015) carried out gas permeability tests on cylindrical cement discs containing encapsulated colloidal silica (CS). The results reported a decrease in the gas permeability coefficient by 29.4% and 23.1% for specimens with 1% and 5% (by weight of cement) CS microcapsules after 28 days of curing in water, while there was almost no recovery in gas tightness observed in the control samples (Figure 2.43). The authors also found that the incorporation of microcapsule particles produced

a densified structure of the matrix due to their microfiller effect, resulting in an initial lower permeability of the microcapsule-containing samples. However, after the microcapsules ruptured and released their core materials for healing, the residual shells remained in place creating a void, which might increase the permeability to some extent. This explained the observation that specimens with 5% microcapsules had the lowest permeability both in the reference samples and recovered samples, but a lower recovery rate compared to samples with only 1% microcapsules.

In summary, the self-healing performances of microencapsulated agents can depend on the concentration of microcapsules, microcapsule properties (size, shell thickness, shell material nature), crack size, curing condition, and healing duration.

(a)
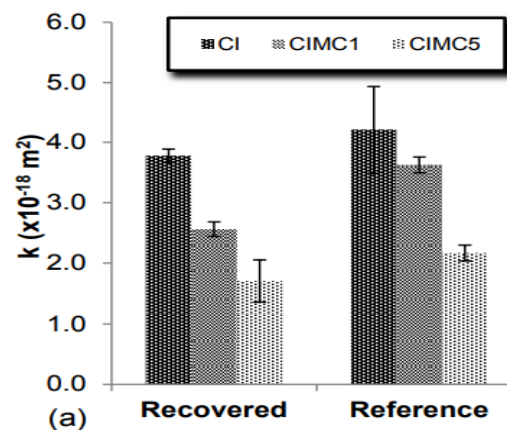
Figure 2.43 Gas permeability coefficients of cement composites containing 1% and 5% microcapsules (shell: PU, core: chloride silicate) after 28 days of healing (Litina & Al-Tabbaa 2015).

2.3.6 Effects of microcapsules on properties of cementitious matrix

Apart from self-healing efficiency, it is also necessary to understand the effects of microcapsule addition on the material properties of the cemetitous matrix. The incorporation of microcapsules is reported to have an influence on the properties of fresh cementitious compositites, such as viscosity, setting time, heat of hydration, etc., and also on the properties of the hardened cementitious matrix, such as mechncial properties, porosity, permeability, etc.

Among previous studies, the effects of microcapsules on the mechanical properties have received the most attention. The addition of microcapsules to cementitious materials is generally reported to decrease the compressive strength of the matrix. Similar to concrete additives and admixtures, the degree of this effect depends primarily on the contents of the microcapsules. Parameters such as the particle sizes and shell properties of the microcapsules themselves can also influence the composite material.

For example, Dong et al. (2017) measured the initial compressive strength of mortar specimens contaning UF microcapsules with epoxy cores that were added at different contents from 0–8% by weight of cement. The compressive strength only decreased slightly at a small addition of microcapsules of 2%, but dramatically decreased by 25% when the addition of microcapsules increased to 8% (Figure 2.44a).

The results also demonstrated the effect of microcapsule particle size on compressive strength. When added at the same content, microcapsules with larger sizes caused more reduction in compressive strength. The authors also analyzed the pore structures of microcapsule-contaning samples to better explain the negative effect of microcapsules on compressive strength. As shown in Figure 2.44b, the addition of microcapsules obviously modified the pore distribution of the mortar samples and increased the number of larger pores (>200 nm) which was considered harmful to the strength of the sample. The porosity of mortar specimens also increased with increasing addition contents from 4% to 8%. As a result, increased porosity led to decreased compressive strength of the cementitious matrix, and this negative effect became more significant at addition contents above 4%.

Kanellopoulos et al. (2016) reported a similar decreasing trend in the compressive strength of mortar specimens with increasing contents of gelatine/gum acacia microcapsules, as shown in Figure 2.45a. The authors also measured the elasticity modulus but the results did not show a clear pattern of the effect of microcapsules. The reason for this is not yet clear. The authors also found that the addition of microcapsules to some extent provided an increase in the flexural strength and fracture toughness of the specimens compared to the controls (Figure 2.45b). However, large numbers of microcapsules significantly increased the viscosity of cement mixes, which could potentially lead to poor compaction of the cement mixes and hence low

levels of adhesion between the embedded microcapsules and the host matrix. As a result, the flexural strength and fracture toughness decreased instead at high concentrations of microcapsules. Wang et al. (2013) also reported significant reduction in the flexural strength of mortar specimens when the concentration of UF/epoxy microcapsules was above 3% by weight of cement, which was attributed to the weaker interface bonding strength of the microcapsules.

| (a) | (b) |
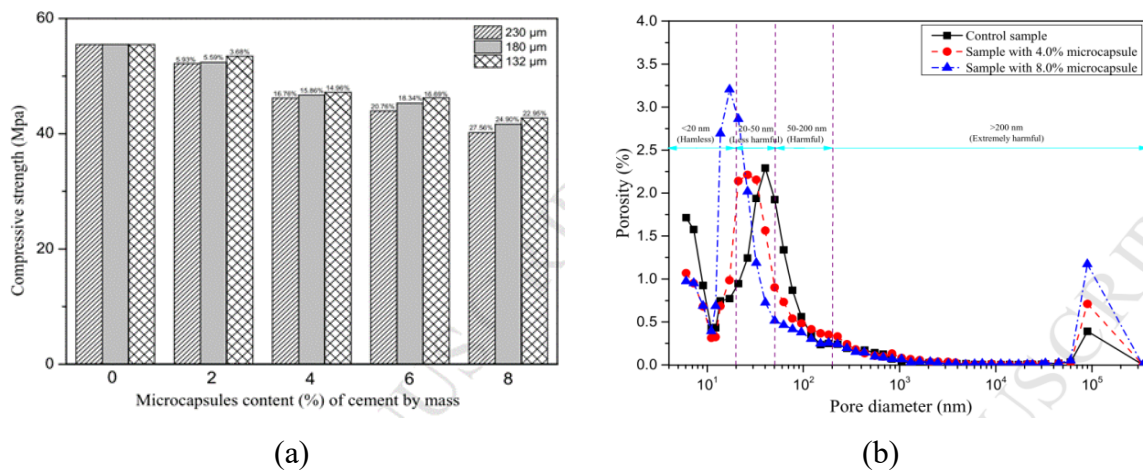
Figure 2.44 (a) Compressive strength of mortar specimens contaning UF/epoxy microcapsules with three different average sizes of 132, 180 and 230 µm; (b) Pore size distribution of mortar specimens containing UF/epoxy microcapsules (Dong et al. 2017).

| (a) | (b) |
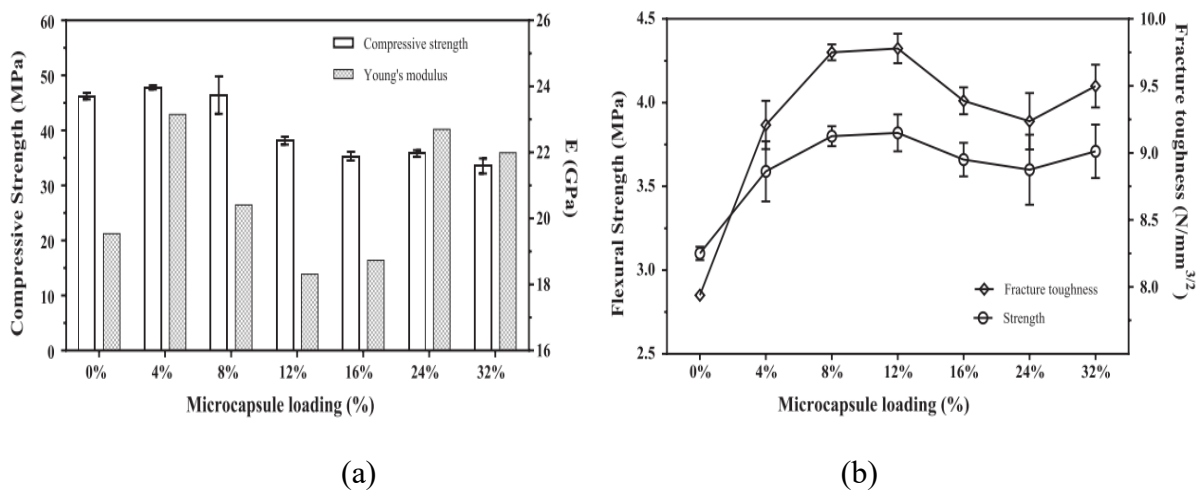
Figure 2.45 Mechanical properties of mortar specimens containing different volume fractions of microcapsules (shell: gelatine/gum acacia, core: SS, 290–700 µm) (a) Compressive strength and Young's modulus; (b) Flexural strength and fracture toughness (A. Kanellopoulos et al. 2016).

84

The effects of microcapsules on the properties of fresh cementitious mixes should also be taken into consideration when using them with cementious materials. The effects of microcapsules on viscosity, one of the representative parameters of rheology properties, have been investigated by several researchers. Kanellopoulos et al. (2016) reported that the addition of spherical microcapsule particles caused a viscosity increase. As shown in Figure 2.46, a linear increase in viscosity was observed as the volume content of microcapsules increased up to 12%. However, a sharp increase was seen when the concentration increased to 16% and above, reaching a maximum of more than 200% increase for concentrations above 24%. Litina et al. (2016) and Giannaros (2017) also saw similar increasing trends in viscosity with increasing concentrations of microcapsules. At low microcapsule concentrations, the increase in viscosity was mainly caused by microcapsules filling the spaces between cement particles to reduce the inter-particle distance which is usually much larger than the particle size. When the inter-particle distance reduced to a scale comparable to the microcapsule size, microcapsule particles started to agglomerate and reduce the free volume, thereby significantly increasing the viscosity via a space-crowding effect (Faroughi & Huber 2014).
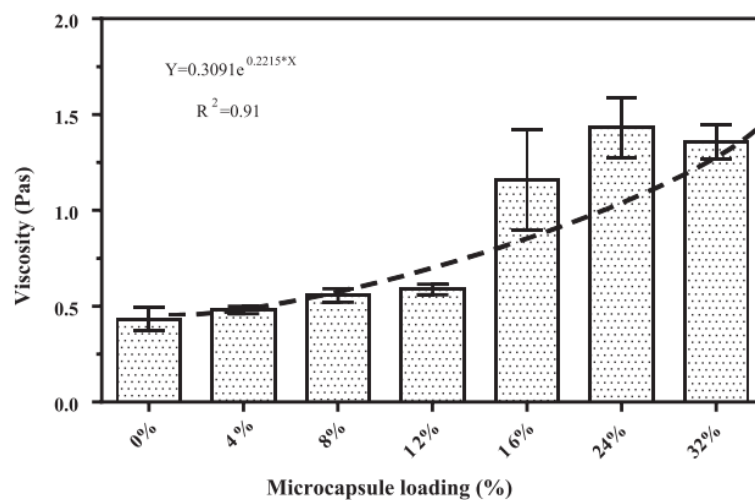
Figure 2.46 Viscosity of mortar specimens containing different volume fractions of microcapsules (shell: gelatine/gum acacia, core: SS, 290–700 µm) (A. Kanellopoulos et al. 2016).

The effects of microcapsules on cement hydration rate and setting time have also been reported. As mentioned above, Giannaros (2017) measured the profiles of cement hydration of mortar

mixes containing microcapsules with gelatine/gum acacia wall and SS core using calorimetry, and the results showed that the inclusion of microcapsules both at low concentration (4% by volume of cement) and much higher concentration (32% by volume of cement) had a negligible effect on the hydration process and setting time. The author also tested another type of microcapsule with PUrea shell wall and SS core, but found accelerated hydration and a shortened setting time (by 26%) of the fresh mortar mixtures containing 4% microcapsules. However, in other research by Litina et al. (2016), a reduction in setting time of 16% was observed when adding 5% microcapsules with PU shell and CS core. Apparently, the effects on cement hydration are inconclusive and varied when using different types of microcapsules.

In summary, the effects of microcapsules on the fresh and hardened properties of cement materials are highly dependent on the characteristics of the added microcapsules as well as the microcapsule addition contents. The addition of microcapsules in large amounts can negatively influence the flowability of fresh cement slurries and the mechanical strength of hardened cement. Therefore, it is also important to determine an optimum amount of microcapsules for their application based on overall consideration about their self-healing effciciency and effects on cement properties.

2.4   Summary

As the dominant construction material, cement has been widely used in various construction fields worldwide, including not only civil infrastructures, but also some specialised applications such as wellbores in the oil field. Well cementing is a very critical operation in oil wellbore constructions, and the resultant annular cement sheath plays a critical role in well integrity by providing adequate zonal isolation, stabilizing the formation and protecting the casing from corrosion. Hence, improper cementing jobs and defects of the cement sheath can severely undermine the well integrity. By reviewing the well integrity problems occurring at different stages, it was found that a majority of those problems originate from cement shrinkage and shrinkage-induced cracking, as well as cracking induced by other external stresses. The shrinkage can result in increased permeability of the cement sheath and microannulus at the cement/formation and cement/casing interfaces, further leading to gas/oil leakage. The

cracking of the cement sheath also creates pathways for gas/oil fluid migration. Therefore, cement shrinkage and cracking should be targeted as the main problems to be addressed for improving well integrity.

As reviewed in Section 2.2, the addition of expansive additives is a commonly used way to compensate for shrinkage. MgO is one of the expansive additives used in cementitious systems to produce expansion based on the internal pressure exerted upon crystallization of the hydration product brucite ($Mg(OH)_2$). MgO additives have been reported to be effective at reducing different types of cement shrinkage including autogenous shrinkage, drying shrinkage, and thermal shrinkage. Compared to other expansive additives, MgO expansive additives have advantages for the use in oil well cement including good thermal stability, low water demand for hydration and more importantly, designable expansion properties. Additionally, the expansion of MgO under restrained annular spaces between the formation layer and steel casing was seen to be beneficial for the compressive and shear bond strengths of the cement sheath, which further contributes to improvement in well integrity.

MgO additives currently used in oil well cement are calcined at high temperature (hard-burnt or dead-burnt). These MgOs with low reactivity are suitable for high-temperature borehole conditions where the wellbore temperature can be up to 260 °C in many cases. However, at lower temperatures, these less reactive MgOs cannot generate effective expansion due to their slow hydration process, which limits MgO use in low-temperature wellbores. By contrast, reactive grade MgO with high reactivity hydrates much more rapidly than hard-burned or dead-burned MgO, which will provide larger expansion when cured at lower temperatures. Therefore, it is deemed that reactive MgO possesses greater potential in producing more effective expansion under low-temperature downhole conditions. However, the reactivity and hydration properties of reactive grade MgO samples also vary significantly depending on their origin and calcination temperatures. There are very few reports on the effect of different reactive MgOs on the expansion performance of oil well cement. A holistic assessment on the effects of different reactive MgOs on oil well cement properties such as rheology, cement hydration and mechanical strength is also lacking.

Self-healing technologies that target cracking issues in cementitious materials were reviewed. Self-healing cementitious materials that can automatically respond to damage and help to restore the performance of structures is very attractive for the oil and gas industries in addressing cracking problems in well cement sheaths. Self-healing is an intrinsic property of cementitious materials, attributed to the unhydrated cement. However, the healing ability of autogenous healing is very limited, and even more so under wellbore conditions at elevated temperature. The self-healing ability can be enhanced by the addition of healing agents such as adhesive agents and mineral-based admixtures, which promote autonomic healing. To achieve effective healing, vascular or capsule-based delivery systems are used to provide the controlled and timed release of healing agents. Compared to a complex interconnected vascular system, independent capsules are more suitable for field application in underground wellbores.

Micro-sized capsules (<1 mm) have been very popular as they can be simply added to cementitious mixtures and dispersed more homogenously throughout the cementitious matrix. Microencapsulation techniques were discussed, together with the variety of shell and core materials used to produce microcapsules for self-healing cementitious materials. The shell properties are very critical in determining the survivability of microcapsules during mixing, retention of core material under aggressive environments, and, more importantly, the fracture behaviour on the release of core material upon triggering. Currently developed polymeric shell materials in the literature show good stability in the cementitious matrix. Among the encapsulated healing agents, sodium silicate (SS) is regarded as an excellent mineral-based agent that is compatible with the cement matrix in terms of the healing products (C-S-H gels) as well as showing significant self-healing efficiency. Mineral-based healing agents like SS generally have good thermal stability, which is advantageous over commonly used adhesive agents for high temperature uses. The self-healing performance of SS and other adhesive or mineral healing agents encapsulated within various polymeric shell walls has been reported in terms of the mechanical strength recovery and durability recovery of cementitious materials. The addition of microcapsules was seen to affect the properties of cementitious materials such as rheology, porosity, permeability, and mechanical strength, which should be taken into consideration during the use of microcapsules.

However, current research into microcapsule-based self-healing cementitious materials is mainly focused on the use under ambient conditions. Their use in extreme environments such as underground wellbores is rarely reported. A microcapsule-based self-healing system that can accommodate wellbore conditions is currently lacking. To develop such a system, microcapsules that are able to remain stable when exposed to challenging high temperature borehole conditions are needed. The thermal stability of both the shell material and the healing agent should be considered. To maintain long-term performance of oil well cement sheath after healing, the healing agents and their healing products are required to be compatible and durable in cementitious environment at high temperature. The self-healing efficiency of the microcapsules under high temperature as well as their effects on the properties of oil well cement needs to be comprehensively investigated.

Therefore, the work discussed herein comprises a step forward in the application of MgO-based expansive system and microcapsule-based self-healing system in oil well cement. In the expansive system, reactive MgOs with different reactivities are investigated on their expansion characteristics and shrinkage reduction performance in oil well cement. In the self-healing system, sodium silicate-based microcapsules are evaluated on their self-healing efficiency in oil well cement. A hybrid system that combines the use of reactive MgO and self-healing microcapsules is also proposed to further enhance the well cement performance.

Chapter 3 Materials and Experimental Methods

3.1 Introduction

In this chapter, a detailed description of the materials, sample preparation, and experimental methods and procedures used in this study is presented. This chapter introduces the materials and experimental details adopted for the expansive cement system and the self-healing cement system. For the expansive oil well cement (OWC) system, cement samples incorporating reactive MgO additives were prepared for evaluation of their expansion characteristics and shrinkage reduction performance in OWC pastes. For the self-healing OWC system, cement samples containing microcapsules were prepared for evaluation of their self-healing performance. The effects of MgO and microcapsules on the fresh properties and mechanical properties of OWC pastes were investigated, respectively. In the end, the combined system with both MgO and microcapsules was also prepared for investigation.

3.2 Materials

3.2.1 Oil well cement

Class G oil well cement (API) was used for preparing the cement paste specimens. Class G cement was chosen since it has the widest application among oil well cements. API Class G Grade cement (High Sulphate Resistant) was supplied by Dyckerhoff, Germany. The chemical compositions and physical properties of the oil well cement are presented in Table 3.1.

3.2.2 MgO expansive additives

Three types of reactive MgOs with different reactivity values were used as expansive additives (Figure 3.1). MgO N50, with the highest reactivity, was synthesized from seawater, supplied by Lehmann & Voss, Netherlands. MgO MAG-R with medium reactivity and MgO 92/200 with lowest reactivity were produced from the calcination of magnesite and were supplied by Sanyuan, China and Richard Barker Harrison, UK, respectively. The chemical compositions and physical properties of the three MgOs are presented in Table 3.2.
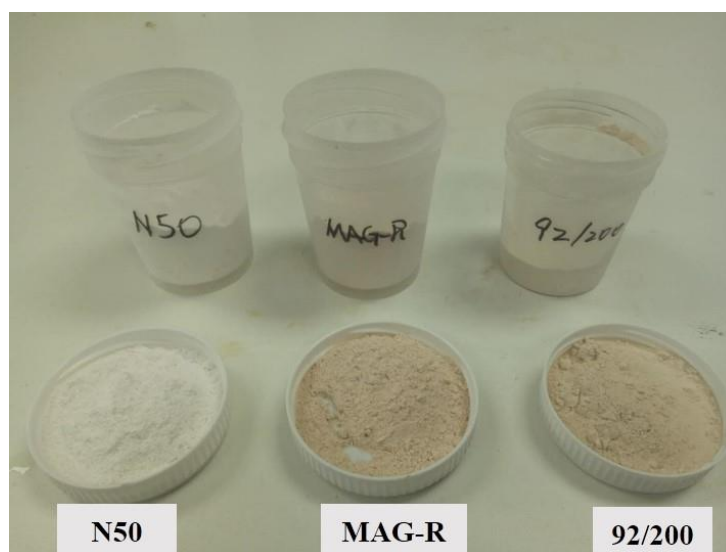
Figure 3.1 Different types of reactive MgOs: N50 synthesized from seawater; MAG-R and 92/200 from calcination of magnesite.

Table 3.1 Chemical and physical properties of API Class G oil well cement.

Chemical composition (%)		Physical properties	
C_3S	48–65	Specific surface area (m^2/kg)	385
C_2S	-	Thickening time test (min)	90–120
C_3A	≤3.0	Maximum consistency during 15 to 30 min(Bc)	30
$C_4FA+ 2C_3A$	≤24.0	Compressive strength (8 hours 38 ºC and atmospheric pressure) (MPa)	2.1
MgO	≤6.0	Compressive strength (8 hours 60 ºC and atmospheric pressure) (MPa)	10.3
SO_3	≤3.0		
Loss on Ignition (LOI)	≤3.0		
Insoluble Residue	≤0.75		
Equivalent Alkali (as Na_2O)	≤0.75		

Table 3.2 Chemical composition and physical properties of MgO N50, MAG-R, and 92/200.

Chemical composition (%)								
	CaO	SiO_2	Al_2O_3	Fe_2O_3	SO_3	Na_2O	MgO	LOI
N50	1.00	-	-	0.07	0.85	-	97.50	8.00
MAG-R	1.68	1.10	0.10	0.75	-	-	92.01	5.72
92/200	0.90	0.90	0.22	0.50	-	-	93.20	2.80
Physical properties								
	Bulk density (g/cm^3)		Particle size			Specific surface area (BET) (m^2/g)		
N50	220		residue on sieve (45 μm):0.005%			150		
MAG-R	-		residue on sieve (80 μm):<10%			55		
92/200	302		-			9		

3.2.3 Self-healing microcapsules

Two types of polymeric microcapsules, T1 and T2, were used for self-healing in oil well cement. The T1 and T2 microcapsules were manufactured by Thies technology Inc using interfacial polymerization with polyurea as the shell wall and solid sodium silicate as the core material. All groups of microcapsules generally consist of ~90% SS core materials and ~10% polyurea shells. The T1 and T2 microcapsules had the same core but mainly differ in the polyurea shell. The T1 microcapsules had a rigid shell while the T2 microcapsules had a rubbery shell. There were two batches of T1 and T2 microcapsules used: OT1 and OT2 from the old batch produced at an earlier time, and NT1 and NT2 from the new batch produced at a later time. After microcapsules of the old batch were used up, microcapsules of the new batch continued to be used in the tests. The basic characteristics of the T1 and T2 types of microcapsules are summarized in Table 3.3. More detailed characterization work on the T-series microcapsules such as the morphology, particle size, and thermal stability will be carried

out to evaluate their suitability for use in oil well cement, and the results will be given in Chapter 5, Section 5.2.

Table 3.3 The basic characteristics of microcapsules.

Type of microcapsules		Production method	Shell	Core	Shell/Core content (%)
T1	OT1	interfacial polymerization (oil-in-water system)	Polyurea (rigid)	Semi-crystalline sodium silicate in solid state	Shell: ~10% Core: ~90%
	NT1				
T2	OT2		Polyurea (rubbery)		
	NT2				

3.3   Characterisation on MgO and microcapsules

3.3.1 Reactivity of MgO

The reactivity of the three types of MgO was evaluated by the acetic acid reactivity test method (Chau & Li 2008). This method measures the time needed for the MgO to neutralize an acid (acetic used here), where a smaller neutralization time indicates a higher reactivity. The reactivity test was conducted by reacting 5.0 g MgO with 100ml of acetic acid solution (1 mol/L) while gently stirring with the experimental setup as shown in Figure 3.2. The reactivity value of MgO was expressed as the time in seconds required for the complete neutralization between MgO and acid (at pH=7). The neutralization process was monitored and the pH change of the solution was recorded by pH meter.

Figure 3.2 Set up for the reactivity test of MgO.

3.3.2 Characterisation of microcapsules

When using microcapsules in oil well cement, it is necessary to comprehensively investigate the properties of the microcapsules that will have a decisive influence on the healing efficiency under the specific environmental exposure conditions and application specifications. The properties of the microcapsules were studied using an optical microscope, scanning electron microscopy (SEM), and thermogravimetric analysis (TGA). These techniques were also used for microstructure analysis of the cement paste samples, which will be introduced later in detail in Section 3.9. First, the morphology of the microcapsules was investigated using an optical microscope and SEM. Based on the microscopy images, the particle size distribution of the microcapsules was analyzed using the imaging software Image J. The thermal stability of the microcapsules was evaluated using TGA. To further evaluate the survivability of the microcapsules in a high-temperature and alkaline environment in oil well cement, the microcapsules were placed in a sealed container with saturated $Ca(OH)_2$ solution placed in the oven at 80 ºC, which was used to simulate the high temperature and alkaline condition. The microcapsules were examined for their stability using a microscope over a period of 14 days.

3.4   Sample preparation and curing

The Class G oil well cement with a constant w/c of 0.44 was used as the control mix during the tests. Cement pastes containing different additives were cast. For the expansive cement system, three types of MgO were added at different contents of 0, 4%, 8%, and 12% by weight of cement. For the self-healing system, microcapsules were added at 0, 1.25%, 2.5%, 5%, and 7.5% by weight of cement. For the combined cement system, both MgO and microcapsules were added to the cement at an optimal content.

The sample preparation process is illustrated in Figure 3.3. Cement samples were mixed using a Kenwood 1500 W food blender consisting of a stainless steel bowl and blade. The additives were mixed thoroughly with cement powders, and then water was added and mixed at a high agitation speed. The total mixing process was carried out for 8 mins, including 3 mins for dry mixing and 5 mins for wet mixing. After mixing, the cement paste was placed into the oil-wet moulds and compacted using a vibration table. The moulds with samples were covered with multiple layers of plastic film in order to prevent loss of water through evaporation during curing, and were then left to cure at laboratory room temperature or at different temperatures in the incubators for a specific period. After demoulding, the samples were cured under different conditions according to the curing regimes required for different tests.
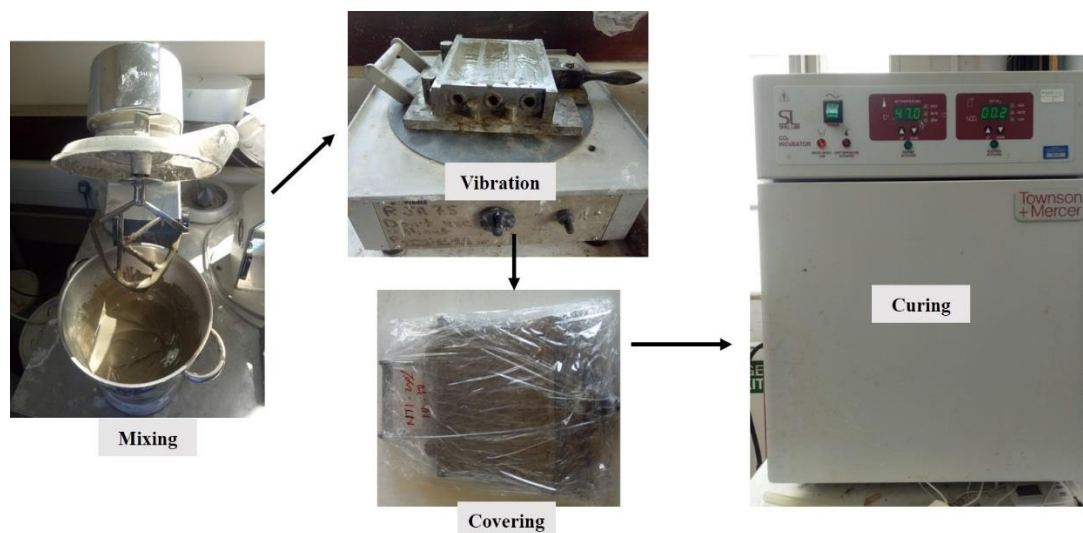
Figure 3.3 Sample preparation procedure of cement paste specimens.

3.4.1 Cubes

Two types of 40 mm × 40 mm × 40 mm cube moulds were used to determine the compressive strength of unrestrained and restrained cement pastes, shown in Figure 3.4a,b. The cube mould in Figure 3.4a was used for casting unrestrained cement pastes. The cube mould assemblies with top cover in Figure 3.4b were specially designed for three-dimensionally restrained cement pastes by simulating the restrained condition of oil well cement pastes between the casing and the formation.

The cast cement samples with moulds were cured at 80 ℃ in the incubators with relative humidity ≥ 95% before demoulding. The unrestrained cube samples were demoulded after 6 h, and then cured in water at the same temperature of 80 ℃ until the age for compressive tests. The restrained cube samples were cured within the restrained moulds at all times under the same conditions until the age for compressive tests.

(a)   (b)   (c)
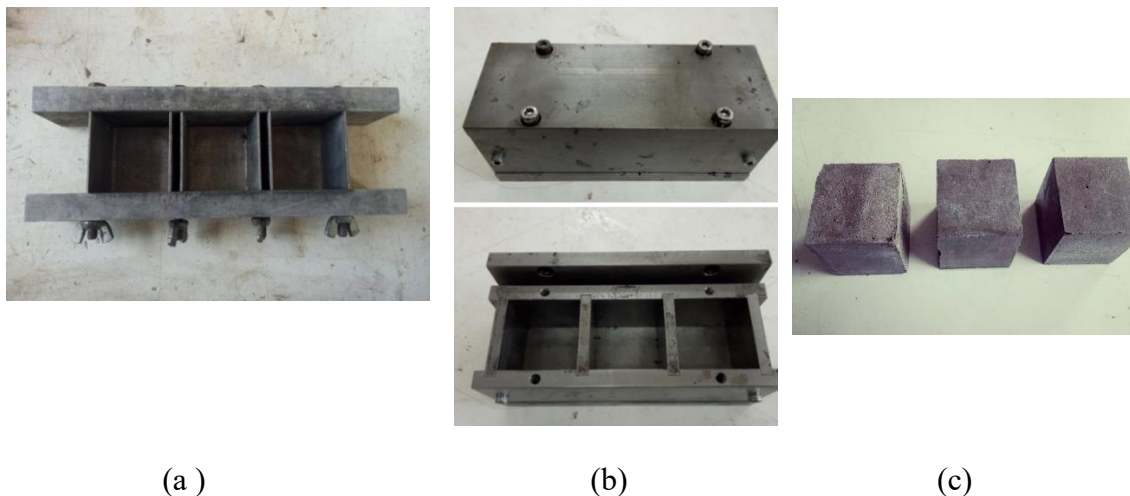
Figure 3.4 40 mm × 40 mm × 40 mm cube mould (a) Unrestrained cube mould; (b) Restrained cube mould assemblies; and (c) Cement cubes after demoulding.

3.4.2 Prisms

Three types of cement prism sample were prepared for different test series. Prism moulds 40 mm × 40 mm ×160 mm (Figure 3.5a) and 50 mm × 50 mm × 250 mm (Figure 3.5c) were used to prepare samples for unrestrained and restrained length change measurements, respectively. The 40 mm × 40 mm ×160 mm prism mould was fitted with shrinkage studs at

both ends. The 50 mm×50 mm×250 mm prism mould had a restrained cage made of two 10mm thick end-plates with 6 mm diameter threaded rod in the centre. The unrestrained and restrained cement samples after demoulding are shown in Figure 3.5b and 3.5d, respectively. The cast unrestrained prism samples were cured at 20 °C under ambient conditions, and at 40 °C, 60 °C and 80 °C in the incubators with relative humidity ≥ 95% for 24 h (at 20 °C and 40 °C) or 6 h (at 60 °C and 80 °C) before demoulding. The restrained prism samples were cured only at 80 °C in the incubator before demoulding. After demoulding, the samples were cured at different conditions (in water, sealed, unsealed) according to the types of experiment that they were used in. These will be introduced in Section 3.6.

| (a) | (b) |

| (c) | (d) |

Figure 3.5 (a)&(b) 40 mm × 40 mm ×160 mm prism mould and unrestrained cement samples after demoulding; (c)&(d) 50 mm × 50 mm × 250 mm prism mould and restrained cement samples after demoulding.

Prism moulds 40 mm × 40 mm ×160 mm (Figure 3.6a) were used to prepare cement pastes for self-healing performance tests. A steel wire, 1.6 mm in diameter and 130 mm in length was

used to prevent complete sample separation under loading. This wire was cast into the cement prism's compressive section with a cover of 10 mm from the top. The cement samples after demoulding are shown in Figure 3.6b. The cast prism samples with moulds were cured at 80 °C in the incubators with relative humidity ≥ 95% for 6 h before demoulding. After demoulding, the prism samples were cured in a water container at 80 °C, as shown in Figure 3.6c, until the age of tests.
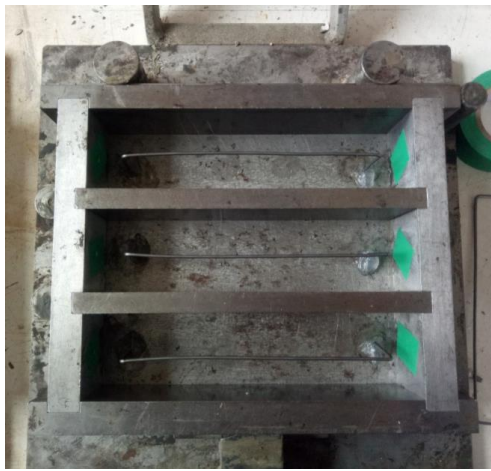
(a)   (b)
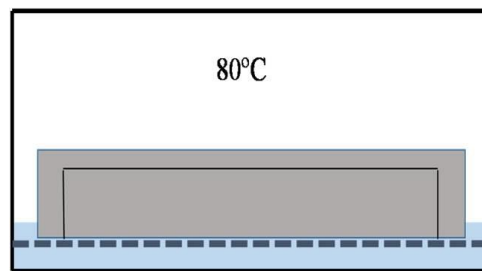
(c)

Figure 3.6 (a) 40 mm × 40 mm × 160 mm prism mould with steel wire glued on the base; (b) Prism cement sample after demoulding; (c) Demoulded prisms cured in a water container with the water level 2~3 mm above the bottom of the prisms at 80 °C, in the incubator.

3.4.3 Cylindrical disks

Cylindrical disk samples (50 mm in diameter and 10 mm in thickness) were cast for evaluating their self-healing performance by the gas permeability test. The disk moulds and samples after

demoulding are shown in Figure 3.7a and 3.7b. The cast disk samples with moulds were cured at 80 °C in the incubators with relative humidity ≥ 95% for 6 h before demoulding. After demoulding, the prism samples were cured in a water container at 80 °C in the incubator as shown in Figure 3.7c.

A summary of different types of cement paste samples and their corresponding curing conditions during the periods before and after demoulding is given in Table 3.4.

(a)

(b)

(c)
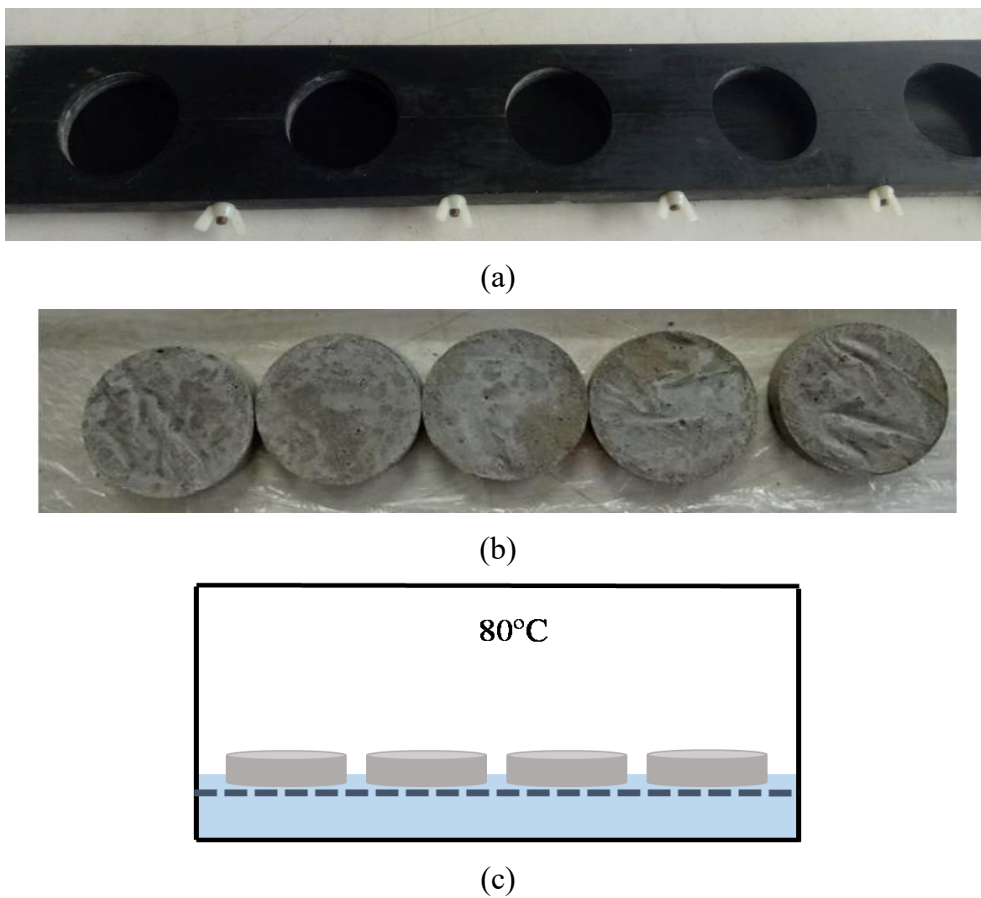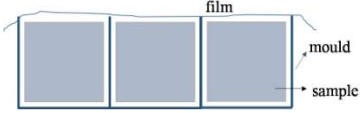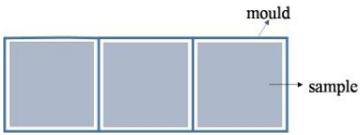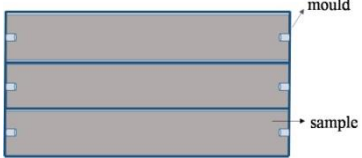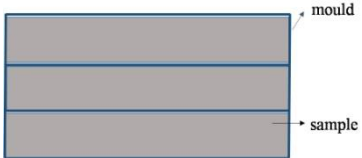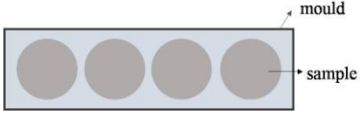
Figure 3.7 (a) Cylindrical disk mould (Ø50 mm × 10 mm); (b) Cement disks after demoulding; (c) Demoulded prisms cured in a water container with the water level 2~3 mm above the bottom of the prisms at 80 °C in the incubator.

Table 3.4 Summary of different types of cement paste samples and their curing conditions.

Sample type		Before demoulding (in incubator, RH≥95%)	After demoulding, before testing	T (ºC)
Cubes	unrestrained		in water*	80
	restrained		cured with mould before testing	
Prisms for expansive cement system	unrestrained		in water*	20, 40, 60, 80
			sealed	80
			unsealed	80
	restrained		in water*	80
			unsealed	
Prisms for self-healing cement system			in water**	80
Cylindrical disks for self-healing cement system			in water**	80

Note: Specimens that needed to be cured in water at an elevated temperature were stored in a water container placed in the incubator. *submerged in water; ** with a thin water level of 2~3 mm above the bottom of the sample.

3.5   Effects on the fresh properties of oil well cement slurries

3.5.1 Rheological properties

Additives may adversely affect the rheological properties of oil well cement slurries. The effect of different additives (MgO, microcapsules, or both) on the viscosity and yield stress needs to be investigated. A Brookfield DV3T Rheometer connected with a water bath was used to measure the viscosity of cement slurries containing different additives (Figure 3.8). The viscosity of the cement slurries was tested at two different temperatures, 20 °C and 40 °C. The w/c ratio was kept constant at 0.44 and the cement slurries were prepared by mixing 30 g cement, 13.2 g water and the corresponding additives in varying quantities together in a plastic cup using a vortex mixer. After mixing, cement slurries were placed into the rheometer sample cup for testing. The heating chamber was pre-heated to the test temperature before sample preparation.
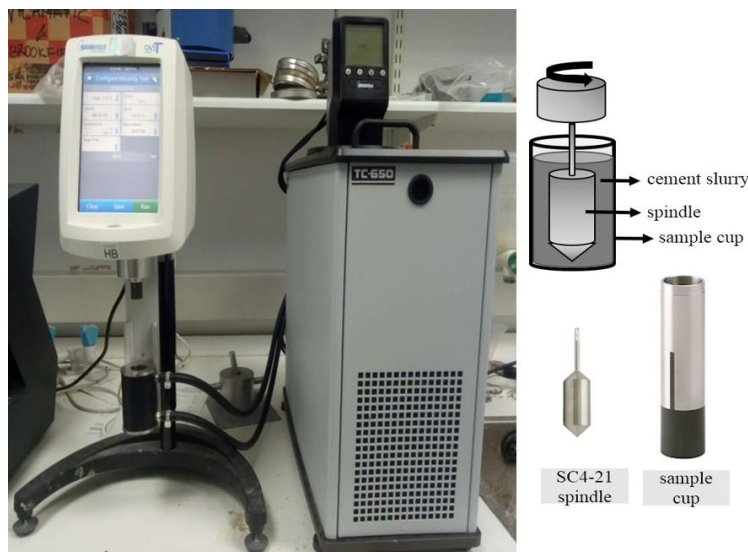
Figure 3.8 Brookfield DV3T Rheometer connected with a water bath used to measure the viscosity of fresh cement slurries.

The viscometric testing scheme used was adapted from Shahriar & Nehdi (2012), as seen in Figure 3.9. The measurements were taken at 20 different shear rates starting from 5.11-230 s^{-1} after a continuous rotation of 10 s at each speed to obtain the up-flow curve, and then at a descending shear rate from 230 to 5.11 s^{-1} to obtain the down flow curve. Before starting to

take measurements, pre-conditioning was carried out on the sample for 3 mins at a shear rate of 115 s^{-1} under the test temperature. After obtaining the hysteresis loop of the cement slurry, the plastic viscosity and yield stress were calculated from the shear rate-shear stress down curve based on the Bingham model as introduced in Chapter 2, Section 2.1.3.2. The down-curve was chosen since it better fitted the Bingham plastic model than the up-curve (Shahriar & Nehdi 2012).

(a)   (b)
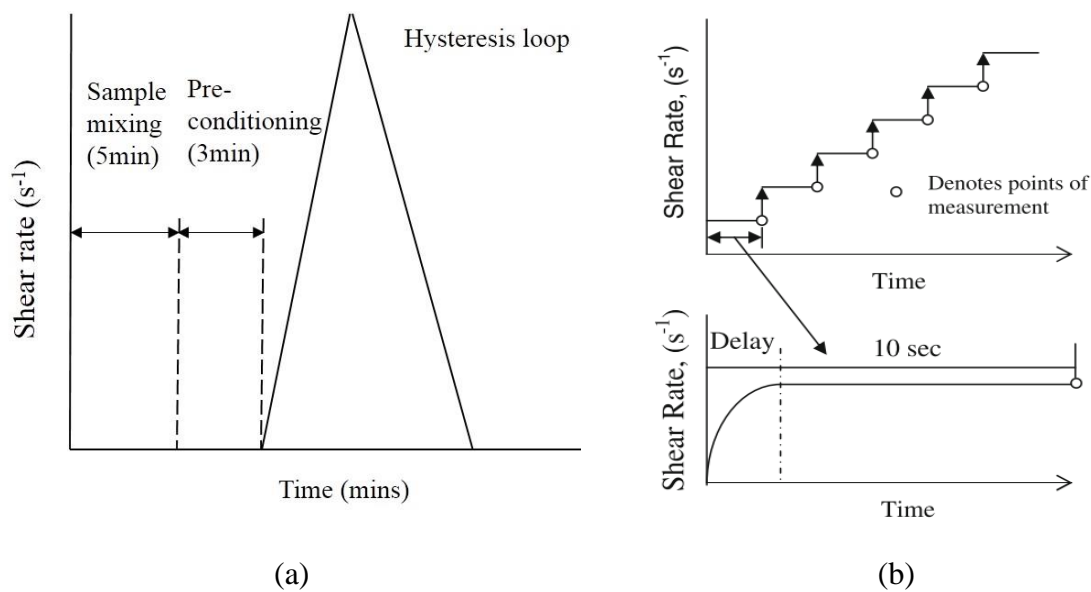
Figure 3.9 (a) Testing scheme of the viscosity test; (b) Schematic representation of the stepped ramp of shearing, adapted from (Shahriar & Nehdi 2012).

3.5.2 Isothermal calorimetry

The effects of additives (reactive MgOs and microcapsules) on the cement hydration process were investigated using a Calmetrix I-Cal 2000 HPC High Precision Isothermal Calorimeter in accordance with ASTM C1679 (Figure 3.10a). In isothermal calorimetry tests, the rate of cement hydration is represented by the heat flow rate while the total degree of hydration is represented by the cumulative heat evolution. The addition of admixtures may change the shape of the heat flow curve, and the admixture effects on cement hydration can therefore be investigated. A typical rate of heat evolution of cement hydration is shown in Figure 3.10b. As the heat flow rate changes, different stages of the hydration process can be clearly viewed: (I) rapid initial processes; (II) dormant period; (III) acceleration period; (IV) retardation period

and (V) longer term reactions (Gatner et al. 2002). Through isothermal calorimetry, all stages of the hydration process can be easily followed.

(a)

(b)
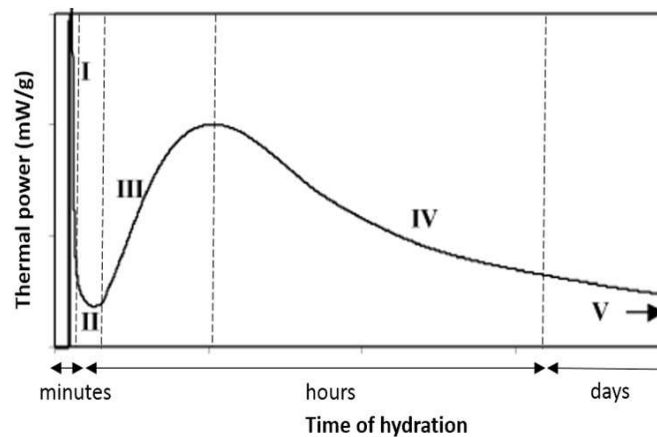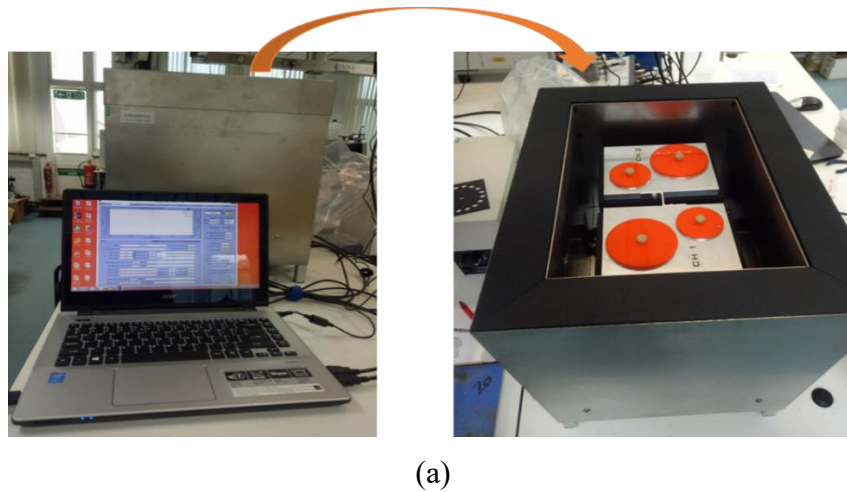
Figure 3.10 (a) Calmetrix I-Cal 2000 HPC High Precision Isothermal Calorimeter connected to laptop data logging; (b) Typical rate of heat revolution curve of cement hydration (Gatner et al. 2002).

Before starting the test, the thermostat was set to the designated test temperature (20 °C and 40 °C) and the test chamber was then left to stabilize for 24 hours. Dry cement mixtures and mixing water were prepared. For each cement mixture, the quantity of cement was 50 g/sample and the additives were added at different contents (0~12% by weight of cement for reactive MgO, and 0~7.5% by weight of cement for microcapsules). The water was added at a constant w/c ratio of 0.44 (22 g/sample). Pre-conditioning of the cement mixtures and water was carried out in the stabilized test chambers for at least 2 hours. All the ingredients were mixed together

for 1 minute in the sample cup. As soon as the sample cup was placed back into the test chamber, the logging of the heat of hydration started immediately and lasted for 50 hours.

3.6   Effects on the mechanical properties of hardened oil well cement pastes

3.6.1 Compressive strength

Compressive strength tests were performed on the cement paste samples to evaluate the effect of different additives on the strength of oil well cement pastes. Three cubes were tested for their unconfined compressive strength (UCS) at different ages of 1, 3, and 7 days after casting. Prior to the test, the dimensions of the specimens were measured by digital slide callipers (Figure 3.11a) and the weight was measured using a digital scale to 0.01 g accuracy (Figure 3.11b). The cubic specimens were then tested using a 250 kN servohydraulic testing frame with a Controls 50-C9030 compression device at the loading rate of 2400 N/s in accordance with BS EN 196-1 and API Specification 10A. The compressive strength f_c was calculated using the Equation 3.1:

$$f_c = \frac{P_{max}}{A}$$

Equation 3.1

where P_{max} is the ultimate compressive failure load (kN), and A is the cross-section area of individual specimen tested.

(a)

(b)

(c)

Figure 3.11 Unconfined compressive strength tests (a) Dimension measurements; (b) Weight measurements; (c) Loading of cubic samples using 250 kN servohydraulic testing frame with a Controls 50-C9030 compression device.

3.7   Expansion performance of MgO in oil well cement pastes

The expansion of MgO in class G well cement pastes was characterized by the expansion rate and magnitude which were determined by measuring the linear deformation of the prism specimens. Unrestrained 40 mm × 40 mm ×160 mm prisms (Figure 3.12a) and restrained 50 mm × 50 mm × 250 mm prisms were both used for testing (Figure 3.12b). A digital length comparator was used for measuring the linear deformation of the prism specimens, as shown in Figure 3.12. The initial measurements were taken immediately after demoulding, then all the specimens were cured under water in the incubators at different temperatures from 20 to 80 °C as shown in Table 3.4. Samples cured at 20 °C were stored in a water tank at a constant laboratory temperature of 20±1 °C (Figure 3.13a). Samples cured at elevated temperature were stored in sealed water containers placed in the incubator (Figure 3.13b). The subsequent length

change measurements were taken at different time intervals over 60 days. Three replicate prisms were used for measurements of each mix group. The linear length change ΔL was calculated as in Equation 3.2.

$$\Delta L = \frac{L_t - L_i}{L} \times 100\%$$ Equation 3.2

where L_t is the length at curing time t, L_i is the initial length on the first comparator reading and L is the length of the reference rod, which is 160 mm for unrestrained (40 mm × 40 mm × 160 mm) prisms and 260 mm for restrained (50 mm × 50 mm × 250 mm) prisms.

The linear deformations of 40 mm × 40 mm × 160 mm sealed prisms were also measured to evaluate the effects of MgO on autogenous shrinkage reduction at 80 °C. After the initial measurements, the specimens were first sealed using a layer of adhesive aluminium tape and then another layer of cling film to prevent moisture exchange with the surrounding environment, as shown in Figure 3.14. These sealed prism specimens continued to cure at the same temperature of 80 °C in the incubator. The length change measurements were taken at different time intervals over 28 days.

The linear deformations of unsealed cement paste prisms exposed to drying condition were measured to evaluate the effects of MgO on drying shrinkage reduction at 80 °C. Unrestrained 40 mm × 40 mm ×160 mm prisms and restrained 50 mm × 50 mm × 250 mm prisms were both used for testing. After initial measurements, the 40 mm × 40 mm ×160 mm prisms were then stored at different humidities (high humidity of 90%, low humidity of 25%) at 80 °C in the incubator (Figure 3.15a). The restrained prisms were first stored in water for 7 days at 80 °C and then dried at RH of 25% at 80 °C in the incubator (Figure 3.15b). In the following curing ages, subsequent length change measurements were taken at different time intervals over 28 days.

(a)   (b)
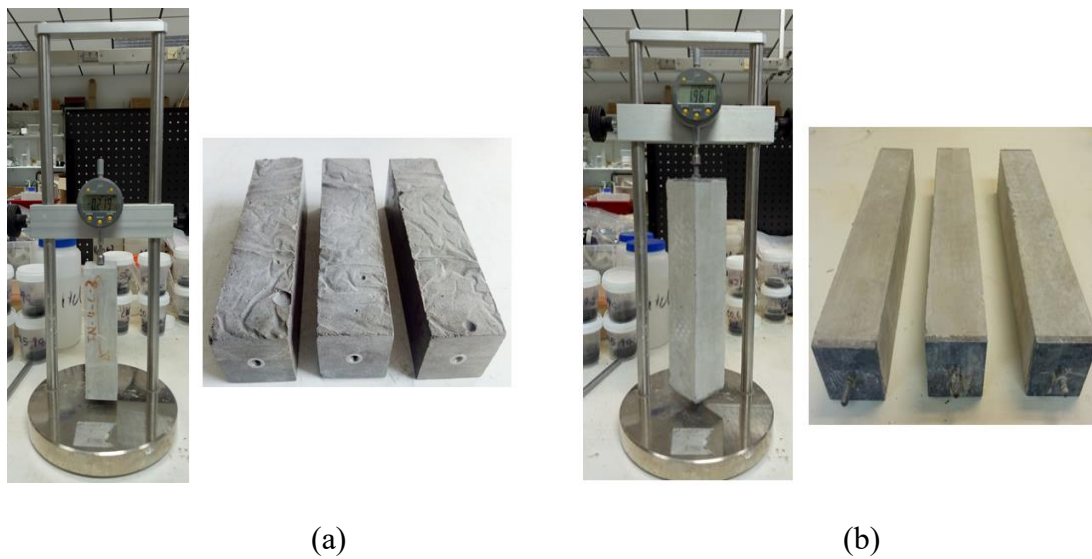
Figure 3.12 Linear deformation measurements of cement paste prisms using digital length comparator (a) Unrestrained 40 mm × 40 mm × 160 mm prisms; (b) Restrained 50 mm × 50 mm × 250 mm prisms.

(a)   (b)
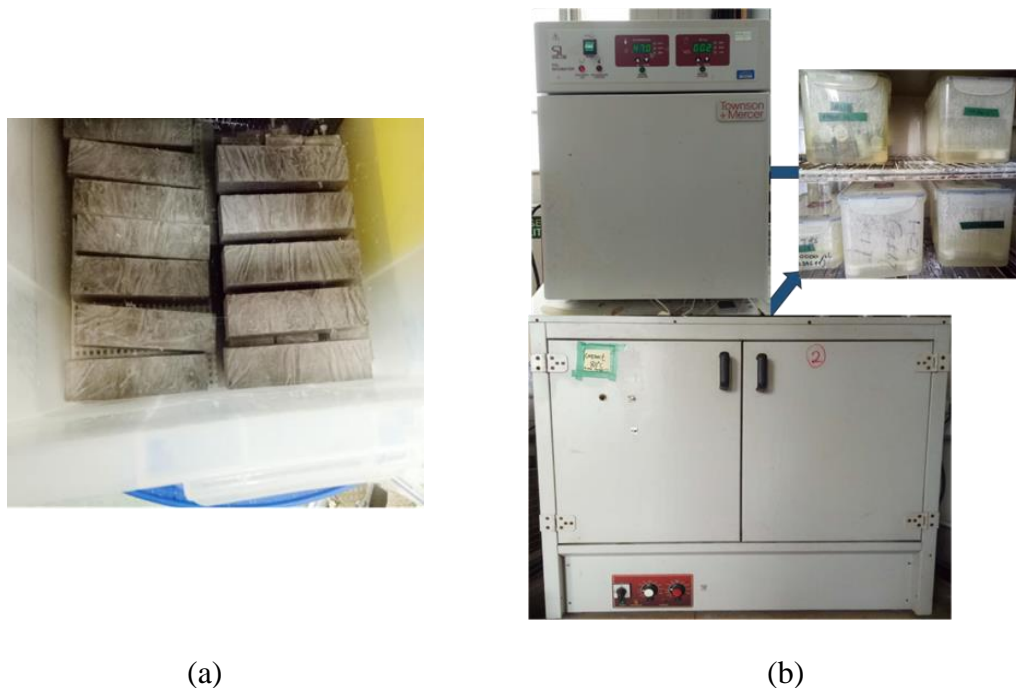
Figure 3.13 Unrestrained 40 mm × 40 mm × 160 mm prisms and restrained 50 mm × 50 mm × 250 mm prim cured in water at different temperatures from 20 to 80 °C. (a) In water tank at 20 °C; (b) In sealed water container at elevated temperature (40, 60, and 80 °C) in incubator.
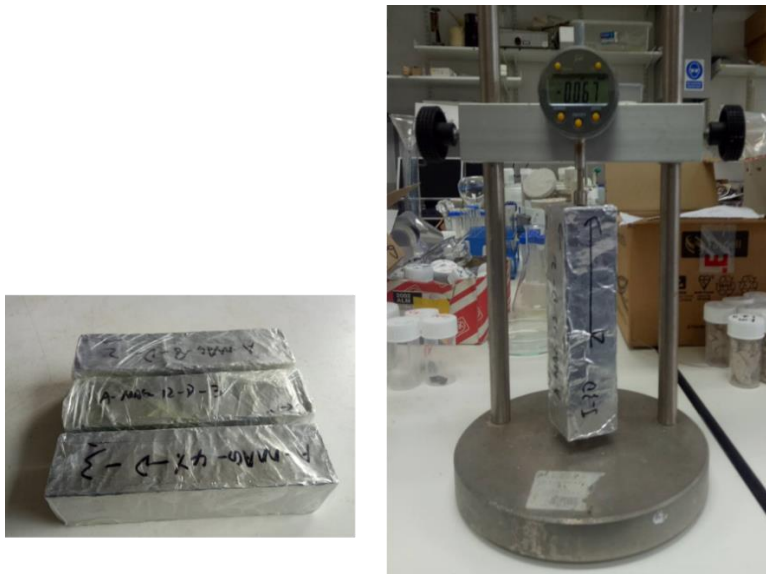
Figure 3.14 Linear deformation measurements of sealed 40 mm × 40 mm ×160 mm cement pastes prisms using digital length comparator.

| (a) | (b) |

Figure 3.15 Unsealed cement specimens stored at different humidity at 80 ºC in the incubator (a) Unrestrained 40 mm × 40 mm ×160 mm prisms; (b) Restrained 50 mm × 50 mm ×250 mm prisms.

3.8   Self-healing performance of microcapsules in oil well cement pastes

3.8.1 Inducing controlled cracks in cement specimens

40 mm × 40 mm × 160 mm prisms and Ø 50 mm × 10 mm cylindrical disks were prepared for evaluating the self-healing performance of oil well cement pastes containing microcapsules. The prism specimens were used for the capillary water absorption test and flexural strength recovery test, while the disk specimens were used for the gas permeability test.
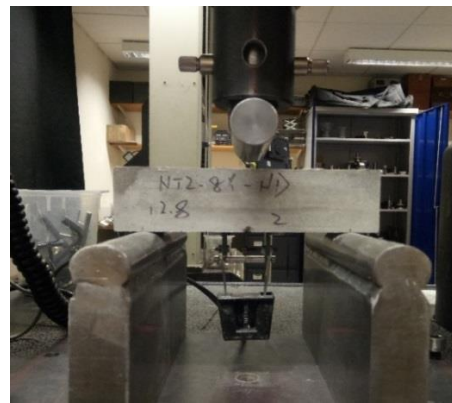
(a)   (b)
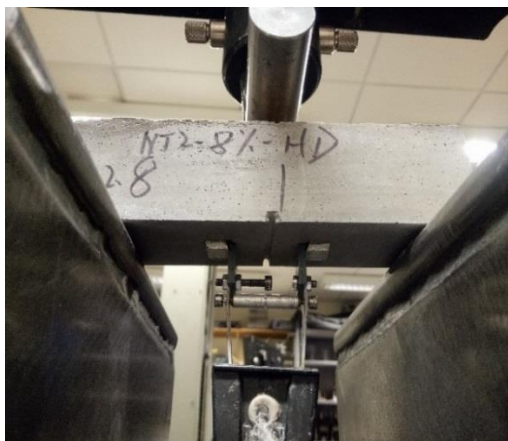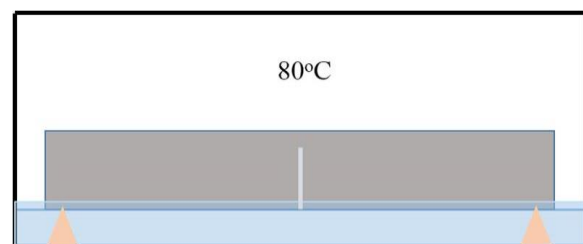
(c)   (d)

Figure 3.16 (a) Notched 40 mm × 40 mm × 160 mm prisms with two knife edges fixed on both sides of the notch; (b) Three-point bending test set-up; (c) Control of crack width using a clip gauge attached to the glued knife edges at the bottom of the specimens; (d) Curing conditions of the cracked prism specimens at 80 ℃.

(a)   (b)

(c)
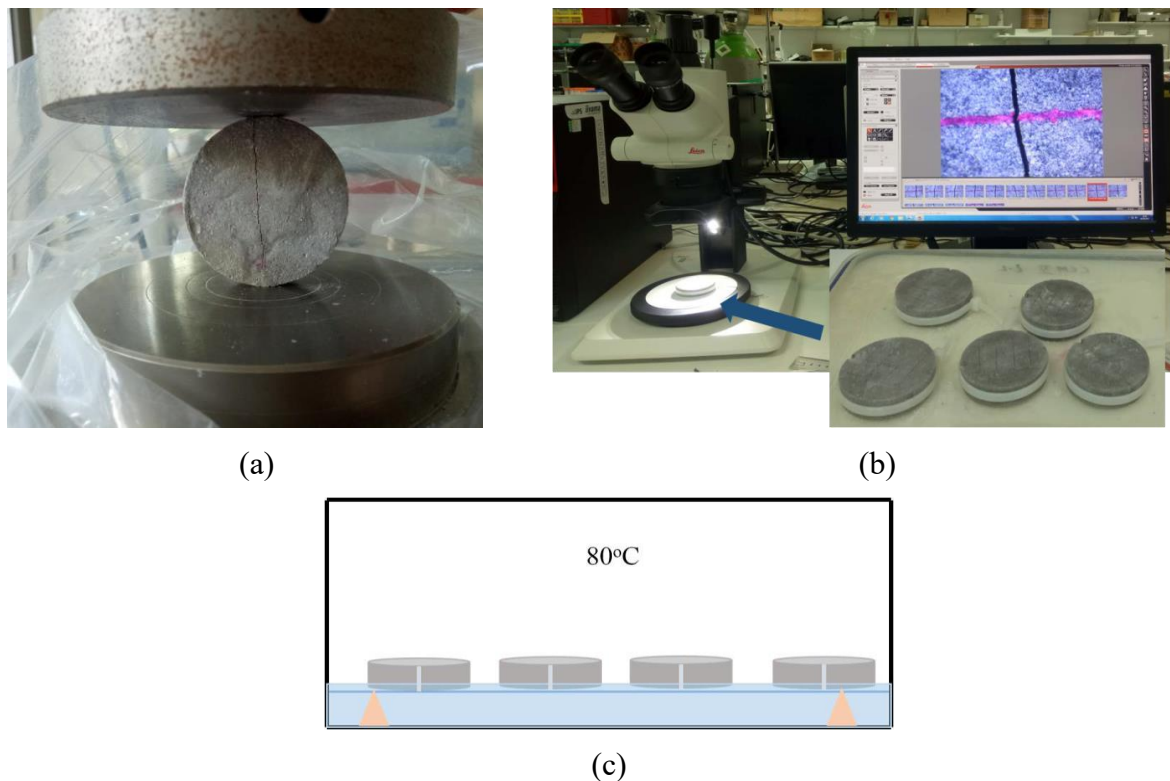
Figure 3.17 (a) Cylindrical disk cracked using the 50 kN CONTROLS UNIFRAME testing machine; (b) Two parts of the cracked disk were glued together at the ends and fixed with a flexible cable tie with a controlled crack width with of 150-200 µm under a microscope; (c) Curing condition of the cracked disks at 80 ºC.

For the prism specimens, the three-point bending test was used to induce cracks in the specimens. The specimens were taken out from the incubator for cracking after 3 days following the date of casting. Prior to cracking, all the specimens were notched (1.5 mm depth and 2 mm width) with a rotating diamond blade (Figure 3.16a) in order to ensure the crack initiated in the centre of the specimens. The notched samples were then mechanically cracked by 3PB test using an Instron 30 kN static testing frame at a rate of 0.10 mm/min and loading span of 125 mm (Figure 3.16b). The crack width was controlled using a clip gauge that was attached to the bottom of the specimens through two knife edges fixed on both sides of the notch (Figure 3.16c). The cement prisms were loaded to a crack mouth opening displacement (CMOD) of 200 µm with a residual crack width ranging within 90-170 µm. The cracked specimens were then cured in the incubator at 80 ºC in a sealed container containing water at a

level of 2-3 mm above the bottom of the specimens, as shown in Figure 3.16d. The water could be absorbed into the crack by capillary force to assist the healing process.

The cylindrical disk specimens were cracked using the 50 kN CONTROLS UNIFRAME testing machine as shown in Figure 3.17a. The specimens were cracked into two separate pieces and then these two separate pieces were fixed at a crack width of 150-200 μm (Figure 3.17b) by fixing together the two ends and stabilising with a flexible cable tie. The cracked disks were cured at the same condition as that for the cracked prisms as described above, shown in Figure 3.17c.

3.8.2 Observation of cracks and crack depth measurement

The cracks induced in the prism specimens were observed using a microscope (Figure 3.18). Images were captured at four positions marked along the crack (3 points along the bottom side and 1 point on the lateral side) at different time intervals from the day of cracking to the end of the healing period. The crack width was measured on the captured images using Image J and an average value of the four measurements for each specimen was calculated. The crack mouth width healing efficiency was calculated according to Equation 3.3:

$$\text{Crack mouth width healing} = \frac{w_i - w_a}{w_i} \times 100\% \qquad\qquad \text{Equation 3.3}$$

where w_i is the initial crack width before healing, and w_a is the crack width after healing for 7 days at 80 °C.
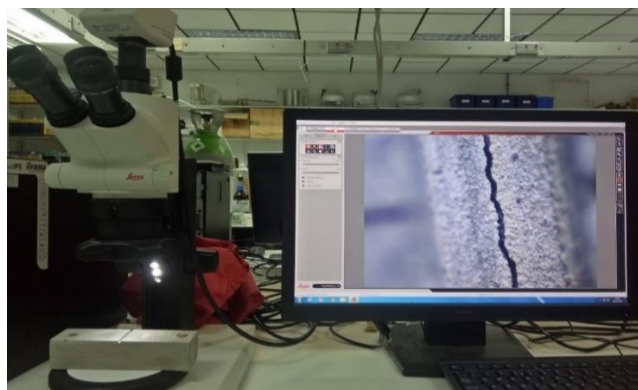
Figure 3.18 Observation of cracks in prism specimens using microscope.

Measurement of the crack depth in the prism specimens was carried out using an ultrasonic pulse velocity test instrument (PUNDIT-PL 200) (Figure 3.19a). The testing device complies with British standard BS 1881: Part 203. As illustrated in Figure 3.19b, two 150 kHz transducers were placed on either side of the crack on the base of the specimen. Two measurements were taken of the ultrasonic wave transmission time of the pulse to transit distances 2b and 4b, respectively. The time (t_1 and t_2) taken for the ultrasonic waves to travel between the two points was recorded and the crack depth d was then calculated based on Equation 3.4.

$$d = b\sqrt{\frac{4t_1^2 - t_2^2}{t_2^2 - t_1^2}}$$

Equation 3.4

<div align="center">(a)   (b)</div>
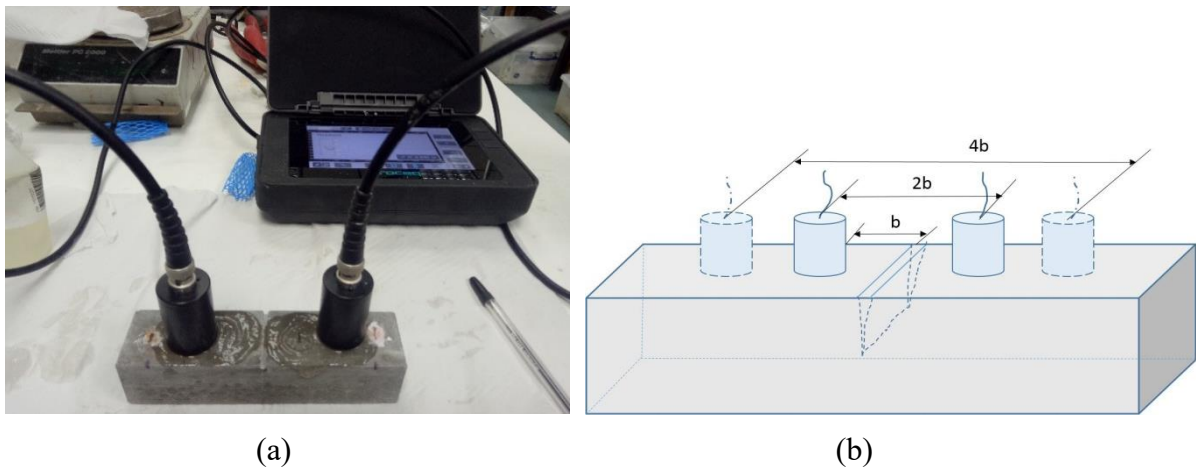
Figure 3.19 (a) Ultrasonic pulse velocity test instrument (PUNDIT-PL 200) for crack depth measurement; (b) Schematic diagram of crack depth measurement.

3.8.3 Capillary water absorption

The capillary water absorption (sorptivity) test was carried out on prism specimens to evaluate their recovery in water tightness after healing. Sorptivity is an indicator of the ability of concrete ability to absorb and transmit liquid through it by capillary suction (Sabir et al. 1998). Following the testing procedure in ASTM C1585 (ASTM C1585 2013) and RILEM report (De Rooij et al. 2013), a short-term one-dimensional capillary water absorption test was conducted on the prism specimens after healing for 7 days. The testing procedure is illustrated in Figure 3.20. The cracked prism specimens were first dried in a vacuum chamber until the mass

changes were less than 0.1% between 24 h periods. The specimens were then wrapped on the bottom and lateral sides with aluminium tape but the crack area was left uncovered for exposure to capillary water suction. The top side of the specimens was also covered with cling film to prevent moisture evaporation from the specimens during the test. Specimens were placed on supports in a tank containing a shallow water level which was maintained at ~3 mm throughout the test. Weight changes in the specimens due to capillary water uptake were monitored at required time intervals during a period of ~4.5 hours. The sorptivity coefficient was calculated based on Equations 3.5 and 3.6 according to (Hall & Tse 1986):

$$M_w = \frac{\Delta m}{A\rho} \qquad\qquad\text{Equation 3.5}$$

$$M_w = C + S\sqrt{t} \qquad\qquad\text{Equation 3.6}$$

where M_w is the water uptake quantity per unit area of inflow surface (mm), Δm is the change in specimen weight (g), A is the area of inflow surface (mm^2), ρ is water density (g/mm^3), and S is the sorptivity coefficient (mm/min$^{1/2}$) determined by calculating the slope of curve between M_w and the square root of measurement time t (min$^{1/2}$).

Figure 3.20 Illustration of the capillary water absorption testing procedure.

3.8.4 Gas permeability

The gas permeability test was carried out on disk specimens to evaluate the improvement of gas permeation performance after healing. The testing method proposed by Alshamsi & Imran (2002) was adopted in this study to measure the gas permeability coefficient of the cracked cement paste disks. Liquid methanol was used as the permeating gas source due to its low boiling temperature (65 °C). Before testing, the disk specimens were dried in a vacuum chamber until the mass changes were less than 0.1% between 24h periods. The test set-up is illustrated in Figure 3.21.
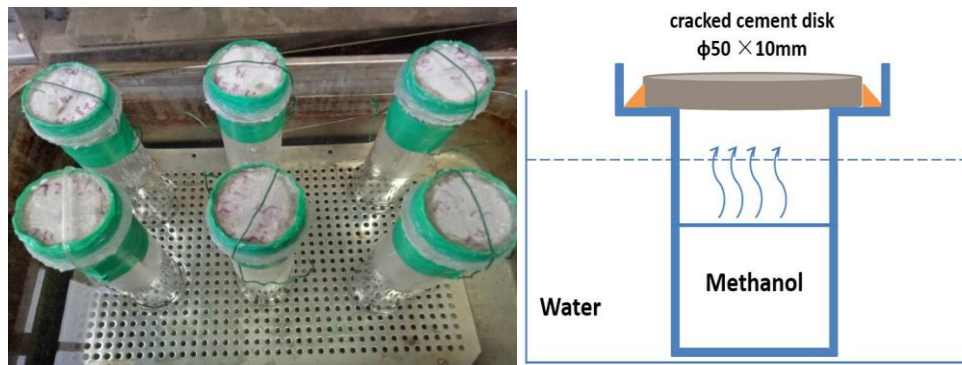
Figure 3.21 Illustration of the gas permeability test on cracked disk specimens.

The disks were then fixed with epoxy sealant and tape to the top of the glass pressure cells containing one-third of liquid methanol. The glass cells were placed in a 40 °C water bath and the weight loss of each glass cell was recorded every 10 minutes until a steady weight loss was reached. The permeability coefficient (k) was calculated according to Equations 3.7 and 3.8.

$$k = \alpha \frac{L}{A} m^*$$

<div align="right">Equation 3.7</div>

$$\alpha = 2\eta T R_u \frac{P_2}{(P_1^2 - P_2^2)}$$

<div align="right">Equation 3.8</div>

where L is the length of the sample (m), A is the cross-sectional area perpendicular to the direction of flow (m^2), m* is the rate of mass loss (g/h), α is a constant for methanol in a particular temperature and pressure difference calculated in Equation 3.7, η is the dynamic viscosity (Ns/m^2), T is the absolute temperature (K), R$_u$ is the gas constant (8.3 J/mol K, for

methanol), P_1 is the inlet pressure (N/m²), and P_2 is the outlet pressure (N/m²). The value of α for methanol used in this study was 1.684 ×10⁻¹⁷.

3.8.5 Recovery in flexural strength

Following the water absorption tests after 7 days curing, the specimens were recracked to evaluate their recovery in flexural strength using the three-point bending test. The initial flexural stress of each specimen was determined during the initial cracking of the specimens as described in Section 3.8.1. The flexural stress was calculated using Equation 3.9 according to BS EN 12390-5:2009.

$$\sigma_f = \frac{3PL}{2bd^2} \qquad \text{Equation 3.9}$$

where σ_f is the stress in the surface at the midpoint (MPa), P is the load (N), L is the support span (mm), b is the width (mm), and d is the depth (mm) of the specimen.

The strength recovery R_f (%) after healing was calculated according to Equation 3.10:

$$R_f = \frac{\sigma_1}{\sigma_2} \qquad \text{Equation 3.10}$$

where σ_1 is the maximum stress of the original specimen and σ_2 is the maximum stress of the specimen after healing.

3.9   Microstructure analysis

The microstructures of the hydrated cement pastes with MgO expansive additives as well as self-healing products from the cracking surface were investigated using powder X-ray diffraction (XRD), thermogravimetric analysis (TGA), scanning electron microscopy (SEM), and energy dispersive X-ray spectroscopy (EDX) techniques.

1. Powder X-ray diffraction (XRD)

XRD analysis was used to explore the crystalline phases present in the cement paste samples. XRD patterns were collected on a Siemens D500 X-ray diffractometer with a Cu-Kα radiation (wavelength λ=0.1541 nm) at 40 kV and 35 mA (Figure 3.22). Scanning was operated in the 2θ range from 5° to 60°, at a counting time of 1 s/step and a resolution of 0.02°/step. The peaks

from the obtained XRD patterns were searched and matched in the PDF-2004 database using X'pert Highscore software. For analysis of the hydrated cement pastes with MgO additives, microstructure samples were obtained from small chips of the crushed cubic samples from the compressive tests. The collected chips were first treated with isopropanol to stop hydration of the cement and MgO. Before testing, the cement chips were taken out from the isopropanol and dried at 50 °C for 4 hours to remove the isopropanol. The dried chips were ground to pass a 75 µm mesh sieve for the XRD tests. For analysis on the self-healing products of microcapsules in cement pastes, microstructure samples were extracted from the crack surface of vacuum-dried prism samples using a SAPHIR 520 polishing machine with P80 silicon carbide abrasive paper (Figure 3.23). The powders were then collected and passed through a 75 µm mesh sieve and prepared for the XRD tests.
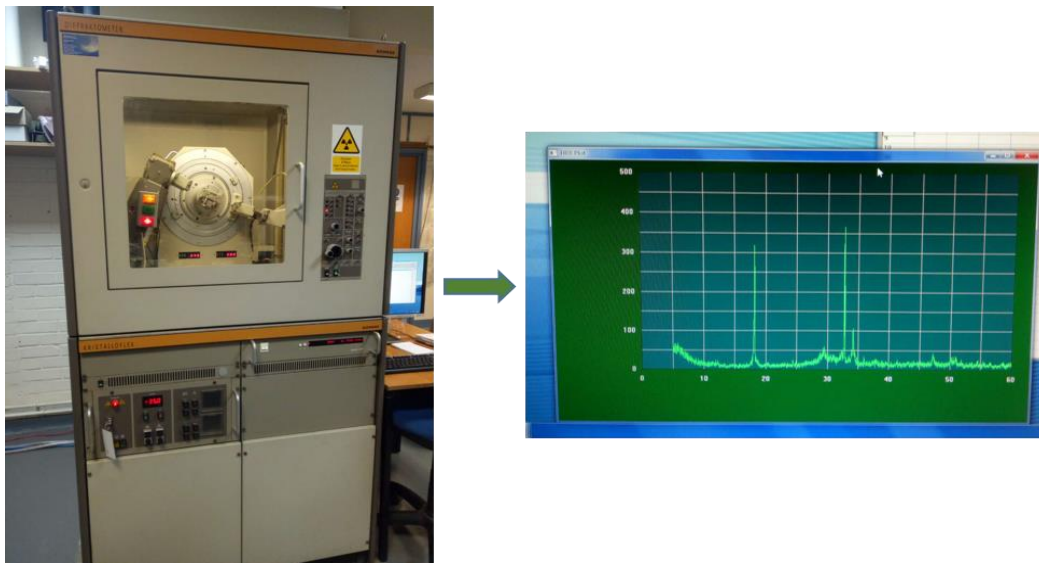
Figure 3.22 Powder X-ray diffraction (XRD) analysis using a Siemens D500 X-ray diffractometer.

Figure 3.23 Powder sample extraction from the crack surface of cement prisms containing microcapsules.

2. Thermogravimetric analysis (TGA)

TGA was used both for characterizing the microcapsules and studying the microstructure samples of the cement pastes containing MgO and/or microcapsules. TGA tests were conducted using a METTLER TOLEDOTGA/DSC 1 instrument (Figure 3.24a) and a PerkinElmer STA6000 instrument (Figure 3.24b). For microcapsule characterization, a small amount of microcapsule samples (3~5 mg) was placed into a ceramic crucible and heated within the temperature range of 50 to 650 $^{\circ}$C at a rate of 10 $^{\circ}$C/min in a nitrogen environment using a METTLER TOLEDOTGA/DSC 1. The cement paste powder samples prepared for the XRD tests as above were also used for the TGA tests. The powder samples (15±2 mg) were heated within the temperature range of 50 to 800 $^{\circ}$C at a rate of 10 $^{\circ}$C/min in air using the PerkinElmer STA6000.

3. Scanning electron microscopy (SEM) and energy dispersive X-ray spectroscopy (EDX)

SEM was used to characterize the surface morphology of the original microcapsules, MgO hydration products in the cement pastes, self-healing products, and microcapsules embedded on the crack surface. EDX was used to study the elemental composition of the materials observed under SEM. SEM and EDX were conducted using a FEI Nova NanoSEM FEG machine (Figure 3.25). Small chips were collected from the crushed cubic samples containing MgO additives, and from the crack surface of prism samples containing microcapsules. Similar sample preparation processes as described in the XRD sample preparation were used, such as

the prevention of hydration and drying in a vacuum chamber. The prepared microcapsule samples or chips were mounted onto aluminum stubs using adhesive carbon tape and silver patching. The stubs with the samples were then coated with gold film to ensure good conductivity and signals in the tests.
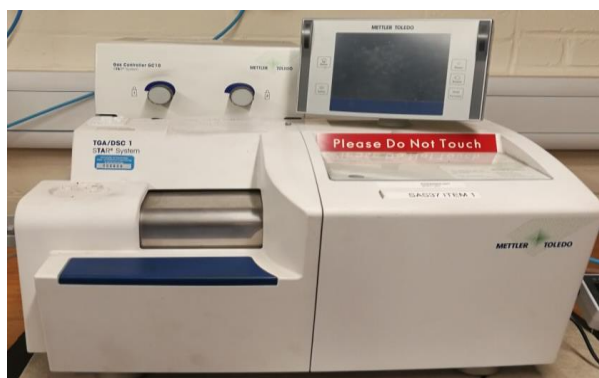
(a)
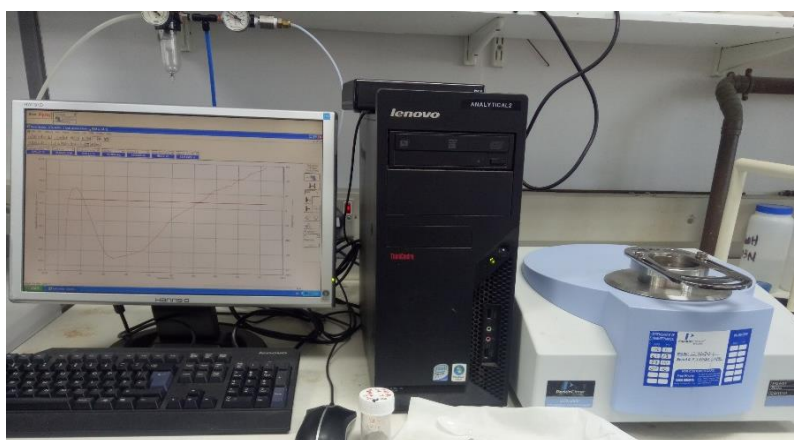
(b)

Figure 3.24 (a) METTLER TOLEDOTGA/DSC 1; (b) PerkinElmer STA6000 instruments for thermogravimetric analysis.

Figure 3.25 FEI Nova NanoSEM FEG for characterisation on MgO hydration products as well as self-healing products of sodium silicate microcapsules in cement pastes.

Chapter 4 Expansion performance of oil well cement with reactive MgO additives

4.1 Introduction

Most of the MgO expansive additives currently used in oil well cements are hard-burned or dead-burned types with low reactivity, that are mainly effective under high wellbore temperatures (usually above 150 °C). Therefore, reactive MgOs from higher reactivity grades are expected to be suitable for applications under lower wellbore temperatures. In this study, three types of reactive MgOs were used as expansive additives in oil well cements: N50 produced from seawater, and MAG-R and 92/200, both produced from low temperature calcination of magnesite, as detailed in Section 3.2.2. Their reactivities were examined by the acetic acid reactivity test. First, the expansion characteristics of the three reactive MgOs in oil well cement pastes were investigated by considering different influencing factors including MgO reactivity, MgO addition content, curing temperature, and restrained condition. For most low temperature wellbores, 80 °C is a representative temperature level which was therefore set as the target curing temperature in this study. After understanding their expansion characteristics, the effects of MgO reactivity and content on autogenous shrinkage reduction were studied under sealed conditions. The effects of MgO reactivity and content on drying shrinkage reduction as well as cracking resistance were examined under drying conditions with different relative humidities. In addition, the influences of the three types of reactive MgOs on oil well cement properties such as rheology properties, cement hydration, and compressive strength were also evaluated. On the basis of all the testing results, an overall evaluation was made on the suitability of the three reactive MgOs for use in oil well cements at lower wellbore temperatures.

4.2 MgO reactivity

The reactivities of MgO were tested by the acetic acid reactivity test and the results are given in Table 4.1. A smaller value for the neutralisation time (in seconds) represents higher reactivity. N50 synthesised from seawater has the highest reactivity among the three reactive

MgOs, followed by MAG-R produced from magnesite. 92/200, also produced from magnesite, has the lowest reactivity. According to the classification system of Jin & Al-Tabbaa (2014) mentioned in Chapter 2, Section 2.2.3.3, these three MgOs all belong to the reactive MgO group. N50 can be categorised as high reactivity with typical reactivity values of $\leq$ 30 s and SSA values $\geq$ 60 m^2/g. MAG-R can be categorised as medium reactivity with typical reactivity values between 30–300 s and SSA values between 10–60 m^2/g. The reactivity value of 92/200 belongs to the range of medium reactivity while its SSA value falls into the range of low reactivity ($\leq$ 10 m^2/g). Considering its significant difference from MAG-R in reactivity and SSA values, 92/200 is categorised as low reactivity in this study.

Table 4.1 Reactivity of the three reactive MgOs used in the study.

MgO type	Source	Reactivity (s)	SSA (m^2/g)	Reactivity grade
N50	seawater	~10	150.0	high reactivity
MAG-R	magnesite	75±20	54.9	medium reactivity
92/200	magnesite	140±16	9.0	low reactivity

4.3 Mix design of oil well cement samples

Different groups of cement mixtures were designed to study the expansion characteristics of reactive MgOs in oil well cement pastes as well as their shrinkage reduction performance and their influences on oil well cement properties. As shown in Table 4.2, mix groups I to III were prepared for tests on their expansion characteristics according to different influencing factors including the MgO reactivity and content, curing temperature, and restrained condition (free or restrained). Mix group IV samples were prepared for tests on the effects of MgO reactivity and content on autogenous shrinkage reduction under sealed conditions. Mix group V samples were prepared for tests on the effects of MgO reactivity and content on drying shrinkage reduction under drying (unsealed) conditions of different relative humidity (RH). Samples for restrained drying shrinkage at low RH were also prepared in this group to investigate the effects of reactive MgOs on the cracking resistance of oil well cement pastes. The remaining three mix groups (VI, VII, and VIII) were prepared for tests on evaluating the influences of reactive

MgOs on the rheological properties and hydration processes of fresh oil well cement slurries as well as the compressive strength of hardened oil well cement pastes. Throughout all mix groups, the three types of reactive MgO, namely N50, MAG-R and 92/200, were notated as RM1, RM2 and RM3, respectively. All the samples were prepared at a constant w/c ratio of 0.44.

Table 4.2 Mix design of oil well cement pastes with MgO additives.

Mix group	MgO type	MgO content (%)	temperature (ºC)	Restraint condition	Curing condition
I (MgO reactivity and content)	RM1	4, 8, 12	20	free	in water
	RM2	4, 8, 12	20		
	RM3	4, 8, 12	20		
II (curing temperature)	RM1	12	20, 40, 60, 80	free	in water
	RM2	12	20, 80		
	RM3	12	20, 40, 60, 80		
III (restraint condition)	RM1	12	20,80	restrained	in water
	RM2	12	20,80		
	RM3	12	20,80		
IV (autogenous shrinkage reduction)	RM1,RM2, RM3	4,8,12	80	free	sealed
V (drying shrinkage reduction)	RM2	4,8,12	80	free	unsealed at high RH 90%
	RM3	4,8,12			
	RM2, RM3	8	80	free	unsealed at low RH 25%
	RM2, RM3	8	80	restrained	water curing for 7 days then drying at low RH 25%
VI (rheology)	RM1, RM2, RM3	4,8,12	20, 40	-	-
VII (cement hydration)	RM1, RM2,RM3	12	20, 40	-	-
VIII (compressive strength)	RM1, RM2,RM3	4,8,12	80	free, restrained	in water

4.4 Expansion of oil well cement pastes with MgO

4.4.1 Expansion characteristics of reactive MgO in oil well cement pastes

4.4.1.1 Effect of MgO reactivity and content

According to mix group I in Table 4.2, class G oil well cement pastes containing reactive MgO with different reactivity values (RM1>RM2>RM3) at different contents of 4%, 8%, and 12% by weight of cement cured in water at 20 ºC were prepared to investigate the effect of MgO reactivity on their expansion performance. The length change of the cement pastes in mix group I were measured over a curing period of 60 days. The standard deviation for all measurements was less than 0.01%.

To distinguish the effect of MgO reactivity on expansion, Figure 4.1 presents the expansion curves of cement pastes with RM1, RM2 and RM3 at the same addition content level of 4%, 8% and 12% in Figures 4.1a–c, respectively. First of all, the addition of all three types of MgO increased the expansion of class G oil well cement pastes compared to the control samples. A very slight expansion was also observed in the control samples without MgO, which is due to the reabsorption of water as reported by Acker (2004).

The expansion trends depicted in Figure 4.1 indicate that MgOs with higher reactivity have a faster expansion rate and larger expansion magnitude at the early age, and experience a relatively shorter expansion period before plateauing at a later age. This can be attributed to their high SSA and porous microstructure which promotes their hydration at an early age. (Canterford 1985). According to the expansion model proposed by Mo et al. (2010), MgO with high reactivity has porous structures and a high volume of interior pores, which allows hydration to take place quickly both at the surface and interior pores of the MgO grains at an earlier age. As a result, it hydrates faster at an early age to form more brucite crystals which generate greater stress to expand the cement matrix, thus a larger expansion magnitude was observed with RM1 and RM2 at early age.
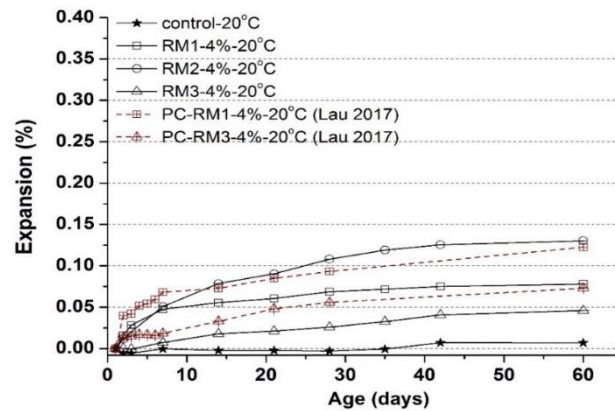
(a)
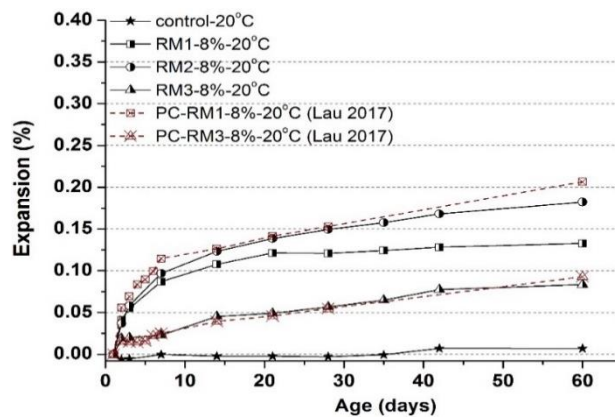
(b)
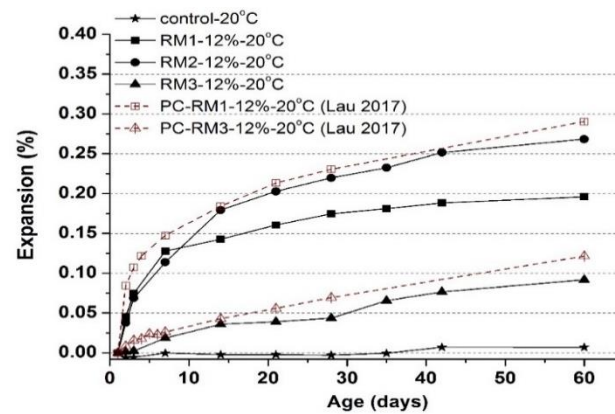
(c)

Figure 4.1 Expansion performance of mix group I oil well cement pastes (black solid lines) containing three types of reactive MgO with different reactivities (RM1>RM2>RM3) at the same addition content of (a) 4%; (b) 8%; (c)12% by weight of cement, cured in water at 20 ºC over 60 days, compared with ordinary Portland cement pastes (w/c=0.35) containing the same type RM1 or RM3 cured in water at 20 ºC.

125

Meanwhile, the faster hydration means a higher initial hydration degree at an early age, therefore resulting in a shorter expansion period before stabilising. The higher the MgO reactivity, the higher the hydration degree at the same curing age, as demonstrated by Li et al. (2010) and Mo et al. (2010). RM2 has lower reactivity than RM1 and thus experienced a longer expansion duration. It was also noted that RM2 produced a larger overall expansion at a later age than RM1. This can be explained from the expansion model of Mo et al. (2010). RM1 has even higher SSA and a more porous structure than RM2, so that RM1 grains have more interior space to accommodate the brucite crystals. Thus a smaller expansion stress was produced to expand the cement pastes despite the higher hydration degree. Another possible reason is that the expansion occurs too quickly for RM1 when the cement paste is still in the fluid state so that it may not generate effective expansion.

By contrast, RM3, with the lowest reactivity, showed delayed expansion property. It has much smaller SSA and a less porous microstructure than RM1 and RM2, thus slower hydration and smaller expansion at early age. According to Mo et al. (2010), the hydration products brucite mainly deposit at the MgO grain boundaries and will induce larger expansion force after accumulating at the boundary over an induction period. Thus the low reactivity MgO will experience faster and larger expansion at a later age. In the same way, RM3 was expected to have accelerated hydration over the long term curing after 60 days, reaching a larger expansion magnitude than RM1 and RM2.

Cement pastes with three MgOs at other two content levels of 4% and 8% had similar trends to those described above: MgO with higher reactivity expanded faster with a larger expansion magnitude at early age; MgO with lower reactivity had slower and smaller expansion at an early age but larger ultimate expansion at a later age.

In general, the reactive MgOs showed consistent expansion trends with those results reported in literature as reviewed in Section 2.2.3.1. Especially, the expansion performances of these reactive MgOs were also compared with the results by Lau (2017) who used the same type MgO RM1 and RM3 in ordinary Portland cement system, as shown in Figure 4.1. It showed that MgO RM3 with low reactivity had similar expansion trends and expansion magnitudes in the oil well cement pastes as in ordinary Portland cement pastes. But for MgO RM1 with high

reactivity, despite of similar expansion trends, oil well cement pastes with RM1 showed smaller expansion magnitude than that of ordinary Portland cement pastes with RM1 in the study of Lau (2017), especially at later age. This is likely due to the higher w/c ratio of oil well cement pastes (0.44) than that of ordinary Portland cement pastes (0.35). Higher water content can promote MgO hydration at early age. The accelerated hydration of highly reactive RM1 occurred at an early age could be ineffective to generate expansion in the cement paste due to its low strength, thus leading to smaller overall expansion magnitude at the later age. By contrast, the influence of w/c ratio was insignificant to RM3 with low reactivity due to its very slow hydration at the early age.

It was noticed that the expansion magnitude generally increased proportionally with increasing MgO content. A higher content of MgO meant more hydration products and thus a larger expansion stress was generated to expand the cement pastes. This positive relationship between MgO content and the resultant expansion magnitude can be more directly viewed in Figure 4.2 a–c which replot the expansion curves in Figure 4.1 in terms of the variation in MgO addition contents for each type of MgO. For cement pastes with RM1 the expansion at 60 days was ~0.08% at an MgO content of 4% and this value increased to ~0.13% and ~ 0.2% at content of 8% and 12%, respectively. Similarly, by increasing the content from 4% to 8% and 12%, the expansion after 60 days of cement pastes with RM2 increased from 0.13% to 0.18% and 0.27%, respectively. The expansion of the least reactive RM3 showed a relatively insignificant difference with increasing addition content. This was attributed to its delayed expansion property which resulted in slow hydration and expansion at an early age.
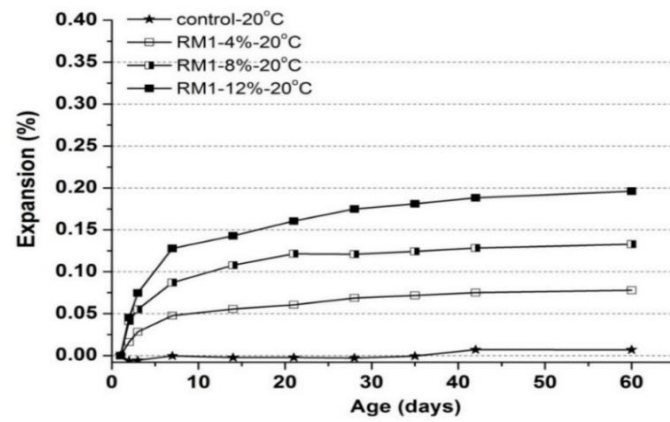
(a)
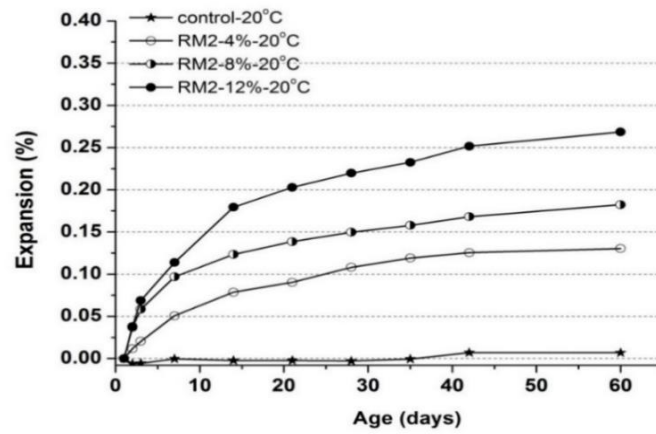
(b)
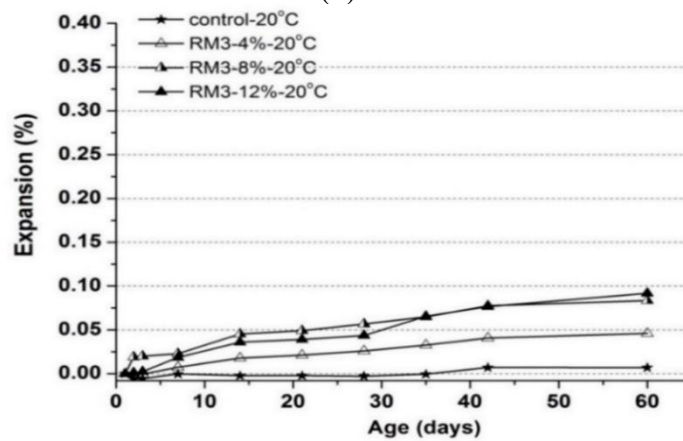
(c)

Figure 4.2 Expansion performance of oil well cement pastes containing three types of reactive MgO with different reactivities (RM1>RM2>RM3) at the same addition content of (a) 4%; (b) 8%; (c)12% by weight of cement, cured in water at 20 ℃ over 60 days.

4.4.1.2 Effect of curing temperature

In mix group II, cement pastes with the three MgOs were cured at different temperatures in water and were measured for length changes over a period of 60 days. The standard deviation for all measurements was less than 0.01%.

Figure 4.3 compares the expansion performance of the cement pastes with 12% RM1, RM2, and RM3 cured at 80 °C with those cured at 20 °C. It is apparent that an acceleration of hydration occurred for all the MgOs so that the expansion of the cement pastes stabilised earlier compared to those cured at 20 °C. At 80 °C, the expansion of the cement pastes with RM1 and RM2 levelled off quickly within the first 3 days, and the one with RM3 kept expanding until around 14 days. According to Rocha et.al (2004), the hydration rate of MgO can be promoted by increasing the temperature and thus ensuring a higher degree of conversion into $Mg(OH)_2$. Therefore, faster expansion was generated by MgO in the cement pastes as the temperature increased.
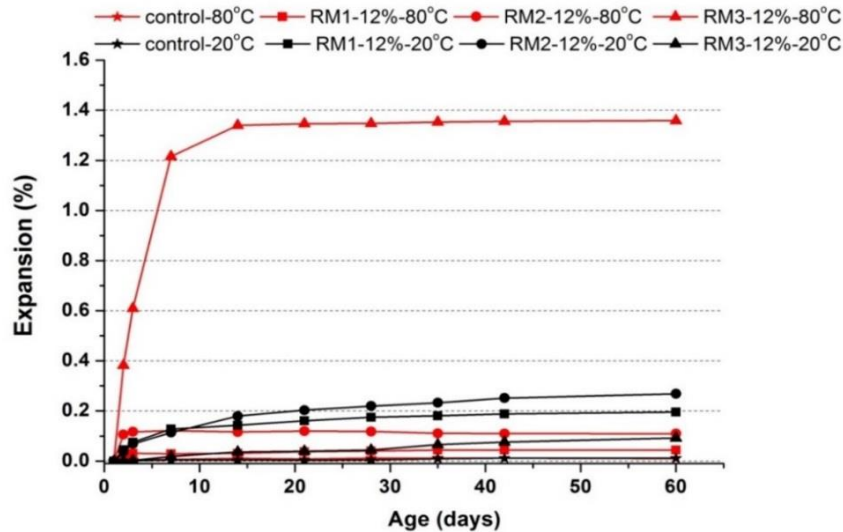
Figure 4.3 Expansion performance of oil well cement pastes containing three types of MgOs at 12% by weight of cement cured in water at 20 °C and 80 °C, respectively.

The trends for the expansion magnitude, however, varied significantly from that at 20 °C. It can be seen that cement pastes with RM3 produced the largest expansion magnitude throughout the whole curing age and reached an ultimate expansion as high as ~1.36%, followed by the

one with RM2 of ~0.12% ultimate expansion. RM1 showed the least expansion among the three MgOs with only ~0.05%. It seems that MgO with a higher reactivity had a smaller expansion magnitude at high temperature of 80 °C, which is contrary to the trends observed among the three MgOs at 20 °C as described above in Section 4.4.2.
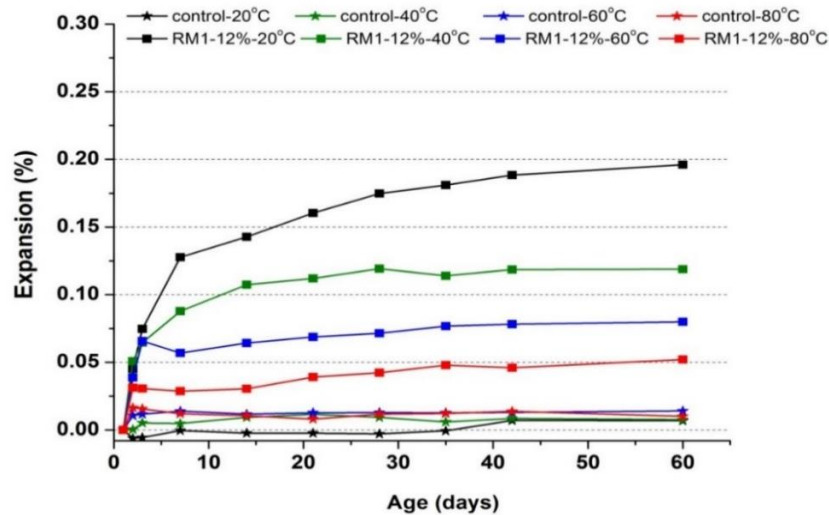
(a)
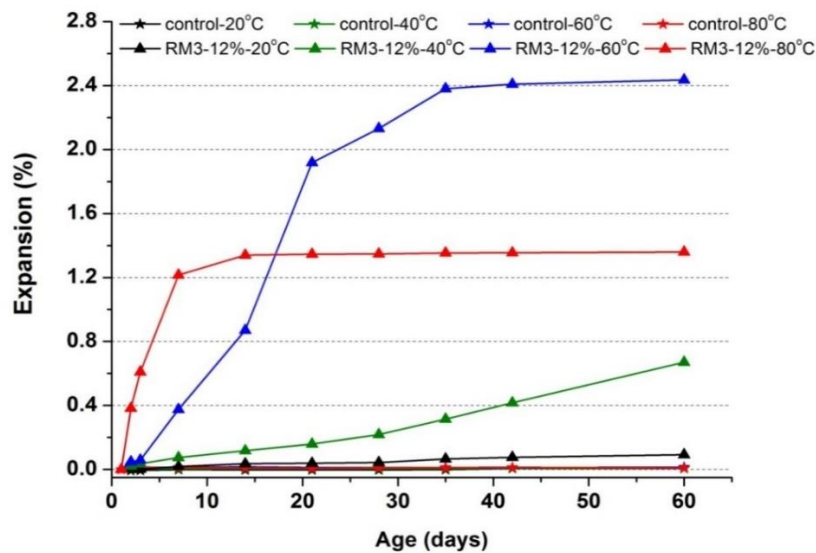
(b)

Figure 4.4 Expansion performance of oil well cement pastes containing MgO (a) RM1 with the highest reactivity and (b) RM3 with lowest reactivity, at content of 12% by weight of cement cured at four temperature levels of 20, 40, 60 and 80 °C in water.

To better observe the variation in trends of expansion behaviour, especially in the expansion magnitude with temperature, length changes of cement pastes with MgO cured in water at four different temperature levels of 20, 40, 60 and 80 ºC are compared in Figure 4.4. RM1 with the highest reactivity and RM3 with the lowest reactivity were selected as representatives from the three MgOs, and their addition content is 12% by weight of cement.

In Figure 4.4a, as the curing temperature was raised from 20 ºC to 40 ºC, 60 ºC and 80 ºC, the expansion period of RM1 was gradually shortened. At 20 ºC, cement pastes with RM1 kept expanding until ~42 days before levelling off. When cured at 60 ºC and 80 ºC, the expansion of RM1 levelled off at very early age within 1 days. This clearly shows that the higher the curing temperature, the faster the expansion.

However, despite the accelerated expansion rate, the expansion magnitude of the cement pastes with 12% RM1 decreased with increasing temperature. The higher the temperature, the lower the expansion magnitude of the cement pastes. When the temperature increased from 20 ºC to 40, 60 and 80 ºC, the ultimate expansion at 60 days experienced a gradual decrease from 0.196 % to 0.119%, 0.08% and 0.052%, respectively. Such a decreasing trend of expansion magnitude could be attributed to a combination of several factors. Firstly, MgO has a higher hydration degree at early ages at elevated temperatures, as mentioned above. RM1, with the highest reactivity, hydrated too fast at high temperature and thus the expansion was too early to generate effective expansion stress upon the cement matrix. If the hydration and crystallisation of MgO occurs too early when the cement slurry is in the fluid phase, the cement system is unable to sustain the expansive forces (Ghofrani& Plack 1993). In addition, the measurements started after demoulding. As previously mentioned, it is very likely that a larger proportion of RM1 has already hydrated during the period before demoulding at elevated temperature. Thus less expansion was measured after demoulding. Secondly, the curing temperature can affect the microstructure of the hydration product, brucite. At low temperatures, the brucite agglomerates formed on MgO grains have a porous microstructure while those brucite particles become more compact with smaller crystal size at high temperature (Rocha et al. 2004). The denser microstructure of the hydration products might result in a smaller internal stress for expansion, therefore a smaller expansion is generated in the cement pastes.

131

In Figure 4.4b, cement pastes with RM3 also showed accelerated expansion at elevated temperature which was similar to RM1. But increasing temperature seemed to have a more pronounced influence on promoting the expansion of the least reactive RM3. Its long induction period at 20 ℃ was notably shortened with increasing temperature. At 40 ℃, its expansion accelerated and exhibited near-linear growth during the curing period. When the temperature was raised to 60 ℃, the expansion rate was exponentially increased at an early age and the expansion plateaued at ~35 days. When the temperature reached 80 ℃, the expansion was further accelerated with a much shorter expansion period of ~7 days. The expansion magnitude of the cement pastes with RM3 at an early age was also significantly enhanced by increasing the curing temperature. According to (Mo et al. 2010), MgO with low reactivity has a less porous structure and thus less space to accommodate hydration products. At higher temperatures, there are more hydration products formed at the grain boundary to induce excessive expansive force upon the RM3 grains, leading to earlier breakage of the grains and enlarging the specific surface area. As a result, the induction period was reduced and the least reactive RM3 started to expand faster at an earlier age.

The ultimate expansion magnitude for RM3 at 80 ℃ was much lower than that at 60 ℃. This is consistent with the performance of RM1, as discussed above. Higher temperature accelerates the hydration rate but may lead denser microstructures of MgO hydration products, resulting in a smaller ultimate expansion magnitude. Of course, the faster hydration that occurred at the elevated temperature before demoulding might be another possible reason contributing to the decreased expansion magnitude measured. Therefore it is expected that, given sufficient time, the ultimate expansion of RM3 at low temperature of 20 ℃ and 40 ℃ would exceed that at 60 ℃.
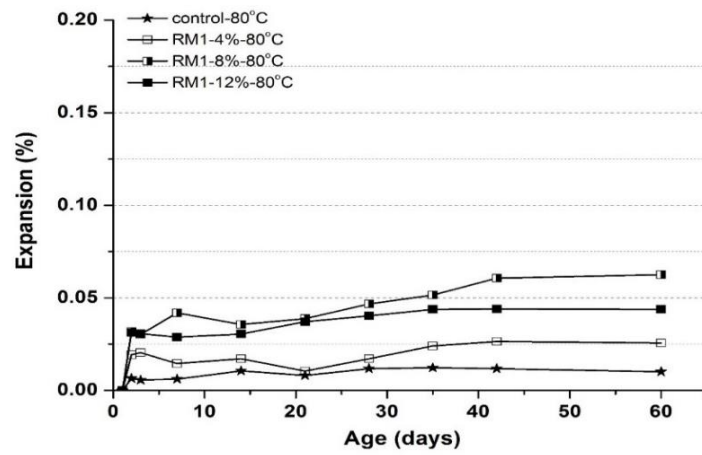
(a)
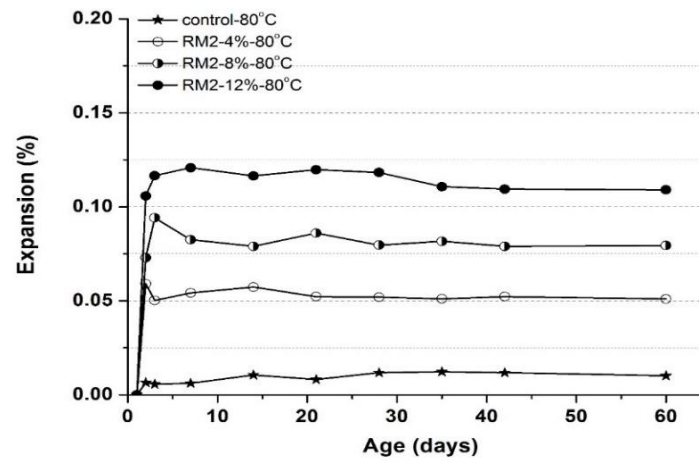
(b)
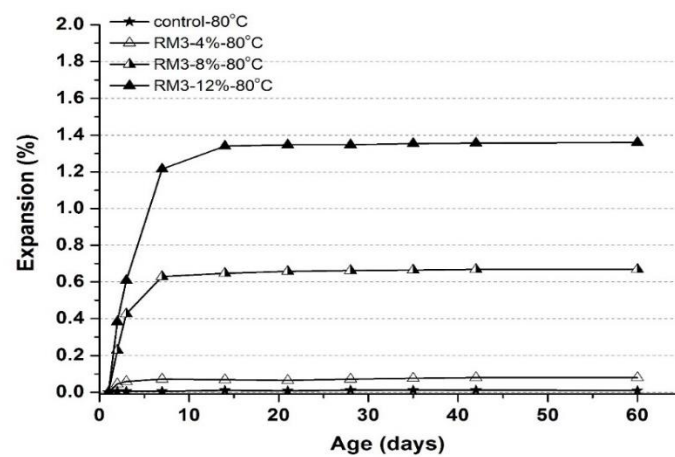
(c)

Figure 4.5 Expansion performance of oil well cement pastes containing MgO (a) RM1; (b) RM2; (c) RM3 at different addition contents of 4%, 8% and 12% cured at 80 ^{o}C in water.

133

Figure 4.5 presents the expansion curves of cement pastes containing RM1, RM2 and RM3 at different addition contents of 4%, 8% and 12% cured at 80 °C. For all three MgOs, a higher content generally resulted in larger expansion which was consistent with the results at 20 °C. But the degree to which the MgO content affected the expansion magnitude of three MgOs at 80 °C was different from that at 20 °C. According to the results reported in Section 4.4.1.1, the increasing MgO content did not show significant improvement in expansion magnitude of RM3 at 20 °C due to its slow hydration during the induction period. When cured at 80 °C, however, the increase of MgO content from 4% to 8% and 12% led to a remarkable increase in the ultimate expansion magnitude from ~0.08% to ~0.67% and ~1.36%, respectively (Figure 4.5c). RM3 had its induction period significantly shortened at high temperature due to accelerated hydration. Therefore, the increasing effect of MgO content on its expansion magnitude was clearly observed within the curing period of 60 days at 80 °C. By contrast, the expansion magnitudes of the cement pastes with RM1 showed indistinct variation with different contents at 80 °C (Figure 4.5a). Obviously, because of its too fast hydration and small expansion at high temperature, the increase in the addition content of RM1 did not efficiently increase the expansion in cement paste.

The above results highlighted that increasing temperature promoted the hydration rate of reactive MgO thus faster expansion at an early age. For the high reactivity RM1, the temperature effect further accelerated its fast hydration at an early age, which can lead to ineffective expansion before cement setting. As a result, the expansion magnitude decreased with increasing temperature. The RM2 with medium reactivity showed a similar trend to RM1 at high temperature, but a higher expansion magnitude than RM1. The RM3 of low reactivity experienced delayed expansion that was significantly advanced by increasing temperature, showing a faster expansion rate as well as a higher expansion magnitude at an early age. At ambient condition of 20 °C, the addition of 12% RM1 or RM2 could generate a fast free expansion of 0.268% and 0.2% respectively, while the addition of 12% RM3 showed much slower and smaller expansion less than 0.1%. At the target temperature of 80 °C, RM1 showed the least expansion less than 0.05% at content of 12% while RM3 had the largest expansion of 1.36% at content of 12% in oil well cement pastes. Considering that the external volumetric

134

reduction in oil well cement is usually a few tenths of 1% (Gotsis et al.1984; Nelson, 2006), RM1 and RM2 seem to be more efficient in compensating for the external volumetric reduction at 20 ºC, while RM3 is the most effective in expansion at 80 ºC.

4.4.1.3 Expansion under restrained condition

Figure 4.6 presents the expansion performance of both unrestrained and restrained oil well cement pastes containing different reactive MgOs at a content of 12% cured at 20 ºC and 80 ºC, respectively. Generally, the restrained samples followed similar expansion trends to the unrestrained samples but with a smaller expansion magnitude at the same age. In Figure 4.6a, both the unrestrained and restrained cement pastes containing RM2 had the largest expansion at 20 ºC. The expansion at 60 days was reduced by ~42% under a restrained condition. For cement pastes with RM1, the expansion at 60 days had a reduction of ~39% from the unrestrained to restrained condition. Cement pastes with RM3 saw the least reduction under restraint due to its delayed expansion property at 20 ºC. At elevated temperature of 80 ºC (Figure 4.6b), the cement pastes with RM3, which expanded the most under free conditions, had the most significant reduction in expansion under restraint.

Cement pastes with higher free expansion had a greater reduction in expansion under restraint. The expansion of cement pastes depends on the expansive energy generated by MgO hydration and crystallisation. If the deformation is confined, the expansive energy will be in turn transferred into pre-compressive stresses which condense the internal microstructure of the cement matrix. The higher the expansion energy, the more the cement will be compressed. MgO with lower reactivity produced larger free expansion which indicated higher expansive stresses exerted on the cement pastes, thus a more significant reduction in expansion under restraint. Such pre-compressive stresses under a restrained condition are beneficial to improving shrinkage cracking resistance as well as the strength of the cement pastes, which will be discussed later in Section 4.4.3 and 4.5.3.
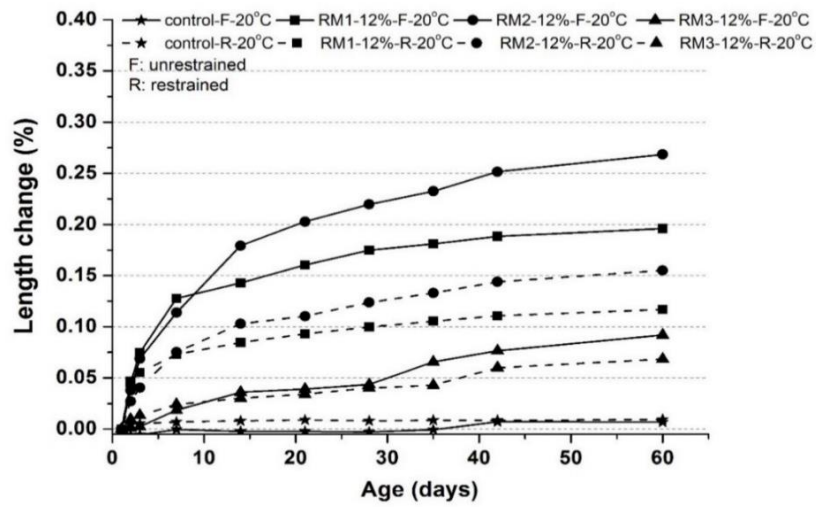
(a)
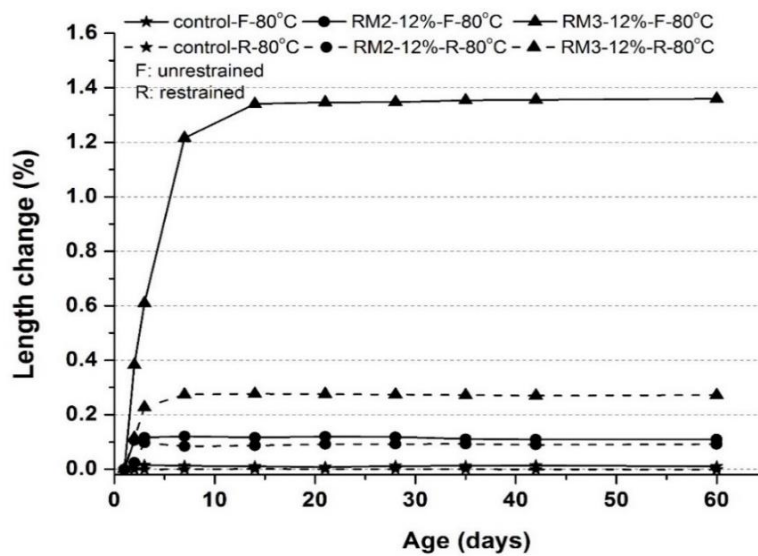
(b)

Figure 4.6 Expansion performance of unrestrained and restrained oil well cement pastes containing different reactive MgOs at a content of 12%, (a) Cement pastes with RM1, RM2 and RM3, respectively, cured at 20 °C; (b) Cement pastes with RM2 and RM3 respectively cured at 80 °C.

4.4.2 Effects of MgO on shrinkage reduction under sealed condition

In mix groups I, II and III, the expansion characteristics of cement pastes with three types of reactive MgO were investigated under water-curing conditions. However, in the underground

wellbore condition, access to water could vary according to the formation conditions. Water is available within a range of aquifers underground. However, in the case of impermeable layers, the cement sheath has very limited access to external water curing. In such condition, the cement is subjected to significant autogenous shrinkage and the hydration of MgO can also be affected. Therefore, it is necessary to investigate the expansion performance of three reactive MgOs under conditions of no water for curing so as to evaluate their ability to compensate for autogenous shrinkage of oil well cement pastes. Accordingly in mix group IV, cement pastes containing three types of MgOs at different contents were cured at 80 $^{\circ}$C under sealed condition. The length change measurements were conducted on sealed cement pastes considering the effects of MgO reactivity and addition contents. The autogenous expansion and shrinkage values are showed as positive and negative, respectively. All the measurements had a standard deviation less than 0.01%, and weight loss was less than 0.5%.

4.4.2.1 Effect of MgO reactivity

Figure 4.7 shows the length change results of cement pastes containing MgOs with different reactivities (RM1, RM2 and RM3) at content of 8% cured under sealed conditions at 80ºC. The control cement paste without MgO addition showed shrinkage under sealed conditions from the beginning of measurements at 6 hours, and had a rapid increase in autogenous shrinkage at an early age and then gradually stabilised. After 60 days, the autogenous shrinkage reached ~ -0.05%. The autogenous shrinkage of cement pastes is caused by capillary forces developing in the cement paste due to self-desiccation, which was discussed in Chapter 2 Section 2.1.4.

In comparison to the control sample, cement pastes with the three types of MgO showed different degrees of reduction in autogenous shrinkage. RM1 with the highest reactivity showed the least shrinkage reduction. After a short and small expansion before the early age of 3 days, cement pastes with RM1 started to shrink. The cement pastes eventually showed a net shrinkage value of ~ 0.01%. Compared to the control sample, the addition of 8% RM1 reduced the autogenous shrinkage by ~80%. Referring to the expansion characteristics of the three MgOs cured in water at 80 $^{\circ}$C in Section 4.4.1, too rapid hydration of RM1 occurring before cement hardening may lead to less effective expansion stresses left to fully counteract the autogenous shrinkage stresses. The fast hydration of RM1 at an early age may also result in

finer pore sizes of the cement pastes which negatively affect the shrinkage reduction performance. Finer pore structures can induce high capillary forces leading to higher autogenous shrinkage (Holt 2001).
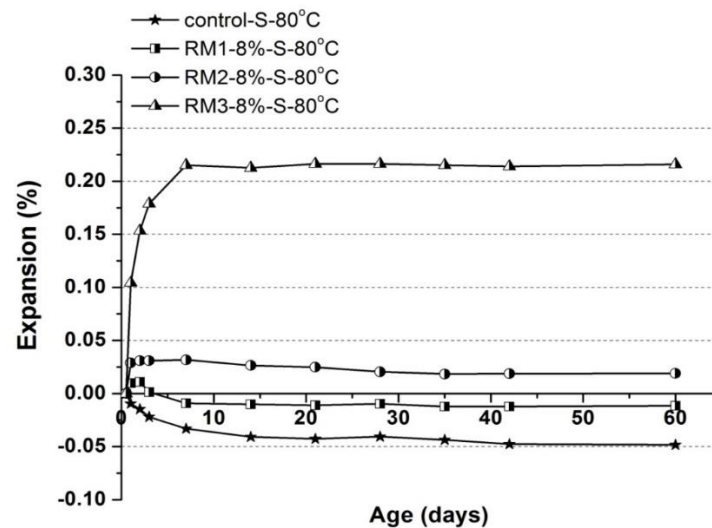
Figure 4.7 Length change of oil well cement pastes containing MgOs with different reactivities (RM1, RM2 and RM3) at a content of 8% cured under sealed condition at 80 $^\circ$C.

By contrast, cement pastes with 8% RM2 or RM3 of relatively lower reactivity showed overall expansion during the curing age under sealed conditions which indicated complete shrinkage compensation. Cement paste with 8% RM2 of medium reactivity had a fast expansion at the early age of ~3 days, which could fully compensate for the shrinkage. As a result, cement pastes with 8% RM2 presented a net expansion value of ~0.02% at 60 days. Compared with the control sample, the addition of 8% RM2 reduced the autogenous shrinkage by ~139%.

The RM3 with the lowest reactivity was the most effective in autogenous shrinkage compensation. Cement paste with 8% RM3 not only had complete shrinkage compensation but also much a larger expansion throughout the curing age than the mix with RM2. It expanded rapidly within 7 days and levelled off at the highest expansion magnitude of ~0.22%, resulting in a dramatic reduction in autogenous shrinkage by ~540%. As discussed in Section 4.4.1, RM3 with the lowest reactivity was able to generate much greater expansion than RM1 and RM2 due to its delayed expansion property. To break the boundary layer around the MgO grains, greater expansion stresses were generated during the hydration of RM3 (Mo et al. 2010), which

138

were more than adequate to counteract the autogenous shrinkage stresses. Compared to RM1 and RM2, RM3 had a longer expansion period with continuous growth in expansion stresses until ~7 days. By then, the autogenous shrinkage of the cement pastes itself had levelled off. Thus the high expansion magnitude produced by RM3 was maintained afterwards.

4.4.2.2 Effect of MgO content

Figure 4.8 presents the length change results of the cement pastes containing different contents (4%, 8%, 12% by weight of cement) of RM1, RM2 or RM3 cured under sealed conditions at 80 °C. The results for cement pastes with RM1 showed that increasing the MgO contents had no significant effects on autogenous shrinkage reduction. All RM1 cement pastes showed comparable net shrinkage at later ages. Cement pastes with RM2 or RM3 had complete shrinkage reduction and showed net expansions at all MgO addition contents. The ultimate expansion magnitude increased from less than ~ 0.01% at content of 4% to ~0.03% by 12% addition of RM2. As for RM3, increasing the MgO content from 4% to 12% led to a dramatic growth in ultimate expansion from ~0.017% to 0.74%.

More MgO addition means more hydration products and thus lager expansion stresses generated for shrinkage reduction and even further expansion. This is consistent with the effects of MgO content on expansion that were observed under water-curing conditions in Section 4.4.1. Mo et al. (2010 & 2012) also reported an increase of expansion with higher MgO contents under non-wet curing conditions. The insignificant effect of MgO content for high reactivity RM1 was related to its hydration at 80 °C being too fast, as explain above in Section 4.4.2.1.

According to the results above, it is evident that medium reactivity RM2 and low reactivity RM3 are more effective in compensating for autogenous shrinkage at the high temperature of 80 °C. High reactivity RM1 had inferior compensation effectiveness due to the expansion rate being too fast at an early age, and the resultant smaller expansion. Additionally, the results also reflected the low water demand for hydration of MgO which enabled expansion even under sealed conditions without an external water supply, as reported in the literature.
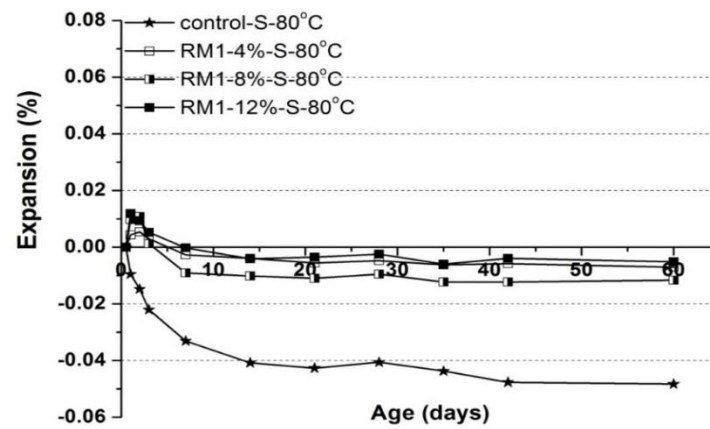
(a)
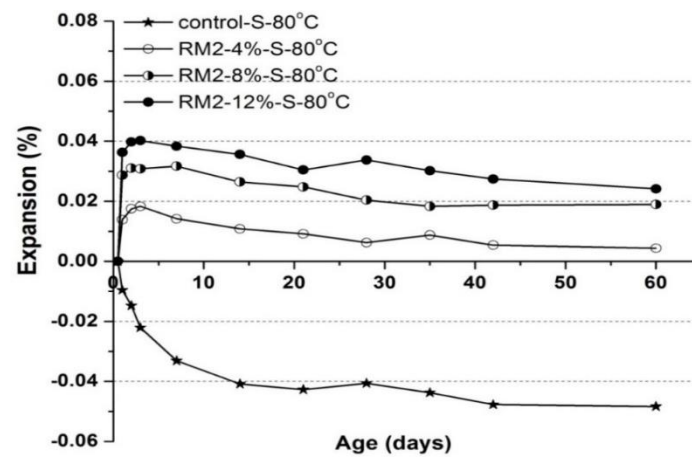
(b)
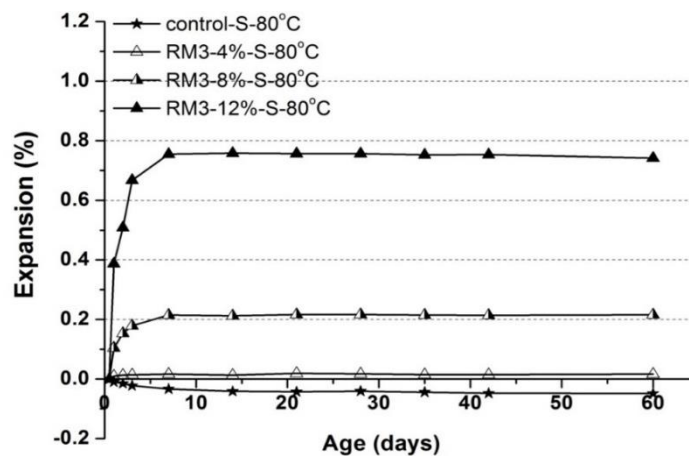
(c)

Figure 4.8 Length changes of oil well cement pastes containing different contents (4%, 8%, 12% by weight of cement) of reactive MgO RM1, RM2 or RM3 cured under sealed conditions at 80 ºC.

4.4.3 Effects of MgO on shrinkage reduction under drying conditions

Cement sheaths in a wellbore may also encounter drying conditions, for example in a porous but non-water-saturated formation layer or high salt layer, in which the drying shrinkage can be induced due to moisture loss. Coupled with the high temperature of a wellbore, the cement sheath is actually subjected to a hot-dry environment. In mix group V, the performance of reactive MgO on shrinkage reduction under drying conditions at 80 °C was investigated with the influencing parameters including MgO reactivity, MgO content, and humidity. Based on their better performance on autogenous shrinkage reduction, the MgOs RM2 and RM3 were selected for use in this mix group and were added in the cement pastes at different contents of 4, 8% and 12%, as shown in Table 4.2. Cement samples were exposed to a high relative humidity (RH) of 90% and low relative humidity (RH) of 25%, respectively.

As reviewed in Chapter 2, Section 2.2.4.2, Lau (2017) reported that the expansion of MgO under restrained conditions was beneficial in reducing shrinkage. Therefore, restrained cement pastes containing RM2 and RM3 at a content of 8% were also prepared for drying shrinkage tests to evaluate their performance under drying conditions of 25% RH at 80 °C.

The length change and weight loss of cement pastes in mix group V over a period of 28 days were measured. All the length change measurements had a standard deviation less than 0.01%.

4.4.3.1 Unrestrained length change under drying conditions

Figure 4.9 presents the length change and the accompanied weight loss of oil well cement pastes containing different contents of reactive MgOs (RM2 or RM3) under drying conditions of 90% RH at 80 °C. When subjected to drying, control cement pastes without MgO showed rapidly increasing shrinkage within the early age of ~5 days, then levelled off at ~14 days (Figure 4.9a). The drying shrinkage is known to be due to moisture evaporation and migration to the dry environment driven by the relative humidity gradient inside and outside the cement pastes (P. Kumar Mehta & Monteiro 2006). The high temperature can also accelerate the hydration of cement, change of internal structure and moisture evaporation (Yang et al. 2014). Thus a rapid growth of shrinkage was seen at an early age.

Cement pastes containing low reactivity RM3 exhibited remarkable drying shrinkage reduction at 90% RH. At an addition content of 4%, cement pastes with RM3 showed almost no shrinkage during the drying period. A slight expansion was observed during the early age before 7 days. When the addition content increased to 8% and 12%, the cement pastes showed even greater increase in expansion and maintained their expansion state throughout the whole drying age. Despite moisture loss under drying (Figure 4.9b), it seemed that RM3 with its strong expansion capability at high temperature was able to produce sufficient expansive stresses which not only compensated for the drying contraction but also induced volume expansion in the cement pastes. In addition, MgO hydration led to additional consumption of internal moisture, which is likely to lower the humidity gradient and inhibit the moisture evaporation. As shown in Figure 4.9b, all cement pastes incorporating reactive MgO showed less weight loss than the control cement pastes.

By contrast, RM2, with medium reactivity, was only effective at compensating for the drying shrinkage at an early age. Within the early age of 3 days, RM2 at content of 8% and 12% showed significant drying shrinkage reduction. In particular, net expansion was observed in cement samples containing 12% RM2. However, because of its short expansion duration at 80 °C, the expansion by RM2 was only able to offset the shrinkage at an early age. After its expansion was completed, the drying shrinkage of RM2 cement pastes continued to increase in the following age. As a result, the drying shrinkage was only partially compensated by ~ 22%.
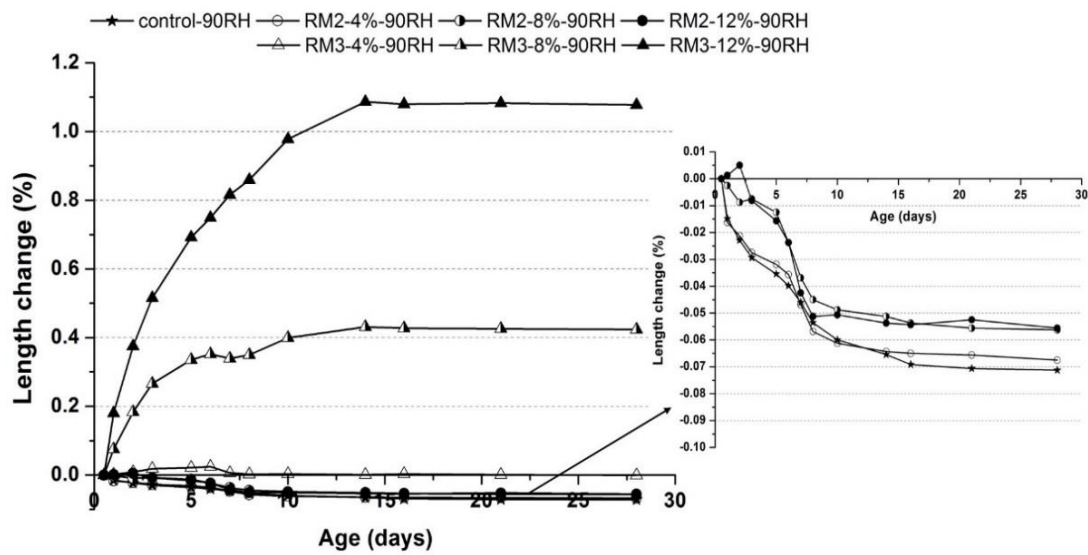
(a)
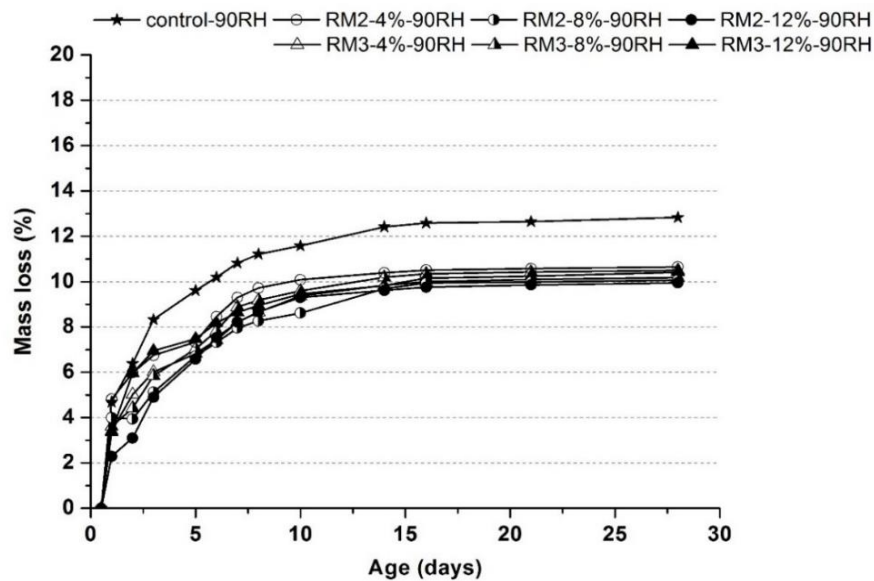
(b)

Figure 4.9 Length change (a) and the accompanied weight loss (b) of oil well cement pastes containing reactive MgOs (RM2 or RM3) at different contents of 4%, 8% 12% by weight of cement under drying conditions of 90% RH at 80 ºC.
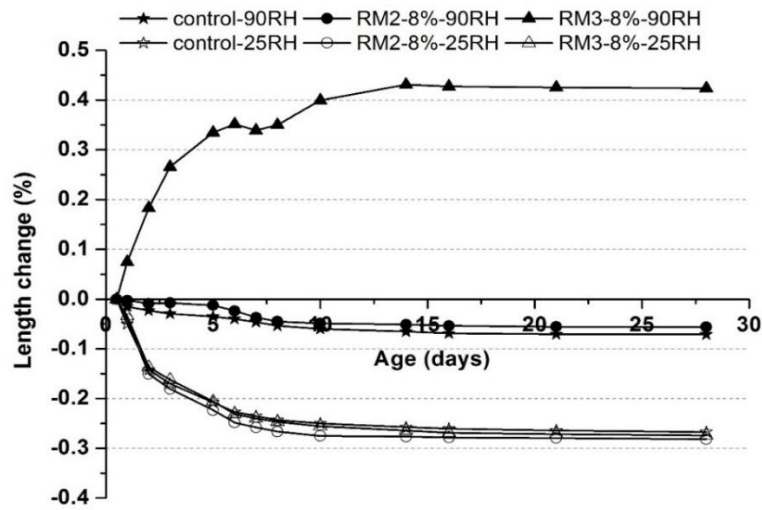
(a)
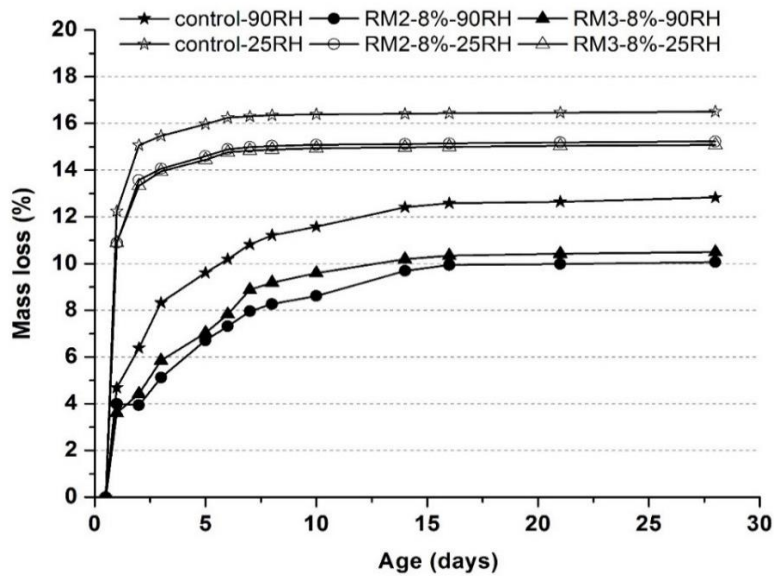
(b)

Figure 4.10 Length change (a) and weight loss (b) oil well of cement pastes with RM2 or RM3 at a content of 8% under different drying conditions of high RH of 90% and low RH of 25% at 80 ºC.

The relative humidity of a drying environment is known to have significant influence on the drying shrinkage of cement. The performance of reactive MgO on drying shrinkage reduction at low RH was also examined. Cement pastes containing RM2 or RM3 at a content of 8% were

144

selected for drying at low RH of 25%. Figure 4.10 compares the performances of reactive MgO (RM2 or RM3) on drying shrinkage reduction under a high RH of 90% and low RH of 25%. Unlike their performance at a high RH of 90%, neither of these two reactive MgOs showed effective drying shrinkage reduction at a low RH of 25%. In Figure 4.10a, both cement samples with RM2 and those with RM3 showed almost identical drying shrinkage to the control samples. Furthermore, the drying shrinkage of all the cement pastes remarkably increased when subjected to low RH drying condition. This might be mainly due to the increase of moisture loss at low RH. A low ambient RH will produce strong gradients near the drying surface, thus increasing the drying rate (Bissonnette et al. 1999). In Figure 4.10b, it is evident that cement pastes under low RH experienced the moisture loss at a faster rate and in higher amounts. Especially at an early age, sharp increases in weight loss were observed in all cement pastes, which induced greater contraction stresses within the cement pastes, thus substantial increase in drying shrinkage. Meanwhile, the substantial moisture loss may possibly inhibit the further hydration and expansion of MgO due to less internal water being available. As a result, there were insufficient expansion stresses from the reactive MgOs to compensate for the contraction stresses.

In conclusion, when exposed to drying conditions at 80 °C, MgO RM3, with the low reactivity, showed complete compensation for the drying shrinkage while MgO RM2 with medium reactivity was only effective in reducing early-age drying shrinkage at a high RH of 90%. At low RH, the addition of reactive MgO was ineffective in drying shrinkage reduction.

4.4.3.2 Restrained length change under drying condition

Figure 4.11 shows the length change of one-dimensional restrained oil well cement pastes containing reactive MgO (RM2 or RM3) at a content of 8% under drying condition of 25% RH of at 80 °C. The restrained cement samples were first cured in water at 80 °C for 7 days which allows for the sufficient hydration of MgO to produce expansion under restraint, which was followed by curing in drying conditions of 25% RH at 80 °C for up to 28 days.

During the period of water curing, MgO blended cement samples showed different degrees of expansion. Cement pastes with 8% RM2 had a short and small expansion that stabilised at the

early age of 3 days, while those with 8% RM3 had more significant expansion that continuously grew during 7 days, which was consistent with the expansion trends of the restrained cement pastes cured in water as described in Section 4.4.1.3. However, when exposed to a low RH environment, all the restrained cement pastes started to shrink due to the contraction stress caused by moisture loss. Rapid length reduction were observed at an early age of drying, particularly for cement samples with the reactive MgOs RM2 or RM3. This is possibly due to the increase in the volume of micropores in the cement caused by the restrained expansion of MgO during the initial water curing period. Under restrained conditions, MgO expansion can lead to a finer pore structure of cement (Zhu et al. 2013). After all the length contractions stabilized at ~21 days, it was found that the cement sample with RM2 had an ultimate restrained drying shrinkage that was higher than the control sample, and the one with RM3 had a comparable value to the control sample. The results indicated that the restrained expansion of MgO at an early age was not effective in reducing drying shrinkage at a later age under a low RH of 25%.

However, the restrained cement pastes incorporating reactive MgO were found to have good performance on the resistance to cracking caused by restrained drying shrinkage. As shown in Figure 4.12a, control cement samples without MgO were subjected to cracking induced by drying shrinkage under restraint during the drying period. The initiation of cracks was observed at ~14 days. By contrast, there were no cracks observed in the restrained cement samples with RM2 (Figure 4.12b) as well as those with RM3 (Figure 4.12c) during the whole drying period until 28 days at low RH. The improvement in the cracking resistance of the cement pastes was attributed to the restrained expansion before drying. Under restrained conditions, MgO expansion can induce pre-pressing stresses on the cement matrix, which can help relax crack stresses and improve the tensile strength of the cement and thus increase its resistance to cracking (Chen et al. 2011).
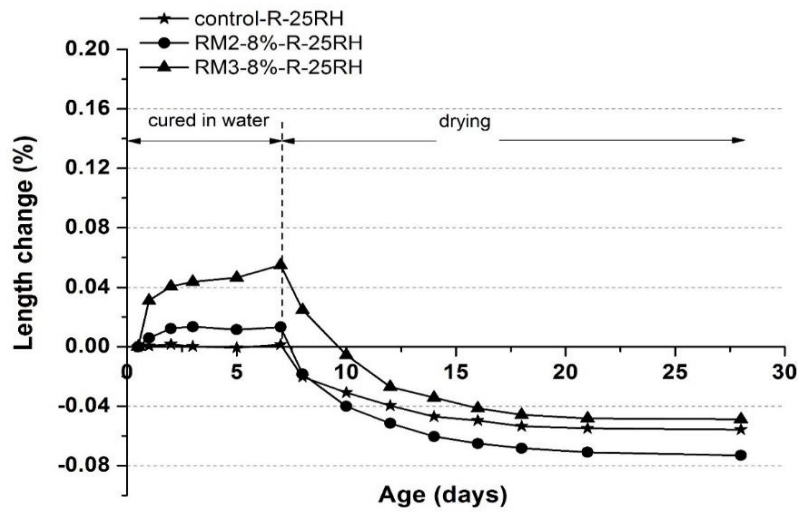
Figure 4.11 Length changes of restrained oil well cement pastes containing reactive MgOs (RM2 or RM3) at a content of 8% exposed to drying conditions of 25%RH after curing in water for 7 days at 80 ℃.
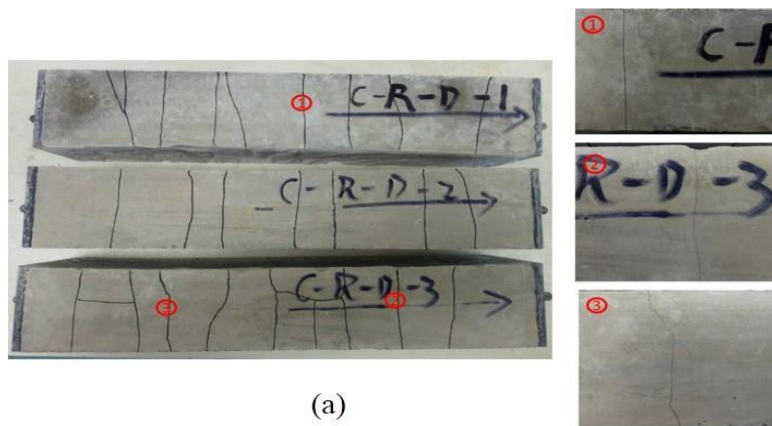
(a)
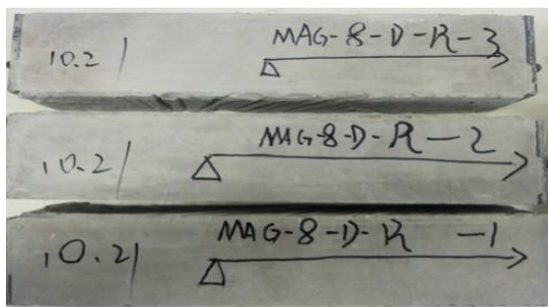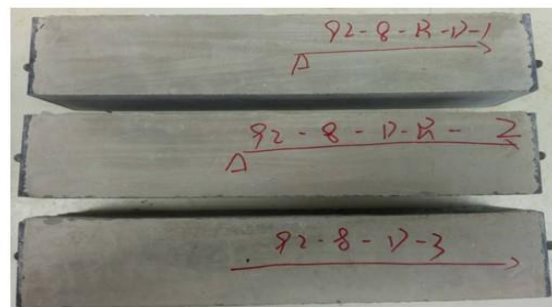
(b)   (c)

Figure 4.12 Restrained oil well cement pastes after drying shrinkage tests at 25% RH at 80 ℃ (a) Control cement samples without reactive MgO; (b) Cement pastes with 8% RM2; (c) cement pastes with 8% RM3.

147

4.5 Effects of MgO additives on the properties of oil well cement

4.5.1 Rheology of fresh cement slurries

Rheology is very important for controlling the slurry mixability and pumpability, and the displacement of drilling fluids during primary cementing. As mentioned in Chapter 2, workability is the energy required to handle and finish a cementitious mixture, whereas pumpability is better represented by the fundamental properties such as yield stress. It also affects the quality of the hardened cementitious matrix. This section investigates the effects of reactive MgO types and their content as well as the coupled effect of reactive MgO and temperature on the rheological behaviour of fresh class G oil well cement slurry.

Figure 4.13 presents the rheological properties (plastic viscosity and yield stress as two typical parameters) of class G oil well cement slurries containing the reactive MgOs RM1, RM2, and RM3 at different contents of 4%, 8% and 12% by weight of cement. Generally, the addition of reactive MgOs seemed to negatively affect the flow behaviour of cement slurries by increasing both the plastic viscosity and the yield stress. This is likely due to reactive MgOs having a higher SSA than cement, and their hydration in contact with water to form less soluble brucite, which increased the water consumption and thus decreased the flowability of cement slurry. It is also noted that the effects of reavtive MgO on the rheological behaviour of slurry is strongly related to MgO reactivity and content. Figure 4.13a shows that cement slurry containing RM1 of high reactivity had obviously higher plastic viscosity and yield stress than the control sample, and both of these two rheological parameters significantly increased with increasing content of RM1. At a content of 12%, the plastic viscosity and the yield stress were remarkably increased by 260% and 176%, respectively. In contrast with RM1, RM2 and RM3 with lower reactivity seemed to have indistinctive influences on the rheological behaviour of cement slurry.
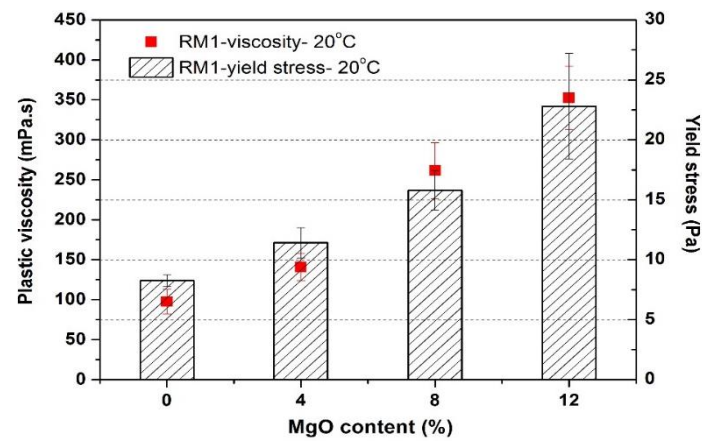
(a)
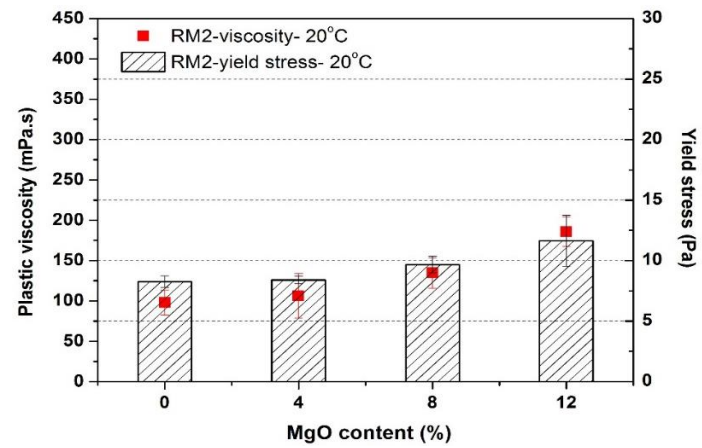
(b)
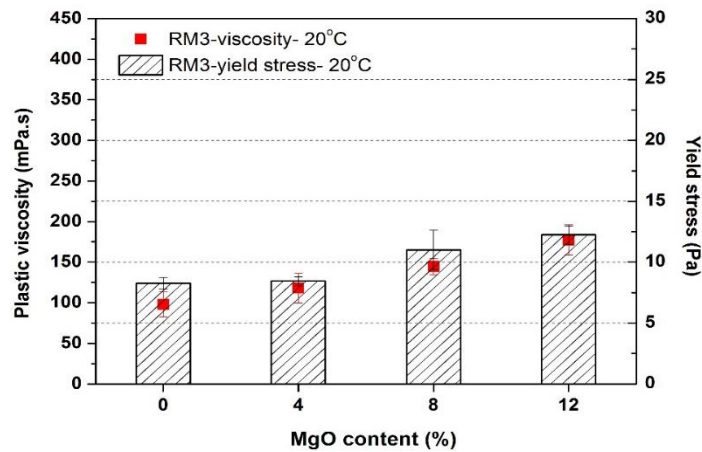
(c)

Figure 4.13 Plastic viscosity and yield stress of oil well cement slurries containing different types of reactive MgO at varied addition contents from 0 to 12% by weight of cement at 20 °C, (a) RM1 (b) RM2 (c) RM3, MgO reactivity: RM1 > RM2 > RM3.

149

The substantial effects of RM1 on the rheological behaviour of cement slurry can be attributed to its high SSA. RM1 can be highly reactive in hydration, and the fast heat release during the hydration of RM1 may also accelerate the cement hydration. The accelerated formation of hydration products can make the cement slurry less flowable. Compared to RM1, RM2 and RM3 both have a relatively smaller SSA and lower reactivity, their additions were unlikely to cause a substantial acceleration in cement hydration. This may explain why the flow behaviour of cement slurry was less affected by the addition of RM2 and RM3. The speculations on the effect of the three reactive MgO on cement hydration will be verified by the hydration heat analysis in the following Section 4.5.2.

The coupled effects of reactive MgO types and temperature on the rheological behaviour of class G cement slurry were also investigated. Figure 4.14 compares the plastic viscosity (Figure 4.14a) and yield stress (Figure 4.14b) values of cement slurries containing RM1, RM2, and RM3 at a content of 12% at different temperatures of 20 ^{o}C and 40 ^{o}C, respectively. For pure cement slurry without MgO, the viscosity and yield stress values showed insignificant change as temperature increased from 20 ^{o}C to 40 ^{o}C. Similar results were also reported by Shahriar (2011) on Class G oil cement slurry at w/c of 0.44. The author also found that the effects of temperature on the plastic viscosity and yield stress of oil well cement slurries were more significant at lower w/c of 0.35 than that of 0.44 and 0.5. However, the addition of reactive MgO seemed to enhance the effects of temperature. It can be observed that, for all three types of reactive MgO, both the plastic viscosity and yield stress increased at 40 ^{o}C, which indicated a reduction in the mobility of cement slurry and more energy required to make the cement slurry flow as temperature increased. This is likely due to the accelerated hydration rate of MgO at higher temperature. The temperature effect was more significant for cement slurry with RM1 due to its high reactivity.

(a)

(b)
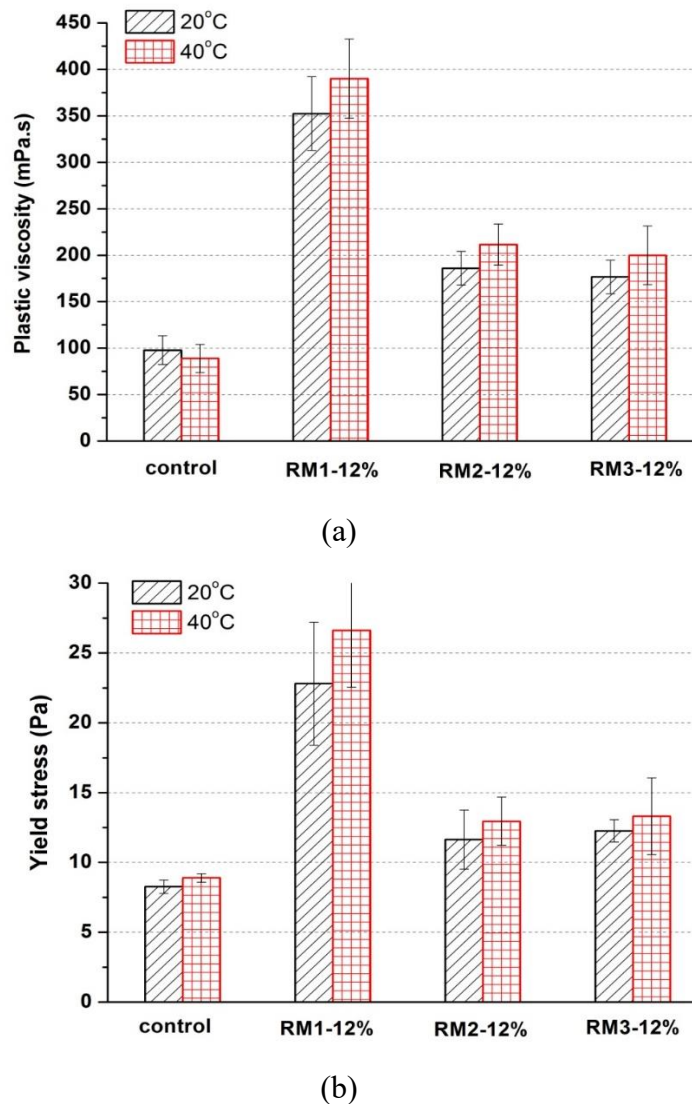
Figure 4.14 (a) Plastic viscosity and (b) yield stress of oil well cement slurries containing different reactive MgOs at a content of 12% by weight of cement at 20 °C and 40 °C.

Overall, the results above showed that the addition of reactive MgO caused an increase in the plastic viscosity and yield stress values of class G cement slurries, indicating a reduction in flowability. The increases were further enhanced at higher temperature. MgO RM1 with the highest reactivity had the most significant effects on the rheological behaviour of cement slurries, both at ambient and elevated temperature. In well cementing practice, the viscosity of oil well cement slurry admixtures are usually controlled within 500 mPa.s. In the case of adding admixtures which can increase the viscosity of cement slurry, the upper limit for the viscosity is 1000 mPa.s. For all three types of reactive MgOs, the viscosity values of MgO-containing

cement slurries are less than 500 mPa.s, which meets the requirements for cementing practice. In addition, in order to reduce the negative effect of MgO addition on the flow behaviour of cement slurries, dispersants can be used to control the viscosity of the slurry (Nelson, 2006).

4.5.2 Hydration of cement

The effects of reactive MgO addition on the hydration of oil well cement pastes were investigated through isothermal calorimetric analysis. Figure 4.15 shows the plots for the heat flow (Figure 4.15 a, c) and total heat curves (Figure 4.15 b, d) for class G oil well cement slurries containing different types of reactive MgO at a content of 12% at 20 °C and 40 °C, respectively. It can be clearly seen from Figure 4.15 that, for all cement slurries, the maximum hydration peaks increased with increasing temperature, while the time to reach the peaks was gradually shortened. The width of the hydration peaks also narrowed with increasing temperature. These results indicated the accelerated hydration of both reactive MgOs and the oil well cement itself at elevated temperature. Correspondingly, the accumulative heat evolution also increased with temperature, which reflected the higher extent of hydration of the cement mixtures at higher temperature.

At 20 °C, as shown in Figure 4.15a, the addition of 12% MgO RM1 accelerated the initiation of the second peak on the heat evolution curve and shortened the induction period. This indicated that RM1 had an accelerating effect on the hydration of oil well cement. By contrast, RM2 at the same content showed only a slight acceleration on initiation of the second peak, while RM3 had a slight delay in the initiation of the second peak. Compared to the other cement slurries, the cement slurry with RM1 had a distinctive initial peak which could be attributed to the hydration of RM1. This suggested that part of RM1 had rapidly hydrated before cement setting. As discussed in Section 4.4.1.1, the formation of hydration products during this period can lead to ineffective expansion and eventually a smaller ultimate expansion. In Figure 4.15b, the addition of reactive MgO showed consistent effects on the total heat curves. The cement slurry with RM1 produced a much higher total heat than the control sample, which indicated acceleration of cement hydration. The cement slurry with RM3 produced a lower total heat than the control sample, which indicated retardation of cement hydration.

The different influences of three reactive MgOs on cement hydration at an early age seem to strongly depend on their reactivity. One of the main theories for explaining the induction period of cement hydration is the $Ca(OH)_2$ nucleation theory which proposes that the induction period ends when $[Ca^{2+}][OH^-]^2$ reaches its maximum supersaturation ratio and starts to nucleate and precipitate (Skalny & Young 1980). As demonstrated in the heat evolution curve of RM1 cement slurry, RM1, with high reactivity, hydrated very fast and its hydration was initiated prior to the induction period of the cement. The fast hydration by RM1 suggested a rapid increase in the concentrations of Mg^{2+} and OH^- ions in the pore solution. Despite the following rapid precipitation of $Mg(OH)_2$, it is speculated that the fast hydration by RM1 lead to an overall increase of the concentration of OH^- which shifted the balance to accelerate the supersaturation of $Ca(OH)_2$, thus shortening the induction period. RM2, with medium reactivity, hydrated slower than RM1, and therefore had an insignificant acceleration effect on the initial hydration of the cement. RM3, with low reactivity, had a much slower hydration rate than either RM1 and RM2 at an early age. Therefore, it can be inferred that during the induction period, the cement (C_3S) hydrated slowly to produce Ca^{2+} and OH^- ions before reaching supersaturation while the RM3 hydrated at an even slower rate to release Mg^{2+} and OH^- ions. However, $Mg(OH)_2$ precipitates earlier than $Ca(OH)_2$ due to its far smaller solubility. As a result, OH^- is consumed for the precipitation of $Mg(OH)_2$, thus leading to an overall reduction of the OH^- concentration which delayed the supersaturation of $Ca(OH)_2$ and prolonged the induction period. Similar retardation effects of low reactivity MgOs have also been reported by Liu et al. (1992).

At 40 °C, the hydration rates of all reactive MgOs and cement were accelerated (Figure 4.15c, d). Especially for RM1, the initial peak was significantly intensified, reflecting its faster hydration rate and higher hydration degree at the very early age. It can also be inferred that the faster hydration of RM1 at higher temperature could result in more ineffective expansion before cement setting, which may also help explain the smaller expansion of RM1 at higher temperature, as discussed in Section 4.4.1.2.
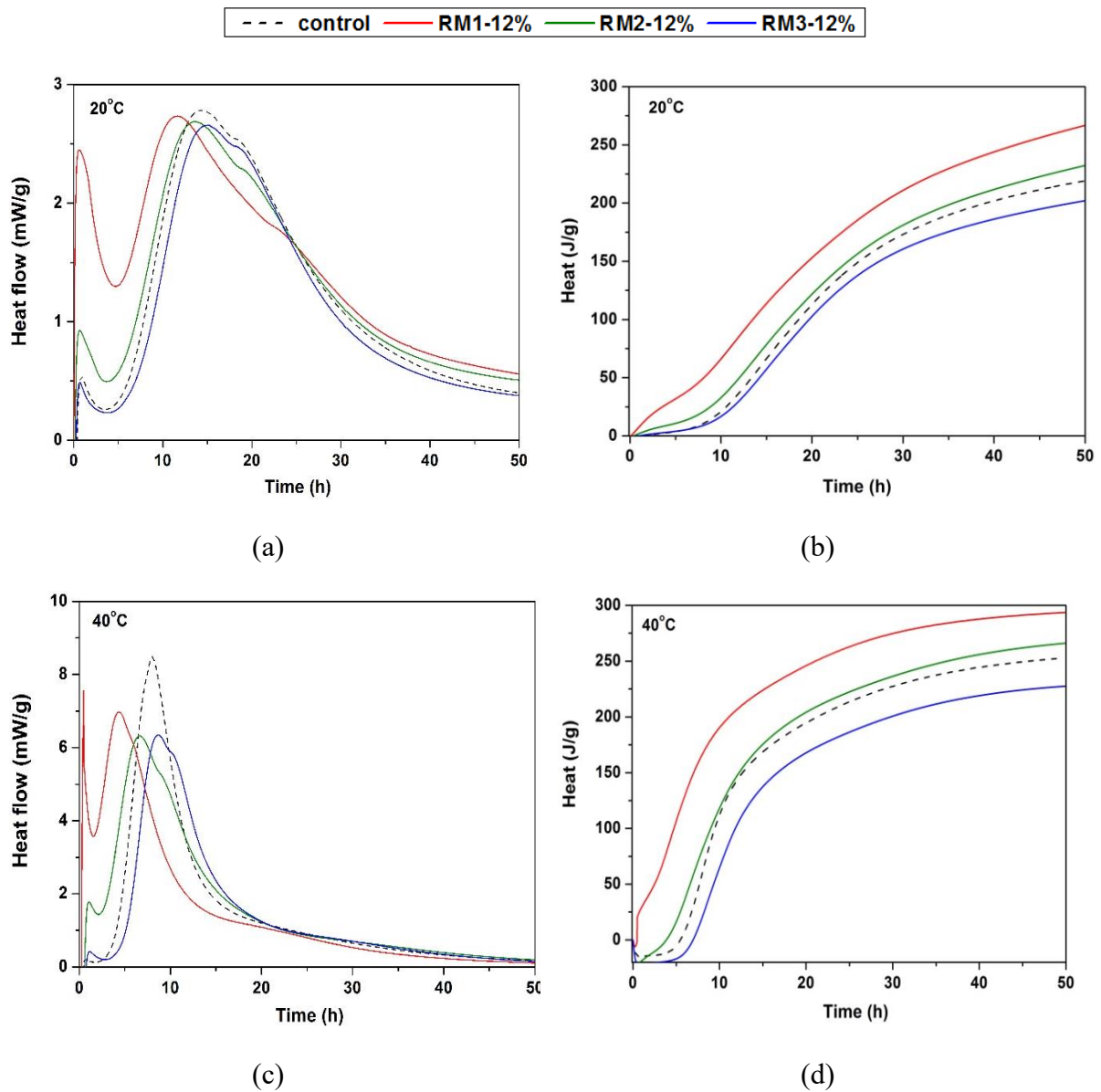
Figure 4.15 (a)&(c) heat flow and (b)&(d) total heat curves for oil well cement slurries containing different types of reactive MgOs (RM1, RM2, or RM3) at a content of 12% tested at 20 ºC and 40 ºC, respectively.

4.5.3 Compressive strength

The effect of reactive MgO additives on the compressive strength of oil well cement was investigated, considering different variables that include MgO type, addition content, and restraint conditions.

154

4.5.3.1 Unrestrained compressive strength

Figure 4.16 presents the effects of reactive MgO types and contents on the compressive strength of unrestrained oil well cement pastes at 80 °C.

RM1 and RM3 were found to negatively influence the compressive strength. As shown in Figure 4.16a, cement pastes incorporating RM1 had lower compressive strength than the control samples at all ages, and the strength further decreased with increasing MgO content. At the early age of 1 day, the compressive strength showed a decrease by 8% to 31.9 MPa at a content of 4% and a higher decrease of 20% to 28.0 MPa at a content of 12%. This decreasing trend among the cement pastes with RM1 continued at the later ages of 3 days and 7 days. As mentioned in 4.5.3, a high content of RM1 substantially reduced the flowability of the cement slurries. This may increase the porosity of the hardened cement and then adversely affect the strength development. Too fast expansion of RM1 at 80 °C occurring before or during cement setting might also induce damage to the newly formed cement skeleton.

The compressive strength of the cement pastes with RM3 as shown in Figure 4.18c was virtually unaltered at the early age of 1 day for all MgO contents, which is different from those with RM1. This is possibly due to RM3 having relatively slower and smaller expansion within the very early age, thus showing indistinct effects on the strength. However, the strength of the cement pastes with RM3 experienced continuous significant decrease in the following ages. At the same age, the strength further decreased with increasing RM3 content. After 7 days, the compressive strength was reduced by 25% and 46% at content of 4% and 12% respectively. This is can be ascribed to the rapid growth in the expansion magnitude of RM3 in cement pastes beyond the age of 1 day at 80 °C as described in Section 4.4.4.1. According to Li (2010), the decrease in strength may be due to the increase of porosity and microcracks in the cement matrix caused by the expansion of MgO. RM3 produced the largest expansion among the three types of reactive MgO, which can significantly increase the porosity and pore size of the cement matrix, thus substantially decreasing the strength.
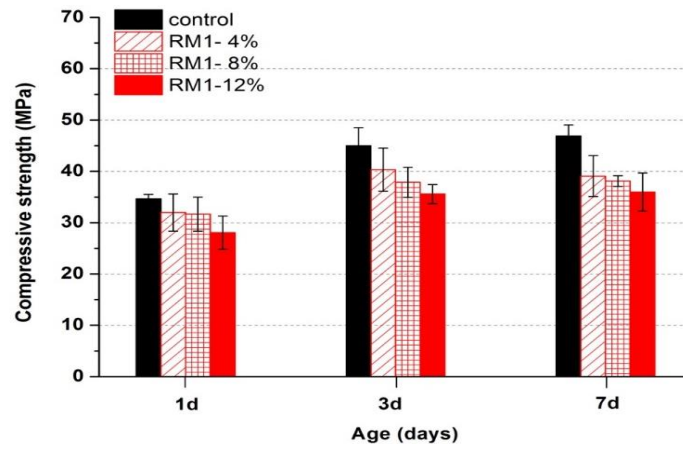
(a)
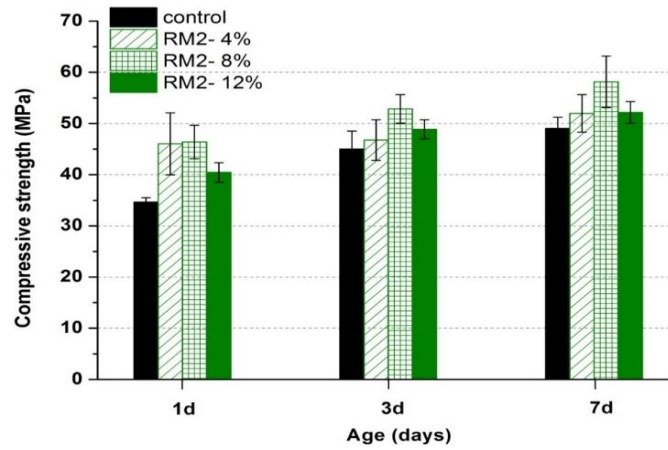
(b)
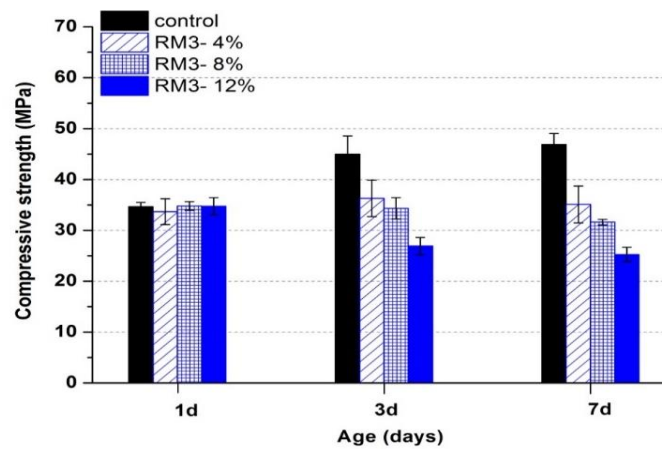
(c)

Figure 4.16 Compressive strength of unrestrained oil well cement pastes containing different reactive MgOs (a) RM1, (b) RM2 and (c) RM3 at different contents of 0–12%, at a curing age of 1, 3, 7 days, cured at 80 °C.

156

Surprisingly, Figure 4.16b shows that the addition of MgO RM2 improved the compressive strength of cement pastes instead of causing strength reduction. Cement pastes containing RM2 generally had higher strength than the reference samples at all MgO contents at three different ages. Cement pastes with 8% RM2 especially seemed to have the highest strength among all the cement samples. After 7 days, the cement strength was increased by 24% at 8% RM2 addition.

There are several possible reasons for the positive effects of RM2 on compressive strength. Firstly, RM2 had a fast expansion speed but a small expansion magnitude at 80 °C which mainly occurred at an early age. The small extent of expansion at an early age seemed to be beneficial for improving the pore structure of the cement matrix by reducing large-sized macropores that were adverse for strength development. Excessive expansion exerted on the cement matrix like that of RM3 is very likely to increase the pore volumes and pore sizes as well as induce microcracks. From this point of view, it seems that cement pastes with RM1 should also show strength enhancement. However, RM1 proved to cause strength reduction, as discussed above. Secondly, the effect of MgO on cement strength might also be related to the microstructures of the hydration product $Mg(OH)_2$. Mo et al. (2015) reported that reactive MgO (reactivity of 50 s) had very dense inner hydration products which were tightly agglomerated together, while less reactive MgO (reactivity of 400 s) had obvious "sheet like" hydration products with larger unfilled inner pores and thus a relatively looser structure. The MgO hydration products from less reactive MgOs with a looser structure may act as "weak points" compared to the surrounding cement hydrates, thus lowering the strength. The denser structure produced by more reactive MgOs like RM2 may help to improve the strength of the cement matrix. This hypothesis will be verified later by SEM observation.

4.5.3.2 Restrained compressive strength

Figure 4.17 compares the compressive strength of three dimensionally restrained and unrestrained oil well cement pastes containing different reactive MgOs at a content of 12% at 80 °C. It was apparent that all the restrained cement pastes with reactive MgOs had increased strength compared to the unrestrained ones, which is consistent with the results reported by Zhu et al. (2013). Under the three-dimensionally restrained conditions, the expansion of MgO

causes densification in the cement matrix, reducing the porosity and large-sized pores. As a result, the restraint expansion contributes to the increases in strength. Under three-dimensional restraint, the compressive strength of cement pastes with RM1, RM2 and RM3 at 7 days increased by 46%, 28% and 91%, respectively, compared to that of the unrestrained cement pastes contaning MgO. The strength of the cement pastes with RM3 in particular had the most significant improvement under restraint, which indicated a higher degree of densification of the cement matrix. As a whole, the expansion of reactive MgO under restrained conditions was beneficial for improving the strength of oil well cement pastes.
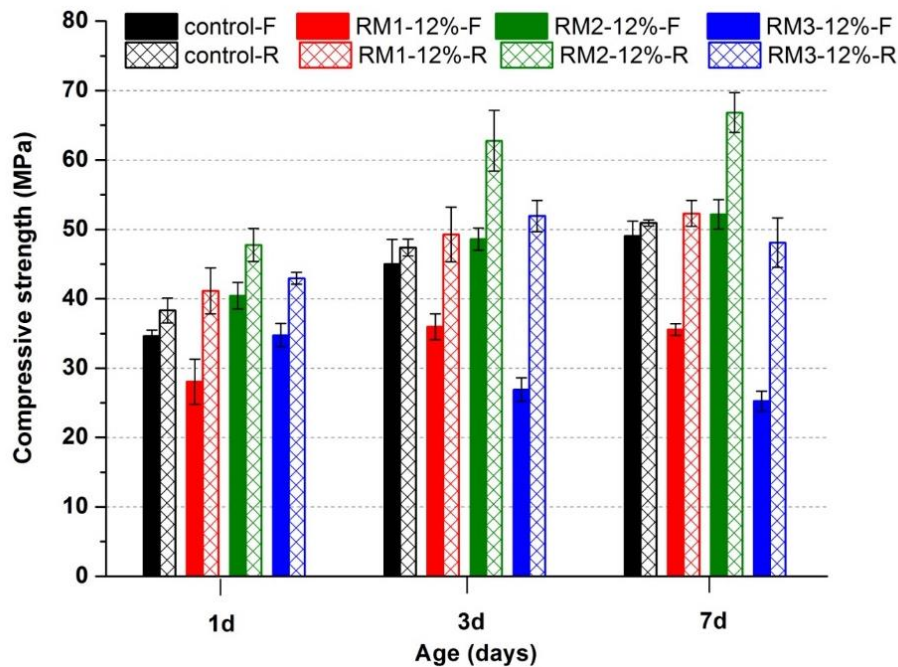
Figure 4.17 Compressive strength of three-dimensionally restrained and unrestrained oil well cement pastes containing different reactive MgOs (RM1, RM2, or RM3) at a content of 12% at 80 ºC.

4.6 Microstructure analysis

To better understand the effects of reactive MgO on expansion behaviour as well as other properties of oil well cement pastes, various techniques including XRD, TGA and SEM were used to carry out microstructure analysis on oil cement paste samples. Cement pastes containing different types of reactive MgOs (RM1, RM2, or RM3) at a content of 12%, at different curing temperatures of 20 ℃ and 80 ℃, and different curing ages of 1 day and 7 days, were prepared for microstructure analysis.

4.6.1 XRD

Figure 4.18 shows the results of the XRD tests on class G cement pastes containing three types of reactive MgO at a content of 12% cured at 80 ℃, at a curing age of 1 day and 7 days, respectively. After 1 day, the peak of MgO was identified at $2\theta=42.9°$ in all cement pastes with reactive MgO. This peak was less intense in the cement pastes with RM1 and RM2 than those with RM3. This indicates that RM1 and RM2 hydrated faster than RM3, and most of the MgO grains had transformed into brucite ($Mg(OH)_2$) (at $2\theta=18.5°$, $38.0°$, $50.9°$, $58.6°$) within the first day of curing at 80 ℃ due to their higher reactivities. Correspondingly, stronger peaks of brucite (especially the main peak at $2\theta=38.0°$) were observed in the cement pastes with RM1 and RM2.

The peak for unhydrated MgO was no longer detected any of the samples with reactive MgOs at a curing age of 7 days, shown in Figure 4.18b, while the peak for $Mg(OH)_2$ at $2\theta=38.0°$ became more intense, implying the full hydration of all three types of MgOs within 7 days. These results further explained the expansion trends of the three types of MgOs at 80 ℃, as previously described in Section 4.4.1. RM1 with high reactivity and RM2 with medium reactivity hydrated fast at an early age to reach a higher degree of hydration at an early age, therefore resulting in a short expansion period. RM3 with a low reactivity had a slower hydration rate and thus experienced continuous expansion until around 14 days. Most of the expansion of RM3 was completed within 7 days, which was consistent with the XRD results.
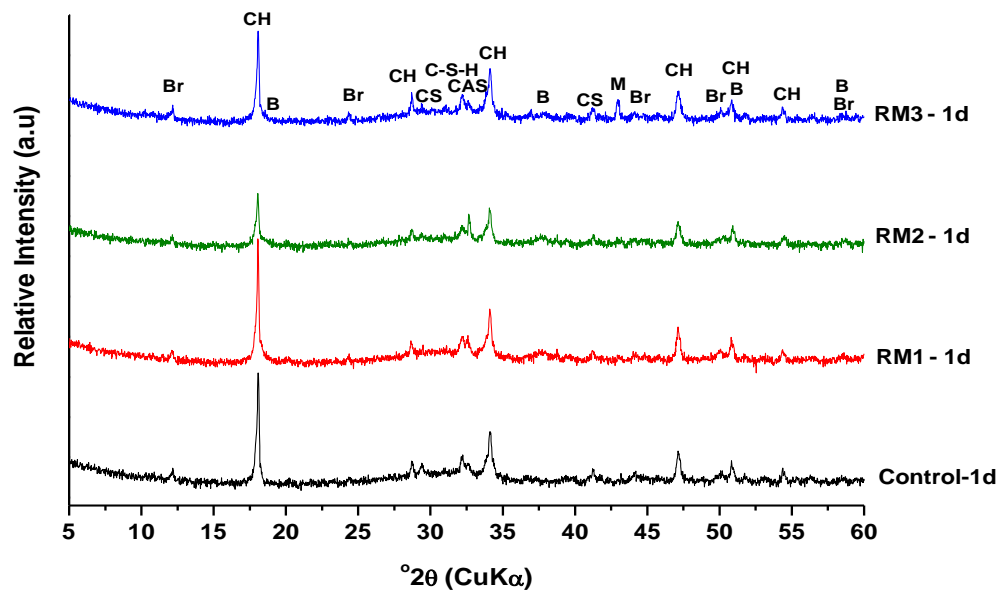
(a)
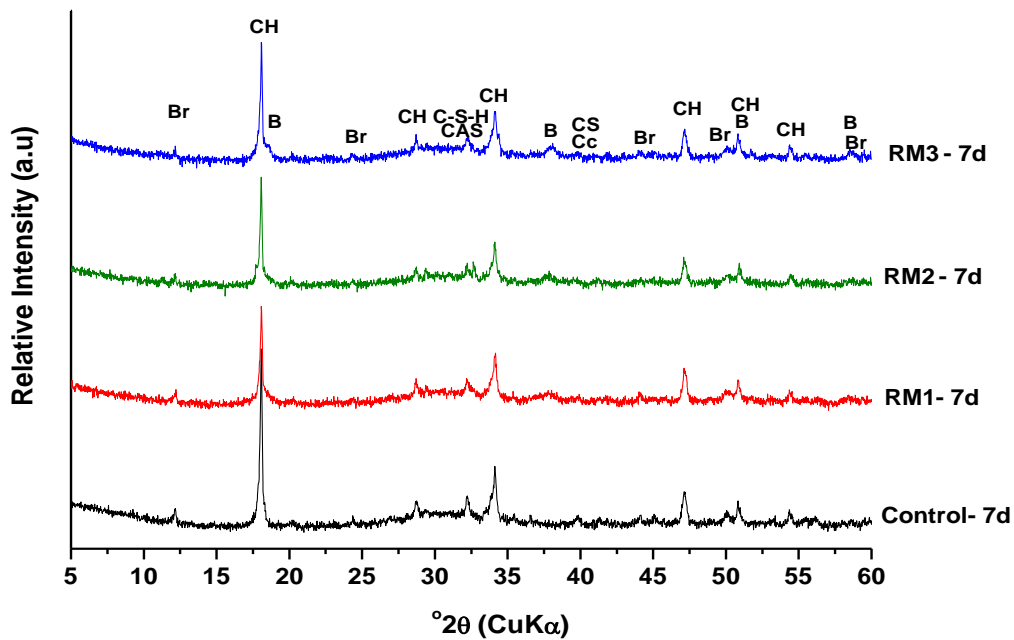
(b)

Figure 4.18 X-ray diffraction (XRD) spectrum for oil well cement pastes containing three reactive MgOs at a content of 12% cured at 80 °C at a curing age of : (a) 1 day; (b) 7 days, where B: Brucite ($Mg(OH)_2$), Br: Brownmillerite, CH: Portlandite ($Ca(OH)_2$), CS: Calcium silicate, C-S-H : Calcium silicate hydrate, CAS: Calcium aluminate monosulfate, Cc: Calcite ($CaCO_3$), M: Magnesium Oxide (MgO).
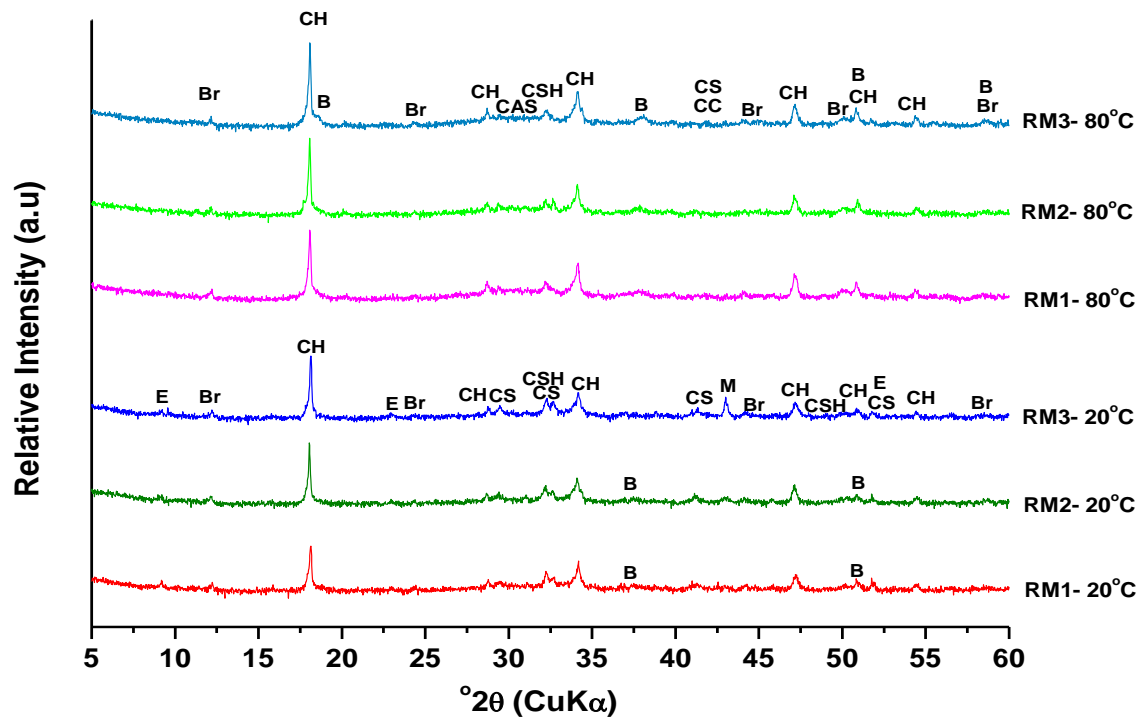
Figure 4.19 X-ray diffraction (XRD) spectrum for oil well cement pastes containing three reactive MgOs (RM1, RM2 or RM3) at a content of 12% cured at (a) 20 °C; (b) 80 °C at 7 days, where B: Brucite (Mg(OH)$_2$), Br: Brownmillerite, CH: Portlandite (Ca(OH)$_2$), CS: Calcium silicate, C-S-H : Calcium silicate hydrate, CAS: calcium aluminate monosulfate, Cc: Calcite (CaCO$_3$), E: Ettringite, M: Magnesium Oxide (MgO).

Figure 4.19 compares the XRD spectrums of 7 day-aged oil well cement pastes with each type of reactive MgO at a content of 12% cured at 20 °C and 80 °C. In general, peaks of unhydrated MgO still can be observed at around 2θ=42.9° for all the MgO-blended cement pastes cured at 20 °C at 7 days. The peak of unhydrated MgO was much more intense for the cement paste with RM3 than those with RM1 or RM2. This suggested the slow hydration of the low reactivity RM3 at 20 °C, thus a large proportion of MgO still remained unhydrated until 7 days. As the temperature rose to 80 °C, the peaks of MgO were no longer detected in all the MgO-blended cement pastes, while the peaks of brucite at 2θ=38.0°, 50.9° became more intense, indicating the acceleration of MgO hydration at high temperature.

In addition, it was also noted that the peaks of ettringite (at 2θ=9.1°, 22.9°) only existed in the cement samples cured at 20 °C. The absence of ettringite at 80 °C was due to its thermal

instability above 70 °C, causing it to decompose into calcium aluminate monosulfate (Jupe et al. 2005).

4.6.2 TGA

Figure 4.20 presents the mass loss and differential thermogravimetry (DTG) results of oil well cement pastes containing three reactive MgOs at a content or 12%, at a curing age of 1 d at 20 °C and 80 °C, respectively. Four main peaks can be observed in the DTG curves of cement samples cured at 20 °C, as shown in Figure 4.20a. The initial weight loss occurring up to 300 °C was mainly attributed to the loss of the chemically bound water from the calcium silicate hydrate (C-S-H) gel layers and also the dehydration of ettringite. The second peak at a temperature range of 320 to 400 °C denoted the decomposition of brucite ($Mg(OH)_2$). During this temperature range, it was evident that the cement pastes with higher reactivity MgO experienced more weight loss. According to the weight loss caused by $Mg(OH)_2$ decomposition, the content of $Mg(OH)_2$ in each cement paste can be roughly calculated and the results are shown in Table 4.3. The cement paste with the RM1 of high reactivity contained the most $Mg(OH)_2$ at 8.1%, indicating that it experienced the highest degree of hydration among the three MgOs at the same age, thus the most hydration products were formed. The cement paste with RM2 of medium reactivity had a $Mg(OH)_2$ content of 4.2%. RM3 showed the least $Mg(OH)_2$ content of 2.6% due to its lower reactivity than RM1 and RM2, and thus its lower degree of hydration. These results confirmed the explanation for the expansion trends of the three MgOs at an early age at 20 °C. MgO of higher reactivity had faster and larger expansion at an early age due to its faster hydration rate and higher hydration degree.

In the following temperature range, the sharp peak at around 410 to 470 °C represents the decomposition of portlandite ($Ca(OH)_2$) and the wide one at 600 to 700 °C represents the decomposition of calcite ($CaCO_3$). The three samples showed only minor variations in weight losses at all peaks, except for the one for the decomposition of brucite, as described above. The slightly higher content of calcite found in the cement paste with RM2 was possibly caused by the carbonation of portlandite during the sample preparation or storage procedures.

The cement samples cured at 80 °C in Figure 4.20b shows consistent trend with those cured at 20 °C in the weight loss at the temperature range of 320 to 400 °C. The cement samples with reactive MgO of higher reactivity had higher weight loss due to the higher degree of hydration. However, the differences between the weight losses of the three cement pastes at this temperature range became less pronounced at 80 °C, due to the accelerated hydration of all three MgOs at high temperature. The accelerating effect of high temperature on the hydration of reactive MgOs is better illustrated in Table 4.3 by comparing the mass loss and $Mg(OH)_2$ contents of cement pastes with each type of MgO cured at 20 °C and 80 °C. At the temperature range of 320 to 400 °C, all cement pastes cured at 80 °C had a significant increase in weight loss compared to those cured at 20 °C, indicating accelerated hydration of the three MgOs, and thus a higher degree of hydration and more hydration products. Such an increase was more remarkable in the cement pastes with RM2 and RM3, which indicated that the increasing temperature had more notable effects on MgO with lower reactivity. Additionally, the absence of the initial peak for the decomposition of ettringite in the cement pastes cured at 80 °C was due to its thermal instability at high temperature, which was also reflected in the XRD results as above.

Table 4.3 $Mg(OH)_2$ contents calculated from the TGA results of oil well cement pastes containing different types of reactive MgO after 1 d cured at 20 °C and 80 °C.

Sample type	20 °C		80 °C	
	Mass loss[*](%)	$Mg(OH)_2$ content (%)	Mass loss[*](%)	$Mg(OH)_2$ content (%)
Cement+12%RM1	2.5	8.1	3.7	11.9
Cement+12%RM2	1.3	4.2	3.5	11.3
Cement+12%RM3	0.8	2.6	3.2	10.3

[*]mass loss between the temperature range of 320 to 400 °C was used for calculation.
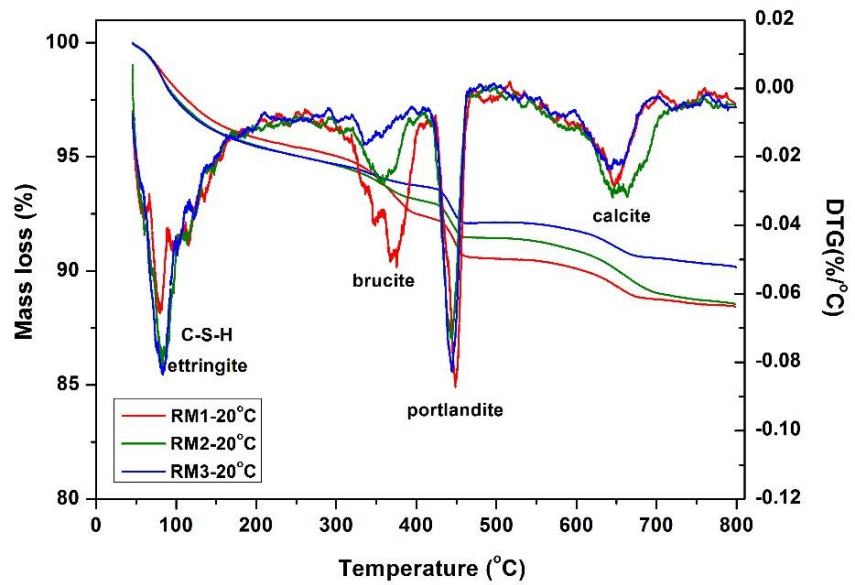
(a)
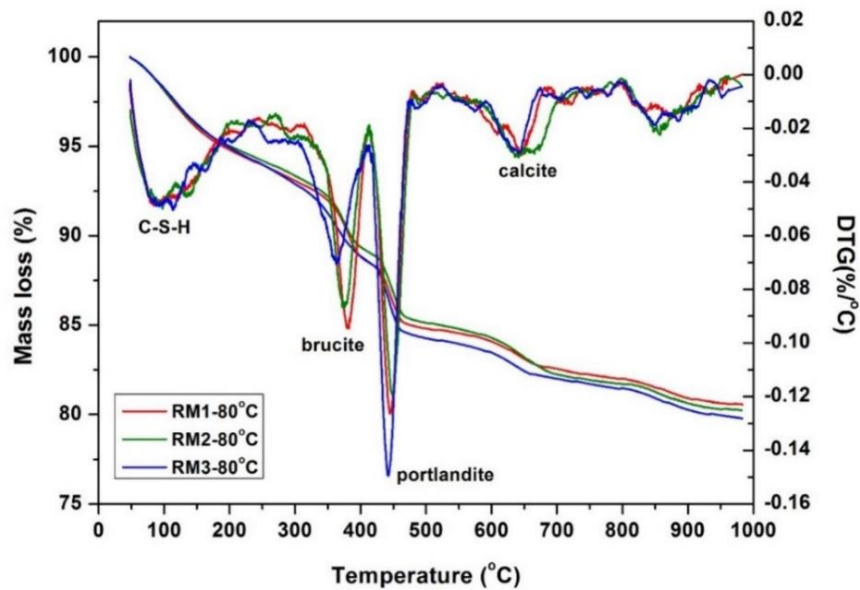
(b)

Figure 4.20 The DTG-TG curves of oil well cement pastes containing the three reactive MgOs (RM1, RM2 or RM3) at a content of 12%, at a curing age of 1 d at (a) 20 ^{o}C and (b) 80 ^{o}C, respectively.

164

4.6.3 SEM

Figure 4.21 presents the morphology of the hydration products of reactive MgOs in oil well cement pastes that were cured in water for 7 days at 80 °C. Figure 4.21a shows that RM1 with high reactivity had inner hydration products of $Mg(OH)_2$ that were agglomerated together, with smaller sized agglomerates being surrounded by various cement hydration phases. Since RM1 with high SSA had a porous structure, the brucite crystals mainly grew locally at the inner pore structures of MgO grains, thus only small crystals were observed at the surface of the agglomerates of hydration products. The brucite crystals for RM2 as shown in Figure 4.21b were also tightly agglomerated together, and the agglomerates seemed to have a very dense structure. It was noted that the hydration products of MAG-R had a larger size than those of RM1. RM2 of medium reactivity had a lower SSA, thus a less porous structure than RM1. Therefore, more of the hydration products grew on the surface instead of inside the inner pores of the MgO grains, thus producing larger sized crystals of the hydration products. By contrast, in Figure 4.21c, the RM3 of low reactivity had obviously lamellar structured hydration products which had even larger crystal sizes but having a looser structure with some unfilled pores among the crystal sheets. These observations confirmed the speculation on the effects of the structure of hydration products on cement strength as discussed in Section 4.5.3.1. The denser structure of the hydration products of RM2 contributed to the improvement in cement strength, while the looser structure of the hydration products of RM3 led to a decrease in cement strength. RM1 had dense hydration products, but caused a reduction in cement strength. This indicated that the roots of its adverse effects on cement strength did not lie in the structure of the hydration products, in but other possible reasons like the expansion being too early before the cement set, as previously proposed in Section 4.5.3.1.

(a)

(b)

(c)
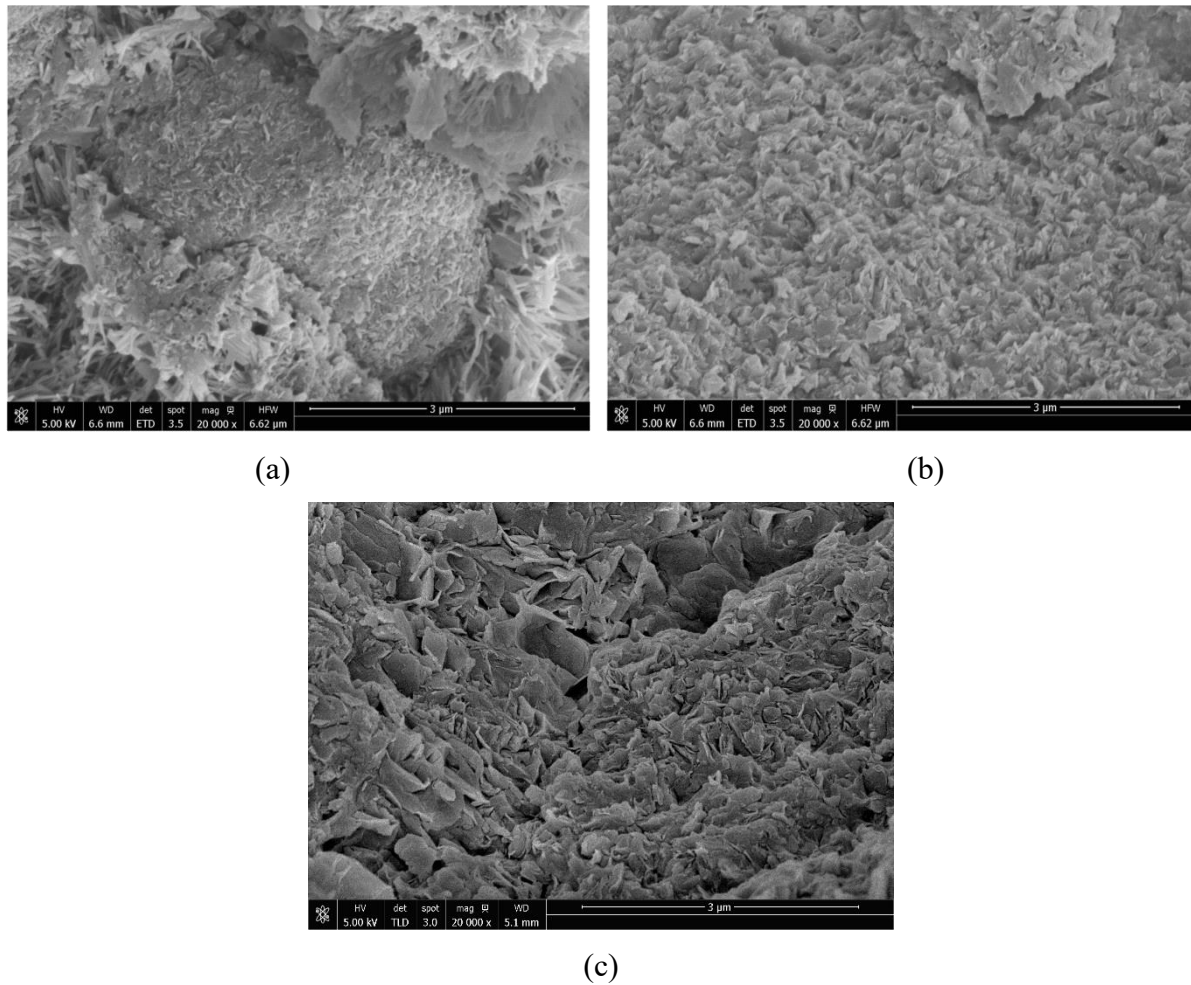
Figure 4.21 Morphology of the hydration products of reactive MgOs in oil well cement pastes that were cured in water for 7 days at 80 °C, (a) RM1; (b) RM2; (c) RM3.

4.7 Summary

This chapter investigated three types of reactive MgO from different sources: N50 (RM1) synthesized from seawater, and MAG-R (RM2) and 92/200 (RM3) from the calcination of magnesite, used as expansive additives in oil well cement. They were first tested on their reactivity values using the acetic acid reactivity test, and were then categorized according to their reactivity and SSA values: N50 was high reactivity, MAG-R was medium reactivity, and 92/200 was low reactivity. These three reactive MgOs were investigated on their expansion characteristics considering different influencing factors: MgO reactivity, addition content, curing temperature, and restraint conditions.

Generally, the results of the three reactive MgOs agreed with the literature that MgO with higher reactivity has a faster hydration rate, thus more rapid expansion at an early age but a smaller ultimate expansion magnitude. Increasing the MgO content induces a larger expansion. N50 of high reactivity had fast expansion that mainly occurred at an early age and levelled off within a short period at a small ultimate magnitude. Its fast early expansion is due to the porous microstructure which promotes a high hydration rate. Despite having a less porous microstructure than N50, MAG-R of medium reactivity also experienced rapid expansion at an early age. Its expansion developed at a relatively slower speed than N50 but lasted for a longer period, and eventually reached a larger expansion magnitude than N50. 92/200 of low reactivity experienced delayed expansion behaviour, which was characterized as a much smaller expansion rate and an expansion magnitude at an early age followed by accelerated expansion at a later age. Such delayed expansion may cause damage to the oil well cement sheath and formation layers. Reactive MgO with a low reactivity like 92/200 is therefore not suitable for use in ambient wellbore conditions.

The accelerating effect of increasing temperature on the MgO hydration, and thus expansion, was also observed in the three reactive MgOs. As the temperature increased from 20 to 80 ℃, the delayed expansion of 92/200 was significantly advanced. The higher temperature, the faster the expansion, as well as the higher the expansion magnitude at an early age. High reactivity N50, which experienced fast hydration at an early age, was further accelerated as the temperature increased but the expansion magnitude decreased. The hydration was too rapid, and largely occurred before cement setting, which was ineffective for expansion, leading to a decreased expansion magnitude. Similarly, the MAG-R with medium reactivity had a faster expansion rate but a reduced expansion magnitude at high temperature. At 80 ℃, the N50 showed very little expansion in the cement pastes during the test period. MAG-R had a short expansion with small magnitude at an early age of 3 days. 92/200 had a fast expansion with a much higher magnitude that continuously grew over 14 days. Therefore, it was inferred that reactive MgO with high reactivity like N50 is unsuited to high temperature conditions, especially at 80 ℃. Under restrained conditions, the MgO cement prisms had similar expansion trends but a reduced expansion magnitude compared to the unrestrained ones.

167

After understanding their expansion characteristics, the three reactive MgOs were tested in oil well cement prisms under sealed or drying conditions at a simulated wellbore temperature of 80 °C, to evaluate their performance in reducing autogenous shrinkage and drying shrinkage reduction, respectively. The results are summarized in Table 4.4.

Table 4.4 The performances of the three types of reactive MgO (at contents of 4, 8, and 12%) on shrinkage reduction at 80 °C.

		N50 (high reactivity)	MAG-R (medium reactivity)	92/200 (low reactivity)
Autogenous shrinkage		partial compensation	complete compensation	complete compensation
Drying shrinkage	High RH 90%	-	early-age reduction (at 8%, 12% content)	complete compensation
	Low RH 25% (unrestrained; restrained)	-	no effective reduction	no effective reduction
	Cracking resistance under restraints	-	improved	improved

Under sealed conditions at 80 °C, N50 of high reactivity was only able to partially compensate for the autogenous shrinkage, and increasing the N50 content had no significant improvement in autogenous shrinkage reduction. The less reactive MAG-R and 92/200 were more effective at reducing autogenous shrinkage. At all contents (4, 8, 12% by weight of cement), their addition could completely compensate for autogenous shrinkage and further induce net expansion in the cement pastes. MAG-R and 92/200 were further examined on their performance in reducing drying shrinkage. Under drying conditions of high RH 90% at 80 °C, 92/200 was still able to fully compensate for drying shrinkage and further produce net expansion in the cement pastes. MAG-R at higher contents of 8, 12% showed significant shrinkage reduction at an early age, though it was not effective in compensating for the drying shrinkage at a later age. Eventually, the addition of MAG-R only showed partial compensation for drying shrinkage in cement pastes at 90% RH. Neither MAG-R nor 92/200 showed drying shrinkage reduction under drying conditions at low RH 25%. Additionally, the expansion of MAG-R or 92/200 (at a content of 8%) in cement prisms at an early age under restrained conditions was found to significantly improve the cracking resistance of cement.

The effects of reactive MgO addition to the properties of oil well cement including rheology, hydration, and compressive strength were also investigated and a summary of the results is given in Table 4.5.

Table 4.5 The effects of the three types of reactive MgO at a content of 12% on the properties of oil well cement.

		N50 (high reactivity)	MAG-R (medium reactivity)	92/200 (low reactivity)
Plastic viscosity & yield stress (20 and 40 °C)		significantly increased	slightly increased	slightly increased
Hydration (20 and 40 °C)		significantly accelerated	slightly accelerated	slightly delayed
Compressive strength (80 °C)	Unrestrained	decreased	increased	decreased
	Restrained	increased	increased	increased

All three reactive MgOs had negative effects on the flow behaviour of oil well cement slurries. Both the plastic viscosity and the yield stress increased with the MgO content. N50 with high reactivity had the most substantial effects on the rheology properties. When coupled with an elevated temperature of 40 °C, the addition of reactive MgO further increased the plastic viscosity and the yield stress of the cement slurries.

N50 and MAG-R had accelerating effects on the hydration of oil well cement slurry, whereas 92/200 showed a slight retardation of cement hydration. At an elevated temperature of 40 °C, the hydration rates of all reactive MgOs and cement were accelerated.

Both N50 and 92/200 caused compressive strength reduction of the oil well cement samples under unrestrained conditions at 80 °C. MAG-R was found to increase the strength of the oil well cement pastes. The compressive strengths of all oil well cement pastes containing reactive MgO were significantly improved under restrained conditions, and were generally higher than those of the cement samples without reactive MgO, which indicates that the expansion of reactive MgO under restraint is benefical for densification of the microstructure of cement.

In summary, among the three reactive MgOs, both MAG-R of medium reactivity and 92/200 of low reactivity are recommended for use in reducing autogenous shrinkage and 92/200 for

drying shrinkage (at high humidity of 90%RH) under the curing temperature of 80 $^{\circ}$C. The use of less reactive MAG-R and 92/200 also have the advantages of marginal influences on the rheology properties and hydration properties of oil well cement, which is beneficial for cementing process. Moreover, the addition of MAG-R increased the compressive strength under both free and restrained conditions. Although the free expansion of 92/200 with low reactivity can cause significant strength reduction, this negative effect can be mitigated as the compressive strength will be increased by the confined expansion.

Chapter 5 Self-healing performance of oil well cement with sodium silicate microcpasules

5.1 Introduction

This chapter investigates a microcapsule-based self-healing oil well cement system. Two groups of polymeric microcapsules, T1 and T2, consisting of solid sodium silicate cores and polyurea shell walls, produced by Thies technology Inc, are used. The T1 and T2 microcapsules mainly differ in their polyurea shell: T1 has a rigid shell while T2 has a rubbery shell. Basic information for these two groups of microcapsules was given in Section 3.1.3. First, two groups of microcapsules were characterised by morphology, particle size distribution, shell thickness, thermal stability, resistance to alkalinity, and survivability during mixing. The chemical reactions of sodium silicate microcapsules in oil well cement pastes at 80 °C were also studied to understand the mechanism of the self-healing process at high temperature. In the following sections, the self-healing performance of oil well cement pastes with addition of two groups of microcapsules at different contents was evaluated using various techniques. These include microscopic observation and ultrasonic wave transmission for measurements of crack closure, gas permeability tests and capillary water sorptivity tests for assessing tightness recovery as well as the three-point bending test for assessing strength recovery. Microstructural analysis was also carried out to characterise the healing products formed on the cracking surface and further verify the release of the encapsulated sodium silicate core material and its healing reactions with the cementitious matrix. Apart from its self-healing properties, the oil well cement properties such as rheology, cement hydration, and mechanical strength were also investigated to obtain a comprehensive evaluation of the effects of microcapsule addition.

Based on the findings of the above tests, a suitable group of microcapsules and the recommended addition content was selected for combined use with reactive MgO, optimised from Chapter 4, in the hybrid expansion and self-healing oil well cement system as proposed in Section 5.8. The effects of the mixed addition of reactive MgO and microcapsules on the expansion, self-healing, and other fresh and hardened properties were all examined for

assessment of the compatibility of two types of additives in the combined oil well cement system.

5.2 Characterisation of microcapsules

5.2.1 Morphology of microcapsules

When observed with the naked eyes, all the polyurea/sodium silicate microcapsules had a very similar powdery appearance which made them suitable for mixing with cement as well as storage and shipment. When observed under the microscope, the microcapsules present as globular shapes surrounded by some tiny debris which might be either from the shell material or unencapsulated sodium silicate, as shown in Figure 5.1. It can be noted that most of the microcapsules are not regular smooth spheres but rough with some dimples on the surface. The uneven shell surface observed in the microcapsules can be related to evaporation of the moisture content from the inner core materials across the shell membrane during the drying process, thus forming an uneven membrane surface. Other researchers have also reported similar phenomenon of the buckled shell due to moisture loss from the core during drying (Scarfato et al. 2007; Souza 2017). Further observations under SEM were carried out to examine the morphology of those microcapsules. The rough surface of these microcapsules could be more clearly observed. By comparing the appearance of two batches of T1 and T2 (see details in Section 3.2.3), it was noted that the newly produced NT1 and NT2 have a relatively smoother surface compared to OT1 and OT2 from the old batch produced at an earlier date.
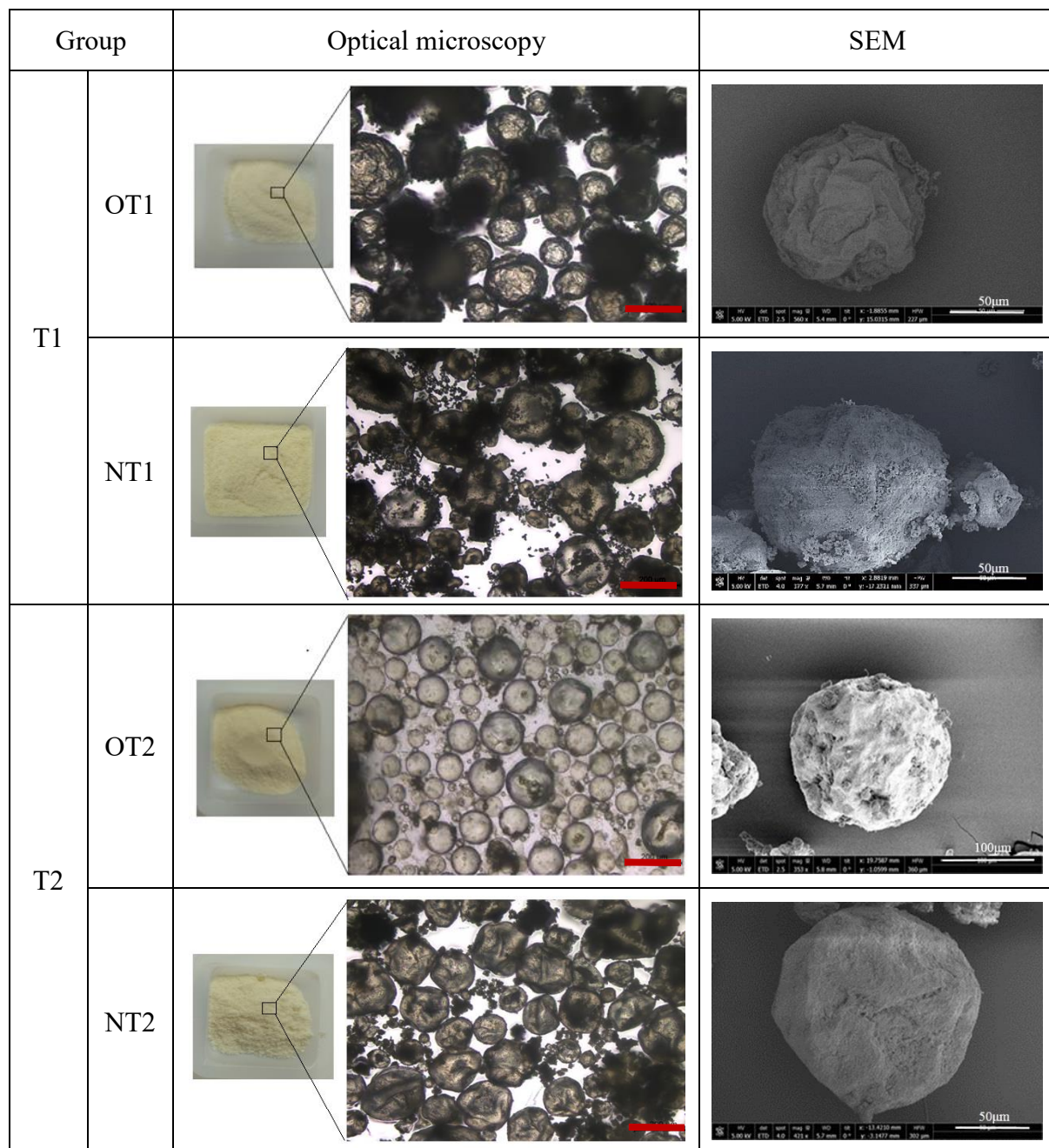
Figure 5.1 The morphology of the two groups of polyurea/sodium silicate microcapsules (T1 group: OT1 and NT1; T2 group: OT2 and NT2) observed under optical microscopy (the red scale bar represents 200 μm) and SEM.

5.2.2 Particle size

The particle size of the T1 and T2 groups of microcapsules was measured using a microscope and then analysed using the image analysis software Image J. At least 150 of each type of microcapsule particles were measured. The results of the particle size distribution are presented in Figure 5.2, and a summary is given in Table 5.1. In the T1 group, the OT1 microcapsules from the old batch have an average size of ~180 μm. The size distribution range is from ~70 to 570 μm but most of the microcapsules lie the range of ~100 – 300 μm. By contrast, NT1 from the new batch had a smaller average size of ~110 μm, and a size range from ~30 to 220 μm. In the T2 group, the OT2 microcapsules had an average size of ~90 μm and the NT2 microcapsules had a slightly larger average size of ~110 μm. It appears that the T2 group microcapsules maintained better consistency in particle size distribution between the old batch and the new batch.

Table 5.1 Average size and size range of the two groups of polyurea/sodium silicate microcapsules (T1 group: OT1 and NT1; T2 group: OT2 and NT2).

Microcapsule type		Average size D_{150} (μm)	Size range (μm)
T1	OT1	~180	~70 to 570
	NT1	~110	~30 to 220
T2	OT2	~90	~20 to 330
	NT2	~110	~20 to 250

(a)

(b)

(c)

(d)
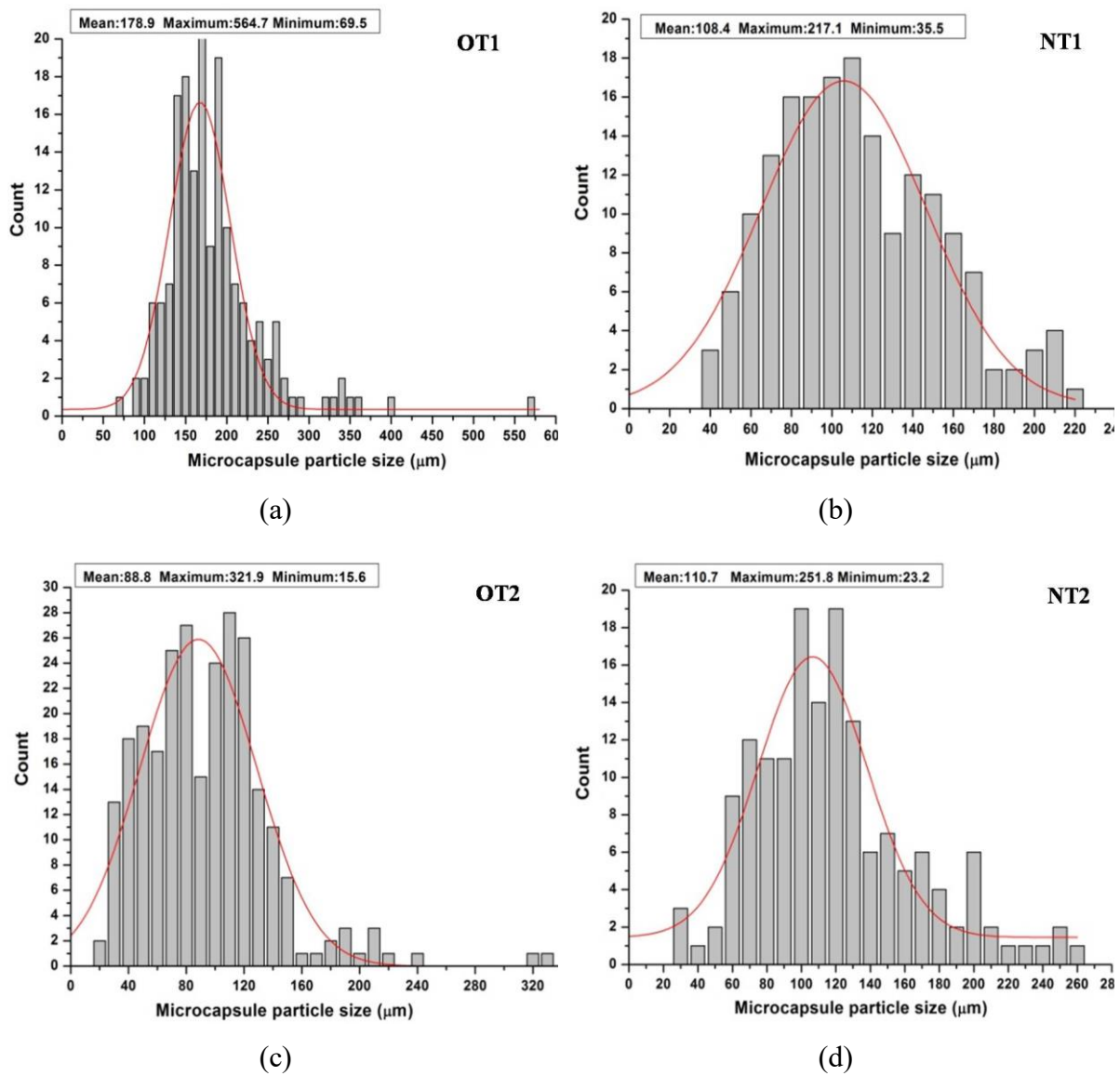
Figure 5.2 Particle size distribution of the two groups of polyurea/sodium silicate microcapsules, T1 group: (a) OT1 and (b) NT1; T2 group: (c) OT2 and (d) NT2.

5.2.3 Thermal stability

The thermal stability of the microcapsules plays a critical role in their application in oil well cement systems under high temperature environments. The microcapsules used are expected to maintain good thermal stability under the targeted application temperature of 80 °C. The thermal stability of the T1 and T2 groups of microcapsules was evaluated using thermogravimetric analysis (TGA). The tests were carried out on the microcapsules as well as

the polyurea shell material. The polyurea shell material was extracted by grinding the microcapsules and dissolving the sodium silicate core using water. Sodium silicate is known to be highly soluble in water while polyurea is insoluble in water. The suspension was then filtered to obtain the shell debris which was dried in an oven at 50 $^{\circ}$C to remove the moisture.

Figure 5.3 presents the TG traces of polyurea microcapsules (OT1, OT2, NT1, NT2) together with their shell materials. All of the TG traces of the microcapsules displayed similar trends that showed the first weight depletion from the initial temperature of 50 $^{\circ}$C and experienced a gradual weight loss over the following wide temperature range up to ~400 $^{\circ}$C, reaching a residual weight of ~70% at 650 $^{\circ}$C. On the other hand for the shell material alone, the shell walls of all the microcapsules generally remained thermally constant up to the higher initial decomposition temperature (varying between ~150 to ~220 $^{\circ}$C for each type of microcapsule) and then decomposed gradually over a temperature range from ~150 to ~490 $^{\circ}$C, finally reaching a residual weight of ~10–26% at 650 $^{\circ}$C. Similar trends in the TG traces of polyurea-type microcapsule shells have also been reported in the literature (Hong & Park 2000; Scarfato et al. 2007).

By comparing the thermal behaviour of the capsules and the shell materials, it can be deduced that the initial weight depletion of the capsules can be mainly attributed to the water loss from the hydrous sodium silicate core across the shell membrane pores. The hydrous sodium silicate crystals become very unstable at elevated temperature and dehydrate gradually as the temperature increases, eventually turning into metasilicate. Sodium silicate hydrates can start dehydrating at the low temperature of ~40 $^{\circ}$C and transform into metasilicate above ~240 $^{\circ}$C (Schmid & Felsche 1983). Dehydration of the sodium silicate hydrates from the debris surrounding the capsules may also contribute to the initial weight depletion. The microcapsules are deemed to remain intact up to the initial decomposition temperature of the shell wall: OT1 with 220 $^{\circ}$C, OT2 with 170 $^{\circ}$C, NT1 with 160 $^{\circ}$C and NT2 with 150 $^{\circ}$C, which are far above the target temperature of 80 $^{\circ}$C.
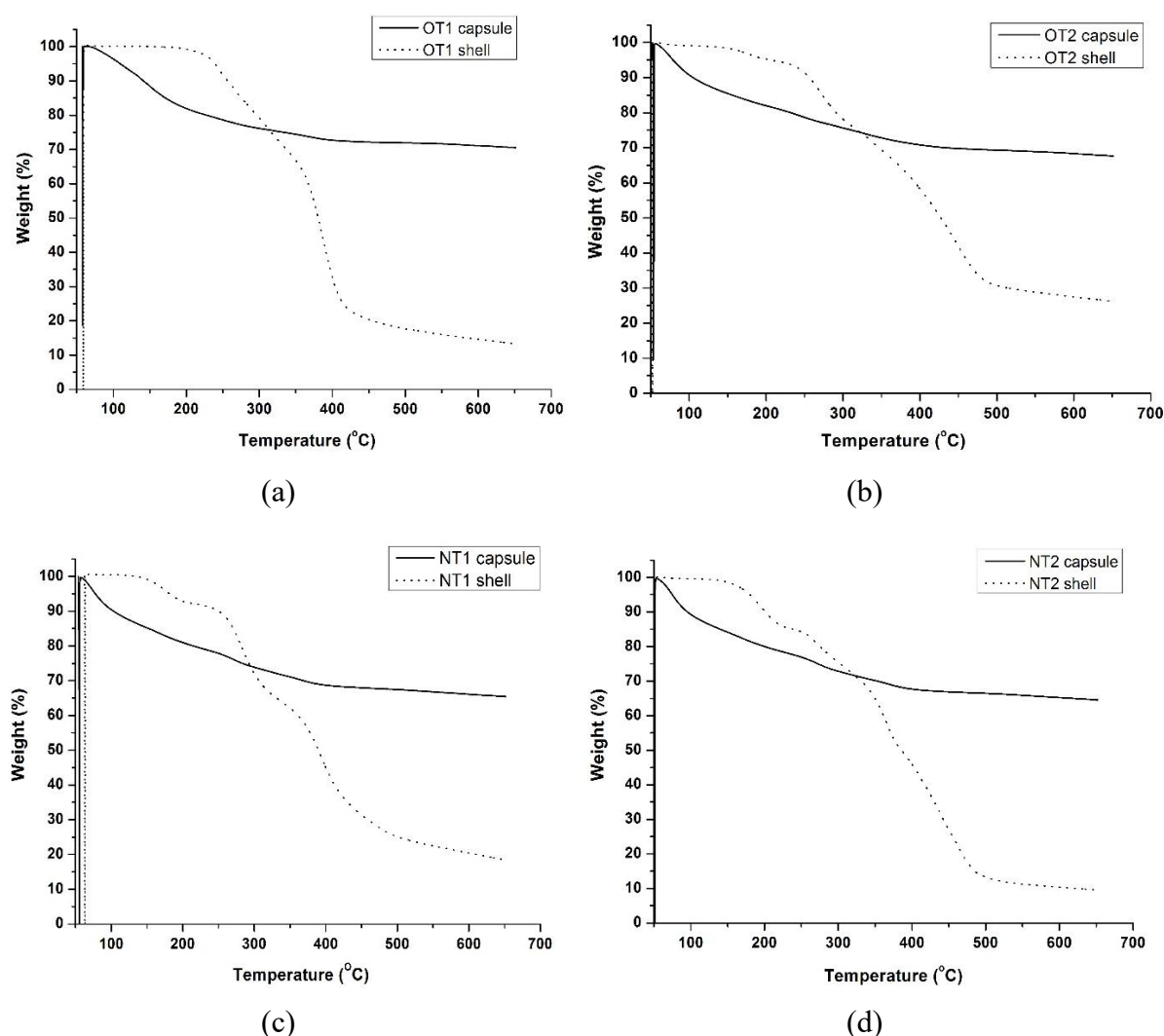
Figure 5.3 TGA analysis of the two groups of polyurea/sodium silicate microcapsules and their shell materials, T1 group: (a) OT1 and (b) NT1; T2 group: (c) OT2 and (d) NT2.

The T1 and T2 microcapsules differ in the rigidity of their polyurea shells, and the shell properties may also vary from batch to batch. Consequently, there were some differences between the thermal reactions of shell materials. By comparing the TG diagrams of OT1 shells with OT2 shells, it was noted that the OT2 shell has a much lower initial decomposition temperature (~170 ^{o}C) than that of OT1 shell (~220 ^{o}C). This reduction in thermal stability of the OT2 shell can be attributed to the incorporation of a flexible diamine monomer in producing the less rigid shell membrane of the T2 group microcapsules. The reactivity of the diamine monomer and the length of the flexible methylene chain in diamine have a decisive influence

177

on the thermal properties of the resultant polyurea shell membrane (Hong & Park 2000). The polyurea shell membrane composed of hard diamine monomer has a higher thermal stability than the shell composed of soft monomer or a mix of hard and soft monomers. However, the NT1 shell was found to have an initial decomposition temperature of 160 °C which is lower than that of OT1. The shell of NT1 might have incorporated soft segments, resulting in a decreased initial decomposition temperature. NT2 had an initial decomposition temperature of ~150 °C, which was close to that of OT2.

5.2.4 Stability in simulated high-temperature and alkaline solution

When used in oil well cement, the microcapsules are not only subjected to high temperatures, but also to the highly alkaline cementitious environment. To examine their stability in the combined high temperature and alkaline conditions, different groups of polyurea microcapsules were immersed in saturated $Ca(OH)_2$ solution (pH≈13) at a temperature of 80 °C that simulated the alkaline cementitious environment and the wellbore temperature. After an exposure of 14 days, the microcapsules were randomly picked from the solution for observation using an optical microscope. As shown in Figure 5.4, the majority of the microcapsules in all groups retained their shell integrity after exposure to the high temperature alkaline solution. The shell wall acts as an important protection layer for the microcapsules. The polyurea shells had good thermal stability as demonstrated by the TG results above. Polyurea materials are also reported to have good resistance to alkalis (Primeaux 2004), which enabled the microcapsules to survive in the high temperature and high alkaline condition. The results suggest that polyurea microcapsules should be able to remain stable in the oil well cement under realistic wellbore conditions. In addition, it was noted that the microcapsules appeared to have a smoother surface than the original ones after immersion in the solution for 14 days. This might be due to the water molecules diffusing across the polyurea shell into the microcapsules. As mentioned above in Section 5.2.1, moisture can escape from the inner core across the shell membrane during drying, leading to an uneven surface with buckles and dimples. When the microcapsules are immersed in water solution, the water molecules can diffuse inwards and unbuckle the microcapsules.
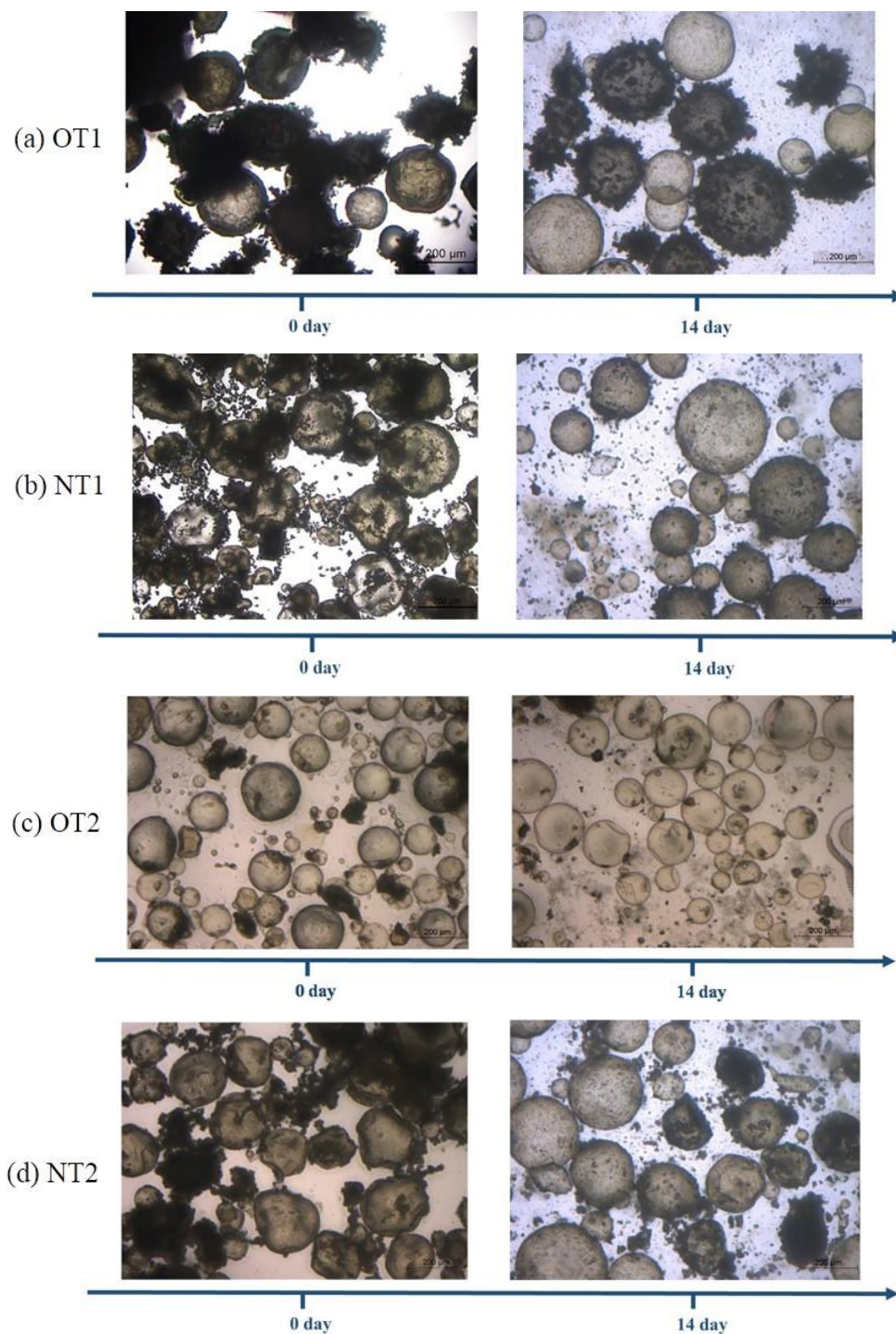
Figure 5.4 Stability of the two groups of polyurea/sodium silicate microcapsules in saturated Ca(OH)$_2$ solution (pH≈13) at a temperature of 80 ºC after 14 days, T1 group: (a) OT1 and (b) NT1; T2 group: (c) OT2 and (d) NT2.

5.2.5 Survivability during mixing

For successful application in a self-healing cement system, one of the primary requirements for the microcapsules is surviving the aggressive mixing process of Class G cement slurry. The microcapsules must resist the stresses generated during high speed stirring. After the standard mixing process, fresh oil well cement slurries containing each type of microcapsules were prepared for investigation of their post-mixing survivability. A glass slide was inserted into the cement slurry to extract a thin layer of slurry mixed with microcapsules. As shown in Figure 5.5, the microcapsules particles mixed into the cement slurry could be observed on the glass slide. The cement slurry on the slide was carefully washed away and the remaining microcapsules were observed under microscope. It seemed that both T1 groups of microcapsules with rigid shells and T2 groups of microcapsules with less rigid shells were sufficiently robust to survive the aggressive mixing process.

SEM observations were also carried out on the microcapsules embedded within the crack surfaces of hardened cement pastes. In Figure 5.6a, the remaining hemispheric shells of ruptured microcapsules were seen to be uniformly distributed through the cement matrix, which further confirmed their survival during mixing. Clearer views of the microcapsules of each group under higher magnification are shown in Figure 5.6b to e. Despite the difference in the rigidity of the shell materials, both the T1 group (rigid) and T2 group (rubbery) microcapsules showed good fracture behavior when triggered for healing. The shells of the microcapsules in each group generally had good bonding with the surrounding matrix. In some cases, the shell partially debonded from the cement matrix upon cracking as shown in Figure 5.7, indicating there was weak bonding at some points between the interfaces. This might be due to the hydrophobic nature of the polyurea shell materials, which are not conducive to building effective chemical adhesion (Souza 2017). As a result, the interfacial bonding between the polyurea shell and cement matrix mainly depends on physical adhesion. However, the microcapsules were still able to rupture upon triggering. The shell thickness of each group of microcapsules was also measured. OT1 microcapsules with a larger mean size (~180 μm), had a shell thickness that varied between 5~10 μm. The microcapsules of OT2, NT1 and NT2 groups with smaller mean size (~90–110 μm) had a shell thickness that varied within a

relatively smaller range between 3~5 µm. The materials remaining inside the shell appeared to be the healing products of calcium silicate hydrate (C-S-H) and other carbonation products, which will be further discussed in Section 5.7.
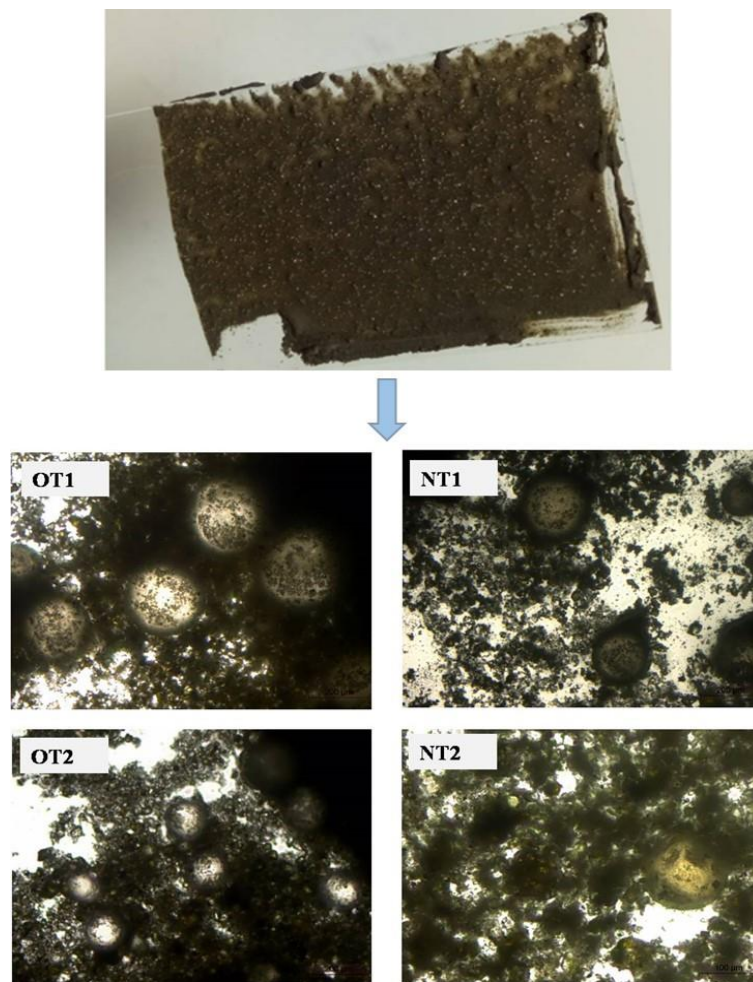
Figure 5.5 Cement slurry containing microcapsules observed under microscope after mixing.
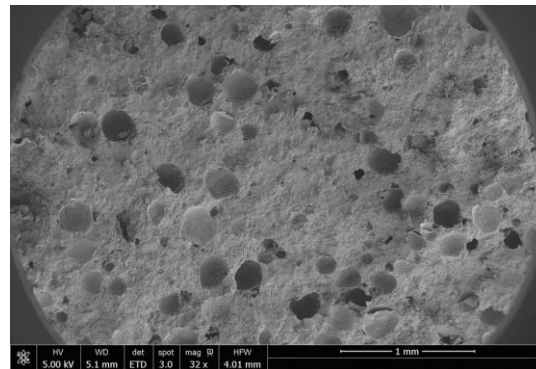
(a)
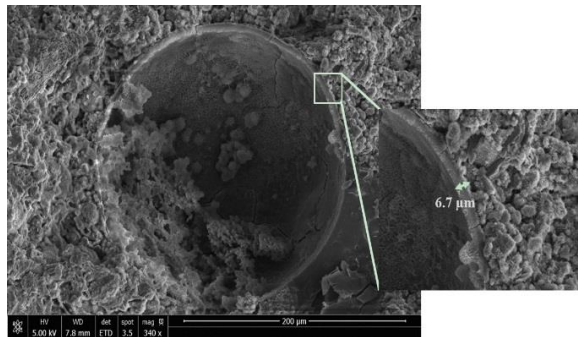
(b) OT1
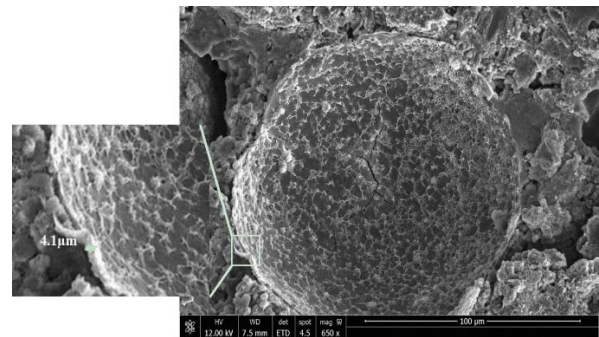
(c) NT1
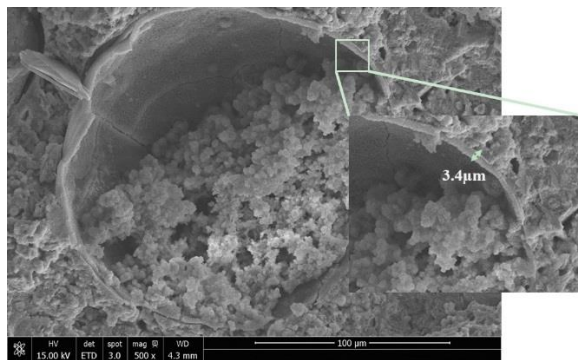
(d) OT2
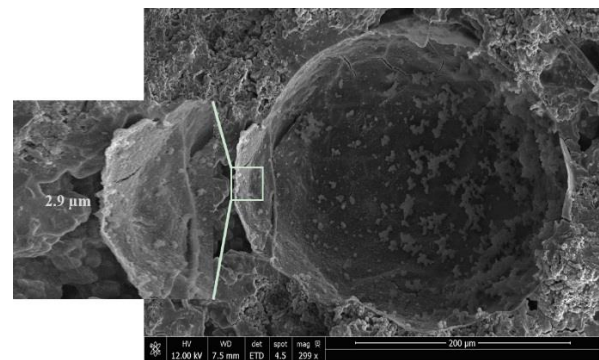
(e) NT2

Figure 5.6 SEM observations on the cracking surface of oil well cement pastes contaning two groups of microcapsules: (a) overview of the cracking surface; ruptured microcapsules (b) OT1, (c) NT1, (d) OT2, (e) NT2 embeded on the cracking surface.

Figure 5.7 SEM images of microcapsule shells debonded from the surrounding cement matrix

5.3 Mix Design

Different groups of oil well cement mixtures were prepared to investigate the self-healing efficiency of the T-series microcapsules as well as the effects on the oil well cement properties of their addition. The mix compositions for each group of tests are shown in Table 5.2. The w/c ratio remained constant at 0.44 and the curing temperature for all cement specimens was 80 ºC.

Table 5.2 Mix composition of oil well cement pastes contaning different groups of polyurea/sodium silicate microcapsules.

Mix		Microcapsule type	Microcapsule content (by weight of cement, %)
Self-healing efficiency	Gas permeability (Ø50 mm×10 mm disks)	OT1, OT2	0, 1.25, 2.5, 3.75, 5.0
		NT1, NT2	0, 5.0
	●Crack width and crack depth measurements; ●Capillary sorptivity; ●Flexural strength recovery (40×40×160 mm prisms)	NT1, NT2	0, 2.5, 5.0, 7.5
Effects on oil well cement properties	Rheology properties	NT1, NT2	0, 2.5, 5.0, 7.5
	Cement hydration	NT1, NT2	0, 1.25, 7.5
	Compressive strength (40×40×40 mm cubes)	NT1, NT2	0, 2.5, 5.0, 7.5
	Flexural strength (40×40×160 mm prisms)	NT1, NT2	0, 2.5, 5.0, 7.5

For tests of their self-healing efficiency, different types of specimens containing varying microcapsule content from 0 up to 7.5% (by weight of cement) were prepared, including Ø50 mm × 10 mm disks for the gas permeability test and 40 mm × 40 mm × 160 mm prisms for crack width and crack depth measurements, capillary sorptivity tests, and flexural strength recovery assessments. After curing for 3 days at 80 °C, the cement samples were cracked to a controlled crack mouth opening displacement (CMOD=0.2 mm) as detailed in Chapter 3. After a healing period of 7 days at the same temperature, the various tests as mentioned above were carried out to evaluate the self-healing performance of the post-healing cement samples. It should be noted that microcapsules from the old batch (OT1 and OT2) were only used in the preparation of small disk specimens in the gas permeability tests due to the limited quantities produced. NT1 and NT2 from the newly produced batch were used for preparation of the prism specimens. To check the consistency between the two batches of microcapsules in self-healing effectiveness, gas permeability tests were also carried out on the disk specimens prepared with NT1 and NT2 for comparison with the old batch.

The effects of the addition of microcapsules at various contents (0–7.5%) on the rheology properties and hydration rate of fresh oil well cement slurries were tested using rheometer and isothermal calorimeters, respectively, at 20 °C and 40 °C. The effects on the mechanical properties of hardened oil well cement pastes cured at 80 °C were studied using 40 mm × 40 mm × 40 mm cubes for the compressive strength test and 40 mm ×40 mm × 160 mm prisms for the flexural strength test. The microcapsules used in the tests of this nature were NT1 and NT2 from the new batch.

5.4 Self-healing mechanism of sodium silicate microcapsules in oil well cement cured at high temperature

To understand the self-healing mechanism of sodium silicate microcapsules in oil well cement cured at high temperature, the chemical reactions between the oil well cement matrix with encapsulated sodium silicate within polyurea microcapsules at 80 °C were first studied in this section using XRD and TGA microstructure analysis. As introduced in Section 5.3, the oil well cement specimens were all cracked after 3 days' curing at 80 °C and left to heal for 7 days at

the same temperature. In this analysis, control oil well cement pastes were ground into fine particles after curing for 3 days at 80 °C to replicate the cement matrix in the cracking area of the cement specimens. The polyurea/sodium silicate microcapsules (OT1 was used here) or unencapsulated sodium silicate powder were added to the ground cement pastes, together with water. The microcapsules were crushed in the mortar using a pestle to ensure the release of the sodium silicate core materials before adding to the ground cement pastes. For reference, a ground cement sample with only water added was also prepared. Each sample contained 10 g ground cement pastes with the addition of 2 g crushed OT1 microcapsules or sodium silicate (SS) powder (20% by weight of cement pastes), and 5 g water. Water was added since it is needed for the reaction of the sodium silicate with hydrated cement. Those mixes were then cured in small plastic vessels at 80 °C for 7 days. The post-curing mixes were dried in an oven at 50 °C for 24 h to remove moisture and then ground for XRD and TGA analysis. The ground cement sample without any additives before healing was also tested. There were four samples tested in total, including (1) oil well cement pastes before healing; (2) oil well cement pastes with only water added after healing; (3) oil well cement pastes with sodium silicate powder and water addition after healing; (4) oil well cement pastes with crushed microcapsules and water addition after healing. This analysis method was adapted from Giannaros et al. (2016) who carried out a similar analysis on the reaction between sodium silicate microcapsules and cement matrix at ambient temperature. A summary of the testing procedure is shown in Figure 5.8.
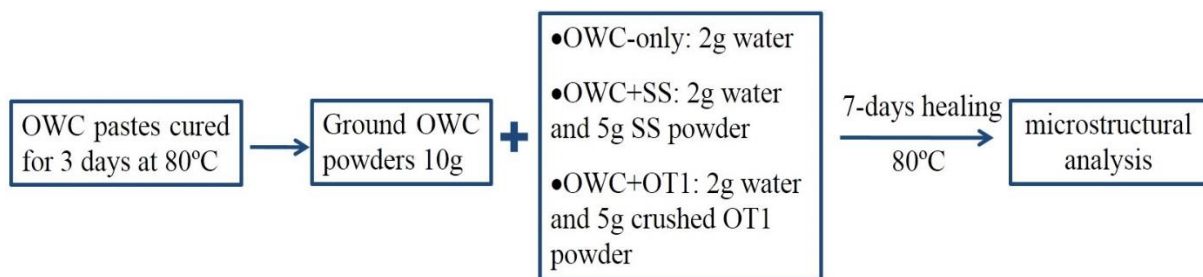
Figure 5.8 Testing procedure for investigating the self-healing reactions of sodium silicate microcapsules in oil well cement cured at 80 °C.

Figure 5.9 presents the cement mixtures before and after healing. It can be clearly seen that the ground cement pastes with only water added (OWC-only) showed almost no change before and after healing, whilst the ground cement pastes with added SS powder (OWC+SS) or crushed microcapsules (OWC+OT1) were bound together into hardened disks after healing for 7 days at 80 °C. This indicated the formation of the C-S-H product by the reaction between sodium silicate and $Ca(OH)_2$, which acted as a binding material that could bridge the hydrated cement particles.

Before healing

OWC only   OWC +SS   OWC +OT1

After healing for 7 days at 80ºC
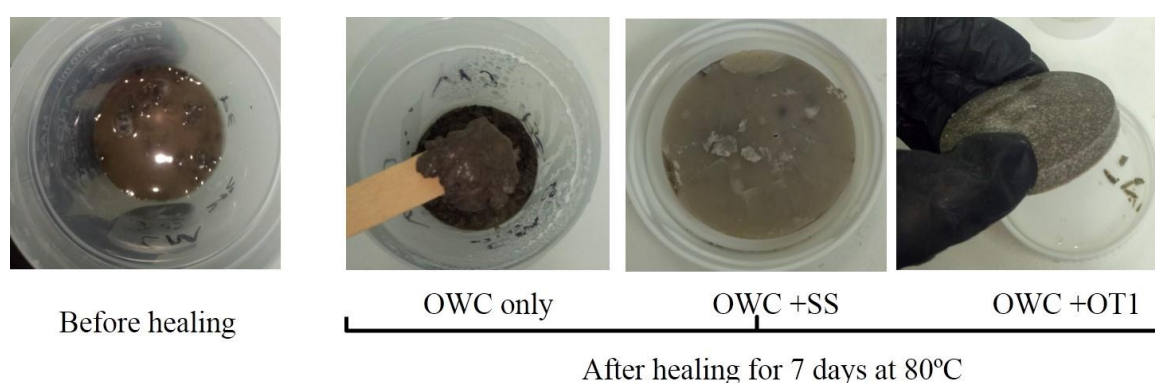
Figure 5.9 Ground oil well cement paste mixtures with only water added, or SS and water, or crushed OT1 microcapsules and water before and after healing for 7 days at 80 °C.

The XRD results of the four samples tested are shown in Figure 5.10. The main peaks of $Ca(OH)_2$ (CH) were identified at $2\theta=18.0°$, $34.1°$, and $47.1°$. Calcium silicate hydrates (C-S-H) did not show intensive peaks due to their poor crystallinity, but appeared as a hump that was observed in the region around $2\theta=29.5°–32.3°$. The CH peaks were very intense in the control sample of oil well cement without any additives before healing. After healing for 7 days at 80 °C, the intensity of the CH peaks was significantly reduced in the samples treated with SS or OT1 microcapsules, indicating the consumption of CH by reacting with sodium silicate. Correspondingly, the hump area of C-S-H was clearly seen to become more distinctive in the samples treated with SS or OT1 microcapsules, suggesting the formation of C-S-H healing products. By contrast, the XRD spectra of the sample treated with only water after healing remained almost identical to that of the control sample before healing. The only healing process in the sample without the addition of healing agents was autogenous healing, based on further hydration of the cement and precipitation of calcium carbonates. It was noted that the peaks of

the unhydrated calcium silicates (mainly C_3S) were absent in all samples, suggesting that most of the oil well cement hydrated within the 3 day curing period at 80 °C. Curing at a high temperature substantially accelerated the cement hydration. In such a case, there was very little unhydrated cement remaining available for further hydration in autogenous healing.
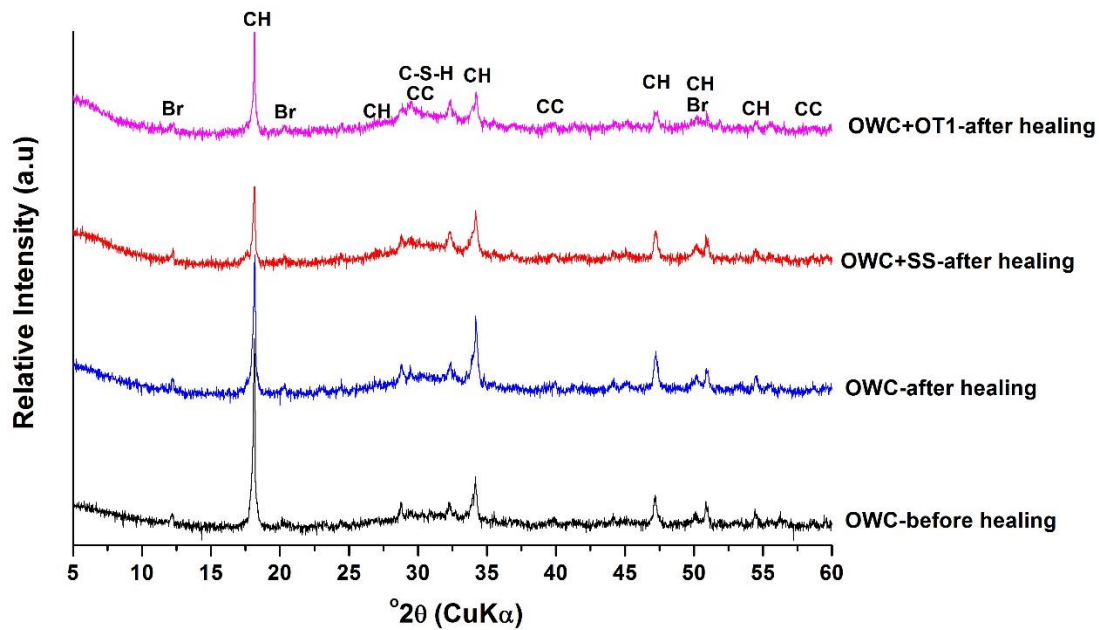
Figure 5.10 X-ray diffraction (XRD) spectrum of the four mixtures investigated: ground oil well cement paste (OWC) before healing, OWC added with only water, SS and water (OWC+SS), crushed OT1 microcapsules and water (OWC+OT1) after healing for 7 days at 80 °C, where Br: Brownmillerite, CH: Portlandite ($Ca(OH)_2$), C-S-H: Calcium silicate hydrate, Calcium aluminate Cc: Calcite ($CaCO_3$).

According to the XRD results above, it was clear that oil well cement cured under a high temperature has very little capability for autogenous healing due to the high degree of cement hydration. The addition of sodium silicate agent induced the consumption of CH and formation of C-S-H, which improved the healing capability of highly hydrated oil well cement pastes. In the studies of Giannaros et al. (2016) and Irico et al. (2017), who used XRD to investigate the chemical reaction of SS with hydrated cement, the reduction of CH peaks and the increase of the hump in the C-S-H region were also observed in the ground cement pastes treated with SS agent. However, the cement samples in their studies were prepared by 7-day curing at 20 °C before grinding. Peaks of unhydrated calcium silicate were still observed, and the intensity of

these peaks was seen to reduce after healing. Obviously, in addition to the reaction between SS and CH, further hydration of the unhydrated cement was also involved in the healing reactions of those ground cements cured at 20 °C.

The TGA tests provided quantitative analysis of the healing reactions between SS and hydrated oil well cement, as supplementary to the XRD analysis. Figure 5.11 presents the TGA results including the weight loss (Figure 5.11a) and the corresponding differential thermogravimetry (DTG) curves (Figure 5.11b-e) of the four samples. As shown in the DTG curves, the sharp peak at around 400 to 500 °C represented the decomposition of portlandite $Ca(OH)_2$ (CH) into CaO and H_2O. The weight loss at 600 to 800 °C represented the decomposition of calcite $CaCO_3$ into CaO and CO_2. The peaks of $CaCO_3$ were not very distinctive in the XRD spectra in Figure 5.10, whilst the $CaCO_3$ content in each sample can be more clearly identified in the TGA results. The C-S-H hydrates showed weight loss over a wide range of temperatures from 50 to 600 °C (mainly between 50 and 400 °C) caused by dehydroxylation and the loss of water present in the interlayer. The relative quantities of these main components in the samples can be calculated from the weight loss results (Lothenbach et al. 2016). The weight loss of CH (WL_{CH}, %) due to the evaporation of water can be used to calculate the amount of CH (M_{CH}, %) present in the samples, using the molecular masses of CH ($m_{CH} = 74$ g/mol) and water ($m_{H_2O} = 18$ g/mol) H_2O as shown in Equation 5.1:

$$M_{CH} = WL_{CH} \times m_{CH}/m_{H_2O} = WL_{CH} \times \frac{74}{18} \qquad \text{Equation 5.1}$$

Similarly, the weight loss of $CaCO_3$ (WL_{CaCO_3}, %) due to the loss of CO_2 can be used to calculate the amount of $CaCO_3$ (M_{CaCO_3}, %) using the molecular masses of $CaCO_3$ ($m_{CaCO_3} = 100$ g/mol) and CO_2 ($m_{CO_2} = 44$ g/mol) as shown in Equation 5.2:

$$M_{CaCO_3} = WL_{CaCO_3} \times m_{CaCO_3}/m_{CO_2} = WL_{CaCO_3} \times \frac{100}{44} \qquad \text{Equation 5.2}$$

The calculated results of the CH and $CaCO_3$ content in the four tested samples are given in Table 5.3. It is difficult to accurately quantify the amount of the C-S-H hydrate phase due to its wide water loss region that spanned from 50 to 600 °C and overlapped between the different weight loss regions of other products within this range. Especially in the sample with crushed

microcapsules, the decomposition of the polyurea shell that mainly occurred between 220 and 400 °C also contributed to the total weight loss.

Generally, the TGA results were consistent with the relative intensity of the CH and C-S-H peaks in the XRD spectra as described above. Through comparison with the control sample before healing, it is evident that the oil well cement sample treated with SS or crushed microcapsules had reduced weight loss between 400 and 500 °C, while there was more weight loss in the temperature range between 50 and 400 °C, suggesting the consumption of CH and subsequently increased content of C-S-H after healing. As shown in Table 5.3, by addition of SS or crushed microcapsules, the content of CH was substantially reduced from 18.8% to 12.4% and 7.7% respectively. The sample treated with only water showed almost identical weight loss in both temperature ranges to the control sample before healing. This further confirmed that there was little continued hydration occurring in the hydrated oil well cement under high temperature curing at 80 °C. The slight reduction in the weight loss of CH was due to the carbonation of CH, which can be identified by the increased weight loss of $CaCO_3$ between 600 and 800 °C. According to the calculations, the content of $CaCO_3$ in the control cement pastes increased from 3.2% to 4.1% after healing. The increased content of $CaCO_3$ was also observed in the other two post-healing samples with SS and crushed microcapsules.

It is noted that the sample treated with crushed microcapsules showed even more reduction in CH content as well as more weight loss in the C-S-H region than the sample with SS. The carbonation of CH is one possible reason for the greater reduction of CH. SS is highly soluble in water and its solubility increases with temperature. Direct addition of SS may induce very rapid reaction with $Ca(OH)_2$ at high temperature. The quickly formed C-S-H gel may deposit on the surface of cement particles, which is likely to inhibit further reaction between the $Ca(OH)_2$ leached from the cement particles. Therefore, less CH was consumed to form C-S-H. As illustrated in Figure 5.9, a thin layer of gel products was formed on top of the bound mixtures of the oil well cement with SS after healing. By contrast, a more full reaction seemed to be achieved between the sodium silicate released by the crushed microcapsules and $Ca(OH)_2$ from the ground cement particles.

(a)

(b)

(c)

(d)

(e)
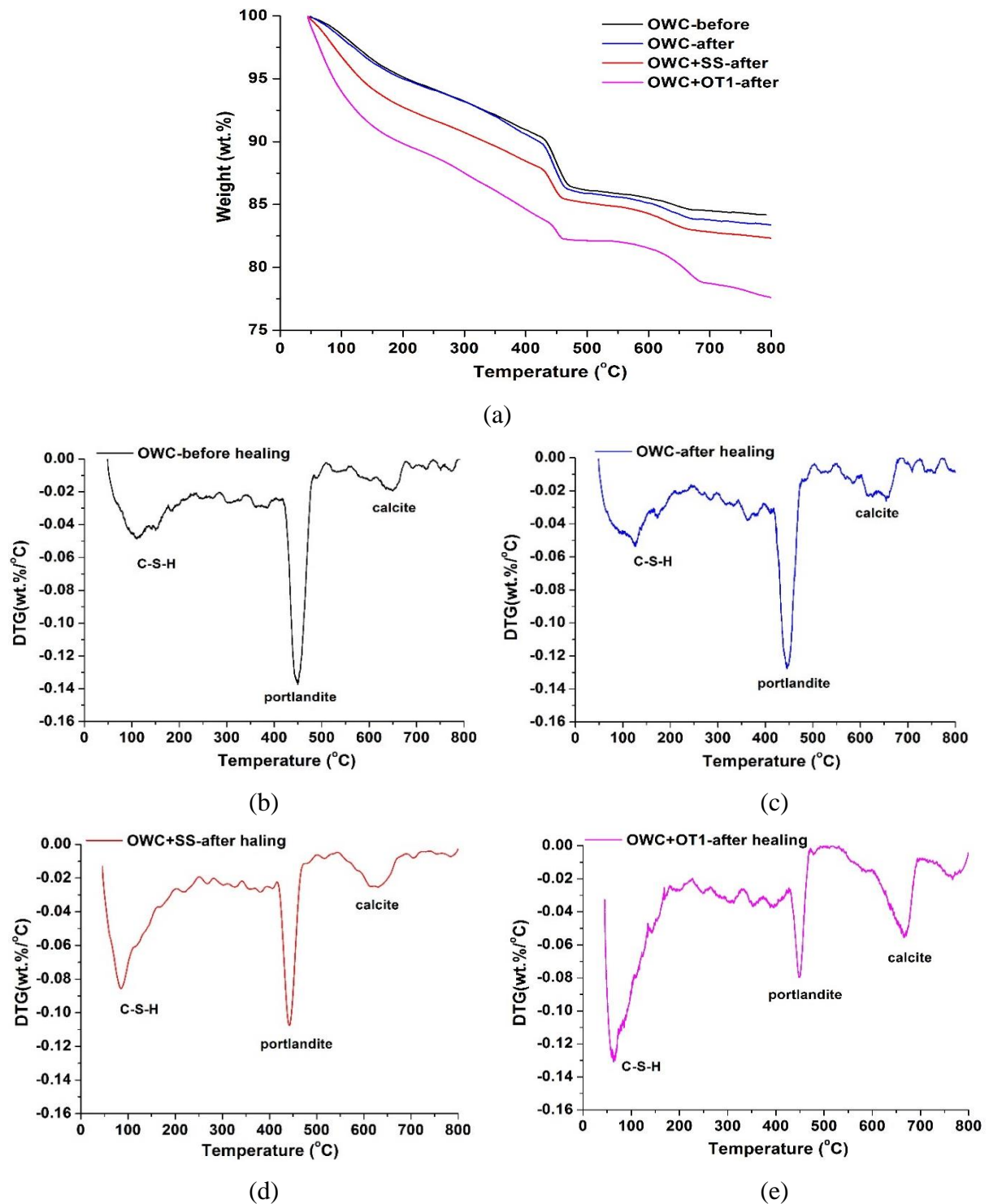
Figure 5.11 Weight loss (a) and DTG curves of (b) ground oil well cement paste (OWC) without any additives before healing; (c) ground cement pastes with only water added; (d) SS and water (OWC+SS); (e) crushed OT1 microcapsules and water (OWC+OT1) after healing for 7 days at 80 °C.

Table 5.3 The relative contents of Portlandite $Ca(OH)_2$ and calcite $CaCO_3$ in the four mixtures tested using TGA analysis.

Cement paste type	$Ca(OH)_2$		$CaCO_3$	
	Weight loss (%) 400–500°C	Content %/g cement paste	Weight loss (%) 600–800°C	$CaCO_3$ %/g cement paste
OC-before	4.4	18.8	1.4	3.2
OC-after	4.2	17.9	1.8	4.1
OC+SS	2.9	12.4	1.9	4.3
OC+OT1	1.8	7.7	3.2	7.3

5.5 Self-healing efficiency

5.5.1 Visualisation of crack closure

5.5.1.1 Crack width

After 3 days of curing at 80 ºC, the 40×40×160 mm oil well cement prisms containing NT1 or NT2 microcapsules at various contents were loaded under three points of bending at a controlled crack mouth opening displacement (CMOD) of 0.2 mm. Microscope images were taken of the cracks generated in the cement samples after loading, and their residual crack widths were measured. The results showed that the cracked cement samples had residual crack widths ranging between 0.09–0.17 mm. After healing for 7 days at 80 ºC, the post-healing crack widths of the cracked cement samples were compared to the original ones to determine the degree of crack width healing. The results of the crack mouth width healing efficiency calculated according to Equation 3.3 are presented in Figure 5.12. Microscope images of the cracks in cement samples before and after healing are shown in Figure 5.13.
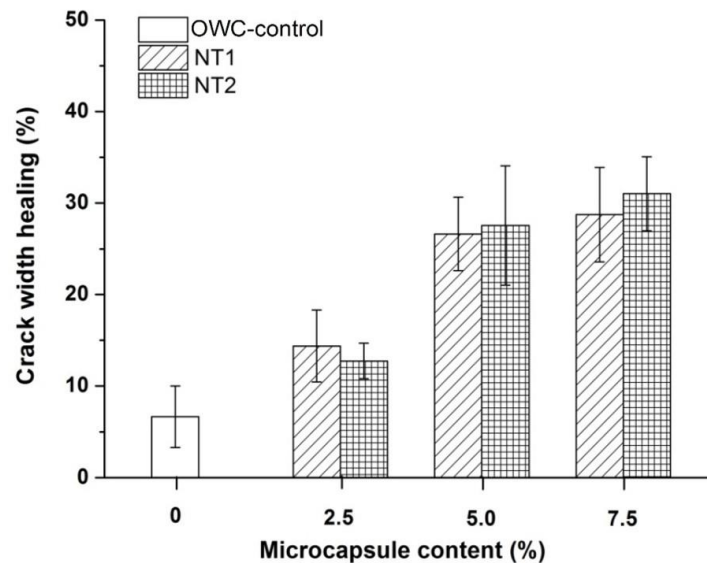
Figure 5.12 Crack mouth width healing of cracked oil well cement prisms containing a varying content of NT1 or NT2 microcapsules from 0 to 7.5% by weight of cement after healing for 7 days at 80 °C.

As seen in Figure 5.12, compared to the control samples, the cement samples containing microcapsules showed better performance in crack mouth width healing. Cement samples with higher microcapsule content had higher degrees of crack width healing. The crack width healing degree in the control samples was less than 7%. With addition of microcapsules (NT1 or NT2) at a content of 7.5%, the crack width healing degree was improved to about 29~31%. Figure 5.13 also shows that the cement samples with microcapsules generally showed improved crack width healing, with healing products filling in the cracks that were presumably precipitates of calcium carbonates and the reaction products of sodium silicate with the hydrated cement. Cement samples with NT1 and NT2 microcapsules showed similar degrees of crack width healing.

Other researchers have also reported the improved crack width healing in a cementitious matrix using encapsulated sodium silicate agents. For example, Giannaros (2017) reported that the degree of crack width healing (0.11~0.17 mm) in mortar samples was improved from 40% to about 80% by the addition of sodium silicate microcapsules (average size 290 μm) from 0 to 8% (by weight of cement). Kanellopoulos et al. (2015) even obtained complete crack mouth

filling of crack widths of 0.3–0.4 mm CMOD of mortar samples after healing by using sodium silicate encapsulated in glass capsules that had much larger sizes than microcapsules (<1 mm).

It appeared that the improvements of the crack width healing in this study were less prominent than those of the previous studies as mentioned above. However, it should be noted that the samples in previous studies were cured at ambient temperature, while the oil well cement samples of this study had high temperature curing at 80 °C. In the former cases, the healing process involved contributions both from autogenous self-healing by continued cement hydration and precipitation of calcium carbonates, and from autonomic self-healing by reactions of sodium silicate with the hydrated cement. In the study of Giannaros (2017), the crack width healing degree of the control samples already reached about 40%, suggesting that the samples cracked at a young age of 7 days possessed a high potential for autogenous healing. For microcapsule-containing samples, the healing of cracks took advantage of both autogenous healing and autonomic healing. The resulting high degrees of crack width healing are thus not surprising. In the case of oil well cement samples cured at 80 °C, by contrast, the healing process largely depended on autonomic healing by SS microcapsules while the contributions from autogenous healing were very limited. Most of the oil well cement had completed hydration within the first 3 days before cracking, as analysed in Section 5.4, thus very little unhydrated cement was available for continued hydration after cracking. The precipitation of calcium carbonates at the crack mouth may also be influenced by high temperature curing due to the reduced solubility of CO_2 in water with increasing temperature. The precipitation of calcium carbonates was regarded as the most important contribution for filling the crack mouth. As a result, the control samples had a very low degree of crack width healing. Considering the challenging conditions for self-healing at high temperature, the crack width healing achieved by adding microcapsules (NT1 or NT2) can be still seen a significant improvement compared to the control samples.

The microscope images only presented an indication of the healing degrees at the cracking mouth but did not reflect the healing conditions inside the cracks. Therefore, investigations on the healing of the crack depth were carried out in the following section to obtain more comprehensive information about the healing degree within the cracks.

Figure 5.13 Microscope images of cracked oil well cement prisms containing a varying content of NT1 or NT2 microcapsules from 0 to 7.5% by weight of cement before and after healing for 7 days at 80 ºC. The red scale bar represents 0.5 mm in all images.

5.5.1.2 Crack depth

A non-destructive method using ultrasonic equipment was employed to measure the depth of the cracks in oil well cement prisms after healing for 7 days at 80 °C. This method is based on the fact that ultrasonic waves travel much easier in hardened cementitious matrix (4000–5000 m/s) than in water (1480 m/s) or air (350 m/s). As a result, they will travel around the open cracks leading to an increase in transmission time. When the crack is sealed, the waves will be able to travel through the formed healing products that fill in the cracks, thus reducing the transmission time. By measuring the wave transmission time, the depth of cracks can be calculated according to Equation 3.4. The results of the calculated crack depths of the cement samples after healing for 7 days at 80 °C are shown in Figure 5.14.
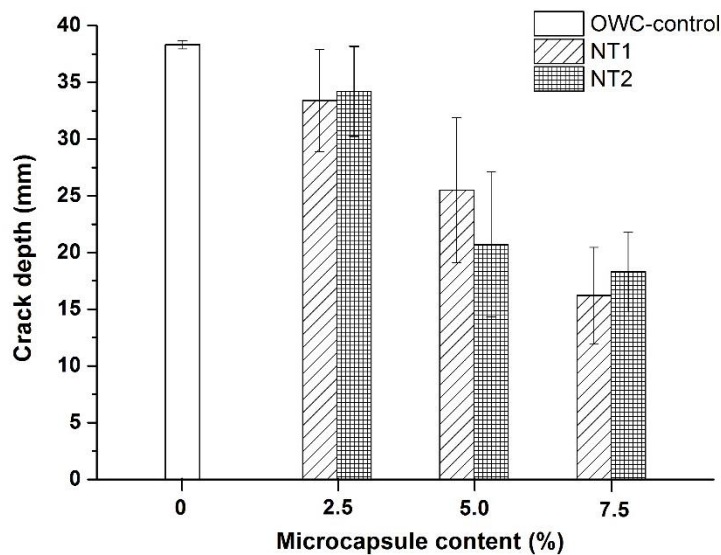
Figure 5.14 Ultrasonic crack depth measurements of cracked oil well cement prisms containing a varying content of NT1 or NT2 microcapsules from 0 to 7.5% by weight of cement after healing for 7 days at 80 °C.

All the cement samples containing microcapsules showed lower crack depths than the control samples after healing. Increasing the content of microcapsules achieved greater reduction in the crack depth. At a content of 2.5%, cement samples with NT1 microcapsules, a crack depth reduction of ~13% was achieved compared to the control samples. The increased addition of NT1 to 7.5% resulted in a greater crack depth reduction of ~58%. Similarly, the addition of NT2 microcapsules from 2.5% to 7.5% resulted in increased crack depth reduction from ~11%

to ~53%. The increased crack depth reduction suggests that there was improved healing inside the cracks. Mostavi et al. (2015) also observed a crack depth reduction of 35% after 14 days of healing achieved by adding 5% (by weight of cement) SS microcapsules in the mortar samples. Giannaros (2017) reported that increasing the proportions of SS microcapsules up to 10.7% resulted in crack depth reduction of 68% after 28 days of healing. At similar concentrations of SS based microcapsules, the oil well cement samples here cured at high temperature obtained comparable levels of crack depth reduction as those samples cured at ambient temperature in the aforementioned studies after a shorter healing period of 7 days. This indicates that that high temperature curing may induce fast healing. Although high temperature curing may suppress the autogenous healing of cement samples as discussed above in Section 5.5.1.1, it also can accelerate the autonomic healing process based on the reaction of sodium silicate agents with cement hydration products.

5.5.2 Recovery in tightness

In this section, gas permeability tests and water sorptivity tests were carried out to evaluate the self-healing behaviour of oil well cement samples containing microcapsules in terms of the recovery of tightness. As introduced in Table 5.2, gas permeability tests were conducted on cement disks containing OT1 or OT2 microcapsules from the old batch. Water sorptivity tests were conducted on cement prisms containing NT1 or NT2 microcapsules from the new batch. Before testing, those cement samples were cracked after curing at 80 ℃ for 3 days and were then left to heal for a further 7 days at the same temperature.

5.5.2.1 Gas permeability

Figure 5.15 presents the results of the gas permeability test on the cracked disc samples after healing for 7 days at 80 ℃, as well as their uncracked counterparts. The cracked disks had an average crack width range of 0.13–0.16 mm. The uncracked samples all showed very low permeability coefficients below 1×10^{-17} m^2. The addition of OT1 and OT2 microcapsules at small contents up to 2.5% had negligible effects on the gas permeability of the oil well cement samples. At higher addition contents, the cement samples with microcapsules saw a slight increase in the gas permeability compared to the control samples. This is possibly due to the

influence of microcapsules on the porosity of the cementitious matrix. The addition of microcapsules can increase the porosity of cement (Dong et al. 2017), thus increasing the permeability.
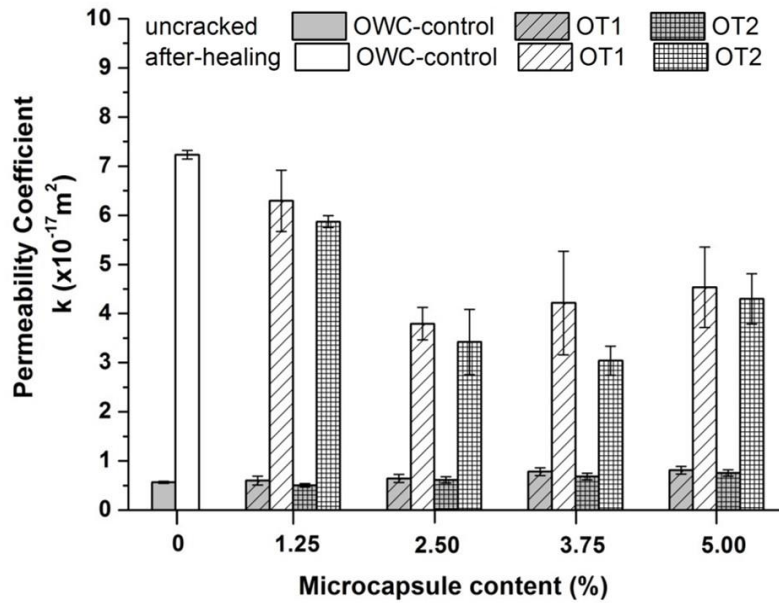
Figure 5.15 Gas permeability coefficients of uncracked and cracked oil well cement prisms containing a varying content of NT1 or NT2 microcapsules from 0 to 7.5% by weight of cement after healing for 7 days at 80 °C.

In the post-healing cement samples, the addition of OT1 or OT2 microcapsules resulted in a reduced gas permeability coefficient of the cracked samples after healing compared to the control ones, indicating a recovery in the gas tightness. The gas permeability coefficients of the post-healing cement samples decreased as the microcapsule content increased. Adding 2.5% microcapsules substantially reduced the permeability coefficient by ~48% for the samples with OT1 and ~53% for the samples with OT2. However, when the content of microcapsules increased to 3.75% and above, the permeability coefficients of the post-healing cement samples showed no further decrease but a slight increase instead. It is speculated that after the microcapsules ruptured and released their core materials for healing, the residual shells remained in place creating voids on the crack surface which provided paths for gas flow, thus increasing permeability (Litina & Al-Tabbaa 2015). Microcapsules OT1 with larger average size may generate larger sized voids after rupture for healing, which allows more gas flow. As

a result, the post-healing samples with OT1 generally obtained less reduction in permeability than those with OT2. Nonetheless, the addition of microcapsules achieved an overall reduction in gas permeability of the cracked cement samples after healing, indicating their effectiveness in improving the gas tightness recovery of cracked cement samples. Although it is recognised that the gas permeability coefficient of unhealed cracked samples could be of interest, this was not measured in this research.
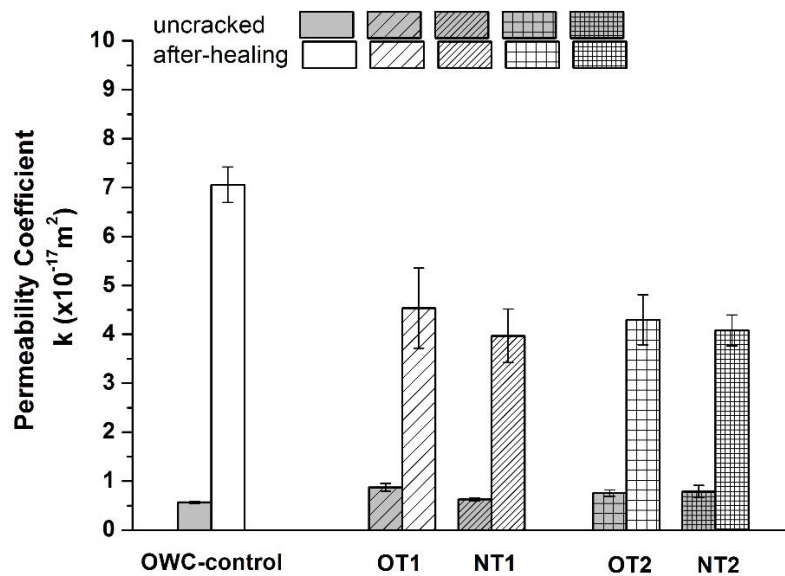
Figure 5.16 Gas permeability coefficients of uncracked and cracked oil well cement prisms containing new batch microcapsules (NT1 and NT2) compared to the samples with old batch microcapsules (OT1 and OT2) at a content of 5% after healing for 7 days at 80 °C.

In addition, the gas permeability test was also conducted on the cement samples containing NT1 or NT2 microcapsules at an addition content of 5%. Figure 5.16 compares the gas permeability results between the old batch and the new batch of microcapsules. For both the T1 and T2 groups, microcapsules from the new batch (NT1 or NT2) showed comparable performance to the old batch (OT1 and OT2) on gas permeability reduction in the post-healing samples.

5.5.2.2 Water sorptivity

Figure 5.17 presents the water sorptivity results of the oil well cement prism samples containing NT1 or NT2 microcapsules after healing for 7 days at 80 °C, as well as those of the uncracked

ones. The representative plots of cumulative water uptake over the testing time of the post-healing samples and their uncracked counterparts are given in Figure 5.17a and Figure 5.17b. The corresponding sorptivity coefficients are shown in Figure 5.17c. Figure 5.17a, shows that the water uptake by capillary sorption through the cracks was substantially reduced in the post-healing cement samples containing microcapsules, compared to the control samples without microcapsules, which indicates a recovery in water tightness after healing. The sorptivity coefficients of post-healing cement samples with microcapsules were consistently lower than the control samples, as shown in Figure 5.17c. There was a general trend that the sorptivity coefficients of the cement samples decreased with the increasing content of NT1 or NT2 microcapsules, suggesting improved healing of the cracks at higher microcapsule content. This trend was consistent with that observed in the crack width and crack depth measurements on the same prism samples. At an addition content of 2.5%, the sorptivity coefficients of post-healing cement samples with NT1 and those with NT2 were reduced by ~31% and ~38% compared to the control samples. As the addition of microcapsules increased to 7.5%, the reduction in the sorptivity coefficients reached ~76%. This decreasing trend was not linear, as reduced reduction in sorptivity coefficients was gained by increasing the microcapsule addition from 5% to 7.5%. This is possibly due to the large amount of void spaces occupied by the ruptured microcapsules after healing that can create connecting pores within the cracking area of the matrix, and which may increase the sorptivity.

Other researchers have also obtained considerable reductions in sorptivity coefficients by using different types of sodium silicate microcapsules (Antonis Kanellopoulos et al. 2016; Giannaros 2017). In the study of Giannaros (2017), addition of the aforementioned gelatine/gum acacia microcapsules up to 5.33% by weight of cement resulted in reduction of the sorptivity coefficients by ~54% after 28 days of healing at ambient temperature. Obviously, the NT1 and NT2 microcapsules in this study achieved faster recovery against the water sorption which can be attributed to faster healing in high temperature curing conditions. Kanellopoulos et al. (2016) also found that the ability of the hydrophilic gelatine/gum acacia shell materials to absorb water might increase the sorptivity of the cementitious marix. However, the hydrophobic polyurea shell material of the microcapsules in this study seemed to reduce the sorptivity to some extent,

as indicated by the water uptake measurements (Figure 5.17b) as well as the sorptivity coefficients of the uncracked samples (Figure 5.17c). The microcapsule-containing samples generally absorbed less water than the control samples without microcapsules, and so had lower sorptivity coefficients. The characteristic of reduced water absorbency of the cement matrix can be beneficial to its durability in water tightness. As a whole, the water sorptivity results together with the results of the gas permeability, clearly showing that the recovery in durability of oil well cement samples will be improved by the addition of T1 and T2 groups of microcapsules.
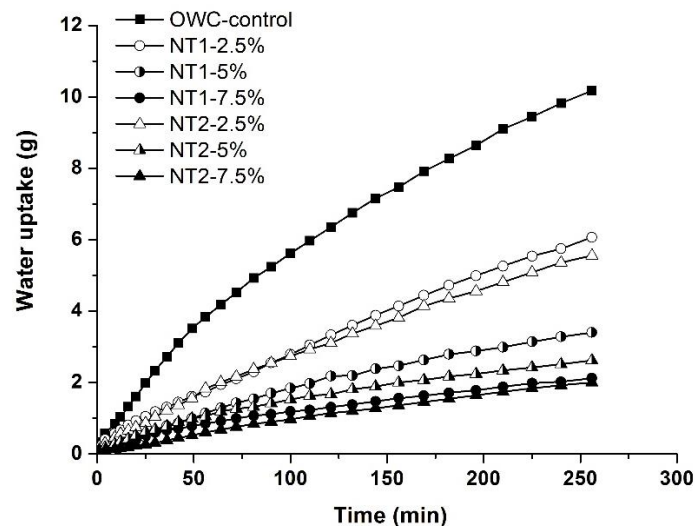
(a)
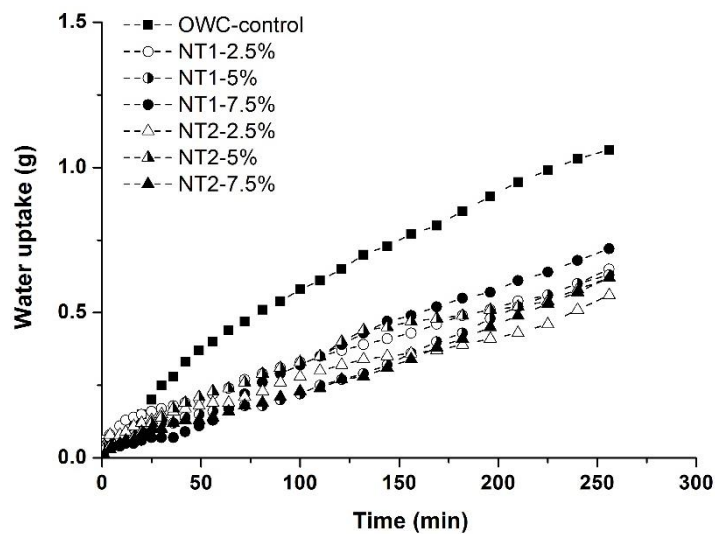
(b)
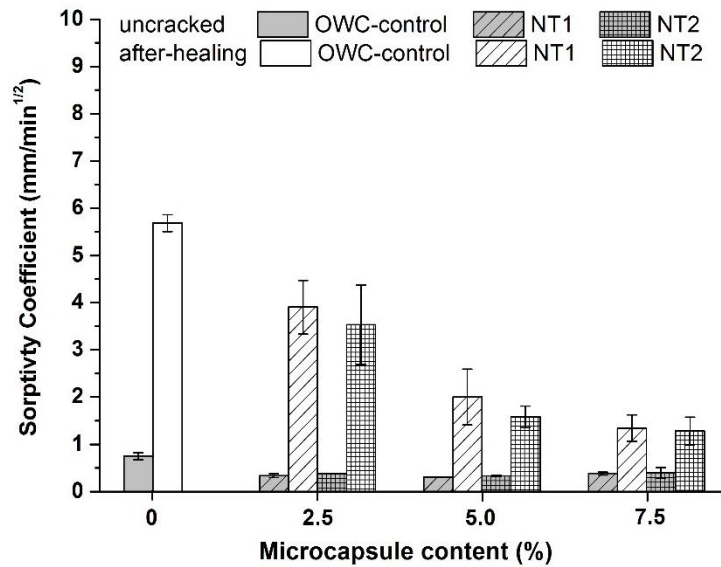
(c)

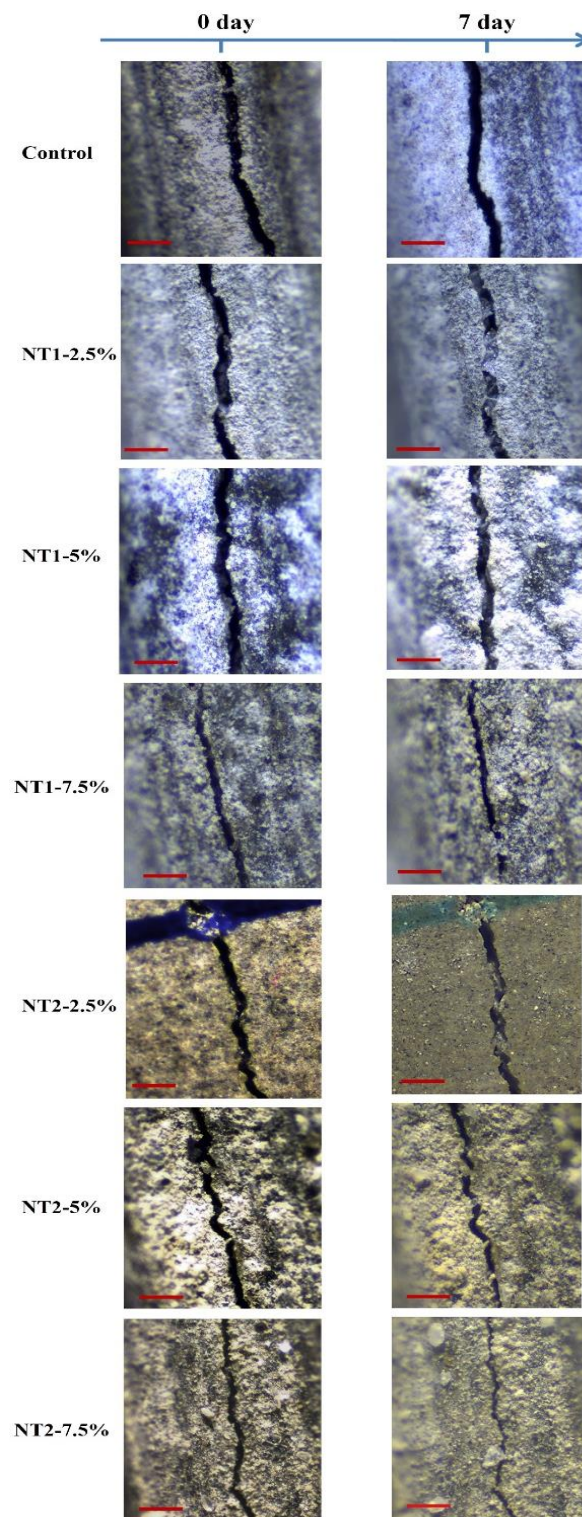Figure 5.17 Capillary sorptivity results on water uptake of (a) cracked and (b) uncracked oil well cement prisms containing a varying content of NT1 or NT2 microcapsules from 0 to 7.5% by weight of cement after healing for 7 days at 80 °C. The corresponding sorptivity coefficients are given in (c).

5.5.3 Recovery in flexural strength

After the measurements of capillary sorptivity, the post-healing prism samples were re-loaded under three-point bending to examine their flexural strength regain which was calculated according to Equation 3.9. As shown in Figure 5.18, the addition of NT1 or NT2 microcapsules increased the regain in the flexural strength of oil well cement samples after healing for 7 days at 80°C. The control samples obtained a flexural strength regain less than ~3%. Such low strength recovery is not surprising since the contributions from autogenous healing are substantially weakened at high temperature curing, as previously mentioned. The addition of NT1 or NT2 microcapsules from 2.5% up to 7.5% improved the strength regain by ~7% to 27%. A higher microcapsule content resulted in a greater strength regain. In the autonomic healing by sodium silicate agent, the main healing product C-S-H is similar to the main hydration phase of cement which is considered to be the main strength giving component of the hardened cement matrix. The formed C-S-H can provide effective binding within the cracking area, thus contributing to the strength recovery. As illustrated in Section 5.4, the ground cement particles with addition of unencapsulated sodium silicate agent or the sodium

silicate microcapsules were both seen to be bound together after healing for 7 days, which are strong indications of the effectiveness of sodium silicate in improving strength recovery.

In the literature, there are also records of improved strength recovery with the use of encapsulated sodium silicate agents. For example, Pelletier et al. (2010) measured the flexural strength recovery of concrete specimens containing 2% PU microcapsules with sodium silicate by volume of cement and found that the samples containing microcapsules restored 10–12% more of their flexural strength than the samples without microcapsules after 7 days healing at ambient temperature. However, the concrete specimens in their study were only loaded to induce internal minor cracks but not to complete failure. At similar addition contents of microcapsules, those ones loaded to failure in this study restored comparable strength recovery within the same healing duration. From this point of view, the high-temperature healing by T1 and T2 microcapsules seemed to achieve more effective strength recovery. Gilford III et al. (2014) reported that the shell thickness had a significant influence on the healing efficiency of strength recovery. Microcapsules with too-thin shells might be too fragile to survive the mixing processes, while those with too-thick shell might be too strong to be ruptured by cracking. The best strength recovery of 11% was achieved by sodium silicate microcapsules with an optimal shell thickness at the highest content of 5% by weight of cement. NT1 and NT2 microcapsules used here had similar shell thickness but different rigidity. Considering that both groups of microcapsules showed good survivability during mixing as well as successful fractures upon triggering according to the SEM observations in Section 5.2.6, the different shell properties of NT1 and NT2 should have no significant effect on their healing performance. However, cement samples with NT2 were found to attain higher strength recovery rates than those with NT1 at higher content of 5% and 7.5%. This may be because the cement samples with NT2 had lower initial strength than those with NT1, especially at higher microcapsule contents (reported in Section 5.7.3.2), thus and relatively higher strength recovery rate. The strength regain achieved by NT2 was similar to that by NT1.
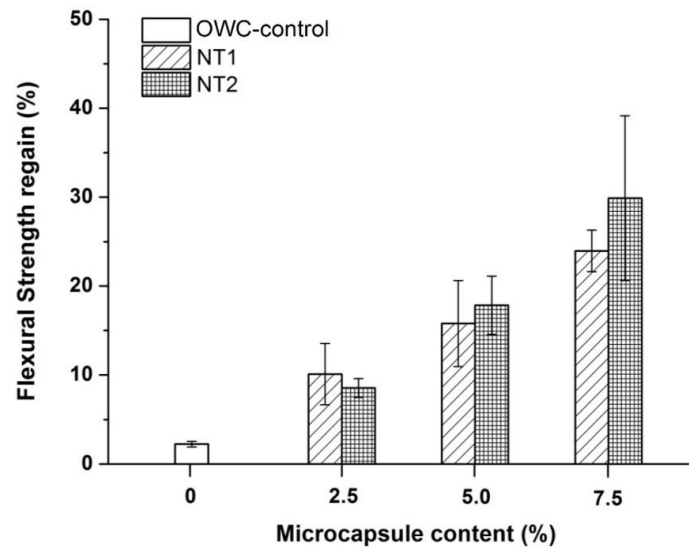
Figure 5.18 Flexural strength recovery of cracked oil well cement prisms containing varying contents of NT1 or NT2 microcapsules from 0 to 7.5% by weight of cement after healing for 7 days at 80 °C.

5.6 Microstructure analysis

5.6.1 SEM and EDX

After re-cracking under three-point bending, the post-healing oil well cement prisms containing microcapsules (NT1 or NT2) were completely separated and small chips were extracted from the cracking surface for SEM observations. On the cracking surface, both types of microcapsules were seen to be meanly distributed in the cement pastes, and the majority of them were successfully ruptured by cracking, as shown previously in Figure 5.6 in Section 5.2.5. Taking a closer look at these ruptured microcapsules, the core materials seemed to be successfully released, leaving the empty shell wall embedded in the cement pastes. As shown in Figure 5.19, clusters of fibrous products were observed around the residual shells of the NT1 (Figure 5.19a) or NT2 (Figure 5.19b) microcapsules on the cracking surfaces, which appeared to be C-S-H. Within the shells, there were also small quantities of C-S-H-like products attached to the internal shell wall. In addition to the fibrous products, plate-shaped crystals were also observed to grow on the cracking surface, as shown in Figure 5.19e. Those crystals are likely to be $CaCO_3$ formed by the carbonation of $Ca(OH)_2$ from the cracking surface.

203

(a)

(b)

(c)

(d)

(e)

(f)
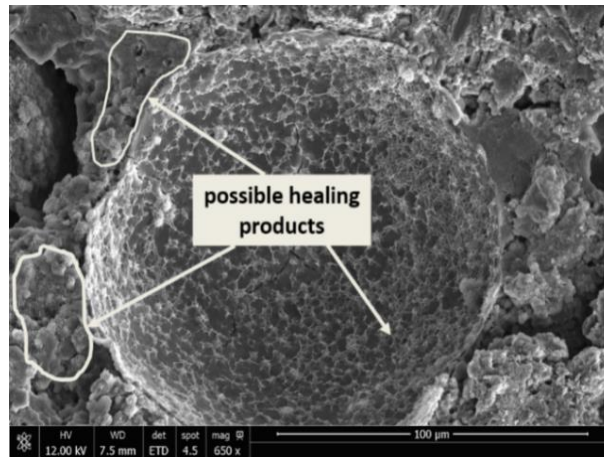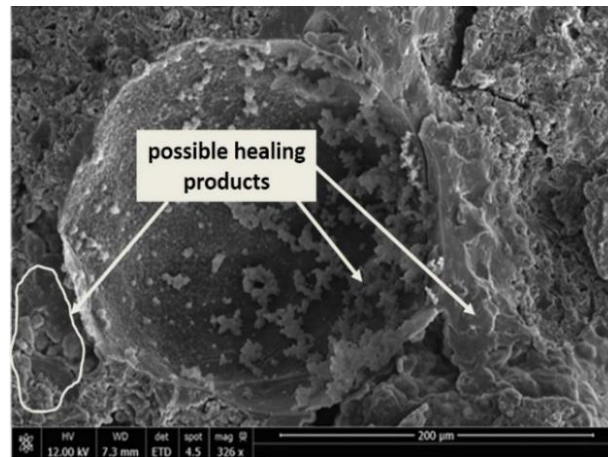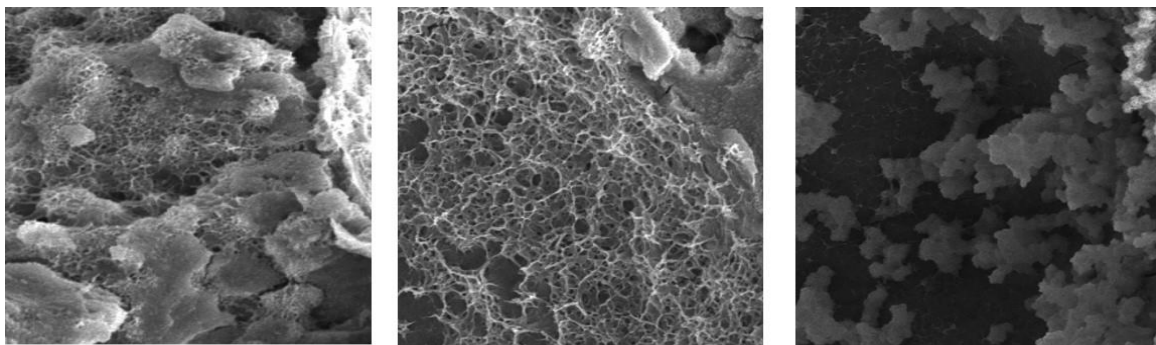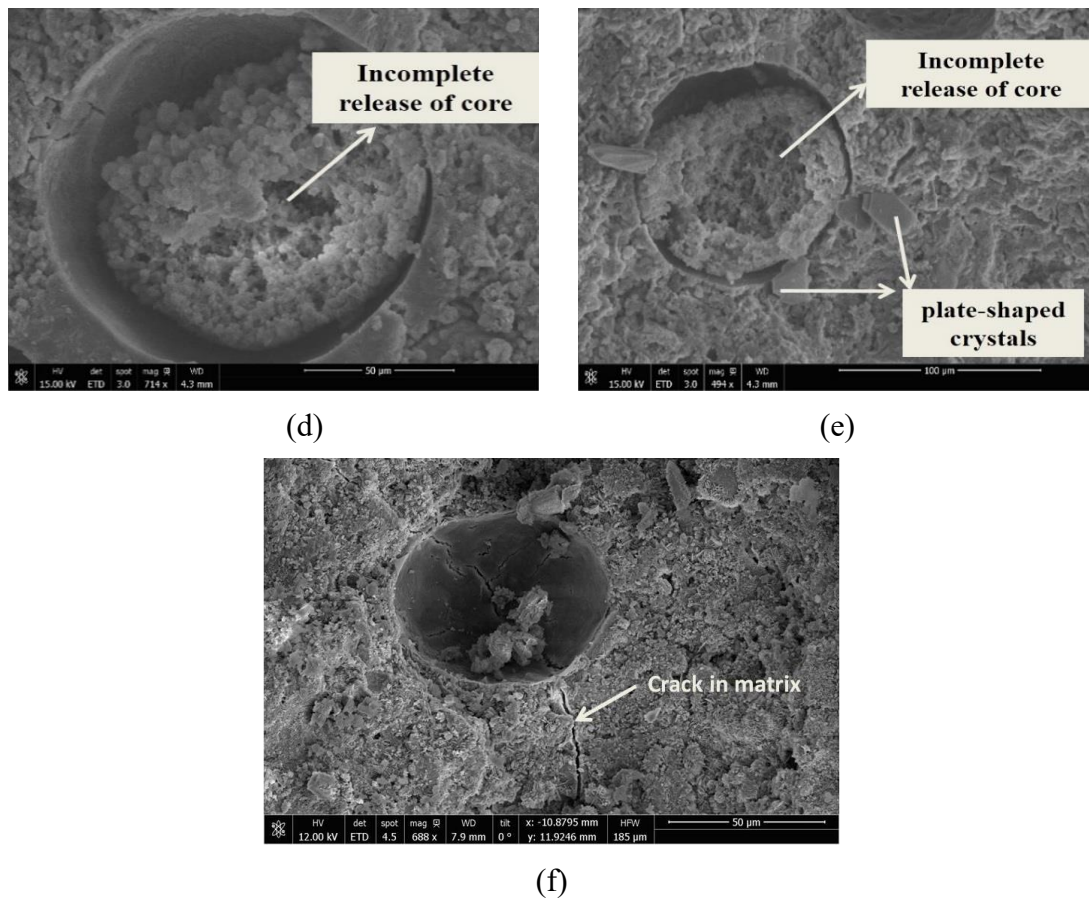
Figure 5.19 SEM observations of re-cracked oil well cement prisms containing NT1 or NT2 microcapsules after healing for 7 days at 80 °C: ruptured microcapsules (a) NT1 and (b) NT2 with C-S-H-like healing products (c) formed inside and outside around the residual shells; (d)&(e) incomplete release of core materials; (f) microcapsule cracked by propagation of microcracks in the cement matrix.

Occasionally in a few microcapsules, large quantities of clusters were found remaining within the shell (Figure 5.19d & e), which implied that the sodium silicate core materials may not be released out from the microcapsules but reacted mainly within the shell. In some cases as shown in Figure 5.19f, the microcapsule might be cracked by the propagation of microcracks in the cement matrix prior to the designated cracking induced by three point bending. In practical situations, the microcapsules are supposed to rupture by cracking for healing in similar way to the microcapsule in Figure 5.19f. This further illustrated that these polyurea microcapsules can be triggered for healing wherever cracks develop in the cement pastes.

To further analyse these healing products, energy-dispersive x-ray spectroscopy (EDX) was used to determine their elemental composition. EDX analysis was carried out on different locations both inside, outside, and around the ruptured microcapsules. As shown in Figure 5.20b and Figure 5.20d, a variety of chemical elements, mainly calcium, silicon, oxygen, and sodium, were detected in those fibrous products inside or around the microcapsules. Those fibrous products were therefore verified as C-S-H which contained calcium, silicon, and oxygen as the main chemical elements. Sodium was a unique element from the sodium silicate core materials. Its presence in the C-S-H products around the microcapsules further confirmed the successful release of sodium silicate to the cracking surface for the healing reaction with calcium hydroxides. Occasionally in the case of unsuccessful release, the cluster of healing products that remained in the microcapsules turned out to be mainly C-S-H, as suggested by the similar traces of chemical elements in Figure 5.20f. Additionally, traces of carbon also indicated the formation of calcite as healing products.

A calcium-silicon-sodium (Ca-Si-Na) ternary composition diagram was plotted based on the normalized atomic mass percentages of the EDX results, as shown in Figure 5.21. In the control samples without the presence of the sodium, the tested points generally showed Si/Ca ratios of less than 0.4. Those points with Si/Ca ratios of 0.2–0.4 were verified as the hydration products C-S-H while those with a very low Si/Ca ratio (<0.05) suggested the presence of portlandite and calcite. In the samples with microcapsules, it was found that the Si/Ca ratio (0.5–0.9) of the tested points around the NT1 or NT2 microcapsules was generally higher than that of the control samples. The resulting higher Si/Ca ratios from the addition of microcapsules again illustrated the reaction of sodium silicate core to form silicon-rich C-S-H healing products. Giannaros (2017) also observed a greater Si/Ca ratio (>0.5) of the healing products produced by sodium silicate microcapsules in the cracking area.
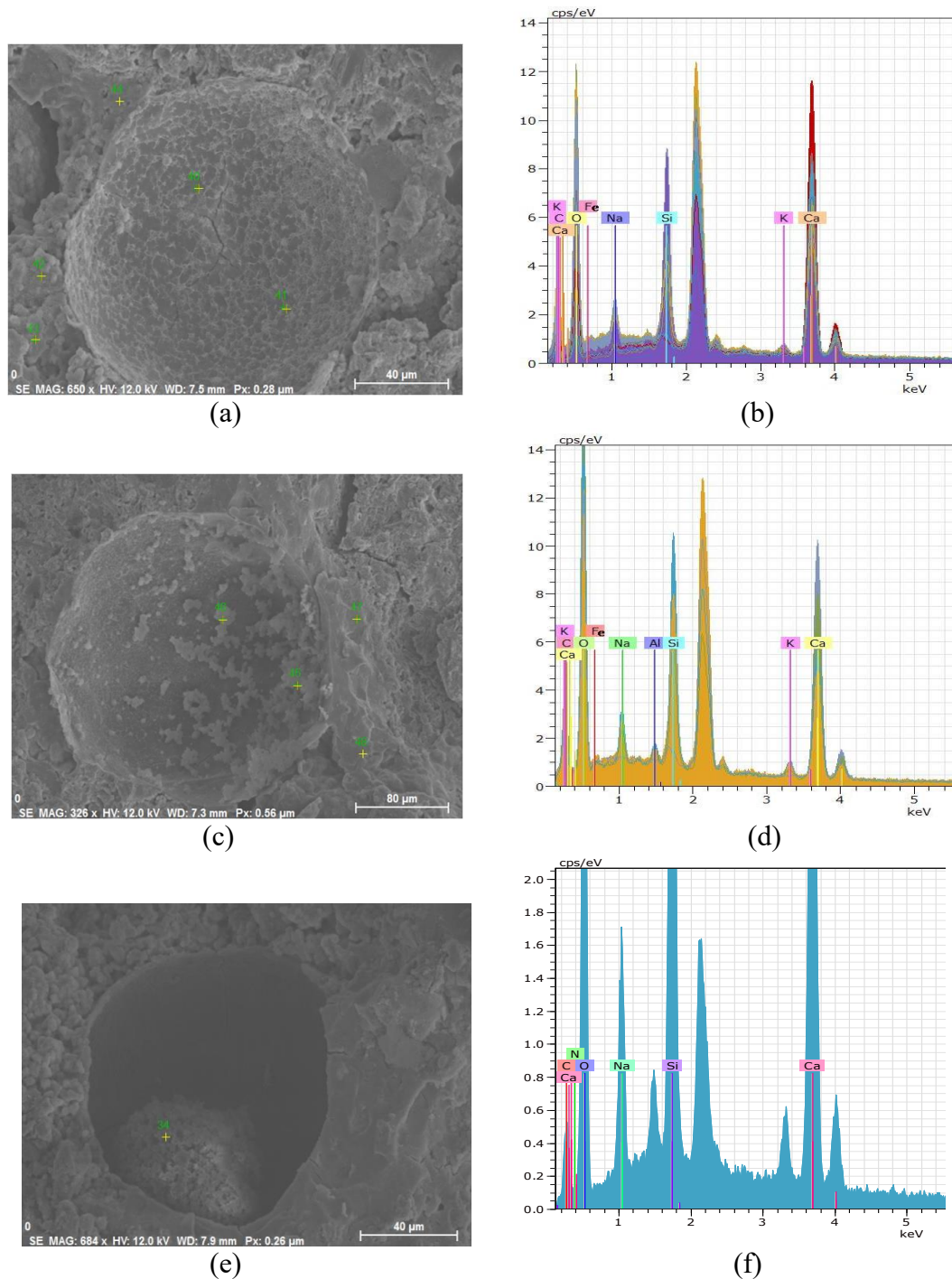
Figure 5.20 SEM images and the corresponding EDX analysis results of ruptured microcapsules (a) & (b) NT1 and (c) & (d) NT2 microcapsules; (e) & (f) microcapsules with unreleased core materials.
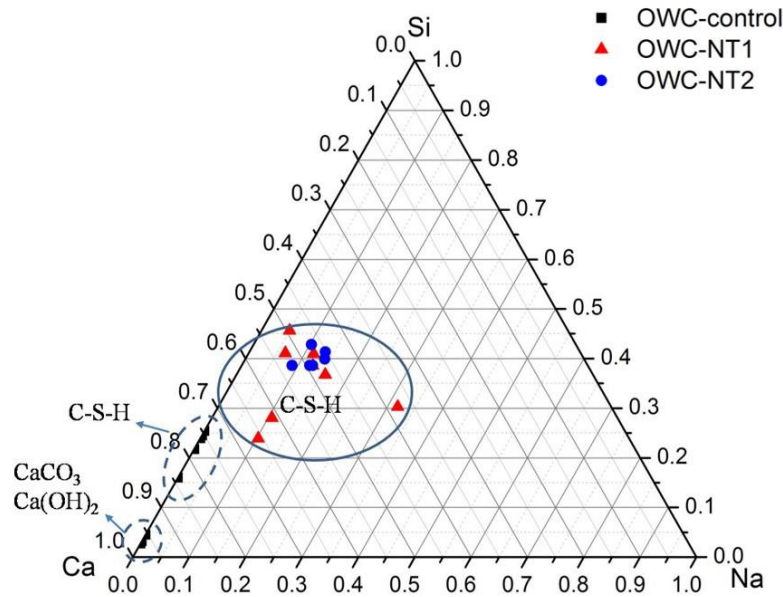
Figure 5.21 Ca-Si-Na ternary composition diagram for EDX results of the cracking surface of oil well cement prisms containing NT1 or NT2 microcapsules after healing for 7 days at 80 °C.

5.6.2 XRD

After 7 days of healing at 80 °C, the powder samples were extracted from the cracking surface of re-cracked oil well cement prisms containing NT1 or NT2 microcapsules (at content of 7.5%) as well as the control samples for XRD analysis. The obtained spectra are plotted in Figure 5.22. In all the tested samples, the typical peaks of portlandite (CH) were identified mainly at $2\theta=18.0°$, $34.1°$, and $47.1°$. Due to the poor crystallinity, C-S-H did not show intensive peaks, but a hump in the region around $2\theta=29.3°-32.3°$. The peaks of calcite formed by the carbonation of CH were observed at $2\theta=29.4°$ which overlapped with the hump of C-S-H, together with other small peaks at $2\theta=39.6°$, $56.5°$. The three tested samples did not show very distinct differences in the XRD spectra, which can be due to the small quantities of healing products obtained from the cracking surface. Nonetheless, it still can be seen that the hump region of C-S-H at $2\theta=29.3°-32.3°$ appears to be more intensive in both samples (OWC-NT1, OWC-NT2) extracted from the microcapsule-containing specimens compared to the sample from the control specimen. This observation suggests the formation of C-S-H healing products by reaction between the released sodium silicate and portlandite, which is inconsistent with the analysis of the healing mechanism in Section 5.4.
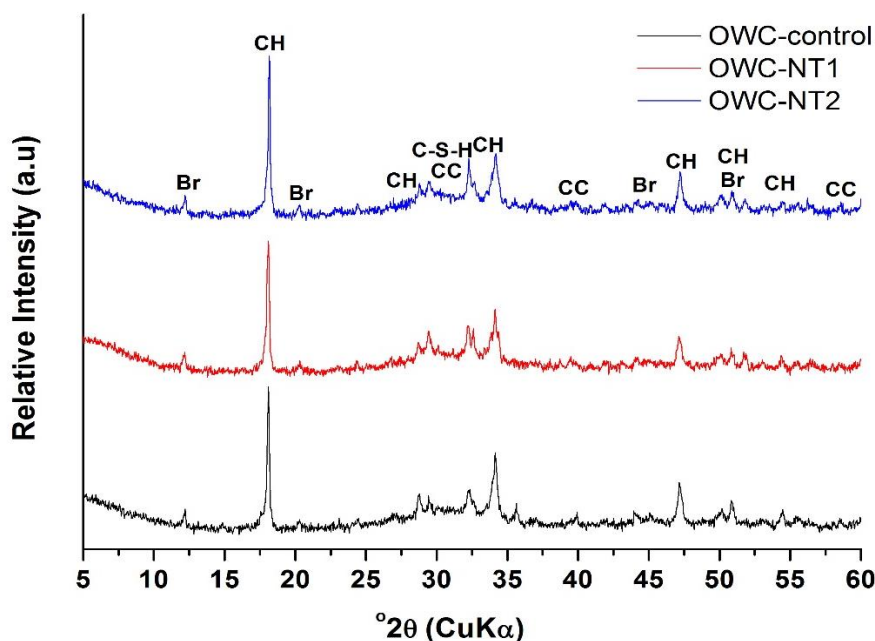
Figure 5.22 X-ray diffraction (XRD) spectrum of samples extracted from the cracking surface of oil well cement prisms containing NT1 or NT2 microcapsules at a content of 7.5% after healing for 7 days at 80 °C, where Br: Brownmillerite, CH: Portlandite ($Ca(OH)_2$), C-S-H : Calcium silicate hydrate, Calcium aluminate Cc: Calcite ($CaCO_3$).

5.6.3 TGA

TGA tests were also carried out on the extracted powder samples. The weight loss and the corresponding differential thermogravimetry (DTG) curves of the three test samples were plotted in Figure 5.23. The C-S-H hydrates showed weight loss over a wide range of temperatures from 50 to 600 °C due to water loss from the interlayer and dehydroxylation. Within the temperature range between 50 and 400 °C, the control samples had less weight loss (~9.7%) than the samples from the microcapsule-containing specimens (~10.5%), indicating the increased content of C-S-H hydrates in the cracking area with microcapsules after healing. Meanwhile, the weight loss between 400 and 500 °C represented the decomposition of portlandite into CaO and H_2O. The sample from the control specimens showed greater weight loss (~3.6%) than the samples from microcapsule-containing specimens (~2.5%) between 400 and 500 °C. These results suggest the consumption of CH by reacting with the sodium silicate agents released from the ruptured NT1 or NT2 microcapsules to produce C-S-H healing products. In addition, the weight loss between 600 to 800 °C due to the decomposition of calcite

($CaCO_3$) was also observed in the three tested samples, indicating the carbonation of CH to form calcite during healing.
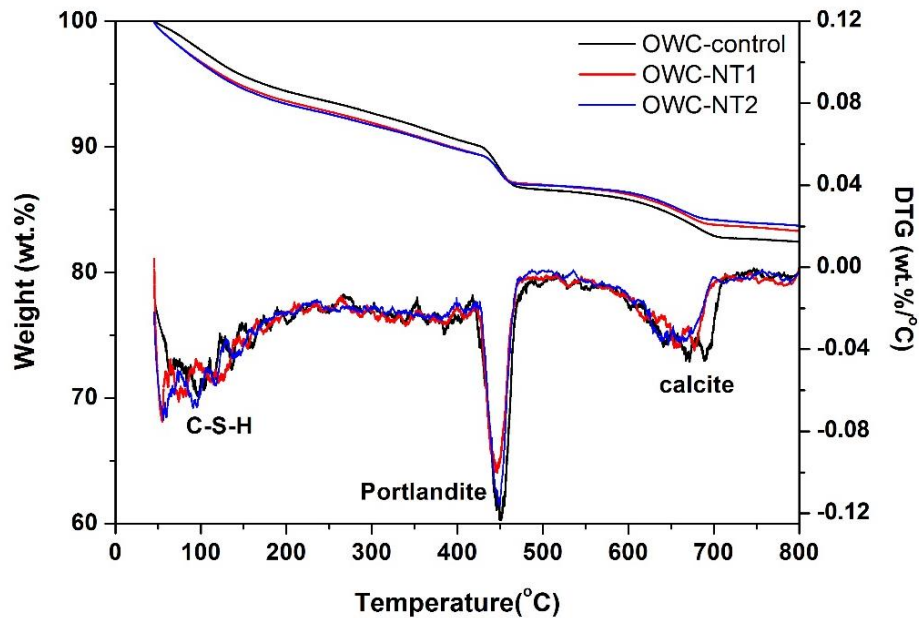
Figure 5.23 Weight loss and DTG curves of samples extracted from the cracking surface of oil well cement prisms containing NT1 or NT2 microcapsules at a content of 7.5% after healing for 7 days at 80 °C.

Based on the microstructure analysis results above, it is clear that the encapsulated sodium silicate agents were successfully released to react with $Ca(OH)_2$ from the cement matrix around the microcapsules, producing C-S-H healing products, which supported the observations of the improved healing performance of oil well cement samples by the addition of T1 and T2 microcapsules as discussed in Section 5.5.

5.7 Effects of microcapsules on oil well cement properties

5.7.1 Rheology of fresh cement slurries

The effects of microcapsule addition on the rheological behaviour of fresh oil well cement slurry were investigated both at 20 °C and 40 °C. Figure 5.24 presents the variation in plastic viscosity and yield stress of oil well cement slurries with increasing added NT1 or NT2 microcapsule contents from 0 to 7.5% at 20 °C. Generally, NT1 (Figure 5.24a) and NT2 (Figure 5.24b) microcapsules showed similar influencing trends on the rheological properties. Between

addition contents from 0 to 5%, the plastic viscosity and yield stress showed an almost linear increase with the increasing microcapsule content. However, a substantial increase was seen in both the plastic viscosity and yield stress when the microcapsule content increased to 7.5%. The plastic viscosity and yield stress of the cement slurries containing NT1 increased by 83% and 61%, respectively, and the plastic viscosity and yield stress of the cement slurries containing NT2 increased by 111% and 72%, respectively. At low microcapsule concentrations, the increase in viscosity was mainly caused by microcapsules filling the spaces between cement particles to reduce the inter-particle distance which is usually much larger than the particle size. When the inter-particle distance reduced to a scale comparable to the microcapsule size, microcapsule particles started to agglomerate and reduce the free volume, thereby significantly increasing the viscosity via a space-crowding effect (Faroughi & Huber 2014).

This explains the significant influence of NT1 and NT2 microcapsules on the viscosity of cement slurries above content of 5%. As the flowability decreased, higher energy was needed to initiate flow of the cement slurries, thus increasing the yield stress. In addition, there was some tiny debris (polyurea shell or sodium silicate core materials) mixed within the powdery T1 and T2 microcapsules as observed in Section 5.2.1. This debris from the sodium silicate core materials could react with cement hydrates $Ca(OH)_2$ and accelerate cement hydration, which might also cause an increase in viscosity and yield stress.

Figure 5.25 compares the plastic viscosity (Figure 5.25a) and yield stress (Figure 5.25b) of oil well cement slurry containing NT1 or NT2 microcapsules at contents of 7.5% at 20 °C and 40 °C. At the higher temperature of 40 °C, cement slurries with T1 or T2 microcapsules showed an increase in both plastic viscosity and yield stress compared to those at 20 °C. Increasing the temperature can accelerate the hydration of the cement, which may lead to an increase in the viscosity and yield stress. Such effects of increasing temperature were more prominent in oil well cement slurry with a low w/c ratio of 0.35 (Shahriar 2011). Therefore, the control cement slurry with a high w/c ratio of 0.44 was barely affected by increasing the temperature from 20 to 40 °C. The addition of microcapsules had already increased the viscosity and yield stress at 20 °C due to the filling effect and crowding effect. When coupled with the effect of temperature,

the microcapsule-containing cement slurries showed further increases in viscosity and yield stress.
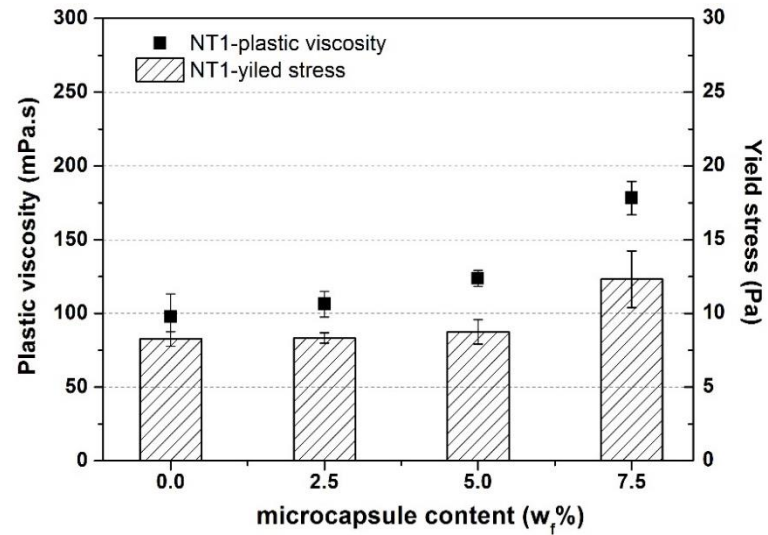
(a)
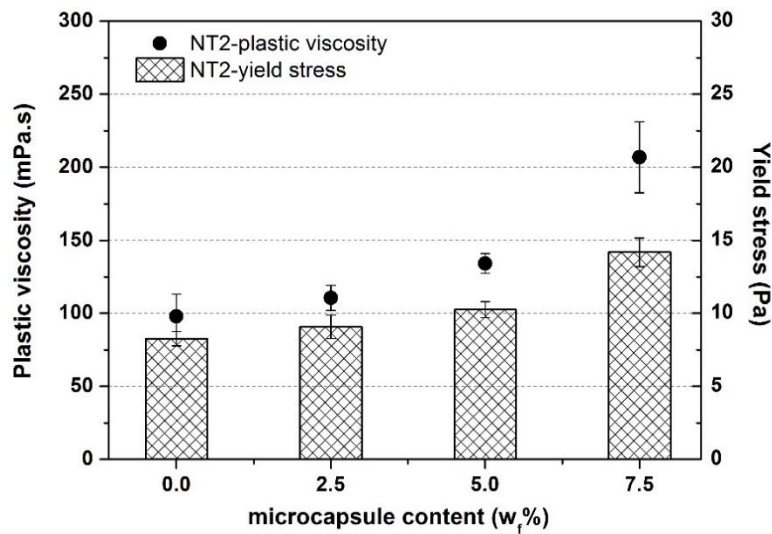
(b)

Figure 5.24 Plastic viscosity and yield stress of oil well cement slurries containing polyurea/sodium silicate microcapsules (a) NT1 and (b) NT2 at varying addition contents from 0 to 7.5% by weight of cement at 20 °C.
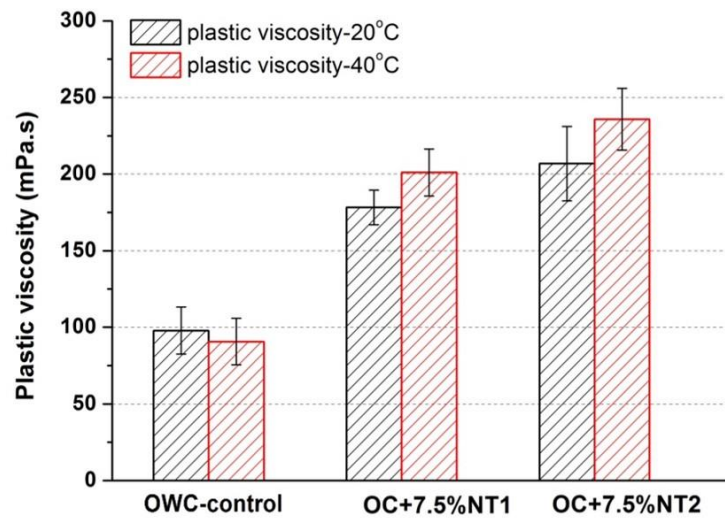
(a)
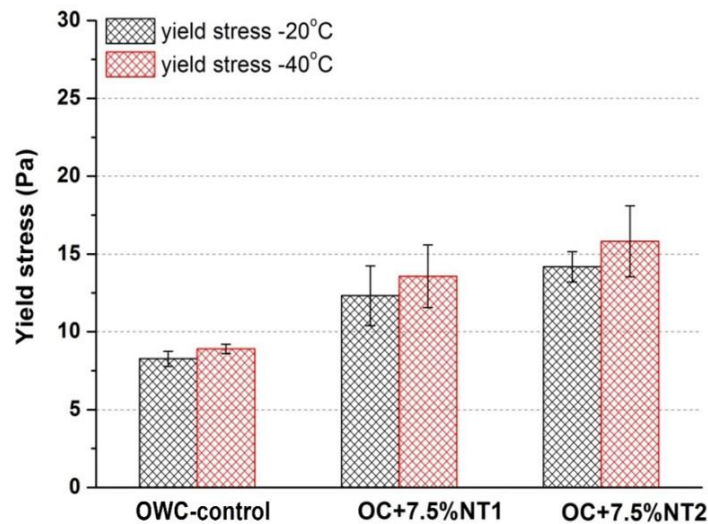
(b)

Figure 5.25 (a) Plastic viscosity and (b) Yield stress of oil well cement slurries containing NT1 or NT2 polyurea/sodium silicate microcapsules at a content of 7.5% by weight of cement at different temperatures of 20 ºC and 40 ºC.

In summary, the addition of NT1 and NT2 microcapsules negatively affected the flow behaviour of oil well cement slurries. They caused a significant increase in the plastic viscosity and yield stress at higher contents above 5%, indicating decreased flowability and pumpability.

At higher temperatures, the microcapsule-containing cement slurries showed further increases in viscosity and yield stress.

5.7.2 Hydration of cement

The effects of adding microcapsules to the hydration of the oil well cement pastes were investigated using an isothermal calorimeter. Figure 5.26 shows the plots for the heat flow (Figure 5.26a) and total heat curves (Figure 5.26b) for oil well cement slurries containing NT1 or NT2 microcapsules at contents of 1.25% and 7.5% tested at 20 ℃. Compared to the control slurries, the addition of both NT1 or NT2 microcapsules at a content of 1.25% slightly shortened the induction period and accelerated the initiation of the second peak on the heat evolution curve, which indicates an acceleration of cement hydration. At a high content of 7.5%, the accelerating effect of microcapsule addition became more significant. The peak values of heat flow and the accumulative heat values were seen to be reduced by the addition of microcapsules. The accelerating effect on cement hydration was also reported by Giannaros et al. (2016) who used a similar type of polyurea/sodium silicate microcapsules. The acceleration of cement hydration was thought to be due to the debris of sodium silicate core materials but not due to breakage of the microcapsules. As mentioned in Section 5.2.1, small debris of sodium silicate core or polyurea shell materials that formed during the emulsion polymerisation process were found in the microcapsule powders. The sodium silicate debris can react with the cement hydration product $Ca(OH)_2$. leading to a decrease in the initial pH of the pore solutions of cement pastes, thus accelerating the cement hydration. The reduction in the peak values of heat flow and accumulative heat can be attributed to water absorption of the debris, including the water consumption by the reaction between sodium silicate and $Ca(OH)_2$. This resulted in less water being available for cement hydration, and then reduction of in the hydration heat release.

At the higher temperature of 40 ℃, the effects of the addition of microcapsules on heat flow curves and total heat curves were similar to those at 20 ℃ (Figure 5.27). The hydration of the cement itself, as well as the reaction between the sodium silicate core debris and $Ca(OH)_2$, were both accelerated at elevated temperature, as reflected by the obviously shortened induction period and intensified peak values of the heat flow curves at 40 ℃.
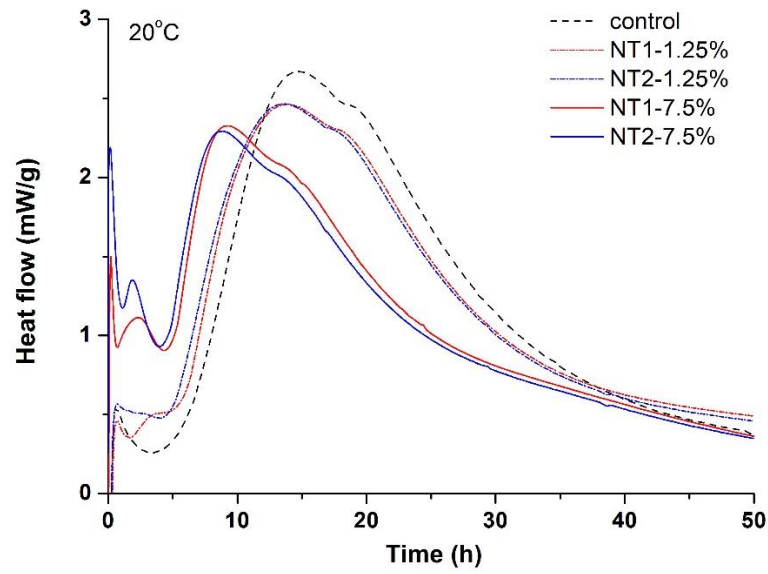
(a)
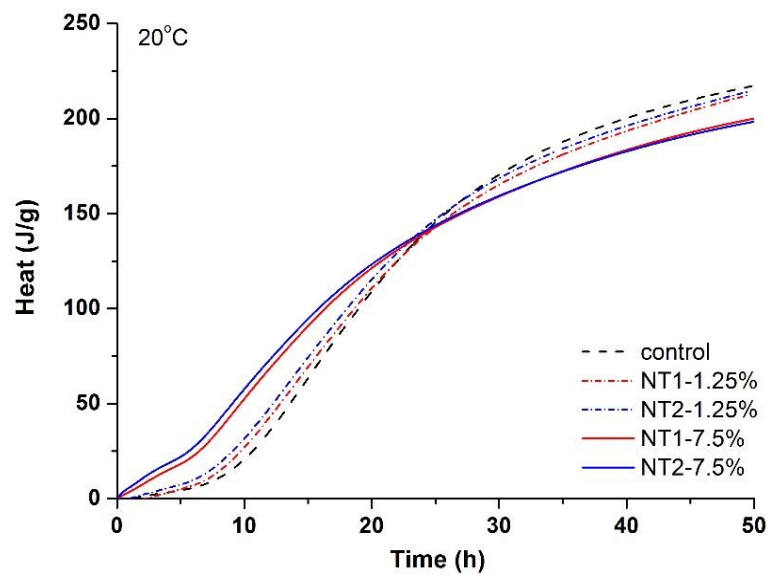
(b)

Figure 5.26 (a) Heat flow and (b) Total heat curves of oil well cement slurries containing NT1 or NT2 polyurea/sodium silicate microcapsules at a content of 1.25% and 7.5% by weight of cement at 20 ^{o}C.

(a)

(b)
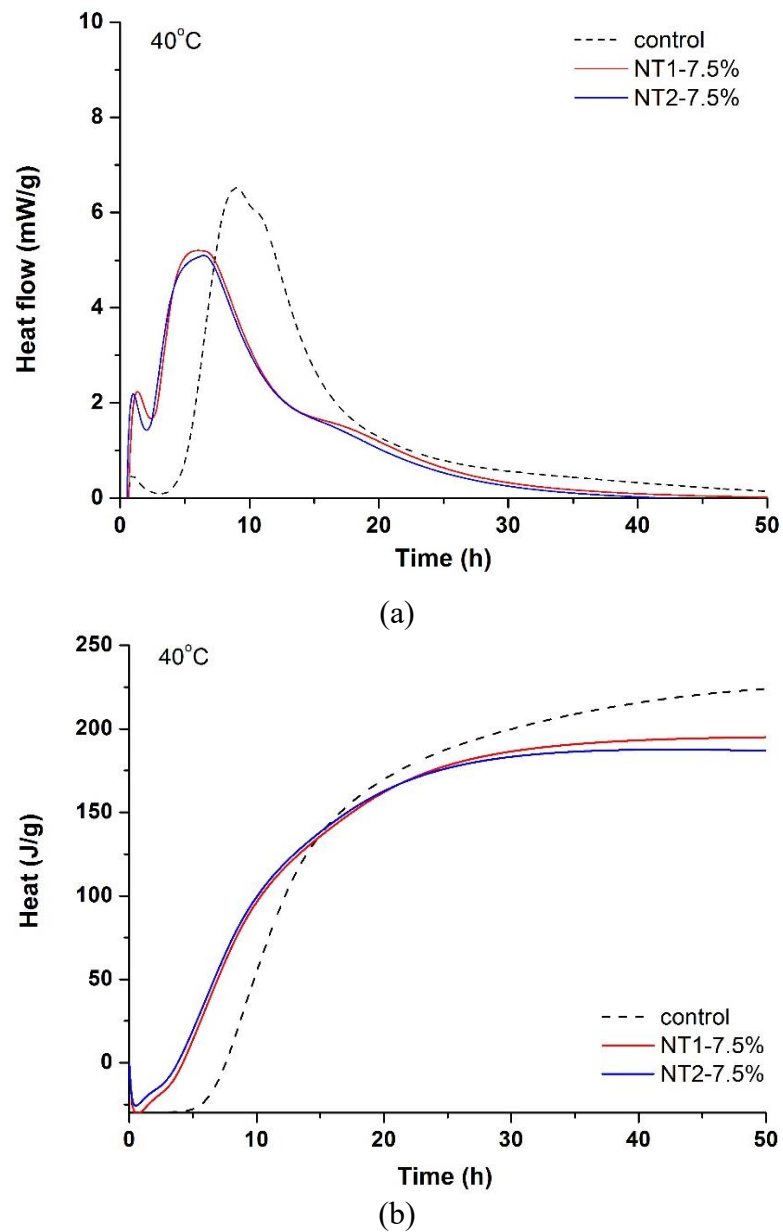
Figure 5.27 (a) Heat flow and (b) Total heat curves of oil well cement slurries containing NT1 or NT2 polyurea/sodium silicate microcapsules at a content of 7.5% by weight of cement at 40 °C.

216

5.7.3 Mechanical properties

The compressive strength of oil well cement pastes containing NT1 or NT2 microcapsules at different contents from 0 to 7.5% was tested at 3 days. The flexural strength values at the age of 3 days were also obtained from prism samples loaded under three-point bending. The peak values at which the prisms were loaded to failure were used for calculation of the flexural strength.

5.7.3.1 Compressive strength

As shown in Figure 5.28, for both types of microcapsules, their addition generally caused a decrease in the compressive strength of oil well cement pastes, which became more significant as the microcapsule content increased. When the addition content increased up to 7.5%, the compressive strength of the cement pastes with NT1 decreased by ~26%, while the strength reduction of cement pastes containing NT2 reached about 40%. The decreasing trends on compressive strength with increasing microcapsule additions agreed with previous research in the literature. Dong et al. (2017) reported that the compressive strength was significantly decreased by about 5% to 25% with an increase in the addition of 2% to 8% (by weight of cement) microcapsules sized between 132~230 μm. Kanellopoulos et al. (2016) also found that when the volume fractions of microcapsules increased to 12% (2.3% by weight of cement) and above, the effect of microcapsule addition became noticeably detrimental, decreasing the compressive strength by 17% to 27%.

The decrease in compressive strength could be attributed to several reasons. First, the cement matrix usually possesses a much higher modulus than the polymeric microcapsules Wang et al. (2013). The microcapsules may become defects in the cement matrix, leading to a decrease in strength. Furthermore, the effects on the compressive strength seem to also depend on the different shell properties of the microcapsules themselves. Comparison between the two groups of microcapsules showed that NT1 caused less compressive strength reduction than NT2 at the same addition content. This may be mainly because T1 group microcapsules have rigid shells which are stronger than T2 group microcapsules with rubbery shells, thus having a less negative effect on the strength of the cement matrix. In addition, the increased viscosity of cement

217

slurries with larger amounts of microcapsules may also lead to a less compacted cement matrix, thus decreasing its strength.
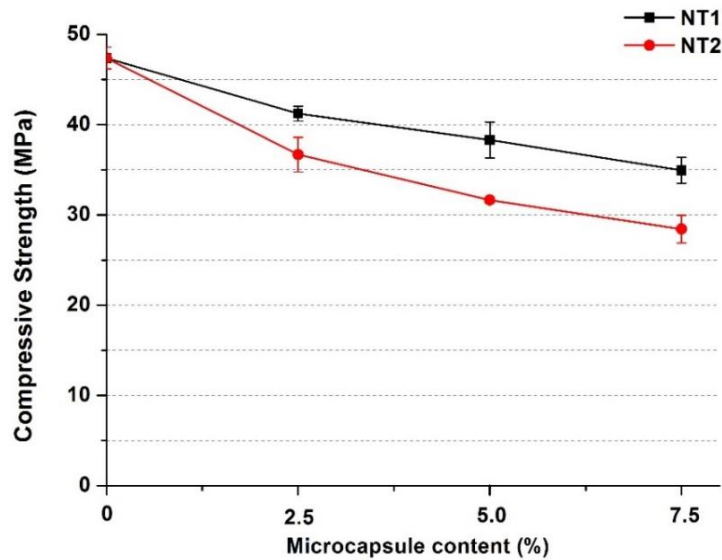
Figure 5.28 Compressive strength of oil well cement pastes containing a varying content of NT1 or NT2 microcapsules (0–7.5%) after 3 days curing at 80 ℃.
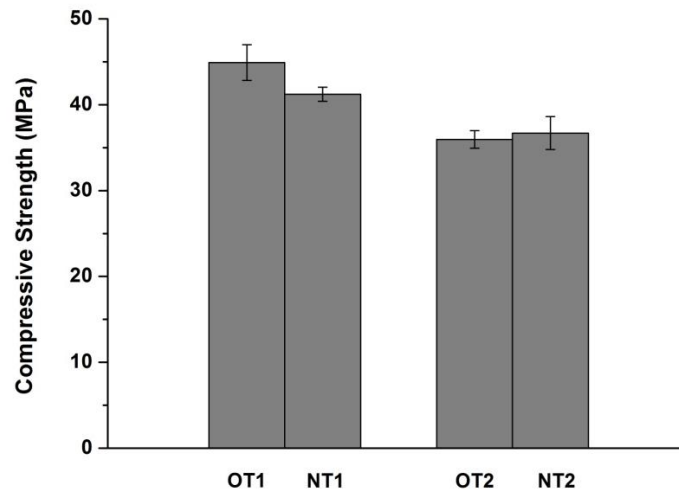
Figure 5.29 Compressive strength of oil well cement pastes containing 2.5% microcapsules of the old batch (OT1, OT2) compared to the new batch (NT1 and NT2).

The effects of microcapsules of the old batch (OT1 and OT2) on the compressive strength of cement pastes were also tested and compared to the new batch, as shown in Figure 5.29. At the same content of 2.5%, cement pastes with OT1 were noted to have higher compressive strength than those with NT1, while the strength of samples with OT2 was similar to those with NT2.

As suggested by the TG results in Section 5.2, the shell materials of NT1 might incorporate some soft segments, which possibly led to a decrease in the rigidity of the shell. The larger sized microcapsules were also reported to cause a greater reduction in the compressive strength (Dong et al. 2017). OT1 microcapsules have a larger average size (~180 μm) than the other three (~90 to 110 μm) groups of microcapsules, but caused the least strength reduction. This again could be ascribed to the higher rigidity of its shell walls.

5.7.3.2 Flexural strength

Figure 5.30 shows the flexural strength of the oil well cement pastes containing NT1 or NT2 microcapsules at different contents from 0 to 7.5%. Similar to the compressive strength, the flexural strength of all the cement samples showed a decreasing trend with increasing microcapsule content. At a microcapsule content of 2.5%, the flexural strength of the cement samples with NT1 and NT2 decreased by ~17% and ~19%, respectively. When the content of microcapsules increased to 7.5%, the flexural strength reduction increased to ~25% and ~32%, respectively. Wang et al. (2013) also reported significant reduction in the flexural strength of mortar samples when adding similar-sized organic microcapsules with UF shells (average size of 166 μm) at contents above 3% by weight of cement. The author concluded that the flexural strength reduction could be mainly attributed to the weaker interface strength of the organic microcapsules compared to the original strength of the matrix. However, Kanellopoulos et al. (2016) observed a general increase in the flexural strength of mortar samples containing microcapsules with gelatine/gum acacia shells. They attributed the improvements in flexural strength to good adhesion of the gelatine/gum acacia shell with the cementitious matrix. The hydrophilic nature of the shell allowed cement hydration products to form directly on the shell, inducing effective chemical bonding with the matrix. Obviously, the interfacial bonding of the microcapsules strongly influenced the flexural strength and the bonding was inherently affected by the shell nature. The UF shell of the microcapsules used by Wang et al. (2013) and the polyurea shell of the microcapsules used in this study are hydrophobic materials. As mentioned above in Section 5.2.6, the interfacial bonding between the polyurea shell and cement matrix mainly depends on physical adhesion with a lack of chemical adhesion due to its hydrophobic nature, leading to the lower flexural strength the of cement pastes under loading. Additionally,

the cement samples with NT1 generally have higher flexural strength than those with NT2, which was consistent with their compressive strength. The shell of NT1 is more rigid than those of NT2. More stresses are needed to crack the NT1 microcapsules under loading, thus achieving a higher flexural strength.
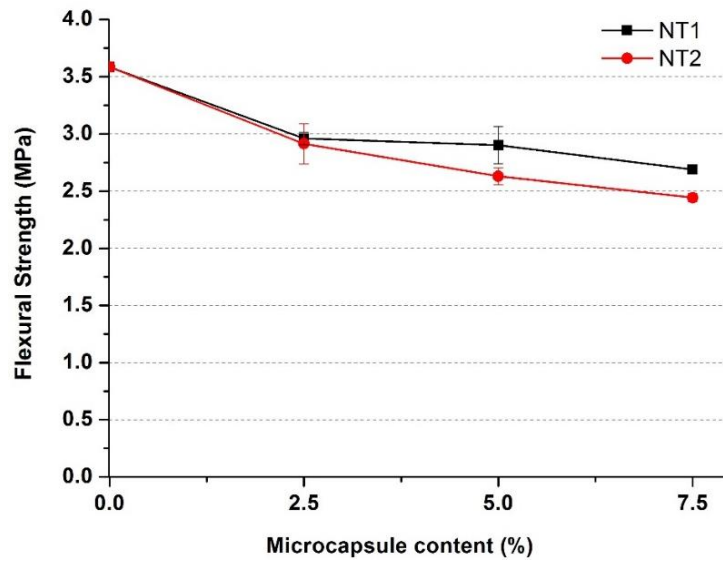
Figure 5.30 Flexural strength of oil well cement pastes containing varying contents of NT1 or NT2 microcapsules (0–7.5%) after 3 days of curing at 80 ℃.

5.8 Oil well cement combining reactive MgO and sodium silicate microcapsules

5.8.1 Introduction

In this section, a combined oil well cement system is proposed that incorporates both reactive MgO and sodium silicate microcapsules. First, suitably reactive MgO and microcapsules were selected based on the previous testing results. The expansion performance of the three types of reactive MgO and their effectiveness in shrinkage reduction in oil well cement were examined in Chapter 4. The results showed that MgO MAG-R with medium reactivity and MgO 92/200 with low reactivity had superior expansion performance and effectiveness in shrinkage reduction to MgO N50 with high reactivity under 80 ℃. The former two MgOs with lower reactivity had much less influence on the hydration process, as well as on the rheology properties of the oil well cement pastes. However, MgO-92/200 was found to have significant

negative effects on the compressive strength of the oil well cement. The influence of its large expansion on the stability of the microcapsules in the combined system is also another concern. Excessive expansion stresses may cause damage to the microcapsules. Therefore, MAG-R which had a positive effect on the cement strength and relatively smaller expansion was selected for the combined system.

According to the results in the above Section 5.5 and 5.7, the T1 and T2 groups of microcapsules generally showed similar self-healing efficiency in tightness recovery and strength recovery. Their different shell properties mainly influenced the strength of the oil well cement pastes. The addition of the T2 microcapsules with rubbery shells caused greater strength reduction than the T1 microcapsules with rigid shells. In view of this, T1 microcapsules were selected for the combined system.

Following the results obtained from the individual expansive and self-healing systems, RM2 and NT1 were added at contents of 8% and 5% (by weight of cement), respectively. The expansion behaviour and the self-healing performance of the combined oil well cement system containing RM2 and NT1 at 80 ºC were investigated and compared to the single systems with only MgO or microcapsules. Meanwhile, the coupled effects of reactive MgO and microcapsules on the rheology properties and the mechanical strength of the oil well cement pastes were also examined. The mix composition of the combined system is given in Table 5.4. The testing programmes and curing conditions of the combined mixes are consistent within the individual systems.

Table 5.4 Mix composition of oil well cement pastes containing reactive MgO and sodium silicate microcapsules.

Mix	MgO-RM2 (%)	Microcapsule-NT1 (%)	Temperature (ºC)	w/c ratio
RM2+NT1	8	5	80	0.44

5.8.2 Effects of combined additives on oil well cement properties

5.8.2.1 Rheology of fresh cement slurries

Figure 5.31 compares the effects of the combined additives with the effects of only MgO or microcapsules on the plastic viscosity (Figure 5.31a) and yield stress (Figure 5.31b) of fresh oil well cement slurry at 20 ℃ and 40 ℃. As reported before, MgO RM2 with medium reactivity had an indistinct influence on the rheological behaviour of cement slurry at 20 ℃. But the addition of microcapsules was found to significantly decrease the flowability of cement slurries at a higher addition content of microcapsules (>5%), due to the agglomeration of large quantities of microcapsules. The separate additions of MgO RM2 at a content of 8% or microcapsules NT1 at a content of 5% appeared to produce insignificant changes to the flow behaviour of oil well cement slurries at 20 ℃, as shown in Figure 5.31. Compared to the control sample, MgO RM2 (8%) alone increased the plastic viscosity and yield stress by ~38% and ~17% and the microcapsule NT1 (5%) alone increased the plastic viscosity and yield stress by ~17% and ~6% at 20 ℃. However, under the coupled effects of MgO and microcapsules, the combined addition of these two additives caused a distinct increase in the plastic viscosity and yield stress by more than 100%. Apparently, the addition large amount of MgO aggravated the agglomeration of microcapsules, thus decreased flowability. At the higher temperature of 40 ℃, the hydration of the cement and MgO were both accelerated, leading to a more substantial increase in the plastic viscosity and yield stress.
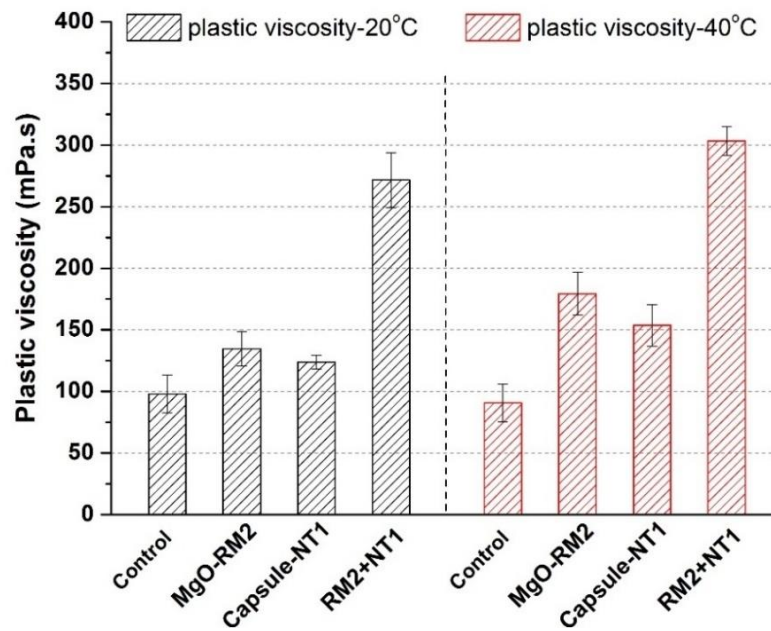
(a)
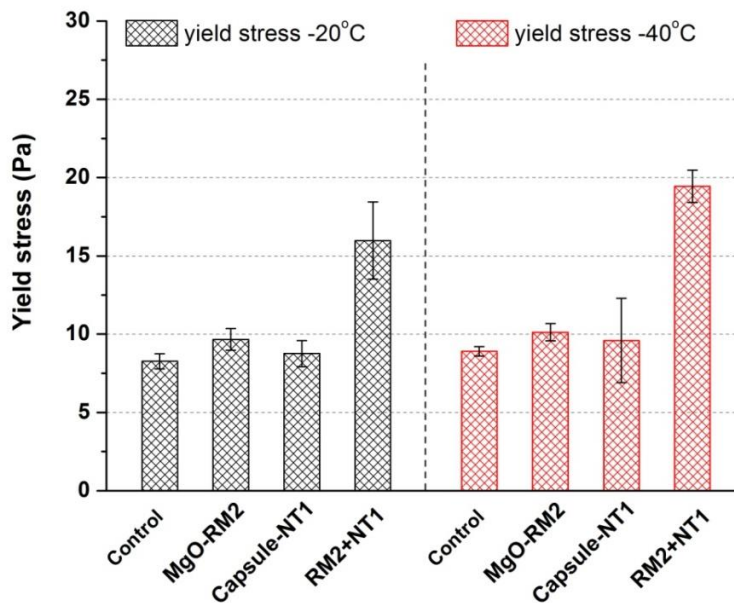
(b)

Figure 5.31(a) Plastic viscosity and (b) Yield stress of oil well cement slurries with the combined addition of MgO RM2 at a content of 8% (by weight of cement) and NT1 microcapsule at a content of 5% (by weight of cement), or the individual addition of MgO and microcapsules at 20 ºC and 40 ºC.

5.8.2.2 Compressive strength and flexural strength

The combined effects of reactive MgO RM2 and NT1 microcapsules on the strength of the oil well cement pastes were also investigated. The compressive strength was tested under three-dimensional restrained condition. As shown in Figure 5.32, the compressive strength of the oil well cement samples after 3 days with the addition of 8% MgO RM2 alone was increased by ~32% compared to the control sample, while that of the samples with only 5% NT1 microcapsules added was decreased by ~19%. As analysed in Section 4.5.3 and Section 5.7.3, the restrained expansion of MgO was beneficial to densifying the pore structure of the cement matrix, thus improving the cement strength. The dense microstructure of the hydration products of RM2 was also considered to be advantageous in improving the cement strength. By contrast, the microcapsules, which usually possess a lower modulus than the cement matrix, thus leading to a decrease in cement strength. The incorporation of microcapsules was also likely to increase the porosity of the cement matrix which adversely affects the strength. By combining both additives, the positive effects of the MgO RM2 on strength could compensate for the negative effect on the strength caused by addition of NT1 microcapsules. As a result, the oil well cement samples that combined both additives showed no strength reduction, but even slightly higher compressive strength than that of the control sample. Similarly, the cement samples containing both MgO RM2 and NT1 microcapsules had higher flexural strength than those samples with individual addition of the microcapsules, as shown in Figure 5.33. The addition of MgO contributed to compensating for the reduction in flexural strength caused by the addition of microcapsules.
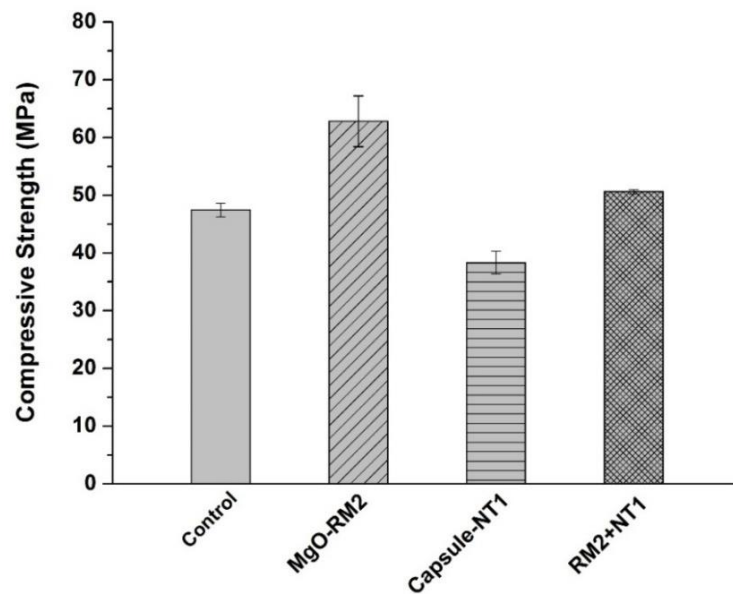
Figure 5.32 Compressive strength of oil well cement slurries containing both MgO RM2 at a content of 8% (by weight of cement) and NT1 microcapsules at a content of 5% (by weight of cement) compared to cement slurries containing only RM2 or NT1 after 3 days of curing at 80 °C.
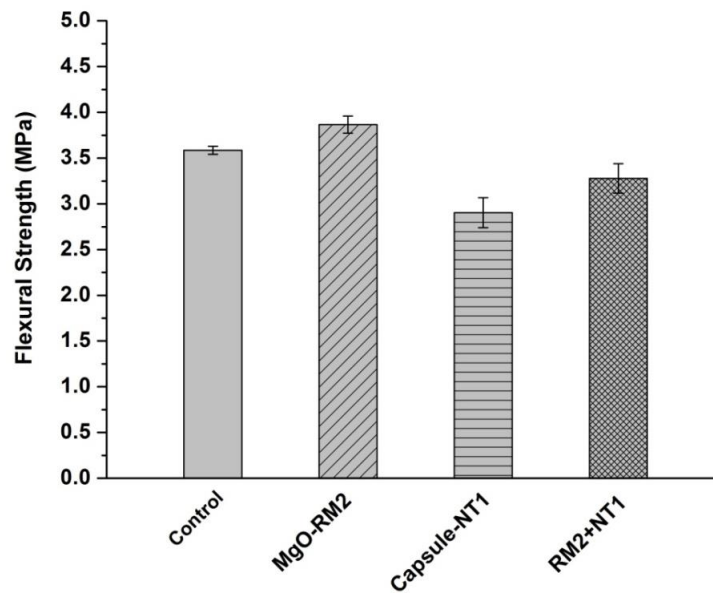
Figure 5.33 Flexural strength of oil well cement slurries containing both MgO RM2 at a content of 8% (by weight of cement) and NT1 microcapsules at a content of 5% (by weight of cement) compared to cement slurries containing only RM2 or NT1 after 3 days of curing at 80 °C.

5.8.3 Expansion performance of the combined oil well cement system

In the combined oil well cement system, the reactive MgO is the expansive component used for generating expansion while the sodium silicate microcapsules are the self-healing component used for inducing autonomic healing. As mentioned in Section 5.2, the microcapsules retained good stability in the cement matrix before being triggered for healing. Their presence in the cement matrix is unlikely to affect the hydration of MgO. Figure 5.34 presents the expansion curves of the oil well cement samples containing MgO RM2 or NT1 microcapsules, or both additives together, cured at 80 °C. It was seen that the cement samples containing the combined additives had similar expansion trends to the samples containing only MgO RM2. The cement samples with the sole addition of NT1 microcapsules showed almost no expansion, just as the control samples did. This indicated that the combined use of NT1 microcapsules with MgO RM2 did not affect the expansion properties of MgO. Accordingly, it can be inferred that the shrinkage reduction performance of MgO RM2 in the cement samples with combined additives should remain consistent with the samples containing only RM2, as reported in Section 4.4.
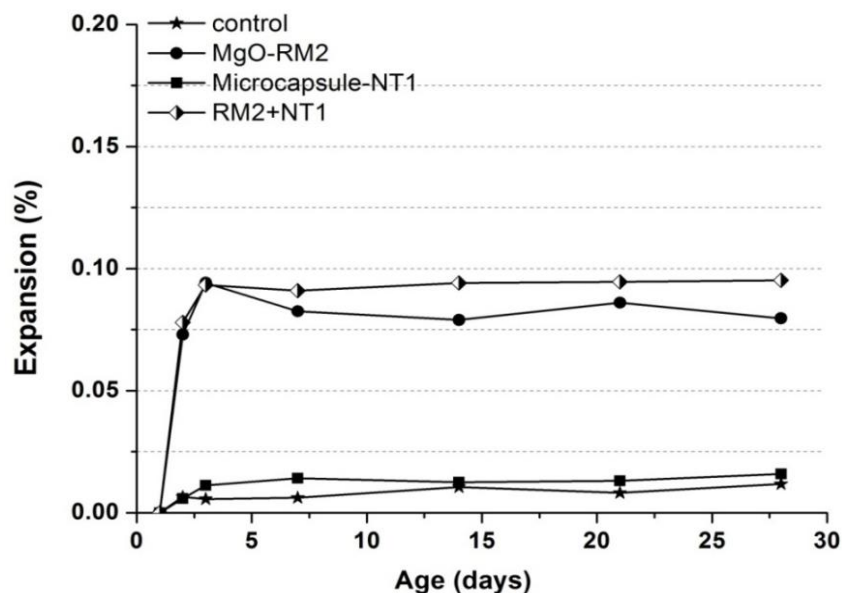
Figure 5.34 Expansion curves of the oil well cement pastes containing different additives (only RM2 at a content of 8%, only NT1 at a content of 5%, or both RM2 and NT1) cured in water at 80 °C over a period of 28 days.

5.8.4 Self-healing performance of the combined oil well cement system

5.8.4.1 Microscopic observations

<table>
<tr><td>(a)</td><td>(b)</td></tr>
</table>
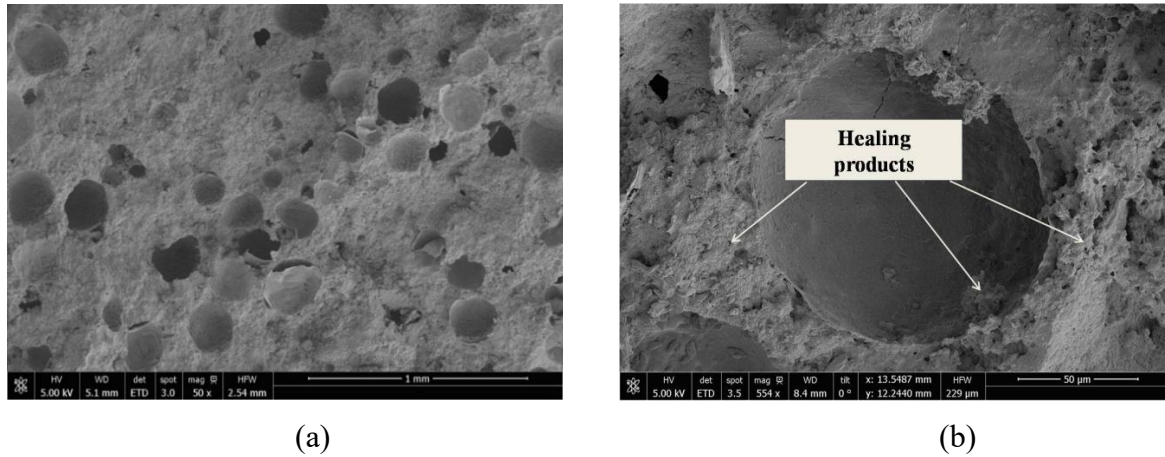
Figure 5.35 SEM images of ruptured NT1 microcapsules embedded into the cracking surface of oil well cement prisms containing both MgO-RM2 and NT1 microcapsules.

Figure 5.35 presents SEM images of small pieces extracted from the cracking surface of oil well cement prisms containing both MgO-RM2 and NT1 microcapsules which were re-cracked under three-point bending after healing. An overview of the cracking surface is shown in Figure 5.35a. The residual hemispheric shells of the ruptured microcapsules are seen to be well embedded in the cement matrix. It seems that the microcapsules were not influenced by the expansion induced by RM2 in the surrounding cement matrix. Most of them should remain stable in the matrix before being triggered for healing, as in the individual self-healing cement system with only the microcapsules. It was also noted that there are slight agglomerations between the microcapsules in the combined cement pastes. As reported in Section 5.8.2, the combined addition of RM2 and NT1 caused a distinct reduction in the flowability of the oil well cement slurries, leading to insufficient dispersion of the microcapsules. Taking closer look at those ruptured microcapsules (Figure 5.35b), it seemed that the core materials were successfully released. The clusters of fibrous products, which were identified as mainly C-S-H healing products in Section 5.6.1, were observed both inside and around the residual NT1 microcapsule.

5.8.4.2 Crack width and crack depth

Typical microscope images of the cracks in oil well cement samples containing different additives (only RM2, or NT1, or combined additives) before and after healing are shown inFigure 5.36. The results of the crack width healing efficiency based on the microscopic observations are presented in Figure 5.37. It was seen that the samples with MgO RM2 alone showed similar healing degree of the crack width as the control samples, which was only around ~8%. No obvious cracking healing was observed in either of the two groups of cracked samples. In the literature, the expansive additive MgO was reported to be capable of improving the autogenous healing of cementitious materials by its continuous hydration to produce the expansion product $Mg(OH)_2$ which could seal the cracks. Qureshi (Qureshi 2016) used reactive MgO and obtained significant improvements in the sealing of drying shrinkage cracks after curing for 14 days at 20 $^{\circ}$C. However, the MgO RM2 used in this study had fast hydration which mainly occurred within the early age of 3 days at the high temperature of 80 $^{\circ}$C, according to the results in Section 4.3. As a result, there was little unhydrated MgO remaining in the cracked cement samples to produce $Mg(OH)_2$ healing products by continuous hydration. By contrast, the cement samples with the combined addition of RM2 and NT1 showed improved crack width healing of ~25% which was comparable to that of the cement samples with NT1 alone.

Similar trends were also observed in the crack depth reduction of the cement samples after healing. As shown in Figure 5.38, the post-healing samples with only MgO RM2 showed almost no reduction of crack depth compared to the control samples without any additives, while cement samples with both RM2 and NT1, as well as the ones with only NT1 microcapsules, obtained increased crack depth reduction after healing.
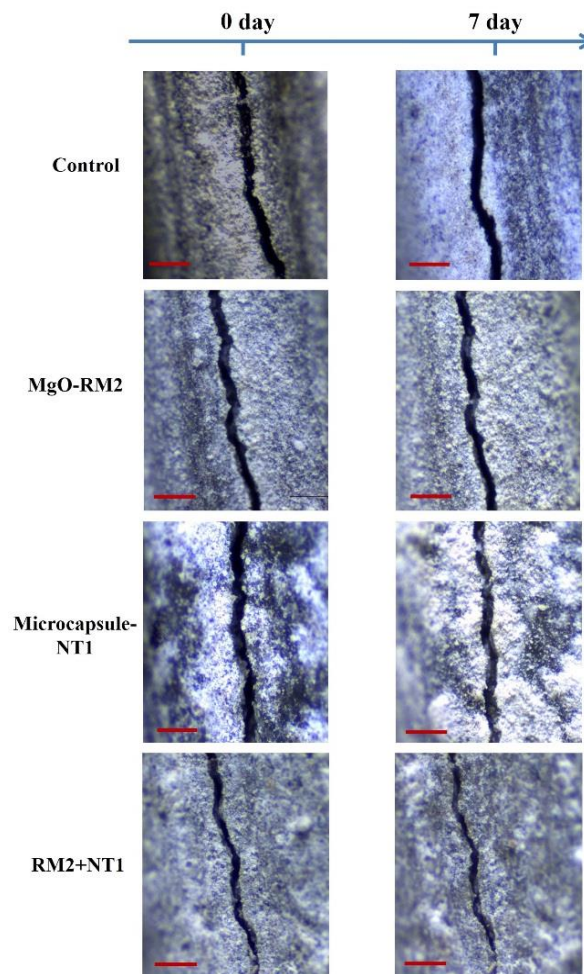
Figure 5.36 Microscopic images of the cracks in oil well cement prisms containing different additives (only RM2 at a content of 8%, or only NT1 microcapsules at a content of 5%, or both RM2 and NT1) before and after healing of 7 days at 80 ℃.
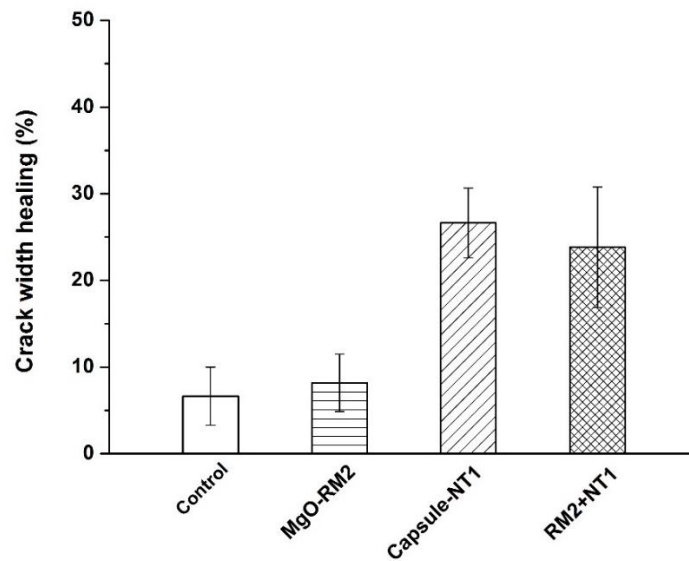
Figure 5.37 Crack width healing efficiency of the oil well cement prisms containing different additives (only RM2 at a content of 8%, or only NT1 microcapsules at a content of 5%, or both RM2 and NT1) after healing of 7 days at 80 °C.
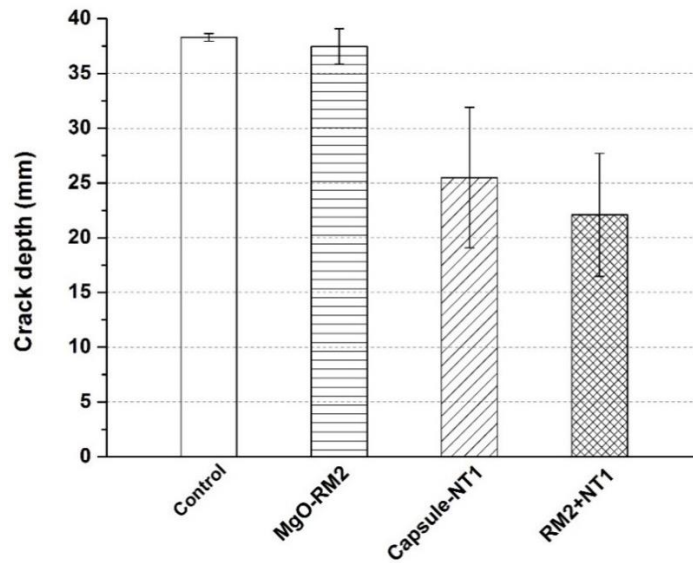
Figure 5.38 Ultrasonic crack depth measurements of the oil well cement prisms containing different additives (only RM2 at a content of 8%, or NT1 microcapsules at a content of 5%, or both RM2 and NT1) after healing of 7 days at 80 °C.

5.8.4.3 Recovery in gas and water tightness

The results of the gas permeability tests on the cracked oil well cement disks containing different additives after healing are compared in Figure 5.39. It was seen that the samples with

the individual addition of MgO RM2 showed almost no improvement in the recovery of gas tightness compared to the control samples. By contrast, the other two group cement samples with microcapsule additions (only NT1, and both NT1 and RM2) showed a significant reduction in the gas permeability after healing. The apparent recovery in gas tightness was mainly attributed to the self-healing reactions by the sodium silicate microcapsules, while MgO RM2 showed little healing effectiveness. This was consistent with the results of the crack width and crack depth measurements. Similarly, the water sorptivity coefficients of the post-healing cement samples with microcapsule addition (only NT1, and both NT1 and RM2) were significantly reduced compared to those of the control samples, as shown in Figure 5.40, suggesting an improvement in the recovery of water tightness achieved by the microcapsules. The post-healing samples with only MgO RM2 showed little improvement in the recovery of water tightness, as reflected in its high sorptivity coefficient compared to that of the control samples.
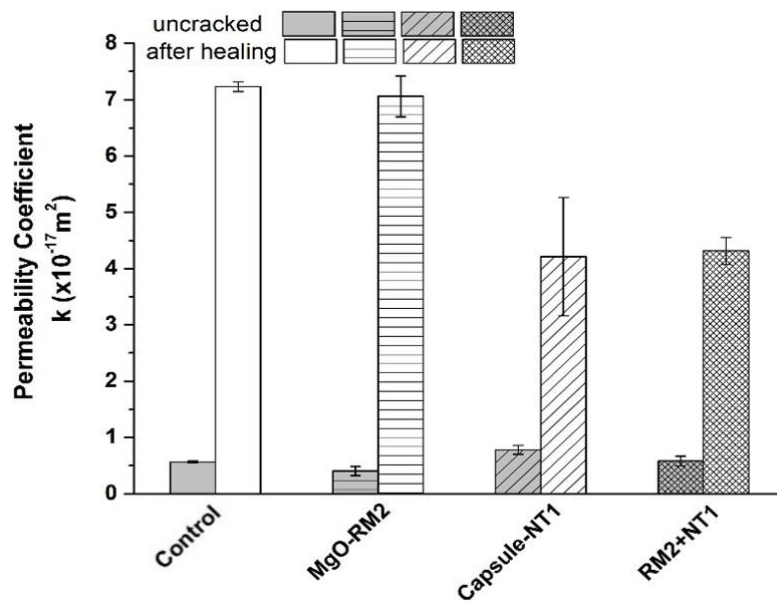
Figure 5.39 Gas permeability of the cracked oil well cement disc samples containing different additives (only RM2 at a content of 8%, or NT1 microcapsules at a content of 5%, or both RM2 and NT1) after healing of 7 days at 80 °C.
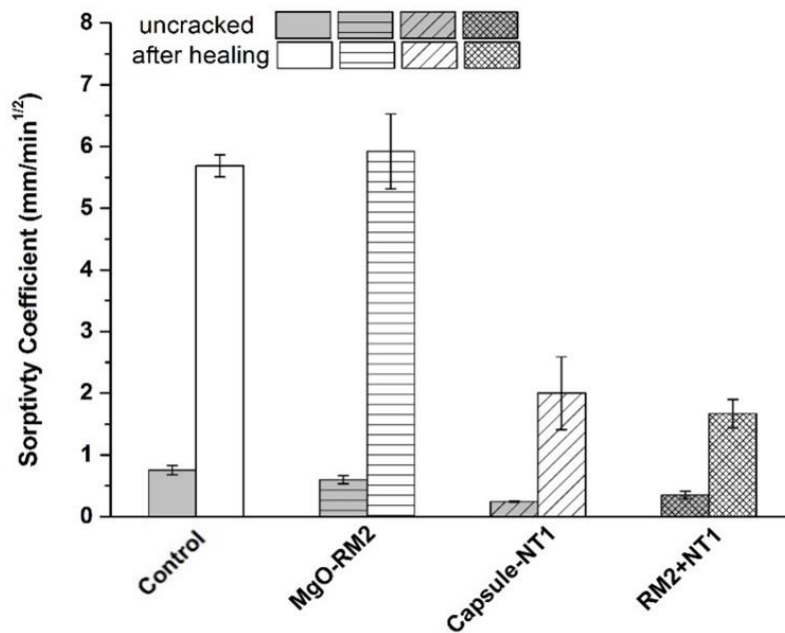
Figure 5.40 Water sorptivity coefficients of the cracked oil well cement prisms containing different additives (only RM2 at a content of 8%, or NT1 microcapsules at a content of 5%, or both RM2 and NT1) after healing of 7 days at 80 °C.

5.8.4.4 Recovery in flexural strength

According to the results on the visualisation of crack closure and self-healing recovery in gas and water tightness, there was a general trend that the healing performance of the cement samples with combined additives remained consistent with those containing only microcapsules, and the self-healing effectiveness of the NT1 microcapsules was largely unaffected by the combined addition of MgO RM2. Such a trend was also found in the results of self-healing recovery in flexural strength as shown in Figure 5.41. As tested in Section 5.5.3, the post-healing cement samples containing 5% NT1 microcapsules had higher flexural strength recovery (~16%) than did the control samples (~2%). The combined cement samples tested in this section also obtained an improved flexural strength recovery of ~14% in contrast with the MgO-only (RM2) samples and the control samples, which showed poor healing.
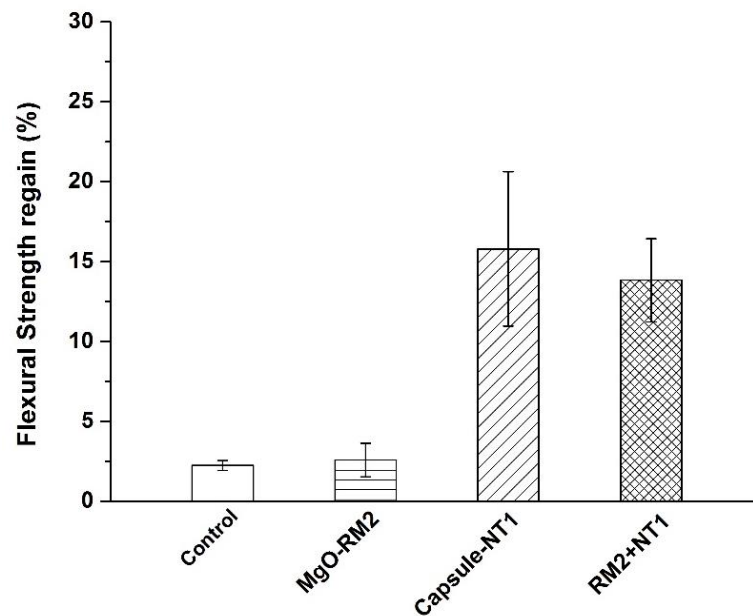
Figure 5.41 Flexural strength recovery of the cracked oil well cement prisms containing different additives (only RM2 at a content of 8%, or NT1 microcapsules at a content of 5%, or both RM2 and NT1) after healing of 7 days at 80 °C.

Based on the above results, it was clear that self-healing in the cement samples with combined additives at 80 °C still mainly depended on the autonomic healing reactions by encapsulated sodium silicate agents. The MgO RM2 was mostly consumed for generating expansion within the early age of 3 days before cracking, and thus there was very limited involvement any unhydrated MgO in the later self-healing reactions after cracking. To a large extent, the expansion by MgO RM2 and the self-healing by NT1 microcapsules worked independently of one other in the combined oil well cement system designed in this section. MgO RM2 is responsible for the expansion at an early age, while the sodium silicate NT1 microcapsules target the healing of cracks generated at a later age.

5.9 Summary

5.9.1 Self-healing system with sodium silicate microcapsules

This system investigated two groups of polyurea/sodium silicate microcapsules, which were first characterised in terms of their important properties such as thermal stability, alkalinity resistance, and survivability during mixing and were then investigated on their effects on the self-healing properties, as well as the fresh and hardened properties, of oil well cement. The T1 and T2 groups of polyurea microcapsules showed good thermal stability up to ~150 $^{\circ}$C and even higher resistance to high alkalinity. Despite having different shell rigidities, the T1 microcapsules with rigid shells and T2 microcapsules with rubbery shells were both strong enough to survive the mixing process. The characterisation results verified their suitability for use in oil well cements under high temperature wellbore conditions at 80 $^{\circ}$C.

Based on the self-healing efficiency by measuring the crack width and crack depth, gas permeability, water sorptivity, flexural strength and microstructural analysis, it was evident that the addition of microcapsules improved the healing performance of oil well cement pastes. Under high temperature curing conditions at 80 $^{\circ}$C, oil well cement itself possesses very limited healing capabilities. Because most of the cement hydrates within the early age of 3 days, there is little unhydrated cement left for continuous hydration in autogenous crack healing. With the addition of microcapsules, the sodium silicate agent was released to react with the hydrated cement matrix to produce calcium silicate hydrates (C-S-H) which helped seal and bind the cracks. This healing reaction was verified by microstructural analysis (SEM & EDX, XRD, TGA), showing a clear consumption of portlandite and the formation of C-S-H healing products. Correspondingly, significantly improved macro self-healing performance was observed in the microcapsule-containing oil well cement specimens after healing. The healing efficiency generally increased with increasing microcapsule content (0–7.5% by weight of cement), as more healing agents were provided for healing.

The microcapsules were found to have negative influences on the fresh and hardened properties of oil well cement, especially at high addition contents. The addition at a content above 5% was found to significantly reduce the flowability of oil well cement slurries. The compressive

strength and flexural strength also decreased with increasing microcapsule contents. Based on the overall consideration of the effects of microcapsules on the oil well cement properties, a content of ~5% seemed to be a suitable dosage for addition.

The T1 and T2 groups of microcapsules that were tested generally showed comparable self-healing efficiency. The different shell properties of T1 and T2 mainly influenced the strength of the oil well cement pastes. The addition of T2 microcapsules with rubbery shells caused more reduction in strength than did the T1 microcapsules with rigid shells. In view of this, T1 is more favourable for use in the combined system.

5.9.2 Combined oil well cement system

The reactive MgO MAG-R with medium reactivity (RM2) and NT1 microcapsules were selected for combined use in one oil well cement system. The combined oil well cement system showed similar expansion performance and self-healing efficiency compared to the individual expansive system with only MgO RM2, and the individual self-healing system with only microcapsules. It seemed that the expansion by MgO RM2 and the self-healing by NT1 microcapsules work independently from each other in the combined oil well cement system. Hydration and expansion of the reactive MgO RM2 occurred within the early age of 3 days, before cracking took place. Therefore, there was little unhydrated MgO remaining in the cracking area for the enhancement of autogenous healing. As a result, the self-healing process in the combined system was still mainly driven by the microcapsules. The effect of MgO expansion on the stability of microcapsules should be taken into consideration in the combined use of these two additives. In this study, the addition of RM2 at 8% showed no significant effects on the stability of the microcapsules.

The combined use of MgO RM2 with NT1 microcapsules was found to be advantageous over the individual system with only microcapsules in terms of the effects on the mechanical properties of the cement pastes. MgO RM2 had the positive effect of improving the cement strength. The addition of RM2 contributed by compensating for the strength reduction caused by NT1 microcapsules.

Chapter 6 Conclusions and recommendations for future work

Oil well cement sheath plays an important role in providing well integrity and ensuring safe well operation. However, the unfavourable shrinkage and cracking problems of oil well cement pose great risks to well integrity. This has motivated research towards the development of oil well cement materials with enhanced properties. In particular, oil well cement with reduced shrinkage and micro-cracks that can provide better well integrity under the extreme downhole environment has attracted much attention. This study has focused on improving the performance of oil well cement by using reactive MgO for shrinkage reduction and self-healing microcapsules for crack repair. This chapter summarizes the conclusions that can be drawn from the current research work, and puts forwards suggestions for future research.

6.1 Conclusions

The conclusions are presented following the order of the thesis chapters.

6.1.1 Literature review

Well cementing is a critical operation in forming annular cement protective layers between the steel casings and formations, as introduced in detail in **Chapter 2**. The annular cement sheath delivers zonal isolation, provides formation stability, and protects the casing from corrosion. Improper well cementing job and cement sheath instability may severely compromise the well integrity, leading to fluid (oil/gas) migration. In particular, the bulk shrinkage and cracks in the oil well cement that occur after cement setting are identified as main causes for well integrity problems in the long term over the lifetime of the wellbore (J. Liu 2012; Shadravan et al. 2014). The microannulus between the cement and the formation/casing induced by cement shrinkage, as well as the propagation of cracks within the cement sheath, can create pathways for fluid migration, resulting in a loss of well integrity.

Expansive additives are a commonly used method for reducing cement shrinkage in oil fields. Traditional expansive additives such as ettringite-based, CaO-based, and MgO-based additives produce expansion based on the internal pressure exerted upon crystallization of the reaction products. Ettringite-based additives have limited applications in oil well cement, however, due

to their instability at elevated temperatures above 70 ^{o}C (Bentz 2009; Nelson 2006). CaO-based additives have the problem of too fast a hydration rate at the early age, and the high solubility of Ca(OH)$_2$. By contrast, MgO-based additives outstand for the good thermal stability of its hydration product Mg(OH)$_2$ (up to 332 ^{o}C) (Marbun 2012). This enables its use in high-temperature downhole conditions. MgO also offers the benefits of lower water demand for hydration, which allows it to be used in low moisture conditions. More importantly, MgO has the unique feature to provide designable expansion rate and magnitude, which enables the delivering of desirable expansion under different downhole conditions. The expansion performance of MgO intrinsically depends on its hydration reactivity and microstructure, which can be adjusted by controlling the production conditions (material source, calcination temperature, and residence time) (Mo et al. 2010; Mo et al. 2012). MgO with high reactivity has fast hydration and high expansion at an early age. MgO with low reactivity exhibits "delayed" expansion properties with a low hydration rate, and shows less expansion during the induction period at an early age but accelerated hydration and much larger expansion at a later age. The expansion performance of MgO is also strongly influenced by curing temperature. The hydration and expansion can be accelerated by increasing the curing temperature. MgO with different reactivities can be used to accommodate the application at different temperature ranges. Based on these properties, MgO exhibits great potential for shrinkage reduction under various conditions and curing stages (autogenous, drying, and thermal). Therefore, MgO is considered to be a suitable expansive additive for use in oil well cement.

The MgO additives currently used in oil well cement are mostly hard-burnt or dead-burnt ones with low reactivity. At ambient temperature, hard-burnt and dead-burnt MgOs usually hydrate too slowly to produce effective expansion at an early age due their low reactivity and low SSA. High temperature is known to have a significant accelerating effect on MgO expansion, especially for low reactivity MgO. Therefore, the hard-burnt and dead-burnt MgOs are suitable for use in high temperature wellbore conditions. Previous studies showed that, those low reactive MgOs were more effective at high temperatures >90 ^{o}C, and their main applicable range is high temperature wellbores (>150 ^{o}C). But at a lower temperature range, the low reactive MgOs, especially dead-burnt MgOs, cannot produce effective expansion at an early

age due to the slower hydration rate as temperature decreases. Moreover, their delayed expansion behavior at the later age can become prominent at lower temperatures, which may cause unwanted damage to the structure of the cement and the formation. As a result, the use of MgO is limited under low-temperature borehole conditions. To extend the usable range of MgO in oil fields, researchers turned to reactive grade MgO. Reactive MgOs usually possess higher reactivity and hydrate much more rapidly than the hard-burned or dead-burned MgOs when cured at normal temperatures. In view of this, reactive MgOs provide great potential for producing more effective expansion under low-temperature downhole conditions. However, the reactivity and hydration properties of the reactive grade MgO samples vary significantly depending on their origin and calcination temperatures. There are very few reports on the effect of different reactive MgOs on the expansion properties of oil well cement, as well as on their shrinkage reduction performance under lower temperature conditions.

The traditional solution to cracking damages of the oil well cement sheath is remedial cementing by injecting cement slurry into cracking locations, which is usually untimely and ineffective. In recent years, self-healing technologies for damage management in cement and concrete structures have drawn extensive attention. Self-healing cementitious materials have the capability to repair structural damage autonomously or with minimal external intervention. A self-healing cement system that can respond to cement sheath damage is therefore a very promising application for oil and gas wells.

Self-healing has long been observed in cement structures as cement possesses some natural healing properties. Through the further hydration of unhydrated cement particles as well as the dissolution and subsequent recrystallization and carbonation of $Ca(OH)_2$, the cementitious matrix is capable of healing cracks by itself under favourable conditions, known as autogenous healing (Van Tittelboom & De Belie 2013). However, this natural autogenous healing capability is limited to very small cracks and is difficult to control. Nonetheless, such self-healing properties can be enhanced or built in for cementitious materials via some innovative approaches. The inclusion of self-healing agents such as mineral additives and supplementary cementitious materials can promote crystallization and sedimentation of healing products in the cracking area through their own hydration or reaction with $Ca(OH)_2$ from the matrix.

However, direct addition may render these self-healing agents ineffective because they usually start reacting immediately upon addition and may be consumed prior to the occurrence of cement cracking.

Encapsulation is an effective way to provide protection for and controlled release of the healing agents. Different encapsulation systems, including vascular networks and discrete capsules, have been investigated to achieve autonomic healing in cementitious materials. Considering the difficulty in the installation of vascular networks in underground wellbores, discrete capsules are deemed more suitable for practical application in an oil well cement system. In particular, micro-sized capsules are likely to cause less disruption to the matrix continuity and the mechanical properties of oil well cement. Microcapsules sequester the healing agent within discrete shell walls until cracking triggers rupture of the shell and the subsequent release of the healing agent to the region of the crack (White et al. 2010). The properties of the shell materials as well as the encapsulated core materials are key parameters for the self-healing performance of a microcapsule-based system. As the protection layer, the shells are required to have enough strength to ensure the survival of microcapsules during the mixing process and also the stability to resist the aggressive alkaline cementitious environment. Particularly when used in high temperature condition, the thermal stability of the shell materials should be of primary concern. The shell walls should also fracture when a crack forms so that the healing agent can be released. Polymeric shell materials such as PF, PU and PUrea generally possess good mechanical properties, chemical and thermal stability which are suited for microencapsulation. PU and PUrea also have the advantage of a relatively simple production process. In terms of healing agents, mineral-based agents have the advantage of better compatibility with the cementitious matrix compared to adhesive healing agents. In particular, silicate-based agents, such as sodium silicate (SS), are the most studied mineral-based healing agents for autonomic self-healing cementitious materials, due to their ability to produce a healing product (mainly C-S-H gels) that is native to the matrix. The encapsulated sodium silicate agents have been reported on their self-healing effectiveness in terms of strength recovery and durability recovery in cementitious materials. Current research on microcapsule-based self-healing cementitious materials mainly

focuses on their use in ambient conditions. Their use under extreme environments and specialised applications such as the underground wellbore has rarely been reported.

The reviews above provide a clearer picture of the potentials of reactive MgO and microcapsule-based self-healing materials for use in improving the performance of oil well cements, and also point out the scarcity of research work in the relevant fields. Therefore, this research project has aimed to investigate the use of reactive MgOs for shrinkage reduction and crack prevention, and sodium silicate microcapsules for crack healing in oil well cement systems. The effect of the combined use of reactive MgO and microcapsules on oil well cement properties was also explored. Accordingly, this research was divided into three parts: the expansive system with reactive MgO, the self-healing system with microcapsules, and the combined system with both additives. The results for the three systems are summarised as follows.

6.1.2 Expansive system with reactive MgO

In the expansive system studied in **Chapter 4**, three types of reactive MgO, N50 (RM1), MAG-R (RM2) and 92/200 (RM3), were used as expansive additives in oil well cement. They were first characterised on their reactivity according to the acid neutralisation time and SSA values: N50 was categorized as high reactivity, MAG-R was medium reactivity, and 92/200 was low reactivity. These three MgOs were then investigated on their expansion characteristics and shrinkage reduction performance in oil well cement as well as their influence on the other properties of oil well cement.

6.1.2.1 Expansion characteristics of reactive MgO in oil well cement

The expansion characteristics of the three reactive MgOs in relation to reactivity and content, curing temperature, and restraint condition, were investigated by length change measurements on oil well cement prisms containing MgO.

The length change results of the cement prisms, containing different reactive MgOs at 4, 8, 12% addition and cured in water at 20 ℃, showed that reactive MgO with higher reactivity has a faster expansion rate but a smaller ultimate expansion magnitude. The expansion magnitude

increased with MgO addition content. This is consistent with the MgO expansion model proposed by Mo et al. (2010), in that high reactivity MgO with a high specific surface area (SSA) and porous structure results in a higher hydration rate. The formed $Mg(OH)_2$ first fill the interior pores and then expand the MgO grains, thus producing a smaller expansion magnitude. MgO N50 of high reactivity had rapid expansion in cement paste which mainly occurred at an early age and levelled off at a small ultimate magnitude within a relatively short period. MgO MAG-R of medium reactivity had lower SSA than the N50, thus it hydrated and expanded at a slightly slower speed, but reached a larger ultimate expansion magnitude. MgO 92/200 had the lowest reactivity and exhibited delayed expansion behaviour, as characterised in the expansion model of Mo et al. (2010) which states that MgO with low reactivity experiences an induction period with very slow expansion rate and small expansion magnitude, but at later age the expansion rate becomes significantly accelerated and reaches a large expansion magnitude. 92/200 has much smaller SSA than N50 and MAG-R, thus its hydration takes much longer. These results were confirmed in restrained MgO cement prisms, which had reduced expansion magnitude but showed similar expansion trends to the free expansion.

Increasing temperature can accelerate the hydration rate of MgO, and thus faster expansion was observed in all MgO cement prisms cured in water at elevated temperatures of 40, 60 and 80°C. The higher the temperature, the faster the observed expansion. In particular, the effect of temperature was more prominent for the low reactivity MgO 92/200 which saw a substantially increased expansion rate at elevated temperature. However, the ultimate expansion magnitude of reactive MgO was found to decrease with increasing temperature. Particularly for the high reactivity N50, very little expansion of the cement prisms was measured when temperatures increased to 80 °C. It was inferred that highly reactive MgO hydrated too fast and hydration almost completed before cement setting, thus leading to ineffective expansion. Another possible reason for the decreased expansion magnitude is that high temperature curing may affect the crystallization of $Mg(OH)_2$, which results in a denser microstructure of $Mg(OH)_2$ crystals.

The XRD and TGA analysis of the hydration degree of reactive MgOs and SEM observations on the microstructures of $Mg(OH)_2$ hydration product further supported the expansion results as presented above.

6.1.2.2 Shrinkage reduction performance

Three reactive MgOs were tested in oil well cement prisms under sealed or drying conditions at a simulated wellbore temperature of 80 °C to evaluate their performance on autogenous shrinkage and drying shrinkage reduction, respectively.

Under the sealed condition, the length change results of MgO cement prisms, at addition contents of 4, 8, and 12% by weight of cement, showed that reactive MgO of lower reactivity was more effective in reducing autogenous shrinkage at 80 °C. Both MAG-R and 92/200 not only completely compensated for autogenous shrinkage but also provided extra expansion under the sealed condition. Moreover, their expansion magnitude also increased with increasing MgO content. In contrast, N50 was only able to partially compensate for the autogenous shrinkage, and increasing the N50 content had no significant improvement on autogenous shrinkage reduction. The results are consistent with their expansion characteristics at 80 °C cured in water. N50 hydrated too fast at 80 °C, thus much less effective expansion was generated after cement setting. Moreover, the hydration product of N50 is of relatively smaller size and denser structure compared to MAG-R and 92/200 at 80 °C, as observed under SEM. As a result, there was insufficient expansive force to counteract the shrinkage stress.

Based on their excellent performance at autogenous shrinkage reduction, MAG-R and 92/200 were further examined on their performance at drying shrinkage reduction at different relative humidities at 80 °C. Under the drying conditions of 90% RH, the addition of MAG-R and 92/200 both reduced shrinkage of oil well cement pastes. The medium reactivity MAG-R at higher content of 8, 12% showed significant shrinkage reduction at early age while it was not effective in compensating the drying shrinkage at later age. In contrast, the addition of 92/200 could fully compensate for the drying shrinkage in oil well cement paste. Especially at higher contents of 8% and 12%, its expansion at 80 °C effectively offset the contraction stresses and further expanded the cement pastes, resulting in an overall net expansion. However, when

exposed to 25% RH at 80 ℃, neither MAG-R nor 92/200 were effective at reducing drying shrinkage. Under low humidity conditions, the increased moisture loss induced not only greater drying shrinkage in the cement pastes but also less water was available for MgO hydration. As a result, no drying shrinkage reduction was observed in any of the MgO cement prisms.

The restrained cement prisms containing 8% MAG-R or 92/200 showed improved cracking resistance when subjected to drying at low RH of 25% at 80 ℃. The restrained expansion of MAG-R and 92/200 during the early-age water curing improved the strength of cement at to resist the cracking stresses.

6.1.2.3 Effects on oil well cement properties

In terms of rheology properties, the addition of reactive MgO had negative effects on the flow behaviour of oil well cement slurries. Both plastic viscosity and yield stress increased with MgO content. N50 had the most substantial effects on rheology properties due to its high SSA and fast hydration. When coupled with high temperature, the addition of reactive MgO further increased the plastic viscosity and yield stress of cement slurries due to the accelerated hydration of MgO at high temperatures.

In terms of cement hydration, N50 and MAG-R had accelerating effects on the hydration of oil well cement slurry whereas 92/200 showed a slight retardation on cement hydration. N50 especially significantly accelerated cement hydration due to its high reactivity. At elevated temperatures, the hydration rates of all reactive MgOs and cements showed acceleration.

In terms of unrestrained compressive strength at 80 ℃, MAG-R was surprisingly found to increase the strength of oil well cement pastes, and the addition of 8% MAG-R led to the most strength improvement. This disagrees with other findings reported in the literature showing that the free expansion of MgO generally caused strength reduction in the cement. This can be attributed to the densification of cement microstructures caused by the expansion of MAG-R at an early age, as well as the dense structure of its hydration products. In contrast, both N50 and 92/200 caused strength reduction of oil well cement pastes. Increasing MgO addition from 4% to 12% led to greater strength reduction. The strength reduction caused by N50 is likely due to its very early expansion occurring before cement setting, causing damage to the cement

skeleton. Its significant negative effects on the rheology properties of cement slurries may also affect the strength development. 92/200 led to significant reduction in strength at a later age (3 days and 7 days), which can be mainly attributed to the increased porosity of cement pastes due to its large expansion and the looser structure of its hydration products. Under restrained conditions, the compressive strengths of all oil well cement pastes containing reactive MgOs were significantly improved and were generally higher than that of cement paste without reactive MgO. This indicates that the expansion of reactive MgO under restraint is benefical for densification of the cement microstructure, thus improving the strength. The effects of MgO expansion on cement pore structure was not investigated in this study, and needs further verification.

Given all the above-mentioned results, it can be concluded that among the three reactive MgOs, both MAG-R of medium reactivity and 92/200 of low reactivity are recommended for use in reducing autogenous shrinkage and 92/200 for drying shrinkage (at high humidity) under the high curing temperature of 80 °C. The use of less reactive MAG-R and 92/200 have marginal influences on the fresh properties of oil well cement slurry (rheology properties and hydration). As for the effects on strength, the free expansion of 92/200 with low reactivity can cause significant strength reduction, but under the restrained conditions, the effect is mitigated as the compressive strength will be increased by the confined expansion. The addition of MAG-R increased the compressive strength under both free and restrained conditions.

6.1.3 Self-healing system with sodium silicate microcapsules

6.1.3.1 Characterisation of microcapsules

In the self-healing system studied in **Chapter 5**, two groups of polyurea/sodium silicate microcapsules were first characterized on their essential properties (particle size, thermal stability, alkalinity resistance) and were then investigated on their effects on their self-healing properties as well as other fresh and hardened properties of oil well cement. The T1 (OT1 and NT1) and T2 (OT2 and NT2) groups of polyurea microcapsules showed good thermal stability up to ~150 °C and even higher. By comparing the two groups, the T1 microcapsules with a rigid shell can withstand a higher temperature than the T2 microcapsules with a rubbery shell.

Both groups of microcapsules showed good stability when exposed to an alkali solution at a high temperature of 80 °C. Despite their different shell rigidities, T1 and T2 were both strong enough to survive the mixing process. When embedded in cement pastes, they were able to be ruptured by cracks and release the healing agents. The characterization results verified their suitability for use in oil well cement under high temperature wellbore conditions (80 °C).

6.1.3.2 Self-healing efficiency

Based on the measurements of crack width, crack depth, gas permeability, water sorptivity, and microstructural analyses, it was evident that the addition of microcapsules improved the healing performance of oil well cement pastes. By analyzing the chemical reactions between the sodium silicate agents and oil well cement, it was revealed that the oil well cement itself possesses very little healing capability when cured under a high temperature at 80 °C. Because cement hydration almost completed within the early age of 3 days, little unhydrated cement was left for continuous hydration in assisting autogenous crack healing. With the addition of microcapsules, the sodium silicate core materials reacted with the hydrated cement matrix to produce calcium silicate hydrates (C-S-H) which helped seal and bind the cracks. This healing reaction was verified by microstructural analysis (XRD and TGA) of the reaction products, showing a clear consumption of portlandite and formation of C-S-H healing products. The healing reactions also involved the carbonation of portlandite as indicated by the increased content of calcium carbonates in the healing products.

Correspondingly, improved macro self-healing performance was observed in microcapsule-containing oil well cement specimens after healing compared to the control specimens without microcapsules. Through optical microscopic observation, enhanced crack width healing was seen in the cement specimens containing microcapsules. Complete crack mouth closure was not observed, however. With the addition of microcapsules (T1 or T2) at 7.5% content, the crack width healing degree was improved from less than 7% to about 30% after healing for 7 days at 80 °C. A non-destructive method using ultrasonic testing was used to measure the depth of cracks in oil well cement prisms after healing. The addition of microcapsules at a content of 7.5% achieved crack depth reduction up to ~58% (NT1) and ~53% (NT2). It was noted that better healing was achieved inside the cracks compared to the crack mouth sealing. Crack

mouth sealing is known to be mainly dependent on the precipitation of calcium carbonates. This process might be inhibited at high temperature curing due to the reduced solubility of CO_2 in water at higher temperatures.

Consistent with the reduced crack mouth width and crack depth, the cracked specimens containing microcapsules obtained enhanced tightness recovery in terms of gas permeability and water sorptivity. The healing efficiency generally increased with microcapsule content as more healing agents were provided for healing. As the addition of microcapsules increased to 7.5%, the reduction in sorptivity coefficients reached ~76%. However, a high microcapsule content might negatively influence the healing efficiency from other aspects. The addition of microcapsules at high content might increase the porosity of the cement matrix and create residual voids on the cracking surface after rupture for healing, leading to increased permeability. The addition of microcapsules above 2.5% did not bring further reduction in gas permeability, but on the contrary increased it. Apart from recovery of water and gas tightness, the sodium silicate microcapsules also showed effectiveness in improving strength recovery. The C-S-H gels formed act as effective bindings within the cracking area, thus contributing to the strength recovery. The addition of microcapsules (T1 or T2) improved the strength recovery by ~27% at a content of 7.5%.

The T1 and T2 groups of microcapsules generally showed comparable self-healing efficiency. T1 and T2 microcapsules mainly differ in the shell properties which are likely to affect their fracture behavior in releasing the core material and further influence the healing efficiency. However, it was demonstrated that both of them showed good fracture behaviour upon cracking and releasing the SS core for healing reaction. Considering the similarities of T1 and T2 in other properties like particle size and core material content, it is reasonable that no significant difference was observed between their healing efficiency.

The microstructure analyses of the cracking surface via SEM and EDX further verified the successful release of the sodium silicate core and its reaction with the cement matrix. The formation of C-S-H healing products was also confirmed by XRD and TGA analyses.

6.1.3.3 Effects on oil well cement properties

The effect of microcapsules on the other properties of oil well cement was also investigated. The results showed that the incorporation of microcapsules generally have negative effects on the cement properties, especially at high addition content. The addition of microcapsules at a content above 5% was found to significantly reduce the flowability of oil well cement slurries. The hydration of cement slurries was obviously accelerated by adding microcapsules at a high content of 7.5% compared to a low content addition at 1.25%. The compressive strength and flexural strength also decreased with increasing microcapsule content. The more microcapsules added, the higher the strength reduction. The different shell properties of T1 and T2 microcapsules mainly influenced the strength of oil well cement pastes, with the addition of T2 microcapsules with rubbery shells causing greater strength reduction than the T1 microcapsules with rigid shells.

Based on the overall effects of microcapsules on the oil well cement properties, the T1 microcapsules with rigid shell are considered more favorable for use in the following combined system, and a content of 5% seemed to be the suitable dosage.

6.1.4 Combined oil well cement system

This part presented the first attempt to develop an expansive self-healing oil well cement system via the hybrid use of MgO expansive additive and self-healing microcapsules. Reactive MgO-MAG (RM2) at 8% content and 5% of NT1 microcapsules were added to the combined oil well cement system. With the combined use of MgO and microcapsules, the effect of MgO expansion on the stability of microcapsules should be taken into consideration. Too great an expansive deformation of the matrix could cause rupture or debonding of the microcapsules and weaken the self-healing performance. This is one of the main reasons why MgO RM2 that produces a relatively smaller expansion mainly at the early age was chosen over MgO 92/200. SEM observation showed that the addition of RM2 at 8% showed no significant effects on the stability of the microcapsules. The combined oil well cement system showed a similar expansion performance and self-healing efficiency to the individual expansive system with only MgO RM2 and the self-healing system with only the microcapsules. It was inferred that

the expansion by MgO RM2 and the self-healing by microcapsule NT1 work independently from each other in the combined oil well cement system. The hydration and expansion of the MgO RM2 was mainly completed within the early age of 3 days before cracking. Therefore, there was little unhydrated MgO remaining in the cracking area to enhance autogenous healing. As a result, the self-healing process in the combined system was still mainly driven by the microcapsules.

In terms of the effect on the mechanical properties of the oil well cement, the combined use of MgO RM2 with NT1 microcapsules was found to be advantageous over the individual system with only microcapsules. MgO RM2 had a positive effect on improving the cement strength, which compensated for the strength reduction caused by the addition of NT1 microcapsules. However, the combined addition of RM2 and NT1 intensified their negative effect on the rheology properties of oil well cement. The plastic viscosity and yield stress of the cement slurries were substantially increased by using two additives compared to the individual additions. In this case, the use of dispersants could be considered to increase the flowability of the cement slurries to meet the requirements for cementing job.

As whole, the combined system takes advantages of the expansive capability of MgO and self-healing capability of microcapsules, which is a promising way to achieve more advanced oil well cement system.

6.2 Recommendations for future work

For the expansive system, the current study mainly focused on the shrinkage reduction performance of reactive MgO at a temperature of 80 ℃, which is a typical temperature level for low-temperature wellbores. In practice, the well temperature usually increases with well depth, forming different temperature zones within one wellbore. In the case of a wide temperature range, a single type of MgO may not be suitable for use at all temperature levels. Further tests can be carried out to specify the range of MgO reactivities which are suitable for shrinkage reduction under specific temperature grades. This information could also be used to instruct the production of reactive MgO for practical oil field use. Thus, a designable expansion oil well cement system could be achieved.

The expansion performance of reactive MgOs in the current study focused on the period after cement setting, and the expansion measurements of cement prisms started from demoulding. However, the expansion behaviours of reactive MgOs within the period before demoulding, which includes the plastic phase before cement setting and the early period of cement hardening, are not well understood. The expansion capability of reactive MgO might be underestimated considering that the expansion occurring during this period was not recorded. Therefore, further tests should be carried out to measure the expansion during this period in order to fully characterise the expansion properties of reactive MgOs.

For better use of reactive MgO, it would also be useful to evaluate the shrinkage reduction performance of reactive MgO under an annularly restrained condition that simulates the realistic condition between the formation layer and steel casing in a wellbore. The shrinkage stresses and MgO expansion stresses are dependent on the restrained condition. In the current study, the effects of reactive MgO on shrinkage reduction were mainly tested under free or one-dimensional restrained conditions. In practice, oil well cement is subjected to radial restraints imposed by the casing and/or the formation. To simulate a realistic condition, the restrained shrinkage ring test method, as described in the studies of Baumgarte et al. (1999) and Mounanga et al. (2011), is suggested for use in further tests on oil well cement shrinkage reduction by reactive MgO.

In addition, reactive MgO was found to significantly affect the strength of the oil well cement under free or restrained conditions. The effect of MgO expansion on the pore structure development of the cement matrix was considered to be one of the main causes. A pore structure analysis of porosity and pore size distribution would be useful to better explain the effect of reactive MgO on the strength development of oil well cement.

For the self-healing system, this study explored the use of SS microcapsules for improving the self-healing properties of oil well cement under a challenging high-temperature borehole environment, with their effectiveness being verified by observing enhanced recovery in mechanical and tightness properties. Nonetheless, there is still a wide range of future work that can be conducted to optimise this microcapsule-based healing system before it can be used for practical purposes in a wellbore.

In terms of microcapsules, optimisation of the shell properties is desirable. The polyurea shell materials in the current study showed good thermal stability and alkalinity resistance, and also stability during mixing, which suited their use in a wellbore environment. However, the incorporation of polyurea microcapsules at high contents caused strength reduction of the oil well cement. The T1 microcapsules with rigid shells were found to cause less strength reduction. A harder shell also was also found to have higher thermal stability. Therefore, microcapsules with more rigid shells is worthy to be explored. It would also be useful to carry out a quantitative analysis of the mechanical properties of microcapsules with different shells in future work.

The addition of encapsulated sodium silicate agents obviously improved the self-healing properties of oil well cement. Optimization of the healing potential of the polyurea/SS microcapsules could be carried out to further enhance the recovery of the cement properties. In the current study, the self-healing efficiency was evaluated at one damage level of CMOD=0.2 mm. Further tests on multiple damage levels would be useful to specify the damage range over which these SS microcapsules would be suitable. They are expected to be more efficient in healing smaller cracks. Meanwhile, the current study assessed the self-healing efficiency of the microcapsules over a healing period of 7 days. For oil well cement system, fast self-healing reactions are desired to obtain timely performance recovery. It is necessary to develop a periodical evaluation of the self-healing efficiency to monitor the self-healing process, which will provide a clearer view on the healing rate of SS microcapsules.

The healing reactions of SS microcapsules require the involvement of water. The curing condition in current microcapsule-based self-healing system simulates the environment where the cement sheath is placed in the section of water-bearing formation in the wellbore. But water access can be limited when cement is placed between a low-permeable formation and casing, or between two concentric casings of different diameters. In such challenging cases, the combined use of water reservoirs such as super absorbent polymers could be considered as an additional water supply.

The combined system takes advantages of the expansive capability of MgO and self-healing capability of microcapsules. But it has a major concern that the MgO expansion may influence

the stability of the microcapsules in the cement matrix, as mentioned in Chapter 5. The MgO used for the combined system should meet the required shrinkage reduction under a specified wellbore condition. In the meantime, it must not produce excessive expansion stresses that may cause damages to the microcapsules. It is useful to investigate the compatibility between different types of reactive MgOs and microcapsules in the cement matrix. Microcapsules with stronger shells would also be beneficial to improve their stability in the combined system. Other delivery methods for healing agents such as coated pellets with higher strength could also be considered in future research.

References

Acker, P., 2004. Swelling, shrinkage and creep: a mechanical approach to cement hydration. *Materials and Structures*, 37(268), pp.237–243.

Alshamsi, A.M. & Imran, H.D.A., 2002. Development of a permeability apparatus for concrete and mortar. *Cement and Concrete Research*, 32(6), pp.923–929.

API Specification 10A, 2010. Specification for Cements and Materials for Well Cementing.

ASTM C1585, 2013. Standard Test Method for Measurement of Rate of Absorption of Water by Hydraulic Cement Concretes. *ASTM International*, 41(147), pp.1–6.

Baumgarte, C., Thiercelin, M. & Klaus, D., 1999. Case Studies of Expanding Cement To Prevent Microannular Formation. *SPE Annual Technical Conference and Exhibition held in Houston, Texas, 3–6 October 1999.*

Bea, R., 2011. Final Report on the Investigation of the Macondo Well Blowout Deepwater Horizon Study Group. , (May 2010), p.126.

Beglarigale, A., Seki, Y., Demir, N.Y. and Yazıcı, H., 2018. Sodium silicate/polyurethane microcapsules used for self-healing in cementitious materials: Monomer optimization, characterization, and fracture behavior. *Construction and Building Materials*, 162, pp.57–64.

Bentz, D.P., 2009. Early-age cracking review: mechanisms, material properties, and mitigation strategies. National Institute of Standards and Technology, Gaithersburg, MD.

Bissonnette, B., Pierre, P. & Pigeon, M., 1999. Influence of key parameters on drying shrinkage of cementitious materials. *Cement and Concrete Research*, 29(10), pp.1655–1662.

Blanc, A., Faure, P., Le Roy-Delage, S. and Fen-Chong, T., 2013. Autogenous shrinkage of hardening cement paste in oil wells. In *Poromechanics V: Proceedings of the Fifth Biot Conference on Poromechanics*, pp. 2517-2525.

Bonett, A. & Pafitis, D., 1996. Getting to the Root of Gas Migration. *Oilfield Review 8*(1),

References

pp.36–49.

Bourgoyne, A.T., Scott, S.L. & Regg, J.B., 1999. OTC 11029 Sustained Casing Pressure in Offshore Producing Wells.

Broni-Bediako, E., Joel, O.F. and Ofori-Sarpong, G., 2016. Oil well cement additives: a review of the common types. *Oil and Gas Research*, *2*(1), pp.1-7.

Buntoro, A., Rubiandini, R. & Key, T., 2001. the Effect of Neat Magnesium Oxide (Mgo) As Expanding Additive With Burning Temperature 1200 O C and 1300 O C.

Canterford, J.H., 1985. Magnesia—An important Industrial Mineral: A Review of Processing Options and Uses. *Mineral Processing and Extractive Metallurgy Review*, 2(March 2015), pp.57–104.

Carey, B., 2010. Wellbore Integrity and CO2 Sequestration. *Los Alamos National Laboratory*.

Chatterji, S., 1995. Mechanism of expansion of concrete due to the presence of dead-burnt CaO and MgO. *Cement and Concrete Research*, 25(1), pp.51–56.

Chau, C.K. & Li, Z., 2008. Accelerated reactivity assessment of light burnt magnesium oxide. *Journal of the American Ceramic Society*, 91(5), pp.1640–1645.

Chen, X., Yang, H.Q., Zhou, S.H. and Yan, J.J., 2011. Crack Resistance of Concrete with Incorporation of Light-Burnt MgO. *Advanced Materials Research*, Vol. 168, pp. 1348-1352. Trans Tech Publications.

Chowdhury, R.A., Hosur, M.V., Nuruddin, M., Tcherbi-Narteh, A., Kumar, A., Boddu, V. and Jeelani, S., 2015. Self-healing epoxy composites: preparation, characterization and healing performance. *Journal of Materials Research and Technology*, *4*(1), pp.33-43.

Chu, I., Kwon, S.H., Amin, M.N. and Kim, J.K., 2012. Estimation of temperature effects on autogenous shrinkage of concrete by a new prediction model. *Construction and Building Materials*, *35*, pp.171-182.

Cohen, M.D. & Richards, C.W., 1982. Effects of the particle sizes of expansive clinker on strength-expansion characteristics of type K expansive cements. *Cement and Concrete*

References

Research, 12(6), pp.717–725.

Cui, X., 2008. Effect of Calcining Temperature and Time on Property of Light-burn MgO. Master thesis. *Master thesis, Nanjing University of Technology*.

Danjusevsky, V.S., 1983. Gefuege und Eigenshaften hydraulicer Bindemitel nach dem Erhaerten Bei Boheren Temperaturen und Laengeren Zeiten. *ITE-Fachberiche*, 107(No:10).

Deng, M., Cui, X., Liu, Y. and Tang, M., 1990. Expansive Mechanism of Magnesia as an additive of Cement (in Chinese). *Journal of Nanjing Institute of Chemical Technology*, *12*(4), pp.1-11.

De Belie, N., Gruyaert, E., Al-Tabbaa, A., Antonaci, P., Baera, C., Bajare, D., Darquennes, A., Davies, R., Ferrara, L., Jefferson, T. and Litina, C., 2018. A Review of Self-Healing Concrete for Damage Management of Structures. *Advanced Materials Interfaces*.

De Rooij, M., Van Tittelboom, K., De Belie, N. and Schlangen, E. eds., 2013. *Self-healing phenomena in cement-Based materials: state-of-the-art report of RILEM technical committee 221-SHC: self-Healing phenomena in cement-Based materials* (Vol. 11). Springer Science & Business Media.

Dong, B., Fang, G., Wang, Y., Liu, Y., Hong, S., Zhang, J., Lin, S. and Xing, F., 2017. Performance recovery concerning the permeability of concrete by means of a microcapsule based self-healing system. *Cement and Concrete Composites*, *78*, pp.84-96.

Dong, B., Fang, G., Ding, W., Liu, Y., Zhang, J., Han, N. and Xing, F., 2016. Self-healing features in cementitious material with urea–formaldehyde/epoxy microcapsules. *Construction and Building Materials*, *106*, pp.608-617.

Dry, C., 1994. Matrix cracking repair and filling using active and passive modes for smart timed release of chemicals from fibers into cement matrices. *Smart Materials and Structures*, 3, pp.118–123.

Edvardsen, C.K., 1996. Water permeability and self-healing of through cracks in concrete. *DeutscherAusschuss für Stahlbeton 455*.

References

Faroughi, S.A. & Huber, C., 2014. Crowding-based rheological model for suspensions of rigid bimodal-sized particles with interfering size ratios. *Physical Review E - Statistical, Nonlinear, and Soft Matter Physics*, 90(5), pp.1–5.

Fathaddin, M.T. & Condition, G.W., 2005. Effects of Additives and Conditioning Time on Compressive and Shear Bond Strengths of Geothermal Well Cement. *Proceedings World Geothermal Congress*, pp.24–29.

Formia, A., Terranova, S., Antonaci, P., Pugno, N.M. and Tulliani, J.M., 2015. Setup of extruded cementitious hollow tubes as containing/releasing devices in self-healing systems. *Materials*, *8*(4), pp.1897-1923.

Gatner, E.M., J.F. Young., D.A. Damidot., I. Jawed., 2002. Hydration of portland cement. In *Structure and performance of cements, Chapter 3*, pp. 57–108.

Ghofrani, R. & Plack, H., 1993. CaO- and/or MgO-Swelling Cements: A Key for Providing a Better Annular Sealing? *Proceedings of SPE/IADC Drilling Conference*, pp.199–214.

Ghosh, S.K., 2006. Functional Coatings and Microencapsulation: A General Perspective. *Functional Coatings: By Polymer Microencapsulation*, pp.1–28.

Giannaros, P., 2017. Laboratory and field investigation of performance of novel microcapsule-based self-healing concrete. *PhD thesis, University of Cambridge.*

Giannaros, P., Kanellopoulos, A. & Al-Tabbaa, A., 2016. Sealing of cracks in cement using microencapsulated sodium silicate. *Smart Materials and Structures, July 2016.*

Gilford III, J., Hassan, M.M., Rupnow, T., Barbato, M., Okeil, A. and Asadi, S., 2013. Dicyclopentadiene and sodium silicate microencapsulation for self-healing of concrete. *Journal of Materials in Civil Engineering*, *26*(5), pp.886-896.

Goboncan, V.C., Dillenbeck, R.L. & Company, B.J.S., 2003. SPE / IADC 79911 Real-Time Cement Expansion / Shrinkage Testing Under Downhole Conditions For Enhanced Annular Isolation. , l.

Gotsis, C., Roy, D.M., Licastro, P.H. and Kaushal, S., 1986. Thermal and Thermomechanical

References

Analysis of a Cylindrical Cementitious Plug Hydrating in a Borehole. *Special Publication*, *95*, pp.49-70.

Hall, C. & Tse, T.K.M., 1986. Water movement in porous building materials-VII. The sorptivity of mortars. *Building and Environment*, 21(2), pp.113–118.

Hassan, M.M., Milla, J., Rupnow, T., Al-Ansari, M. and Daly, W.H., 2016. Microencapsulation of calcium nitrate for concrete applications. *Transportation Research Record: Journal of the Transportation Research Board*, (2577), pp.8-16.

Hearn, N. & Morley, C.T., 1997. Self-sealing property of concrete - Experimental evidence. *Materials and structures*, 30(7), pp.404–411.

Holt, E.E., 2001. Early age autogenous shrinkage of concrete. *VTT Publications*, (446), pp.2–184.

Hong, K. & Park, S., 2000. Preparation of polyurea microcapsules containing ovalbumin. *Materials Chemistry and Physics*, 64(1), pp.20–24.

Huang, H., Ye, G., Qian, C. and Schlangen, E., 2016. Self-healing in cementitious materials: Materials, methods and service conditions. *Materials & Design*, *92*, pp.499-511.

Huang, H. & Ye, G., 2011a. Application of sodium silicate solution as self-healing agent in cementitious materials. *International RILEM Conference on Advances in Construction Materials Through Science and Engineering*, (June 2015), pp.530–536.

Huang, H. & Ye, G., 2011b. Application of sodium silicate solution as self-healing agent in cementitious materials. *International RILEM Conference on Advances in Construction Materials Through Science and Engineering*, (1993), pp.530–536.

Huang, H., Ye, G. & Damidot, D., 2014. Effect of blast furnace slag on self-healing of microcracks in cementitious materials. *Cement and Concrete Research*, 60, pp.68–82.

Irico, S., Bovio, A.G., Paul, G., Boccaleri, E., Gastaldi, D., Marchese, L., Buzzi, L. and Canonico, F., 2017. A solid-state NMR and X-ray powder diffraction investigation of the binding mechanism for self-healing cementitious materials design: The assessment of the

References

reactivity of sodium silicate based systems. *Cement and Concrete Composites*, *76*, pp.57-63.

J. Liu, C.V., 2012. Failure Modes of Oil Well Cement During Service Life. *Hurricanes-2012 Conference Proceedings*, pp.2–3.

Jackson, R.B., Vengosh, A., Darrah, T.H., Warner, N.R., Down, A., Poreda, R.J., Osborn, S.G., Zhao, K. and Karr, J.D., 2013. Increased stray gas abundance in a subset of drinking water wells near Marcellus shale gas extraction. *Proceedings of the National Academy of Sciences*, *110*(28), pp.11250-11255.

Jackson, R.B., 2014. The integrity of oil and gas wells. *Proceedings of the National Academy of Sciences*, 111(30), pp.10902–10903.

Jafariesfad, N., Geiker, M.R., Gong, Y., Skalle, P., Zhang, Z. and He, J., 2017. Cement sheath modification using nanomaterials for long-term zonal isolation of oil wells. *Journal of Petroleum Science and Engineering*, *156*, pp.662-672.

Jafariesfad, N., Gong, Y., Geiker, M.R. and Skalle, P., 2016, April. Nano-sized mgo with engineered expansive property for oil well cement systems. In *SPE Bergen One Day Seminar*. Society of Petroleum Engineers.

Jafariesfad, N., Geiker, M.R. and Skalle, P., 2017. Nanosized Magnesium Oxide With Engineered Expansive Property for Enhanced Cement-System Performance. *SPE Journal,* pp 1-9.

Jaroenratanapirom, D., 2010. Effects of Different Mineral Additives and Cracking Ages on Self-Healing Performance of Mortar. *Annual Concrete Conference 6, thailand Concrete Association*, pp.551–556.

Jensen, O.M. & Hansen, P.F., 1999. Influence of temperature on autogenous deformation and relative humidity change in hardening cement paste. *Cement and Concrete Research*, 29(4), pp.567–575.

Jin, F. & Al-Tabbaa, A., 2014. Characterisation of different commercial reactive magnesia. *Advances in Cement Research*, 26(2), pp.101–113.

References

Joseph, C., Jefferson, A.D., Isaacs, B., Lark, R.J. and Gardner, D.R., 2010. Experimental investigation of adhesive-based self-healing of cementitious materials. *Magazine of Concrete Research*, *62*(11), pp.831-843.

Jupe, A.C., Wilkinson, A.P., Luke, K. and Funkhouser, G.P., 2005. Class H oil well cement hydration at elevated temperatures in the presence of retarding agents: an in situ high-energy X-ray diffraction study. *Industrial & engineering chemistry research*, *44*(15), pp.5579-5584.

Justnes, H., Van Loo, D., Reyniers, B., Skalle, P., Sveen, J. and Sellevold, E.J., 1995. Chemical shrinkage of oil well cement slurries. *Advances in cement Research*, *7*(26), pp.85-90.

K.R.Backe, 1997. Characterising Curing Cement Slurries by Permeability, Tensile Strength and Shrinkage.

Kanellopoulos, A., Litina, C., Giannaros, P. and Al-Tabbaa, A., 2016. Effect of different types of polymeric microcapsules on the self-healing efficiency of cement based composites. *Proceedings of the 9th International Conference on Fracture Mechanics of Concrete and Concrete Structures*.

Kanellopoulos, A., Giannaros, P., Palmer, D., Kerr, A. and Al-Tabbaa, A., 2017. Polymeric microcapsules with switchable mechanical properties for self-healing concrete: Synthesis, characterisation and proof of concept. *Smart Materials and Structures*, 26(4).

Kanellopoulos, A., Giannaros, P. & Al-Tabbaa, A., 2016. The effect of varying volume fraction of microcapsules on fresh, mechanical and self-healing properties of mortars. *Construction and Building Materials*, 122, pp.577–593.

Kanellopoulos, A., Qureshi, T.S. & Al-Tabbaa, A., 2015. Glass encapsulated minerals for self-healing in cement based composites. *Construction and Building Materials*, 98, pp.780–791.

Lau, W.Y., 2017. The Role of Reactive MgO as an Expansive Additive in the Shrinkage Reduction of Concrete. *PhD thesis, University of Cambridge*, (May).

Lau, W.Y. & Mo, L., 2014. Expansion properties of two different reactivity MgOs produced

References

from magnesite and seawater. *34th Cement and Concrete Science Conference*, (197), pp.8–11.

Lavrov, A. and Torsæter, M., 2016. *Physics and mechanics of primary well cementing*. Springer.

Lee, H.X.D., Wong, H.S. and Buenfeld, N., 2010, August. Self-sealing cement-based materials using superabsorbent polymers. *Proceedings of the International RILEM Conference on Use of Superabsorbent Polymers and Other New Additives in Concrete, Lyngby, Denmark*, pp. 15-18.

Li, F.X., Chen, Y.Z., Long, S.Z., Wang, B. and Li, G.G., 2010. Research on the preparation and properties of MgO expansive agent. *Advances in Cement Research*, *22*(1), pp.37-44.

Li, H., 2010. Influence of MgO-bearing Expansive Agent on Deformation and Strength of Cement pastes. Master Thesis (in Chinese).

Li, H., Deng, M. & Mo, L., 2010. Influence ofMgO bearing expansive agent in different activities on deformation of cement pastes. *Journal of Nanjing University of Technology (Natural Science Edition)*, 32, pp.98–102.

Li, W., Zhu, X., Zhao, N. and Jiang, Z., 2016. Preparation and properties of melamine urea-formaldehyde microcapsules for self-healing of cementitious materials. *Materials*, *9*(3), p.152.

Li, W., Jiang, Z., Yang, Z., Zhao, N. and Yuan, W., 2013. Self-healing efficiency of cementitious materials containing microcapsules filled with healing adhesive: Mechanical restoration and healing process monitored by water absorption. *PLoS ONE*, 8(11), pp.1–18.

Litina, C., 2016. Development and Performance of Self - Healing Blended Cement Grouts With Microencapsulated. *PhD thesis, University of Cambridge.*

Litina, C. & Al-Tabbaa, A., 2015. Self-healing of cementitious composites using silica precursors as microencapsulated healing agents. *5th International Conference on Self-Healing Materials*, (Mdi), pp.2–5.

References

Litina, C., Kanellopoulos, A. & Al-Tabbaa, A., 2014. Alternative repair system for concrete using microencapsulated healing agents. *Conference proceedings :5th International Conference on Concrete Repair, At: Belfast, Northern Ireland*, pp.97–103.

Liu, H., Bu, Y. & Guo, S., 2013. Improvement of aluminium powder application measure based on influence of gas hole on strength properties of oil well cement. *Construction and Building Materials*, 47, pp.480–488.

Lothenbach, B., Scrivener, K. & Snellings, R., 2016. *A practical guide to microstructural analysis of cementitious materials*, CRC Press.

Lu, Z., Kong, X., Yang, R., Zhang, Y., Jiang, L., Wang, Z., Wang, Q., Liu, W., Zeng, M., Zhou, S. and Dong, B., 2016. Oil swellable polymer modified cement paste: Expansion and crack healing upon oil absorption. *Construction and Building Materials*, *114*, pp.98-108.

Lv, L., Schlangen, E., Yang, Z. and Xing, F., 2016. Micromechanical properties of a new polymeric microcapsule for self-healing cementitious materials. *Materials*, *9*(12), p.1025.

Lv, L., Yang, Z., Chen, G., Zhu, G., Han, N., Schlangen, E. and Xing, F., 2016. Synthesis and characterization of a new polymeric microcapsule and feasibility investigation in self-healing cementitious materials. *Construction and Building Materials*, *105*, pp.487-495.

Mangadlao, J.D., Cao, P. & Advincula, R.C., 2015. Smart Cements and cement Additives for oil and gas Operations. *Journal of Petroleum Science and Engineering*, 129(April 2010), pp.63–76.

Marbun, B., 2012. Investigation of Self-Manufactured MGO-Swelling Cements for an HPHT Cementing. *PROCEEDINGS, INDONESIAN PETROLEUM ASSOCIATION Thirty-Sixth Annual Convention & Exhibition*, (May).

Marbun, B., 2006. Kinetik der Hydratation von CaO und MgO. Dissertation. , p.142.

Mehta, P.K., 1973. Effect of lime on hydration of pastes containing gypsum and calcium aluminates or calcium sulfoaluminate. *Journal of the American Ceramic Society*, 56(6), pp.315–320.

References

Mehta, P.K. & Monteiro, P.J.M., 2006. *Concrete: microstructure, properties, and materials*.

Mihashi, H., Kaneko, Y., Nishiwaki, T. and Otsuka, K., 2001. Fundamental study on development of intelligent concrete characterized by self-healing capability for strength. *Transactions of the Japan Concrete Institute*, *22*, pp.441-450.

Milla, J., Hassan, M.M., Rupnow, T., Al-Ansari, M. and Arce, G., 2016. Effect of self-healing calcium nitrate microcapsules on concrete properties. *Transportation Research Record: Journal of the Transportation Research Board*, (2577), pp.69-77.

Mo, L., Deng, M., Tang, M. and Al-Tabbaa, A., 2014. MgO expansive cement and concrete in China: Past, present and future. *Cement and Concrete Research*, *57*, pp.1-12.

Mo, L., Deng, M. & Tang, M., 2010. Effects of calcination condition on expansion property of MgO-type expansive agent used in cement-based materials. *Cement and Concrete Research*, 40(3), pp.437–446.

Mo, L., Deng, M. & Wang, A., 2012. Effects of MgO-based expansive additive on compensating the shrinkage of cement paste under non-wet curing conditions. *Cement and Concrete Composites*, 34(3), pp.377–383.

Mostavi, E., Asadi, S., Hassan, M.M. and Alansari, M., 2015. Evaluation of self-healing mechanisms in concrete with double-walled sodium silicate microcapsules. *Journal of Materials in Civil Engineering*, *27*(12), p.04015035.

Mounanga, P., Baroghel-Bouny, V., Loukili, A. and Khelidj, A., 2006. Autogenous deformations of cement pastes: Part I. Temperature effects at early age and micro–macro correlations. *Cement and Concrete Research*, *36*(1), pp.110-122.

Mounanga, P., Bouasker, M., Pertue, A., Perronnet, A. and Khelidj, A., 2011. Early-age autogenous cracking of cementitious matrices: physico-chemical analysis and micro/macro investigations. *Materials and structures*, *44*(4), pp.749-772.

Narayanan, N. & Ramamurthy, K., 2000. Microstructural investigations on aerated concrete. *Cement and Concrete Research*, 30(3), pp.457–464.

References

National Academy of Engineering and National Research Council, 2011. *Macondo Well – Deepwater Horizon Blowout: Lessons for Improving Offshore Drilling Safety*, Available at: www.nap.edu.

Nelson, E.B., 2006. *Well cementing* 2nd edition.

Nelson, E.B., 2012. Well Cementing Fundamentals. *Oilfield Review*, pp.59–60.

Nguon, O., Lagugné-Labarthet, F., Brandys, F.A., Li, J. and Gillies, E.R., 2017. Microencapsulation by *in situ* Polymerization of Amino Resins. *Polymer Reviews*, 58(2), pp.326–375.

Ouarabi, M.A., Antonaci, P., Boubenider, F., Gliozzi, A.S. and Scalerandi, M., 2017. Ultrasonic monitoring of the interaction between cement matrix and alkaline silicate solution in self-healing systems. *Materials*, *10*(1), p.46.

Pang, X., Meyer, C., Funkhouser, G.P. and Darbe, R., 2015. An innovative test apparatus for oil well cement: In-situ measurement of chemical shrinkage and tensile strength. *Construction and Building Materials*, *74*, pp.93-101.

Pang, X., Cuello Jimenez, W. & Iverson, B.J., 2013. Hydration kinetics modeling of the effect of curing temperature and pressure on the heat evolution of oil well cement. *Cement and Concrete Research*, 54, pp.69–76.

Parcevaux, P. a. & Sault, P.H., 1984. Cement Shrinkage and Elasticity: A New Approach for a Good Zonal Isolation. *Proceedings of SPE Annual Technical Conference and Exhibition held in Houston*, p.12.

Pelletier, M.M., Brown, R., Shukla, A. and Bose, A., 2010. Self-healing concrete with a microencapsulated healing agent. *University of Rhode Island, Kingston,USA*, (C).

Perez, G., Gaitero, J.J., Erkizia, E., Jimenez, I. and Guerrero, A., 2015. Characterisation of cement pastes with innovative self-healing system based in epoxy-amine adhesive. *Cement and Concrete Composites*, *60*, pp.55-64.

Perez, G., Erkizia, E., Gaitero, J.J., Kaltzakorta, I., Jiménez, I. and Guerrero, A., 2015.

263

References

Synthesis and characterization of epoxy encapsulating silica microcapsules and amine functionalized silica nanoparticles for development of an innovative self-healing concrete. *Materials Chemistry and Physics*, 165, pp.39–48.

Perignon, C., Ongmayeb, G., Neufeld, R., Frere, Y. and Poncelet, D., 2015. Microencapsulation by interfacial polymerisation: Membrane formation and structure. *Journal of Microencapsulation*, 32(1), pp.1–15.

Plank, J., 2018. Oil well cementing. Available at: http://www.bauchemie-tum.de/master-framework/?p=Tief&i=13&m=1&lang=en.

Primeaux, D., 2004. Polyurea elastomer technology: history, chemistry & basic formulating techniques. *Primeaux Associates LLC*, pp.1–20.

Qian, S.Z., Zhou, J. & Schlangen, E., 2010. Influence of curing condition and precracking time on the self-healing behavior of Engineered Cementitious Composites. *Cement and Concrete Composites*, 32(9), pp.686–693.

Qiao, L., Xue, Y. & Zhang, Q., 2018. Synthesis and characterization of phenol–formaldehyde microcapsules for self-healing coatings. *Journal of Materials Science*, 53(2), pp.1035–1048.

Qureshi, T.S., 2016. The role of expansive minerals in the autogenous and autonomic self-healing of cement based materials. *PhD thesis, University of Cambridge*.

Radonjic, M. & Oyibo, A., 2014. Experimental Evaluation of Wellbore Cement- Formation Shear Bond Strength in Presence of Drilling Fluid Contamination. *5th International Conference on Porous Media and Their Applications in Science, Engineering and Industry*, p.7.

Reddy, B.R., Xu, Y., Ravi, K., Gray, D.W. and Pattillo, P., 2009. Cement Shrinkage Measurement in Oilwell Cementing--A Comparative Study of Laboratory Methods and Procedures. *SPE Drilling & Completion*, *24*(01), pp.104-114.

Reinhardt, H.W. & Jooss, M., 2003. Permeability and self-healing of cracked concrete as a function of temperature and crack width. *Cement and Concrete Research*, 33(7), pp.981–

References

985.

Restuccia, L., Reggio, A., Ferro, G.A. and Tulliani, J.M., 2017. New self-healing techniques for cement-based materials. *Procedia Structural Integrity*, *3*, pp.253-260.

Rocha, S.D.F., Mansur, M.B. & Ciminella, V.S.T., 2004. Kinetics and mechanistic analysis of caustic magnesia hydration. *Journal of Chemical Technology and Biotechnology*, 79(8), pp.816–821.

Rubiandini, R., Siregar, S., Suhascaryo, N. and Efrial, D., 2005. The effect of CaO and MgO as expanding additives to improve cement isolation strength under HPHT exposure. *Journal of Engineering and Technological Sciences*, *37*(1), pp.29-48.

Rudi Rubiandini, R.S., 2000. New Additive for Improving Shearbond Strength in High Temperature and Pressure Cement. *Proceedings of the IADC/SPE Asia Pacific Drilling Technology Conference, APDT*, pp.181–198.

Sabins, F.L. & Sutton, D.L., 1991. Interrelationship Between Critical Cement Properties and Volume Changes During Cement Setting. *SPE Drilling Engineering*, 6(2).

Sabir, B.B., Wild, S. & O'Farrell, M., 1998. A water sorptivity test for martar and concrete. *Materials and Structures*, 31(8), pp.568–574.

Saidin, S., Sonny, I. & Nuruddin, M.F., 2008a. A New Approach for Optimizing Cement Design to Eliminate Microannulus in Steam Injection Wells. *International Petroleum Technology Conference, 3-5 December 2008, Kuala Lumpur, Malaysia*.

Saidin, S., Sonny, I. & Nuruddin, M.F., 2008b. A New Approach for Optimizing Cement Design to Eliminate Microannulus in Steam Injection Wells. *International Petroleum Technology Conference, 3-5 December 2008, Kuala Lumpur, Malaysia*.

Scarfato, P., Avallone, E., Iannelli, P., De Feo, V. and Acierno, D., 2007. Synthesis and characterization of polyurea microcapsules containing essential oils with antigerminative activity. *Journal of applied polymer science*, *105*(6), pp.3568-3577.

Schlangen, E. and Joseph, C., 2009. Self-healing processes in concrete. *Self-healing materials:*

References

Fundamentals, design strategies, and applications.

Schlumberger, 2010. Effective Zonal Isolation for the Life of a UGS Well.

Schlumberger, 2014. Future Self-Healing Cement System. Available at: https://www.slb.com/services/drilling/cementing/self_healing_cement.aspx.

Schmid, R.L. & Felsche, J., 1983. Thermal studies on sodium silicate hydrates. I. Trisodium hydrogensilicate pentahydrate, Na3HSiO4· 5 H2O; Thermal stability and thermal decomposition reactions. *Thermochimica Acta*, 71(3), pp.359–364.

Shadravan, A., Schubert, J., Amani, M. and Teodoriu, C., 2014, March. HPHT cement sheath integrity evaluation method for unconventional wells. *SPE International Conference on Health, Safety, and Environment: The Journey Continues*, 1, pp.73–81.

Shahriar, a. & Nehdi, M.L., 2012. Optimization of rheological properties of oil well cement slurries using experimental design. *Materials and Structures*, 45(9), pp.1403–1423.

Shahriar, A., 2011. Investigation on Rheology of Oil Well Cement Slurries.

Shand, M.A., 2006. *The chemistry and technology of magnesia*. John Wiley & Sons.

Sisomphon, K., Copuroglu, O. & Koenders, E. a B., 2012. Self-healing of surface cracks in mortars with expansive additive and crystalline additive. *Cement and Concrete Composites*, 34(4), pp.566–574.

Skalny, J. & Young, J.F., 1980. International Congress on the Chemistry of Cement.

Souza, L. via R. de, 2017. Design and systhesis of microcapsules using microfluidics for autonomic self-healing in cementitious materials. *PhD thesis, University of Cambridge*.

Souza, P.P., Soares, R.A., Anjos, M.A., Freitas, J.O., Martinelli, A.E. and Melo, D.F., 2012. Cement slurries of oil wells under high temperature and pressure: the effects of the use of ceramic waste and silica flour. *Brazilian Journal of Petroleum and Gas*, 6(3), pp.105–113.

Strydom, C.A., Van Der Merwe, E.M. & Aphane, M.E., 2005. The effect of calcining conditions on the rehydration of dead burnt magnesium oxide using magnesium acetate as a hydrating agent. *Journal of Thermal Analysis and Calorimetry*, 80(3), pp.659–662.

References

Tan, N.P.B., Keung, L.H., Choi, W.H., Lam, W.C. and Leung, H.N., 2016. Silica-based self-healing microcapsules for self-repair in concrete. *Journal of Applied Polymer Science*, *133*(12), pp.1–12.

Thomas, J., Musso, S., Catheline, S., Chougnet-Sirapian, A. and Allouche, M., 2014, September. Expanding cement for improved wellbore sealing: Prestress development, physical properties, and logging response. *SPE Deepwater Drilling and Completions Conference*, *10-11 September, Galveston, Texas, USA*.

Van Tittelboom, K. and De Belie, N., 2013. Self-healing in cementitious materials—A review. *Materials*, *6*(6), pp.2182-2217.

Wang, H., Yuan, Y., Rong, M. and Zhang, M., 2009. Microencapsulation of styrene with melamine-formaldehyde resin. *Colloid and Polymer Science*, 287(9), pp.1089–1097.

Wang, X., Xing, F., Zhang, M., Han, N. and Qian, Z., 2013. Experimental study on cementitious composites embedded with organic microcapsules. *Materials*, 6(9), pp.4064–4081.

Wang, X., Sun, P., Han, N. and Xing, F., 2017. Experimental study on mechanical properties and porosity of organic microcapsules based self-healing cementitious composite. *Materials*, *10*(1), p.20.

White, S.R., Sottos, N.R., Geubelle, P.H., Moore, J.S., Kessler, M., Sriram, S.R., Brown, E.N. and Viswanathan, S., 2001. Autonomic healing of polymer composites. *Nature*, *409*(6822), pp.794–797.

White, S.R., Blaiszik, B.J., Kramer, S.L., Olugebefola, S.C., Moore, J.S. and Sottos, N.R., 2010. Self-healing Polymers and Composites: Capsules, circulatory systems and chemistry allow materials to fix themselves. *American Scientist*, *99*(5), pp.392-399.

Wilcox, B., Oyeneyin, B. & Islam, S., 2016. HPHT Well Integrity and Cement Failure. *SPE Nigeria Annual International Conference and Exhibition*, 2010(August), pp.1–15.

Wu, M., Johannesson, B. & Geiker, M., 2012. A review: Self-healing in cementitious materials and engineered cementitious composite as a self-healing material. *Construction and*

Building Materials, 28(1), pp.571–583.

Yang, J., Keller, M.W., Moore, J.S., White, S.R. and Sottos, N.R., 2008. Microencapsulation of isocyanates for self-healing polymers. *Macromolecules*, *41*(24), pp.9650-9655.

Yang, Y., Li, M., Deng, H. and Liu, Q., 2014. Effects of Temperature on Drying Shrinkage of Concrete. *Applied Mechanics & Materials*, 586, pp.1176–1181.

Yang, Z., Hollar, J., He, X. and Shi, X., 2011. A self-healing cementitious composite using oil core/silica gel shell microcapsules. *Cement and Concrete Composites*, 33(4), pp.506–512.

Yuan, L., Liang, G.Z., Xie, J.Q., Guo, J. and Li, L., 2006. Thermal stability of microencapsulated epoxy resins with poly(urea-formaldehyde). *Polymer Degradation and Stability*, 91(10), pp.2300–2306.

Zhang, J., Weissinger, E.A., Peethamparan, S. and Scherer, G.W., 2010. Early hydration and setting of oil well cement. *Cement and Concrete Research*, 40(7), pp.1023–1033.

Zhu, H., Hua S., Wu Q., Zhang C., Yang T., 2013. Effect of MgO expanding agent on early performance of oil well cement under three dimensional constraint (in chinese). *Journal of China University of Petroleum*, 37(6), pp.1–6.